UNIVERSITY OF CALGARY

Gas-phase Chemistry of Methyl-Substituted Silanes in a Hot-wire Chemical Vapour Deposition Process

by

Rim Toukabri

A THESIS

SUBMITTED TO THE FACULTY OF GRADUATE STUDIES

IN PARTIAL FULFILMENT OF THE REQUIREMENTS FOR THE

DEGREE OF DOCTOR OF PHILOSOPHY

DEPARTMENT OF CHEMISTRY

CALGARY, ALBERTA

August, 2013

© Rim Toukabri 2013

Abstract

The primary decomposition and secondary gas-phase reactions of methyl-substituted silane molecules, including monomethylsilane (MMS), dimethylsilane (DMS), trimethylsilane (TriMS) and tetramethylsilane (TMS), in hot-wire chemical vapour deposition (HWCVD) processes have been studied using laser ionization methods in combination with time of flight mass spectrometry (TOF-MS). For all four molecules, methyl radical formation and hydrogen molecule formation have been found to be the common decomposition steps on both tungsten (W) and tantalum (Ta) filaments. The apparent activation energy ranges from 51.1 to 84.7 kJ · mol^{-1} for the methyl radical formation and 55.4 to 70.7 kJ · mol^{-1} for the formation of H_2. Both activation energy values increase with the number of methyl substitutions in the precursor molecules on W and Ta filaments. The formation of these two species is initiated by Si-H bond cleavage. This cleavage is then followed by Si-CH_3 bond breakage producing methyl radical, whereas two H adsorbates on the surface of the filament recombine releasing H_2 into the gas phase, following Langmuir-Hinshelwood mechanism.

The secondary gas-phase reactions of MMS and DMS in a HWCVD reactor have also been investigated. For DMS as a precursor gas, a competition between silene/ silylene chemistry occurring at low temperature and radical chain mechanism present at high temperature is observed. For MMS, its gas-phase chemistry involves exclusively silylene species, characterized by its insertion and dimerization reactions. It is concluded that both free-radical and silenes/silylenes intermediates play important roles in the gas-phase chemistry of methyl-substituted silanes. A comparison of the secondary gas-phase

reactions of TMS, TriMS, DMS, and MMS revealed a switch in dominance from free-radical chemistry to silene/silylene chemistry as the number of methyl substitution on the precursor molecule is decreased. A study of the effect of deposition parameters, including precursor pressure and filament material, has shown that these parameters influenced significantly the gas-phase chemistry of TriMS and DMS. This is due to the competition between free-radical reactions and silylene/silene reactions. However, these parameters do not affect the gas-phase chemistry of MMS since it involves only one type of intermediate.

Acknowledgements

I would like to take this opportunity to present my appreciation to the people that provided me the possibility to accomplish my PhD study.

Foremost I would like to express my sincere gratitude to my supervisor, Dr. Yujun Shi, for giving me the opportunity to complete my graduate study in her group and for her guidance throughout these years.

Beside my supervisor, I would like to forward my gratitude to my committee members Dr. Hans Osthoff and Dr. Peter Kusalik for their encouragement, and insightful discussions.

It has been a great pleasure to work along each of Dr. Shi's group members, past and present. I would like to thank Brett and Ling for teaching me about the instrument and their help when I started with the lab work. I am also pleased to know Martin, Watheq, Chris, Jimmy, Ismail and Ebenezer. Your company and friendship kept enriched my life with laughter and joy. I specially thank Ismail for his help and contribution in the theoretical calculation carried out in this work.

I would like to thank my friends Yiota, Angela and Samar, who were always great support in all my struggles and frustrations, as well as my achievements through these years. Yiota, even though you are far, your friendship and support is greatly appreciated.

Ibro, I could never thank you enough, you were always there for me.

My sincere thanks go to Bonnie King for her countless hours of support and motivation. I would like to thank also Andy Read and Todd Willis from the science workshop for their tremendous help in fixing and adjusting my instrument, as well as Edward Cairns and Mike Siewert for providing me with assistance with all sorts of electronics.

Last but not least, I would like to thank my parents, Hatem Toukabri and Samira Kedadi for always believing in me. Their love and encouragement provided me with inspiration and driving force to complete this important stage of my life. I also would like to thank my siblings, Ala and Mariem Toukabri, and their families for their understanding and support throughout these last years.

To my parents Hatem Toukabri and Samira Kedadi

Table of Contents

Abstract ii
Acknowledgements iv
Dedication vi
Table of Contents vii
List of Tables x
List of Figures and Illustrations xi
List of Schemes xviii
List of Symbols, Abbreviations and Nomenclature xix
Epigraph xxi

CHAPTER ONE: INTRODUCTION AND BACKGROUND 1
1.1 Thin Film Deposition Processes 1
1.1.1 Physical Vapour Deposition 1
1.1.2 Chemical Vapour Deposition 3
1.2 Hot-Wire Chemical Vapour Deposition (HWCVD) 4
1.3 HWCVD of Silicon Carbide Thin Films 10
1.3.1 Silicon Carbide (SiC) Thin Films 10
1.3.2 Growth of SiC Thin Films Using HWCVD Processes 12
1.3.3 HWCVD of SiC Thin Films Using Methyl-Substituted Silanes 14
1.4 Gas-Phase Chemistry in HWCVD System 15
1.4.1 Detecting the Gas-Phase Reaction Products in a HWCVD Process 15
1.4.2 Gas-Phase Chemistry in HWCVD Using Methyl-Substituted Silanes 19
1.4.3 Chemical Trapping of the Active Intermediates 21
1.5 Objectives of this Thesis 25

CHAPTER TWO: EXPERIMENTAL DETAILS 27
2.1 HWCVD Sources 28
2.1.1 A Collision-Free Setup to Detect Decomposition Species on the Filament 28
2.1.2 A Reactor Setup to Detect Species from Secondary Gas-phase Reactions 30
2.2 Ionization Sources 31
2.2.1 The Single Photon Ionization (SPI) Source 31
2.2.2 The Dual Single Photon Ionization and Laser Induced Electron Ionization (SPI/LIEI) Source 32
2.3 TOF Mass Spectra Collection 34
2.4 Synthesis of MMS-d_3, DMS-d_2 and TriMS-d_1 36
2.5 Sample Preparation and Introduction 39
2.6 Computational Methods 41

CHAPTER THREE: FORMATION OF METHYL RADICALS FROM DECOMPOSITION OF METHYL-SUBSTITUTED SILANES OVER TUNGSTEN AND TANTALUM FILAMENTS 43
3.1 Motivations 43
3.2 The Intensity Profile of Methyl Radical on W Filament 45
3.3 The Activation Energy of Forming Methyl Radicals on W - Effect of Molecular Structures 50

3.4 Effect of Filament Material - W vs Ta....55
3.5 Summary....58

CHAPTER FOUR: STUDY OF HYDROGEN ELIMINATION FROM THE DECOMPOSITION OF METHYL-SUBSTITUTED SILANES OVER TUNGSTEN AND TANTALUM FILAMENT SURFACES....60
4.1 Motivations....60
4.2 Comparison of the Two Ionization Sources....64
4.3 H_2 Formation during the Decomposition of Methyl-Substituted Silanes on a Heated W Filament....69
4.4 Experiments with MMS-d_3, DMS-d_2 and TriMS-d_1....78
4.5 The Activation Energy of Forming H_2 Molecules on W and Ta....84
4.6 1,1-H_2 and 1,2-H_2 Elimination: A Theoretical Study....86
4.7 Summary....106

CHAPTER FIVE: ROLE OF FREE-RADICAL AND METHYLSILENE/DIMETHYLSILYLENE IN THE REACTION CHEMISTRY OF DIMETHYLSILANE IN A HOT-WIRE CHEMICAL VAPOUR DEPOSITION PROCESS....108
5.1 Motivations....108
5.2 Primary Decomposition on Ta and W Filament....111
5.3 Secondary Gas-Phase Reactions on a Ta Filament....112
5.3.1 Possible Secondary Reactions....116
5.3.1.1 Hydrogen Abstraction and Biradical Recombination Reactions....116
5.3.1.2 Reactions Involving Silene and Silylene Intermediates....117
5.3.2 Formation of the Main Products....119
5.3.2.1 Formation of 1,1,2,2-Tetramethyldisilane at Low Filament Temperatures....121
5.3.2.2 Formation of 1,3-Dimethyl-1,3-disilacyclobutane at High Filament Temperatures....124
5.3.2.3 Formation of Trimethylsilane and Tetramethylsilane at High Filament Temperatures....128
5.3.3 Trapping of Active Intermediates....133
5.3.3.1 Trapping Experiment with 1,3-Butadiene....134
5.3.3.2 Trapping Experiments with Ammonia....140
5.4 Effect of Precursor Gas Pressure on DMS Gas-Phase Chemistry....145
5.5 Effect of Filament Material on DMS Gas-Phase Chemistry....157
5.6 Summary....162

CHAPTER SIX: GAS-PHASE CHEMISTRY OF MONOMETHYLSILANE IN A HWCVD REACTOR....165
6.1 Motivations....165
6.2 Primary Decomposition of MMS on W and Ta Filaments....168
6.3 Secondary Gas-Phase Reaction of MMS in a HWCVD Reactor on Ta Filament....171
6.3.1 Possible Secondary Gas-phase Reactions....174
6.3.1.1 Hydrogen Abstraction Reactions and Biradical Combinations....174
6.3.1.2 Reactions Involving Silene and Methylsilylene Intermediates....175

6.3.2 Formation of the Main Products....178
6.3.2.1 Formation of 1,2-Dimethyldisilane....180
6.3.2.2 Formation of 1,3-Disilacyclobutane....182
6.3.3 Trapping of Active Intermediates....183
6.3.3.1 Trapping Experiments with 1,3-Butadiene....183
6.3.3.2 Trapping Experiments with Ammonia....186
6.4 Effect of Filament Materials on MMS Gas-Phase Chemistry....192
6.5 Effect of Source Gas Pressure on MMS Gas-Phase Chemistry....194
6.6 Comparison of Gas-Phase Chemistry with Four Methyl-Substituted Silane Molecules....197
6.7 Summary....200

CHAPTER SEVEN: EFFECT OF TRIMETHYLSILANE PRESSURE ON THE GAS-PHASE REACTION CHEMISTRY IN THE HWCVD PROCESS....202
7.1 Motivations....202
7.2 Gas-Phase Reaction Products from Trimethylsilane in a HWCVD Reactor....203
7.3 Formation of Methane and other Small Hydrocarbon Molecules....208
7.4 Formation of Hydrogen Molecules....213
7.5 Effect on the Radical Recombination and Disproportionation Reactions....215
7.6 Summary....221

CHAPTER EIGHT: CONCLUSIONS AND FUTURE WORK....223

APPENDICES....232

REFERENCES....236

List of Tables

Table 1-1 Material properties of common SiC polytypes[47, 51, 52] 11

Table 2-1 Composition of methyl-substituted silane/He mixtures studied in Chapters 3 and 4 40

Table 2-2 Composition of methyl-substituted silane/He mixtures studied in Chapters 5 and 6 40

Table 2-3 Composition of methyl-substituted silane molecules /trapping agent mixtures studied in this work 41

Table 4-1 Total energies of singlet silene and methylsilylene species and corresponding zero point energies (ZPE) in Hartee's at CCSD(T)/6-311++G(d,p) level 94

Table 4-2 Total energies of triplet silene and methylsilylene species and corresponding zero point energies (ZPE) in Hartee's at CCSD(T)/6-311++G(d,p) level 94

Table 4-3 Activation enthalpies, entropies, and Gibbs free energies for the various decomposition pathways of MMS and DMS 99

Table 4-4 The reaction enthalpies, entropies, and Gibbs free energies for the various decomposition pathways of MMS and DMS 100

Table 5-1 Summary of the intensity ratios of each of the peaks at *m/z* 73, 116, and 118 to that of the parent peak at *m/z* 60 when using 0.12 Torr and 1.2 Torr of DMS in HWCVD reactor at filament temperatures of 1300 and 1400 ^{o}C..... 147

Table 5-2 Comparison of the intensity ratios of each of the peaks at *m/z* 73, 116, and 118 in the presence and absence of ethene ((') indicates the ones with ethene)..... 151

Table 7-1 Summary of the intensity ratios of each of the peaks at *m/z* 146, 116, 130, and 144 to that of the peak at *m/z* 58 when using 0.12 Torr and 4.0 Torr of TriMS in the hot-wire CVD reactor at filament temperatures of 1300 and 1500 ^{o}C..... 207

List of Figures and Illustrations

Figure 1-1: Classification of thin film deposition technologies..... 2

Figure 1-2: A schematic diagram of the PVD process: 1) evaporation from the source, 2) transport of evaporant, and 3) condensation of the evaporant..... 2

Figure 1-3: A diagram of various processes in HWCVD..... 6

Figure 2-1: A schematic of the experimental setup for laser ionization mass spectrometric measurements..... 27

Figure 2-2: A schematic of the HWCVD collision-free flange for detection of direct hot-wire decomposition products. (S.S = stainless steel) 29

Figure 2-3: A schematic the HWCVD reactor for detection of secondary gas-phase products. (S.S = stainless steel)..... 30

Figure 2-4: A schematic diagram of the single photon ionization (SPI) source.[118] (Adapted with permission from Springer Science and Business Media, Journal of the American Society for Mass Spectrometry, 18, 2007)..... 32

Figure 2-5: A schematic diagram the dual SPI/LIEI source..... 33

Figure 2-6: A schematic diagram of the Wiley-McLaren TOF mass spectrometer with a two-stage ion extraction optics configuration..... 34

Figure 2-7: Experimental apparatus for the synthesis of deuterated methyl-substituted silane molecules..... 37

Figure 3-1: 10.5 eV VUV SPI TOF mass spectra of TMS, TriMS, DMS and MMS exposed to a W filament heated to 2000^{o}C at a chamber pressure of ~1 × 10^{-5} Torr. 46

Figure 3-2: The normalized peak intensity of *m/z* 15 (CH_3^+) as a function of the filament temperature for pure MMS, DMS, TriMS, and TMS samples on a W filament at a chamber pressure of 1×10^{-5} Torr..... 46

Figure 3-3: The intensity ratio of a) *m/z* 31 to *m/z* 46 for 8% MMS in He, and b) *m/z* 45 to *m/z* 60 for pure DMS samples as a function of W filament temperature at a chamber pressure of 1×10^{-5} Torr..... 48

Figure 3-4: Apparent activation energy for methyl radical formation from the four methyl-substituted silanes over the surface of tungsten and tantalum surfaces..... 51

Figure 3-5: Temperature profiles of the normalized intensity of methyl radical from W and Ta filaments during the dissociation of a) MMS, b) DMS, c) TriMS, and d) TMS samples. 57

Figure 4-1: Mass spectra of pure DMS taken at a filament temperature of 2000 ^{o}C and a chamber pressure of 1×10^{-5} Torr using a) SPI mode and b) LIEI-SPI mode in the mass region between 0 and 20 amu. 67

Figure 4-2: The intensity of the peak at *m/z* 2 at different W filament temperatures for pure DMS sample using the pure SPI and dual SPI/LIEI ionization sources. 68

Figure 4-3: The mass spectra in the region between *m/z* 1 and *m/z* 4 for MMS, DMS, TriMS and TMS at a filament temperature of 2000 °C and a chamber pressure of 1×10^{-5} Torr using a) SPI mode and b) dual SPI/LIEI source. 70

Figure 4-4: The intensity distributions of the peak at *m/z* 2 at different W filament temperatures for MMS, DMS, TriMS and TMS precursors using a) SPI mode, and b) dual SPI/LIEI ionization mode at a chamber pressure of 1×10^{-5} Torr..... 71

Figure 4-5: Temperature profiles of the normalized intensity of H_2^+ using SPI mode from W and Ta filaments during the dissociation of a) MMS, b) DMS, and c) TriMS samples. 74

Figure 4-6: a) The intensity evolution of the peak at *m/z* 1 as a function of W filament temperatures for MMS, DMS, TriMS and TMS precursors using SPI ionization source at a chamber pressure of 1×10^{-5} Torr, and b) an enlarged plot for the peak 1 evolution from TriMS and TMS samples. 75

Figure 4-7: SPI/LIEI TOF mass spectra of pure a) MMS-d_3, b) DMS-d_2 and c) TriMS-d_1 in the mass region 1 - 5 amu at filament temperatures ranging from 25 °C - 2400 °C and a chamber pressure of 1×10^{-5} Torr. 79

Figure 4-8: The intensity evolution of the peaks at *m/z* 2, 3 and 4 at different W filament temperatures for a) MMS-d_3, b) DMS-d_2, and c) TriMS-d_1 precursors using the dual SPI/LIEI ionization source. 80

Figure 4-9: Apparent activation energy for hydrogen molecule formation from MMS, DMS and TriMS on the two filaments of tungsten and tantalum. 85

Figure 4-10: Optimized structures of a) monomethylsilane, b) methylsilylene, c) silene, and d) methylsilyl involved in the concerted and stepwise 1,1-, and 1,2-H_2 elimination mechanism of MMS. 89

Figure 4-11: Optimized structures of a) dimethylsilane, b) dimethylsilylene, c) methylsilene, and d) dimethylsilyl involved in the concerted and stepwise 1,1-, and 1,2-H_2 elimination mechanism of DMS. 89

Figure 4-12: Optimized structures of a) trimethylsilane, b) trimethylsilyl, and c) dimethylsilene involved in the concerted and stepwise 1,1-, and 1,2-H_2 elimination mechanism of TriMS. 90

Figure 4-13: Optimized structures of the transition states for the concerted and stepwise H_2 elimination processes from MMS. 91

Figure 4-14: Optimized structures of the transition states for the concerted and stepwise H2 elimination processes from DMS. 92

Figure 4-15: Optimized structures of the transition states for the concerted and stepwise H2 elimination processes from TriMS. 92

Figure 4-16: Energy level diagrams for the 1,1-, and 1,2- H_2 elimination pathways of MMS. For each pathway, both stepwise and concerted mechanisms were investigated. Energy values represent the relative enthalpies in kcal/mol at 0 K (ZPE corrections included). 97

Figure 4-17: Energy level diagrams for the 1,1-, and 1,2- H_2 elimination pathways of DMS. For each pathway, both stepwise and concerted mechanisms were investigated. Energy values represent the relative enthalpies in kcal/mol at 0 K (ZPE corrections included). 97

Figure 4-18: Energy level diagrams for the 1,2- H_2 elimination pathways of TriMS. For each pathway, both stepwise and concerted mechanisms were investigated. Energy values represent the relative enthalpies in kcal/mol at 0 K (ZPE corrections included). 98

Figure 4-19: Temperature distribution of Gibbs free energy of activation ($\Delta G^{\neq}$) for the 1,1-, and 1,2- H_2 elimination pathways of MMS. For each pathway, both stepwise and concerted mechanisms were investigated. (ZPE corrections included) 104

Figure 4-20: Temperature distribution of Gibbs free energy of activation ($\Delta G^{\neq}$) for the 1,1-, and 1,2- H_2 elimination pathways of DMS. For each pathway, both stepwise and concerted mechanisms were investigated. (ZPE corrections included) 104

Figure 4-21: Temperature distribution of Gibbs free energy of reaction (ΔG) for the 1,1-, and 1,2- H_2 elimination pathways of MMS. For each pathway, both stepwise and concerted mechanisms were investigated. (ZPE corrections included) 105

Figure 4-22: Temperature distribution of Gibbs free energy of reaction (ΔG) for the 1,1-, and 1,2- H_2 elimination pathways of DMS. For each pathway, both stepwise and concerted mechanisms were investigated. (ZPE corrections included) 105

Figure 5-1: The Intensity ratio of a) $(CH_3)_2SiH^+$ (*m/z* 59) to that of the parent of $(CH_3)_2SiH_2^+$ (*m/z* 60), and b) $(CH_3)_2SiH^+$ (*m/z* 58) to that of the parent of $(CH_3)_2SiH_2^+$ (*m/z* 60) for pure DMS versus the filament temperature at a chamber pressure of 1×10^{-5} Torr. 112

Figure 5-2: a) 10.5 eV SPI TOF mass spectra of 12 Torr 1% DMS/He in the reactor at filament temperatures between 1200 and 1600 ^{o}C. The spectrum at 25 ^{o}C is recorded when the filament is off; b) enlarged spectra in the mass regions of 70-150 amu. 114

Figure 5-3: The intensity ratio of the peak at *m/z* 58 to the parent ion peak at *m/z* 60 from 12 Torr of 1% DMS/He as function of filament-on time over the temperature range of 1100 to 1700 ^{o}C. 116

Figure 5-4: Intensity distribution of peaks at *m/z* 73, 118 and 116 when using 12 Torr of 1% DMS/He and at a filament temperature of a) 1200 ^{o}C, b) 1300 ^{o}C, and c) 1400 ^{o}C. 120

Figure 5-5: 10.5 eV SPI TOF mass spectrum of 0.12 Torr of DMS sample in the reactor at a filament temperature of 1200 ^{o}C in the mass region of 70 - 130 amu. The inset is a mass spectrum of an authentic TMDS sample recorded at room temperature. 122

Figure 5-6: 10.5 eV SPI TOF mass spectrum of 12 Torr of 4% DMS-d_2/He mixture recorded 10 minutes after the filament was turned on at 1200 °C. 123

Figure 5-7: 10.5 eV SPI TOF mass spectra of a) 12 Torr of 4% DMS/He, and b) 12 Torr of 4% DMS-d_2/He in the reactor at a filament temperature of 1400 ^{o}C. 126

Figure 5-8: Intensity distribution of the peaks at a) *m/z* 116 and 118 originated from 4% DMS/He and b) *m/z* 116, 118 and 120 produced from 4% DMS-d_2/He at a filament temperature of 1400 ^{o}C. 127

Figure 5-9: Comparison of the intensity ratio of the peak at *m/z* 116 to the one at *m/z* 118 from the 12 Torr 4% DMS-d_2/He mixture versus filament-on time at 1300 and 1400 ^{o}C. 127

Figure 5-10: 10.5 eV SPI TOF mass spectra of 12 Torr 1% DMS/He in the reactor at filament temperature of 1300 ^{o}C. 129

Figure 5-11: Intensity distribution of the peak at a) *m/z* 73, and b) *m/z* 88 as a function of filament-on time over a temperature range of 1200 to 1700 °C. 130

Figure 5-12: Intensity of the peak at *m/z* 73 observed with 12 Torr of 1% DMS/He mixture at 1300 °C (□), 1500 (○), and 1600 ^{o}C ( ). The contribution to the peak intensity from the photofragmentation of TriMS, TMS, and TMDS combined at 1300 (■), 1500 (●) and 1600 ^{o}C (★) is shown for comparison. 132

Figure 5-13: 10.5 eV SPI TOF mass spectra of 12 Torr 1% DMS + 8% BTD in He in the reactor at filament temperature 1200 ^{o}C after one hour of turning the filament on. 135

Figure 5-14: Intensity of peak at *m/z* 112 and 73 from 12 Torr 8% BTD + 1% DMS/He versus filament-on time at a filament temperature of 1200 ^{o}C. 136

Figure 5-15: 10.5 eV SPI TOF mass spectrum of a) 1,3-Butadiene at room-temperature (Inset: an enlarged picture in the mass region of 0-45 amu), b) 12 Torr of 8% BTD/He mixture recorded 10 minutes after the filament was turned on at 1200 °C. 137

Figure 5-16: a) 10.5 eV SPI TOF mass spectra of 12 Torr 1% DMS + 8% BTD in He in the reactor at filament temperature 1400 ^{o}C (Note the peak at *m/z* 54 is overloaded), b) 10.5 eV SPI TOF mass spectra of 12 Torr of 8% BTD in He in the reactor at filament temperature 1400 ^{o}C after 30 min of reaction time. 139

Figure 5-17: 10.5 eV SPI TOF mass spectra of a) 12 Torr of 1% DMS + 8% NH_3 in He, and b) 12 Torr of 1% DMS/He in the reactor at filament temperature 1300 ^{o}C and after five minutes of turning the filament on..... 141

Figure 5-18: Comparison of the intensity ratio of the peak at *m/z* 75 to the one at *m/z* 73 in the presence and absence of ammonia versus filament-on time at 1300 ^{o}C. . 141

Figure 5-19: Comparison of the intensity ratio of the peak at *m/z* 116 to the one at 118 in the presence and absence of ammonia at 1300 ^{o}C. 142

Figure 5-20: Energy level diagrams for the addition reactions of ammonia to methylsilene and dimethylsilylene species. Energy values represent the relative Gibbs free energy in kcal/mol at 298 K (ZPE corrections included). 143

Figure 5-21: 10.5 eV SPI TOF mass spectra of a) 12 Torr of 1% DMS/He, and b) 12 Torr of 10% DMS/He in the reactor at a filament temperature of 1300 ^{o}C. (Inset: an enlarged spectrum in the mass region of 10-45 amu). 146

Figure 5-22: 10.5 eV SPI TOF mass spectra of 12 Torr of 1% DMS + 8% ethene in He in the reactor at filament temperature 1300 ^{o}C..... 151

Figure 5-23: Comparisons of the intensity of the peaks at a) *m/z* 86, 84, 98 and b) *m/z* 26, 28, 40 versus filament-on time at 1300 ^{o}C observed with 1.2 Torr of DMS. ... 153

Figure 5-24: The intensity of the peaks at *m/z* 73, 118, and 116 versus filament-on time observed with a) 1.2 Torr of DMS at 1300 ^{o}C, b) 0.12 Torr of DMS at 1300 ^{o}C, and c) 0.12 Torr of DMS at 1500 ^{o}C. 154

Figure 5-25: 10.5 eV SPI mass spectra using a) W filament and b) Ta filament for 12 Torr of 1% DMS/He at filament temperature of 1200 °C and filament-on time of 5 min. 159

Figure 5-26: Intensity distribution of peaks at *m/z* 73, 116 and 118 generated from W filament when using 12 Torr of 1% DMS/He at a filament temperature of 1200 ^{o}C..... 161

Figure 5-27: Intensity distribution of peaks at *m/z* 73, 116 and 118 generated from W when using 12 Torr of 1% DMS/He and at a filament temperature of 1400 ^{o}C. 162

Figure 6-1: The intensity ratio of I(*m/z* 44)/I(*m/z* 46) versus the filament temperature for pure MMS sample at a chamber pressure of 1×10^{-5} Torr. 169

Figure 6-2: The intensity ratio of I(*m/z* 45)/I(*m/z* 46) versus the filament temperature for pure MMS sample at a chamber pressure of 1×10^{-5} Torr. 170

Figure 6-3: a) 10.5 eV SPI TOF mass spectra of 12 Torr of 4% MMS/He in the HWCVD reactor at filament temperatures ranging from 900-1400 °C at two minutes of reaction time, and enlarged spectra in the mass region of b) 0-70 amu, and c) 70-200 amu. 172

Figure 6-4:10.5 eV SPI TOF mass spectrum of 12 Torr of 4% MMS/He at the filament temperature of 1400 ^{o}C in the mass region between 80 and 180 amu..... 173

Figure 6-5: The peak intensity in the series of a) *m/z* 88 + n 44 and b) *m/z* 90 + n 44 from 12 Torr of 4% MMS/He as a function of filament-on time at a filament temperature of 1200 ^{o}C. 174

Figure 6-6: The intensity distribution of the peak at *m/z* 88, and 90 as function of filament-on time at filament temperatures a) 1000 °C, b) 1200 °C, and c) 1300 °C. 179

Figure 6-7: 10.5 eV SPI TOF mass spectra of 12 Torr of 4% CH_3SiD_3 in He mixture in the reactor at a filament temperature of 1300 °C in the mass region of 0-100 amu. 181

Figure 6-8: 10.5 eV SPI TOF mass spectra of a) 12 Torr of 4% MMS + 32% BTD in He mixture at room temperature (Inset: enlarged picture in the mass region of 0-50 amu); b) 12 Torr of 4% MMS + 32% BTD mixture in He in the reactor at filament temperature of 1300 ^{o}C; c) 12 Torr of 32% BTD in He mixture in the reactor at filament temperature of 1300 ^{o}C. The peak at *m/z* 54 is overloading. 185

Figure 6-9: 10.5 eV SPI TOF mass spectra of 12 Torr 4% MMS + 32% NH_3 in He in the reactor at a filament temperature of 1300 ^{o}C after 4 minutes of turning the filament on. (Inset: an enlarged mass spectrum in the mass region of 40 to 180 amu. 187

Figure 6-10: The intensity distribution of mass peaks at *m/z* 61 and 90 and 88 in the absence and presence of the trapping agent, NH_3, at a filament temperature of 1300 ^{o}C..... 189

Figure 6-11: The peak intensities in the series of a) *m/z* 88 + n 44 and b) *m/z* 90 + n 44 as a function of filament-on time at a filament temperature of 1300 ^{o}C in the absence and presence of ammonia. 190

Figure 6-12: Comparison of the intensity ratio of the peak at *m/z* 90 to the one at *m/z* 88 as a function of filament-on time at a filament temperature of 1300 ^{o}C in the absence and presence of ammonia. 191

Figure 6-13: 10.5 eV SPI TOF mass spectra using W and Ta filament for 12 Torr of 4% MMS/He mixture at a filament temperature of a) 1200 ^{o}C, and b) 1300 ^{o}C and filament-on time of 3 min. 193

Figure 6-14: The intensity distribution of peaks at *m/z* 90 and 88 generated from W and Ta filaments when using 12 Torr of 4% MMS/He and at a filament temperature of a) 1200 ^{o}C, and b) 1300 ^{o}C. 194

Figure 6-15: 10.5 eV SPI TOF mass spectra of a) 12 Torr of 4% MMS/He, and b) 12 Torr of 10% MMS/He in the reactor at a filament temperature of 1300 ^{o}C in the mass range of 0 to 200 amu. 196

Figure 6-16: The intensity of the peaks at *m/z* 90, and 88 versus filament-on time observed with 0.48 Torr and 1.2 Torr of MMS at a) 1200 ^{o}C and b) 1300 ^{o}C. 197

Figure 7-1: Intensity of the peak at *m/z* 73 (I73') observed with 20 Torr of 20% TriMS/He mixture at 1300 ^{o}C (▼) and 1500 ^{o}C ( ), compared with the calculated contribution to the peak intensity (I73'') from the photofragmentation of TriMS, TMS, and HMDS combined at 1300 ^{o}C (Δ), and 1500 ^{o}C (□). 204

Figure 7-2: 10.5 eV SPI TOF mass spectra of a) 12 Torr of 1% TriMS/He and b) 20 Torr of 20% TriMS/He in the reactor at a filament temperature of 1300 ^{o}C. 206

Figure 7-3: 10.5 eV SPI TOF mass spectrum of an authentic methane sample recorded at room temperature. The inset is a mass spectrum of 4.0 Torr of TriMS sample in the reactor at a filament temperature of 1300 ^{o}C in the mass region of 5 - 20 amu. 209

Figure 7-4: Comparisons of the intensity of the peaks at a) *m/z* 84, 98 and b) *m/z* 16, 26, 40, versus filament-on time at 1300 ^{o}C observed with 4.0 Torr of TriMS. 213

Figure 7-5: The intensity of the peaks at *m/z* 88, 146, 116, 130, and 144 versus filament-on time observed with a) 4.0 Torr of TriMS at 1300 ^{o}C, and b) 0.12 Torr of TriMS at 1300 ^{o}C, and c) 0.12 Torr of TriMS at 1500 ^{o}C. 217

Figure 7-6: The intensity ratio of a) I(*m/z* 116)/I(*m/z* 88), b) I(*m/z* 130)/I(*m/z* 88), and c) I(*m/z* 144)/I(*m/z* 88) as a function of filament-on time for the two TriMS samples of 0.12 Torr and 4.0 Torr at the filament temperatures of 1300 ^{o}C and 1500 ^{o}C. 220

List of Schemes

Scheme 3-1 Adsorption and decomposition of monomethylsilane on a W or Ta surface 53

Scheme 4-1 Chemisorption and decomposition of MMS on a metal surface..... 77

Scheme 4-2 Chemisorption and decomposition of TMS over a metal surface..... 77

Scheme 4-3 Chemisorption and decomposition of MMS-d_3 on a metal surface..... 82

Scheme 4-4 Stepwise and concerted 1,1- and 1,2-H_2 elimination reactions for MMS 87

Scheme 4-5 Stepwise and concerted 1,1-, and 1,2-H_2 elimination reactions for DMS 88

Scheme 4-6 Stepwise and concerted 1,2-H_2 elimination reactions for TriMS 88

Scheme 5-1 Photofragmentation mechanism of 1,1,2,2-tetramethyldisilane. 122

Scheme 5-2 Formation of small hydrocarbons 148

Scheme 6-1 Methylsilylene insertion reactions into Si-H bond of 1,2-dimethyldisilane 177

Scheme 6-2 Methylsilylene insertion reactions into Si-H bond of 1,3-disilacyclobutane..... 178

Scheme 6-3 Reaction of 1,3-butadiene with methylsilylene and silene species..... 184

Scheme 7-1 Disproportionation reactions between Si-containing radicals 215

List of Symbols, Abbreviations and Nomenclature

Symbol	Definition
AE	Appearance potential
Amu	Atomic mass unit
APCVD	Atmospheric pressure chemical vapour deposition
a-SiC:H	Amorphous silicon carbide
BTD	1,3-butadiene
cat-CVD	Catalytic chemical vapour deposition
CCSD(T)	Coupled cluster with single, double and triple excitation
CRDS	Cavity ring down spectroscopy
CVD	Chemical vapour deposition
DMDS	1, 2-Dimethyldisilane
DMDSCB	1,1-Dimethyl-1-disilacyclobutane
DMS	Dimethylsilane
DMSCB	1,1-dimethyl-1-silacyclobutane
E_a^{APP}	Apparent activation energy
EI	Electron ionization
ESD	Evaporative surface decomposition
HMDS	Hexamethyldisilane
HWCVD	Hot-wire chemical vapor deposition
IE	Ionization energy
LIF	Laser induced fluorescence
LiF	Lithium Fluoride
LIEI	Laser induced electron ionization
LOD	Limit of detection
LPCVD	Low pressure chemical vapour deposition
MBE	Molecular beam epitaxy
MMS	Monomethylsilane
MP2	Second-order Møller-Plesset
MP4	Fourth-order Møller-Plesset
MPI	Multiphoton ionization
MS	Mass spectrometry
MSCB	1-Methylsilacyclobutane
Nd:YAG	Neodymium: yttrium aluminum garnet
pc-Si	Polycrystalline silicon
PECVD	Plasma enhanced chemical vapor deposition
PLD	Pulsed laser deposition
PVD	Physical vapour deposition
SCB	Silacyclobutane
SiC	Silicon carbide
$SiGe_x$	Silicon germanium
SiN_x	Silicon nitride
SPI	Single photon ionization
SS	Stainless steel
TIMS	Threshold ionization mass spectrometry

TMDSCB	1,1,3,3-Tetramethyl-1,3-disilacyclobutane
TMS	Tetramethylsilane
TOF	Time-of-flight
TriMS	Trimethylsilane
UV	Ultraviolet
VUV	Vacuum ultraviolet
ZPE	Zero-point energy

Epigraph

Scientific discovery and scientific knowledge have been achieved only by those who have gone in pursuit of them without any practical purpose whatsoever in view.

Max Karl Ernst Planck

Chapter One: Introduction and Background

1.1 Thin Film Deposition Processes

The advancement of the electronic industry has been significantly impacted by the deposition technology, since this technology involves the creation of materials critical for the functionality of electronic devices, such as computers, semiconductors, etc. Deposition technology has seen a significant growth for the past twenty years. This growth is due to the development of the deposition methods and characterization techniques, which provides a better understanding on the properties of the deposited materials. This leads to an expansion in the applications that incorporates these materials.[1]

A significant number of deposition technologies exist.[2-4] These technologies can be categorized as either chemical or physical process. Chemical methods are based on the chemical reactions in the gas phase, whereas physical techniques depend on the evaporation of the material from a source. The classification of these thin film deposition techniques is illustrated in Figure 1-1.

1.1.1 Physical Vapour Deposition

Physical Vapor Deposition (PVD) is a deposition process in which an evaporant is created from a solid or liquid source in the form of atoms or molecules, and transported to the substrate where it condenses to form the thin film deposit.[5] The deposition process in PVD occurs by condensation mechanism. A schematic diagram of the PVD process is shown in Figure 1-2.

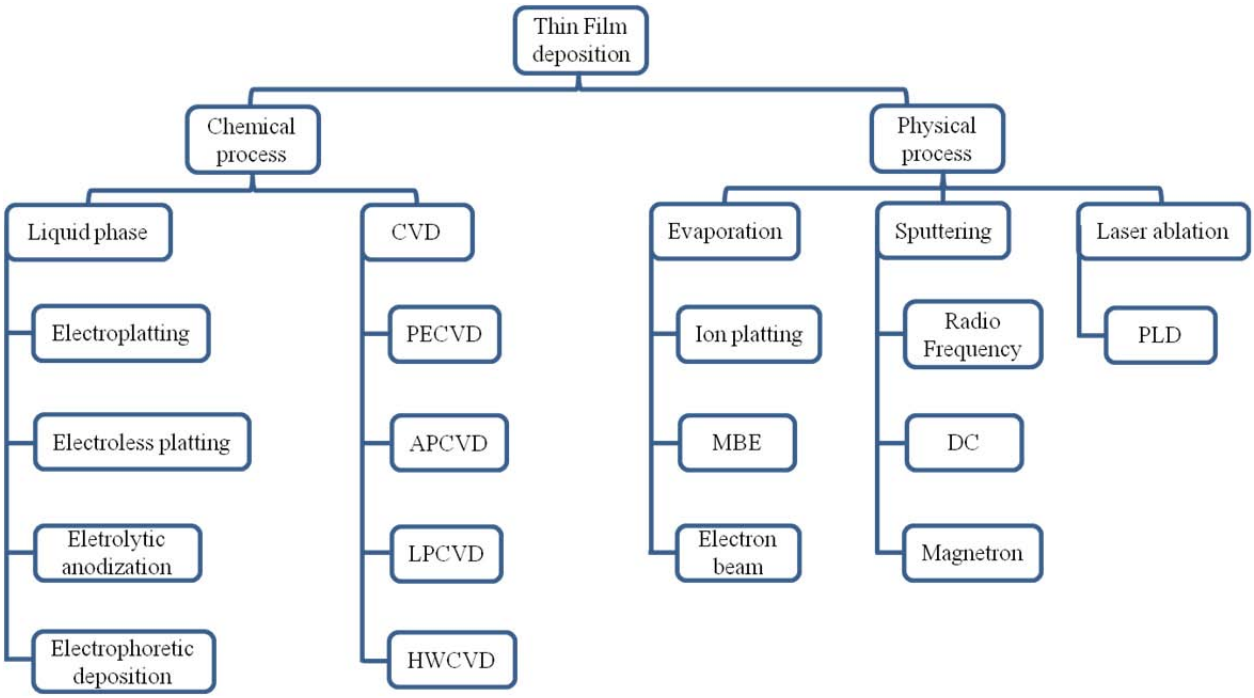


Figure 1-1: Classification of thin film deposition technologies.

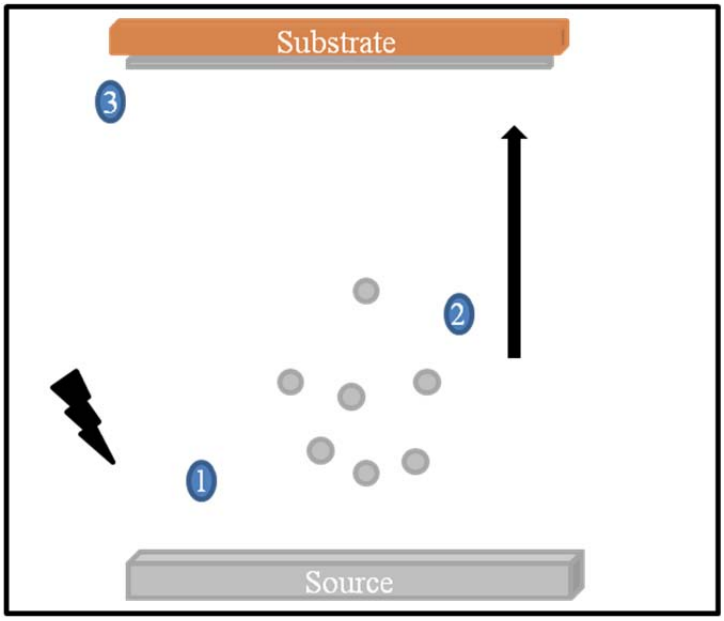


Figure 1-2: A schematic diagram of the PVD process: 1) evaporation from the source, 2) transport of evaporant, and 3) condensation of the evaporant.

PVD processes are used to deposit films with thicknesses in the range of few to thousands of nanometers using substrate of variable sizes. This process can be used in the fabrication of optical, magnetic and optoelectronic devices. This technique is also used in the field of corrosion protection, thermal insulation, and coatings.

1.1.2 Chemical Vapour Deposition

Chemical Vapor Deposition (CVD) is a diverse technology. Two major areas in the application of CVD have been rapidly developed in the last twenty years or so, namely in the semiconductor industry and metallurgical-coating industry, which includes cutting-tool fabrication. CVD consists of the introduction of a precursor into a vacuum chamber containing a substrate to be coated. Chemical reactions occurring on or near the heated substrate result in the formation of thin films.[6, 7] CVD offers several advantages, which make it generally the preferred process in many cases. One of the main advantages is that the deposited materials using CVD are generally quite conformal. Other advantages include relatively high deposition rate, a wide variety of precursors that can be used with high purity, and the fact that CVD does not require a high vacuum. Despite the simplicity of this technique, the CVD process has limitations. One of the major disadvantages lies on the type of substrate to be coated, since the deposition process is carried out at relatively high temperature. Another disadvantage is related to the requirement of having chemical precursors with high vapor pressure which are often hazardous and toxic.

Despite the variety of deposition techniques available, an ideal one would be the one that has a high deposition rate, minimal damage to the deposited film, low substrate

temperature, and low equipment and preparation cost. Recently, a new technique, known as hot-wire CVD (HWCVD) or catalytic CVD (cat-CVD), has been developed that meets these requirements.

1.2 Hot-Wire Chemical Vapour Deposition (HWCVD)

The concept of using catalytic reactions in CVD processes first appeared in a patent by Yamazaki in 1970.[8] He proposed to insert a catalyst in a conventional thermal CVD apparatus to improve film quality and decrease the deposition temperature for silicon nitride film. However, the deposition temperature for obtaining films was similar to that for simple thermal CVD process in his case. Later in 1979, Wiesmann *et al*.[9] reported that they could obtain silicon (Si) films from silane (SiH_4) and heated Tungsten (W) wires or carbon (C) rods. However, their results were not encouraging, due to the inferior electronic properties of their films in comparison with those prepared by plasma enhanced CVD (PECVD).These discouraging results led to several years of inactivity in this field until Matsumura and Tachibana[10] demonstrated in 1985 high-quality hydrofluorinated amorphous silicon (a-Si:F:H) films using silicon tetrafluoride (SiF_4) and hydrogen (H_2) as gas precursors. They claimed that the reaction of H_2 with the heated W filament was catalytic in nature, and thus termed the entire process catalytic CVD (cat-CVD). In a follow-up study in 1986,[11] Matsumura was able to grow high-quality a-Si:H using deposition conditions similar to those used in the a-Si:F:H study. These encouraging results renewed interest in the technique. High-quality a-Si was also grown by Doyle *et al*.[12] under slightly different conditions from those of Matsumura. They named the process as evaporative surface decomposition (ESD), due to the highly

efficient dissociation of the low-pressure feed gas and consequently large flux of deposition radicals. The term “hot wire chemical vapour deposition” was formally introduced by Mahan *et al*. in 1991[13] in a study where the superior properties of amorphous silicon films deposited from HWCVD was demonstrated in comparison to those obtained from PECVD. The work of this group was influential in demonstrating the advantages of this growth method and has led to tremendous growth in this field of research in the past two decades.

In general, the process of HWCVD is quite straightforward. In this technique, the precursor gas is introduced into a vacuum chamber, where a filament, made of either W or tantalum (Ta) typically, is resistively heated up to temperatures between 1500-2000 ºC. The molecules impinging on the hot filament are dissociated by a catalytic process, from which mainly reactive radicals are released from the filament surface into the gas phase. Some of these radicals released from the filament can reach the substrate without encountering any collision, whereas some other undergo secondary reactions as they travel from the filament to the substrate. Secondary gas-phase reactions may occur with other generated radicals or with parent molecule. Products resulting from these reactions and reaching the substrate affect the properties of the growing film.[14] A schematic diagram of the various processes in HWCVD is shown in Figure 1-3.

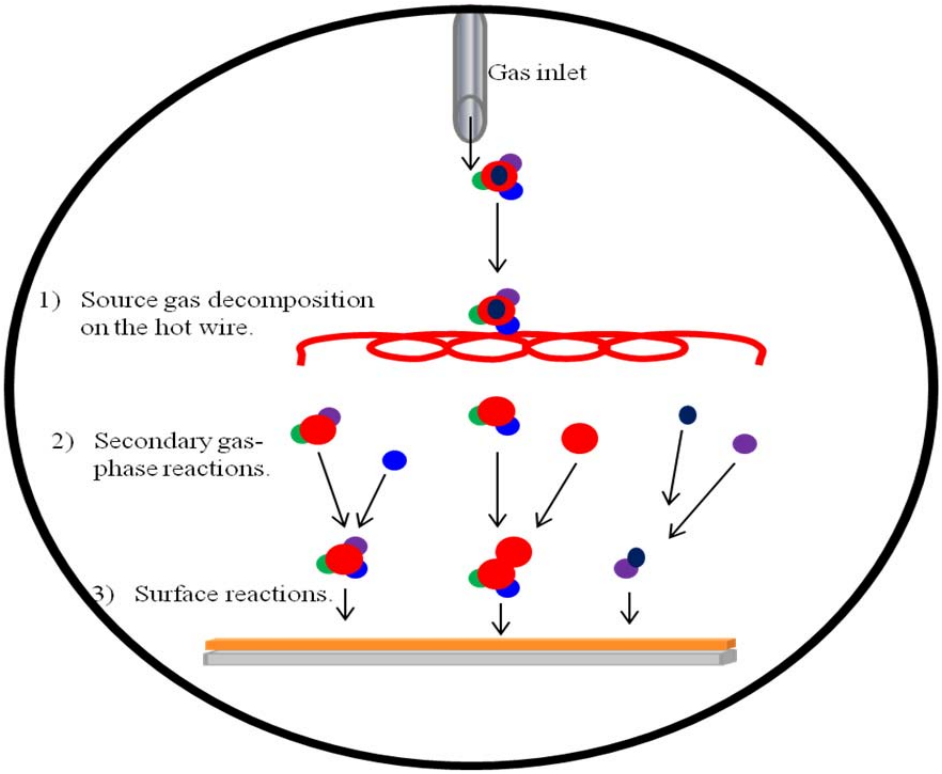


Figure 1-3: A diagram of various processes in HWCVD.

Compared to the conventionally used low pressure CVD (LPCVD) and PECVD, HWCVD offers several advantages as a technique of low-substrate-temperature film formation.[14] For instance, the film can be obtained with high deposition rates of more than 1 nm/s. The high deposition rates are accompanied by high efficiency of gas usage. Since no plasma is used, both the film and the substrate are free from plasma damage or charge-induced damage resulting in the preservation of film quality. This is particularly useful for preparation of passivation films for semiconductor or organic materials. In addition, since the substrate holder is free from electrical potential, various structures can be considered for apparatus design to lower the equipment cost. By enlarging the spanning area of the catalyzer, large-area deposition by HWCVD is feasible.[15] The fast

developing research interest in HWCVD owes a great deal to its advantages. This interest in HWCVD has increased worldwide, particularly in Japan,[15] the United States,[16] and Europe,[17] for the deposition of silicon, silicon germanium ($SiGe_x$),[18-23]silicon nitride (SiN_x),[24-27] and silicon carbide (SiC)[28-32] films.

While knowledge regarding the primary decomposition products from the filament is crucial, ultimately it is the reactions of these primary species with each other and with the source gas itself that produce the final growth precursors. The gas-phase process can be affected by various factors related to the deposition parameters. These include source gas composition, source gas flow rate, gas pressure, filament materials, filament temperature, filament geometry, the distance between the filament and substrate, substrate temperature, substrate morphology, and HWCVD reactor geometry.

Among all of the parameters mentioned above, filament materials and temperature are considered the most critical in studying the gas-phase chemistry in a HWCVD process. Tange *et al.* [33] have studied the decomposition of silane on the surface of three metal filaments: Mo, Ta, and W. They have shown that the Si atoms were the main species desorbed from the W filament at filament temperatures below 1700 K and SiH_2 is the next most abundant radical, followed by SiH_3. From their results, they were able to obtain the activation energy for Si atom production from silane, which was 60 ± 15 kcal/mol (*i.e.*, a 251± 63 kJ/mol) , 23 ± 6 kcal/mol (*i.e.*, a 96± 25 kJ/mol), and 17 ± 5 kcal/mol (*i.e.*, a 71± 21 kJ/mol), for Mo, Ta and W, respectively. These values were significantly lower than the binding energy between Si and metal surface (*e.g.*, 127 kcal/mol (*i.e.*, a 531 kJ/mol) for Si-W system) and depended on the nature of the metal

filament. Their results showed that SiH_4 is catalytically decomposed by the filament rather than through thermal decompositions.

Additionally, Holt *et al.*[34, 35] studied the effect of filament aging on the decomposition chemistry. They have found that with a new wire, Si is produced as the predominant species for temperatures above 1500 K, with a minor contribution from SiH_3 of a low activation energy of 8 kcal/mol (*i.e.*, a 33 kJ/mol), suggesting that the decomposition of the source gas is a catalytic process. When the filament was aged, the gas-phase chemistry is still dominated by the production of Si radical at temperatures above 2100 K, but the high temperature activation energy implies that evaporation from liquid silicon occurred. The recent work of Duan *et al.*[36] on the influence of filament material on radical production from SiH_4 showed the activation energies for Si formation to be 50 – 60 kcal/mol (*i.e.*, a 209 – 251kJ/mol) for W, 40 – 60 kcal/mol (*i.e.*, a 167 – 251kJ/mol) for Re, 120 – 160 kcal/mol (*i.e.*, a 502 – 669 kJ/mol) for Mo, and 140 – 180 kcal/mol (*i.e.*, a 586 – 753 kJ/mol) for Ta. The difference among the activation energies was attributed to the different catalytic capabilities of metals. It should be noted that the energy needed to break Si-H bonds in SiH_4 is 308 kcal/mol (*i.e.*, a 1289 kJ/mol),[37] which is much higher than the activation energy of Si formation on different metal wires. This once again supports the conclusion that the decomposition of SiH_4 is a catalytic process.

Presently, the most common filament materials are W and Ta. In addition to these materials, Mo, V, Pt and graphite were used as filament materials by Matsumura[38] and Morrison[39] during the deposition of a-Si:H materials. Duan *et al.*[36] and Van Veenendaal *et al.*[40, 41] have used Re as the filament material for the deposition of amorphous, microcrystalline, and polycrystalline silicon films. From these studies it was concluded

that filament materials influence the gas-phase chemistry due to the difference in their catalytic capabilities and film properties depend strongly on the filament materials.

In addition to filament materials, filament temperature also plays an important role in HWCVD, for controlling the decomposition of the source gas and the resulting film growth, heat transfer in the gas and secondary gas-phase reaction rates, while also affecting the filament lifetime and contamination of deposited films.[42] HWCVD of a-Si:H films is typically carried out using filament temperatures between 1750 and 1900 ^{o}C.[42] It was found that at lower filament temperatures, the filament is easy to break owing to the formation of silicide, while at high filament temperatures the contamination from the vaporization of the filament should be considered.[43]

Beside the two parameters mentioned above, the effect of precursor pressure is also considered an important factor during the HWCVD process. As reported by Molenbroek *et al*.,[44] the secondary gas-phase reactions, which are responsible for determining the nature of the growth precursor, depend strongly on the mean free path. As the pressure is increased, the mean free path is decreased due to the increased density of molecules in the reaction chamber, yielding a more active gas-phase chemistry. In a study to explore the effect of process condition during the deposition of a-Si:H films in a HWCVD process, Pant *et al*.[45] have noticed a transition from a-Si:H to polycrystalline-Si (pc-Si) thin films with increasing precursor pressure. This transition is explained by the fact that the increase of pressure resulted in a higher consumption of SiH_4 accompanied with an increase in the concentration of the H_2 in the reaction, which in turn is indicative of an increase in the concentration of adsorbed H. These adsorbed H atoms undergo rearrangement reaction at the surface, leading to the formation of pc-Si films.

Despite the extensive number of studies in the field of HWCVD, a clear understanding of the gas-phase process and the effect of various deposition parameters is still lacking. Therefore, a closer examination of the physical and chemical processes occurring at the surface of the wire and in the gas-phase is important for developing a clear understanding of the process.

1.3 HWCVD of Silicon Carbide Thin Films

1.3.1 Silicon Carbide (SiC) Thin Films

Silicon carbide is an extremely hard compound that does exist in nature, as it can be found in meteorites. The earliest observation of SiC compounds goes back to 1824 when Jöns Jacob Berzelius burnt an unknown compound and observed an equal number of silicon and carbon atoms.[46] SiC is one of the leading contenders among the wide bandgap semiconductors that can revolutionize electronic devices. This role is also attributed to its superior electrical and mechanical properties as compared to Si. Since its discovery, especially in the last twenty years, considerable efforts have been made by researchers, who are attracted by its appealing physical properties, to explore synthesis techniques and applications of SiC.

Silicon carbide has been regarded as a promising material for high-temperature, high-power, and high-frequency devices due to its wide bandgap, high thermal conductivity, and stability under severe thermal, chemical and electromagnetic radiation. [47] In addition to its physical properties, another exciting feature of SiC is its occurrence in many different polytypes that depend on the stacking sequence of the SiC bilayer.[48, 49] Over 200 polytypes have been observed having a cubic (C), hexagonal (H), or

rhombohedral (R) Bravais lattice, and only a few are commonly grown in a reproducible form acceptable for use as an electronic semiconductor. The most common polytypes of SiC presently being developed for electronics are 3C- SiC, 4H- SiC, and 6H- SiC. The number in the notation determines the number of layer before the sequence repeats itself and the letter indicates the resulting structure of the crystal. The numerous polytypes of SiC imply a diverse range of electrical characteristics. However, they all share the quality of having a wide bandgap with a high breakdown voltage and a high saturation electron drift velocity which aids in the ability to make suitable high-temperature, high-power, and high-frequency electronic devices. While all SiC polytypes have similar physical and thermal properties, their electrical and optical properties differ.[47, 50] Depending on the designated application, one polytype may have more suitable characteristics than the other, making SiC a versatile semiconductor material. Some of the more important electrical properties of the 3C, 4H, and 6H SiC polytypes are tabulated in Table 1-1 with comparison to silicon.

Table 1-1 Material properties of common SiC polytypes[47, 51, 52]

	Si	6H-SiC	4H-SiC	3C-SiC
Bandgap (eV)	1.11	3.02	3.26	2.39
Thermal conductivity (W/cm-K)	1.5	3-5	3-5	3-5
Breakdown Field (MV/cm)	0.6	3.0	3.2	> 1.5
Electron mobility (cm^2/V-s)	1200	400	800	750

Si has a relatively narrow bandgap of 1.1 eV. A wide bandgap semiconductor is generally defined as one having a bandgap greater than that of silicon. As the temperature

increases above 300 ^{o}C, significant thermal excitation may occur. This is the major reason why Si-based devices fail at temperatures above 250 ^{o}C. The larger bandgap provides energy barrier against thermal excitation and allows SiC device operation at temperatures close to 750 ^{o}C. Another critical parameter for power producing devices is thermal conductivity. The outstanding thermal conductivity of SiC (approximately three times better than Si) allows SiC-based devices to more efficiently remove waste heat, and to operate at a lower junction temperature, which improves device lifetime and reliability. Furthermore, its tight chemical bonding in the diamond-like structure is chemically inactive even at elevated temperatures. Although the electron mobility of SiC is not as good as Si, it is sufficient in the high electric filed regimes where SiC devices typically operate. [51, 52]

These important physical properties of silicon carbide ensure a large range of applications from improved high voltage switching for energy savings in public electric power distribution and electric vehicles, to more powerful microwaves electronics for radar and communications, to sensors and more fuel-efficient combustion chambers for jet aircraft, automobile engines, and for stationary power plants.

1.3.2 Growth of SiC Thin Films Using HWCVD Processes

Conventionally, the formation of SiC thin films in PECVD or HWCVD requires the usage of a mixture of separate Si- (SiH_4, Si_2H_6, or SiH_2Cl_2) and C-bearing (CH_4, C_2H_4, or C_2H_2) source gases. Ferreira *et al.*[53] prepared hydrogenated amorphous SiC (a-SiC:H) by using the gas mixture of C_2H_4 and SiH_4 with PECVD. They obtained a film with bandgaps ranging from 1.85-3.5 eV by controlling the percentage of C_2H_4 in the

mixture. a-SiC:H was also fabricated using the SiH_4 and C_2H_2 mixture with HWCVD in a study by Swain *et al.* on the effect of filament temperature,[54] the process pressure,[28] H_2 dilution[55] and substrate temperature.[56] They found that the C content as well as the bandgap increased with the increase of pressure, H_2 dilution, and filament temperature, while it decreased with the increase of the substrate temperature. Similarly, Tataba *et al.*[30, 57] prepared nanocrystalline cubic SiC (nc-3C-SiC) from a mixture of $SiH_4/CH_4/H_2$ by HWCVD. They found that the filament temperature,[58] total gas pressure, gas flow rates of $SiH_4/CH_4/H_2$, [59] and the filament-to-substrate distance[30] affected the structures of the formed SiC films. Despite the existence of these numerous studies, the use of mixtures presents several drawbacks. For instance, the use of mixtures requires independent flow control of each precursor since the optimum composition of the mixture will vary with deposition temperature, pressure, etc. Additionally, silane and hydrocarbon compounds are either pyrophoric or explosive. In order to circumvent these problems, investigation of alternative single-source precursors containing both Si and C, *e.g.*, organosilicon compounds, has been performed.[31, 32, 60-63] The major advantage in using organosilicon molecules compared to multiple-source precursors is the possibility of preserving Si-C bonds in the grown film. This can potentially translate into improvement in the ratio of Si to C ratio in the resultant films and subsequently in the quality of the film.[64-66] Furthermore, the organosilicon precursors are much safer to handle, and generally need less energy for decomposition than the competing mixtures.

1.3.3 HWCVD of SiC Thin Films Using Methyl-Substituted Silanes

Recently, successful studies in using open chain methyl-substituted silane molecules ($(CH_3)_{4-x}SiH_x$, x =0-3) as precursors for growing SiC thin films using various CVD techniques have emerged. Monomethylsilane (MMS),[31, 32, 39, 61, 67-73] dimethylsilane (DMS),[61, 70] trimethylsilane (TriMS),[32, 61, 67, 70, 73] tetramethylsilane (TMS),[32, 61, 74-77] and hexamethyldisilane (HMDS)[74, 78] have been studied. Among all of these precursors, MMS has been widely used as a single source gas in the preparation of SiC thin films in both PECVD[39, 70] and HWCVD.[31, 32, 39, 68, 69, 73] Lee and Bent[31, 32, 73] studied the effect of different precursor structures (MMS, TriMS, and TMS) on the growth of a-SiC:H by HWCVD. They have shown that the growth mechanism of a-SiC:H film proceeds via Si-H bond cleavage and is dependent on the reaction chemistry of the precursors. They have found that among the three studied materials, TriMS produced thin films with the highest methyl concentration. When Nakayama *et al.*[60] used DMS as a source gas to prepare SiC thin films, they found that filament materials affected the film composition, and the growth rate depended on the filament temperature. Furthermore, the influence of hydrogen dilution, filament temperature and deposition pressure on the deposition rate, the structural and the optoelectronic properties of microcrystalline SiC was investigated by Klein *et al.*[69, 79, 80] using MMS diluted in H_2 in HWCVD system. They have found that with increasing MMS concentration a transition from high to low fraction of crystalline SiC was observed. Additionally, they have determined that high deposition rates without deterioration of the material quality was achieved by the application of low filament temperatures (< 1800 °C) in combination with shorter distance between the filament and the substrate.

1.4 Gas-Phase Chemistry in HWCVD System

Most of the research on HWCVD is focused on the deposition process and the characterization of the films by examining the electrical and physical properties of the deposited films and correlating these properties to the deposition parameters. However, as mentioned in the previous sections, film growth in HWCVD is believed to be induced by precursors generated from direct decomposition on the filament and/or from secondary gas-phase reactions. The properties and quality of the deposited films are determined by these gas-phase precursor species. Therefore, for a better understanding of the HWCVD process and a rational optimization of film deposition process, it is essential to identify the gas-phase chemical species and to study their formation mechanisms and kinetics.

1.4.1 Detecting the Gas-Phase Reaction Products in a HWCVD Process

In a HWCVD system, the decomposition of source gases on the filament results in the formation of radicals, which are difficult to detect because these reactive species have fast rate losses and small number densities in comparison to their molecular precursors.[81] Their detection has become possible after the introduction of several modern, in-situ, real-time analytical techniques. These methods can be divided into three categories: electron-in-ion-out, photon-in-photon-out, and photon-in-ion-out. In electron-in-ion-out method, electrons with an energy above the ionization energy (IE) are used to ionize the species of interest. The conventional 70 eV electron ionization (EI) belongs to this category. This technique has been considered to be a universal ionization method since it can ionize almost all compounds. However, the significant fragmentation that often

accompanies the ionization can greatly complicate the mass spectrum, making it very difficult to identify single components in a complex mixture system. An alternative technique of this type, called “threshold ionization mass spectrometry” (TIMS), can be used. In this technique, the electron energy is chosen to lie just above the IE, which is typically below the appearance energy (AE) of fragment ions. In this way, the only signals obtained are those from ionization of neutral species, and not from their fragmentation.[81] Another method that belongs to this category is laser induced electron ionization (LIEI), developed in the Shi laboratory.[82] The LIEI source consists of a stainless steel rod held 10 mm away from a copper mesh. In this technique, a 355 nm laser radiation is focused onto the stainless steel rod by a quartz lens, and photoelectrons generated by thermionic emission are accelerated towards the ionization regions. This technique has been demonstrated to produce EI-type mass spectra with approximately 70 eV fragmentation patterns, excellent mass resolution, and very high sensitivity. The LIEI source is well suited for studying stable species, which can be readily detected to very low concentrations.

The technique in the second category, photon-in-photon-out, is one where a species is excited by the absorption of a photon followed by relaxation and emission of a new photon, which is indicative of the species of interest. Laser induced fluorescence (LIF) and cavity ring down spectroscopy (CRDS) fall into this category.[83] Both of these techniques have high sensitivity, however only one species can be detected at a time and any photon emission from sources other than the target species can interfere with the detection process.

Photon-in-ion-out technique uses photons energy instead of electron energy for ionization. It involves the use of one, or many, photons from a laser radiation to ionize the neutral species, followed by the ion detection by a mass spectrometer. Two laser ionization methods, known as resonance enhanced multiphoton ionization (REMPI) and SPI, have been used. REMPI involves the excitation of the species of interest to a real energy level, followed by the absorption of a second photon for ionization. This makes the REMPI technique very sensitive and selective. SPI uses a single photon of sufficient energy to ionize the target species, but low enough to avoid fragmentation for most species, thus avoiding convoluted mass spectra.[84] It is considered to be a soft ionization method, because only modest amounts of excess energy are deposited in the resulting ions, and efficient ionization can occur with relatively low laser intensities, minimizing the probability of multiphoton absorption. The ionization selectivity of this technique is given by the ionization energy of the compound and the availability of a wide range of wavelengths. Hence, only those compounds that have an IE lower than the photon energy can be ionized without fragmenting it. Typically, SPI with a VUV laser radiation at 118 nm (10.5 eV), which is the ninth harmonic of the fundamental 1064 nm output of an Nd:YAG laser, is used in HWCVD of SiC thin films, since most of the Si and C containing species have an IE below or at 10.5 eV. In addition, with this wavelength, SPI will not ionize typical background gases, such as He, N_2, O_2, H_2O, or CO_2. SPI has been demonstrated to be a soft and near universal analytical technique, since it provides spectra with reduced background noise and it can ionize most of the species of interest with little or no fragmentation.[85, 86]

Although there are a variety of techniques available for the detection of various species, a careful choice must be made in selecting the most appropriate one for investigating the gas-phase chemistry in the process of HWCVD. Among all of the aforementioned methods, the principle of TIMS is straightforward, however, it requires a very long time for data acquisition and calibration can be a lengthy and complex process. LIF or CRDS are both quite sensitive techniques. Since the foreknowledge of the species to be examined is required and they often can only detect one species at a time, they cannot be effectively applied to study a complex chemistry in an unknown system. Ultimately, it is SPI that has emerged as the most suitable technique for studying the HWCVD chemistry. The "soft" nature of SPI makes it a good choice for the analysis of a complex system, characteristic of a HWCVD or a PECVD system. Furthermore, one-photon ionization cross sections are more uniform from species to species than those using MPI, which makes quantitative analysis feasible by using SPI. In addition to the established SPI method, a new ionization source has also been developed in the Shi laboratory[87] to study the HWCVD chemistry. This source consisted of both LIEI and SPI modes in one, and is therefore called the dual SPI/LIEI source. In this source, the ionization is achieved by directing an unfocused laser beam containing both 118 nm VUV and 355 nm UV radiations to the repeller plate in a TOF mass spectrometer. It is found that the SPI source due to the 118 nm VUV light coexists in the LIEI source. This dual SPI/LIEI source allows for simultaneous observations of all species with IP below and above 10.5 eV, and has therefore proven to be very useful in studying the gas-phase chemistry in the HWCVD processes. Based on these facts, SPI along with the dual SPI/LIEI ionization sources are the two techniques used in this study.

1.4.2 Gas-Phase Chemistry in HWCVD Using Methyl-Substituted Silanes

In their work on the decomposition of methyl-substituted silanes, including MMS, DMS, TriMS, and TMS along with 1,1-dimethyl-1-dilacyclobutane (DMSCB) on W and Re filament in a HWCVD process, Zaharias *et al.*[61] detected the formation of Si and methyl radicals as the two major products during the primary decomposing process by probing the gas-phase species using vacuum ultraviolet (VUV) single photon ionization (SPI) at filament temperatures between 1000 and 1950 ^{o}C. The reaction rate of the aforementioned precursors on the filament decreased with increasing number of methyl groups in the molecule. They have also determined the apparent activation energy (E_a^{app}) of Si formation, and its value increased with increasing methyl substitution in the precursors. For the DMSCB precursor, its decomposition resulted in much lower E_a^{app} value for Si formation due to Si being a part of a four- membered ring leading to a lower barrier. For the methyl production, they have found that MMS, DMS and TriMS produced similar concentrations of CH_3, whereas negligible CH_3 resulted from TMS dissociation. However, they were not able to extract any values for the activation energy for methyl formation since this radical did not follow an Arrhenius behavior under their experimental conditions. Using similar technique as Zaharias, Sharma *et al.*[62] detected SiH_2, CH_3SiH, CH_3, and CH_3Si radicals as the fragmentation products from TriMS and TMS under low-pressure conditions (2.3×10^{-6} Torr).

However, all of these detections were carried out under very low pressures where gas-phase reactions are negligible. Typical deposition pressures for SiC films using HWCVD with either gaseous mixtures of silane and hydrocarbons or single-source precursors range from 0.1 Torr to several Torr.[54, 88] At these relatively high pressures,

secondary gas-phase reactions between the various species produced from the primary decomposition become relevant in understanding the entire process and affect the quality of the deposited film. Unfortunately, little is known about the nature of secondary gas-phase reactions and their products. As a result, the gas-phase chemistry is not fully understood, and details regarding the growth mechanism are unclear.

To gain better insights into the deposition chemistry in HWCVD, the Shi group has previously studied the decomposition and secondary gas-phase reaction chemistry using both open-chain methyl-substituted silanes and four-membered ring (di)silacyclobutane molecules with both W and Ta filaments. In their work, the gas phase chemistry involved in the decomposition of TMS,[89] TriMS,[67] HMDS,[82] silacyclobutane (SCB),[90] DMSCB,[91] 1,1,3,3-tetramethyl-1,3-disilacyclobutane (TMDSCB)[92] and 1-methylsilacyclobutane (MSCB)[93] on a hot W filament and secondary gas-phase reactions in a HWCVD reactor has been investigated using VUV laser SPI coupled with time-of-flight (TOF) mass spectrometry (MS). Among all of these molecules, TMS and TriMS belong to methyl-substituted silane molecules. It was found that TMS decomposed on the W filament to methyl and trimethylsilyl radicals, which react with the abundant parent molecules in the HWCVD reactor, producing more radical species. Self- and cross-combinations of the primary and secondary radicals are the dominant gas-phase reaction pathways. These reactions lead to the generation of small alkenes (C_nH_{2n}, $n \leq 4$), alkyl-substituted silanes, and silyl-substituted alkanes. Si-C bond is found to be the major bond connection in the reaction products of high mass. The study of TriMS revealed the effect of the Si-H bond on the gas-phase reactions. It was found that TriMS decomposed into $(CH_3)_2HSi$, and CH_3 radicals. Similar to TMS, these primary radical products react with

the parent molecule in the reactor, generating more radical compounds. The biradical combination reactions are again found to be responsible for most of the molecules detected in the HWCVD reactor with TriMS. These studies also showed the involvement of silene intermediates in the gas-phase reactions with the two methyl-substituted silane precursors. Silene is a very reactive species which is expected to play an important role in SiC film deposition. Silacyclobutane (SCB), a four-membered ring compound, is known to decompose to produce silene upon pyrolysis. The study of the SCB decomposition on a hot W filament conducted in the Shi group has demonstrated that reactions involving silene and its isomer silylene dominate.

1.4.3 Chemical Trapping of the Active Intermediates

It has been shown that several reactive intermediates, including free radicals, silene, and silylene species, are produced in the primary decomposition of methyl-substituted silane molecules in the HWCVD process. These intermediates are believed to be the driving force in the secondary gas-phase chemistry using these precursors. Therefore, understanding the involvement of these intermediates can provide some insights into their roles in the HWCVD process. Chemical trapping is a useful technique to identify the role of each of the reactive intermediates in the reaction mechanism.

Free radicals play an important role in the pyrolysis chemistry of methyl-substituted silane molecules. Neudorfl and Strausz[94] studied the pyrolysis of MMS and DMS in the presence of ethene as a radical scavenger. In the presence of ethene, the suppression of free-radical chain reaction is observed, while the reaction involving silene/silylene intermediates is still occurring. This suggests that the competition between

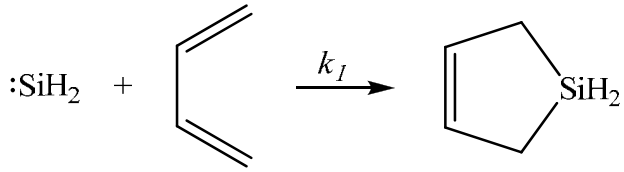
radical chain and silene/silylene mechanism in the pyrolysis of these precursors is taking place. Rickborn *et al*.[95] used toluene to quench radical chain reaction during the pyrolysis of DMS. However, they have found that toluene is an excellent trapping agent only at low temperatures, and with increasing temperature, this trapping agent can itself become a radical source. Another radical scavenger is nitric oxide. Several studies[96-98] showed the effect of NO on the gas-phase chemistry involved in the photolysis of methyl-substituted silanes. It has been found that the products generated from free-radical reactions are suppressed upon using NO, while the ones produced from silene/silylene mechanism are left unaffected.

In addition to free radicals, silylene and silene are believed to play a significant role in the gas-phase chemistry of methyl-substitued silanes, as has been discussed earlier. Silylenes (R_2Si:) have drawn much attention since they were first suggested as reaction intermediates in the decomposition chemistry of methyl-substituted silane compounds.[99] Silylene species have similar geometric structures, electronic configurations, and reactivity similar to carbene. These species are defined as having two covalent bonds and two non-bonding electrons distributed between two non-bonding orbitals. These electrons may occupy the same non-bonding orbital or they may reside in two different non-bonding orbitals. In the lowest singlet state, the electrons have anti-parallel spins and occupy the same nonbonding orbital. In the lowest triplet state, the electrons are distributed between the two non-bonding orbitals. This leads to differences in their chemical behaviour.[100]

Although insertions of silylenes into single bonds can occur, intermolecular insertion into C-H bonds does not take place, except for intramolecular insertions at high

temperatures.[101] Unlike its inertness towards C-H bonds, it has been demonstrated that silylenes insert readily into Si-H bonds through a concerted process.[102, 103] The involvement of silylenes in organosilicon chemistry is not well understood because of the difficulty associated with detecting silylene. Some of these difficulties result from the high reactivity of silylenes. Hence, to verify the existence of silylene and better understand the proposed gas-phase reaction meachnism involving the chemistry of silylene species, several research groups have conducted experiments using different trapping agents, such as methanol, acetylene, 1,3-butadiene, and trimethylsilane, with 1,3-butadiene being most commonly used.[104]

Rogers, O'Neal and Ring[104, 105] carried out a comparative study on the reaction of silylene with 1,3-butadiene, as the reference, versus acetylene and methanol to extract kinetic data to help in choosing the most effective trapping agent for silylenes. The trapping reactions proceed as illustrated by Euqations (1-1) to (1-3).



(1-1)

$$:SiH_2 + CH_3OH \xrightarrow{k_2} CH_3OSiH_3 \qquad (1\text{-}2)$$

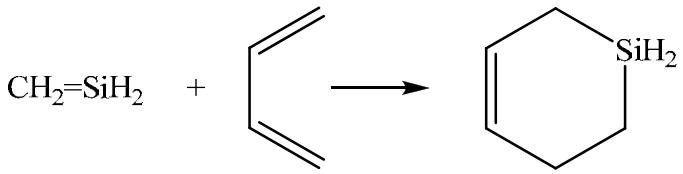
$$:SiH_2 + HC{\equiv}CH \xrightarrow{k_3} HC{\equiv}CSiH_3 \qquad (1\text{-}3)$$

From their kinetic study, they obtained a rate constant ratio to be $\ln {k_1}/{k_2} = (5.91 \pm 0.91) - {(5849 \pm 1529) cal.mol^{-1}}/{RT}$. This indicates a substantial activation

energy for trapping of silylene (:SiH_2) by butadiene. Similarly, a rate constant ratio between the trapping with 1,3-butadiene and acetylene was also extracted to be $\ln {k_1}/{k_3} = (1.51 \pm 0.32) - {(712 \pm 520)cal.mol^{-1}}/{RT}$, which suggests that the reaction to trap silylene by acetylene required less energy. Despite the fact that 1,3-butadiene is the most commonly used chemical to trap silylene intermediates, their results showed that the existence of more suitable trapping agents depended on the experimental conditions such as precursor's pressure.

Silylenes are known to isomerize to silenes by 1,2-migrations of hydrogen, silyl, or methyl groups.[106, 107] Silene intermediates are compounds containing silicon-carbon double bond moiety, having a partial positive charge on silicon and a partial negative charge on carbon. They have also been identified as reactive intermediates in the thermal and photochemical reactions of organosilicon compounds. In the absence of trapping reagents, the most common reactions for these reactive intermediates are dimerizations to give a four-membered-ring compound.[108] Two reactions have been used to trap the short-lived silene species as evidence of their formation. The most commonly used are the 1,2-additions of alcohols or amines across the Si=C double bond and the [2+2] and [4+2]-cycloadditons with alkenes, dienes and carbonyl compounds. [108, 109]Several trapping reagents, including 1,3-butadiene, alcohols, amines, and nitriles, have been suggested for the study of the reactivity of silene. Examples of certain trapping reactions are illustrated by the following equations.

$$CH_2{=}SiH_2 \quad + \quad NH_3 \longrightarrow \quad CH_3SiH_2NH_2 \qquad (1\text{-}4)$$



(1-5)

Chemical trapping of various intermediates involved in the gas-phase chemistry of methyl-substituted silane will provide an insightful understanding on their roles during the HWCVD process. As the most commonly used trapping agent for silene and silylene species, 1,3-butadiene is considered in this work in confirming the involvement of silylene and silene intermediates as well as in differentiating between the mechanism arisen from them and those from free radicals. In addition to 1,3-butadiene, ammonia is used to differentiate between silene and silylene chemistry. It has been proposed that the suppression of the cyclodimerization of methylsilene reaction is achievable in the presence of ammonia due to the fast reactivity of silene molecule with ammonia.[110, 111] However, several studies have emerged claiming that ammonia will also react with silylene moieties.[112-114]

1.5 Objectives of this Thesis

The present study has been undertaken as part of a continuing effort to extend our knowledge of gas-phase chemistry of all methyl-substituted silane molecules in the HWCVD process. Following the previous investigations using TMS and TriMS, this work focuses on the decomposition channels on the filament and dominant chemistry in the reactor, when using MMS and DMS as a single source precursor. The primary decomposition of these precursors on the metal filament under collision-free condition and the secondary gas-phase reactions in a HWCVD reactor are examined in this work

using both SPI and dual SPI/LIEI coupled with TOF MS. With the help of the deuterated isotopomers of MMS and DMS as well as chemical trapping using 1,3-butadiene, and ammonia, the identities of the gas-phase species observed have been elucidated, and their formation mechanisms are discussed.

A further objective of this work was to explore the effect of various deposition parameters on both the primary decomposition of methyl-substituted silanes on the metal filament and subsequent secondary gas-phase reactions. For the formation of methyl radical and hydrogen molecule during the primary decomposition of MMS, DMS, TriMS and TMS, the effects of filament material, precursor gas pressure, and precursor chemical structure have been studied. For the secondary gas-phase reactions of DMS and MMS, the effects of filament material, filament temperature, and precursor gas pressure have been examined.

Regarding the layout of this thesis, background information relevant to the experimental setup and procedures used to conduct the work are provided in Chapter 2. The formation of methyl radical and H_2 molecule from the primary decomposition of the four methyl-substituted silane molecules is presented in Chapter 3 and 4, respectively. Chapter 5 and 6 focuses on the gas-phase chemistry of DMS and MMS, respectively, in the process of HWCVD. Chapter 7 pertains to the effect of precursor pressure on the gas-phase chemistry of TriMS. Finally, conclusions and perspective for future work are provided in Chapter 8.

Chapter Two: Experimental Details

To probe the products from methyl-substituted silane decomposition on the hot filament and from secondary gas-phase reactions in the process of HWCVD, laser-based ionization techniques combined with time-of-flight mass spectrometry (TOF MS) are employed. A schematic of the experimental setup used in this work is illustrated in Figure 2-1. The apparatus consists of a HWCVD source chamber incorporated with a linear TOF mass spectrometer, and a laser ionization source. Details of the apparatus can be found elsewhere.[115]

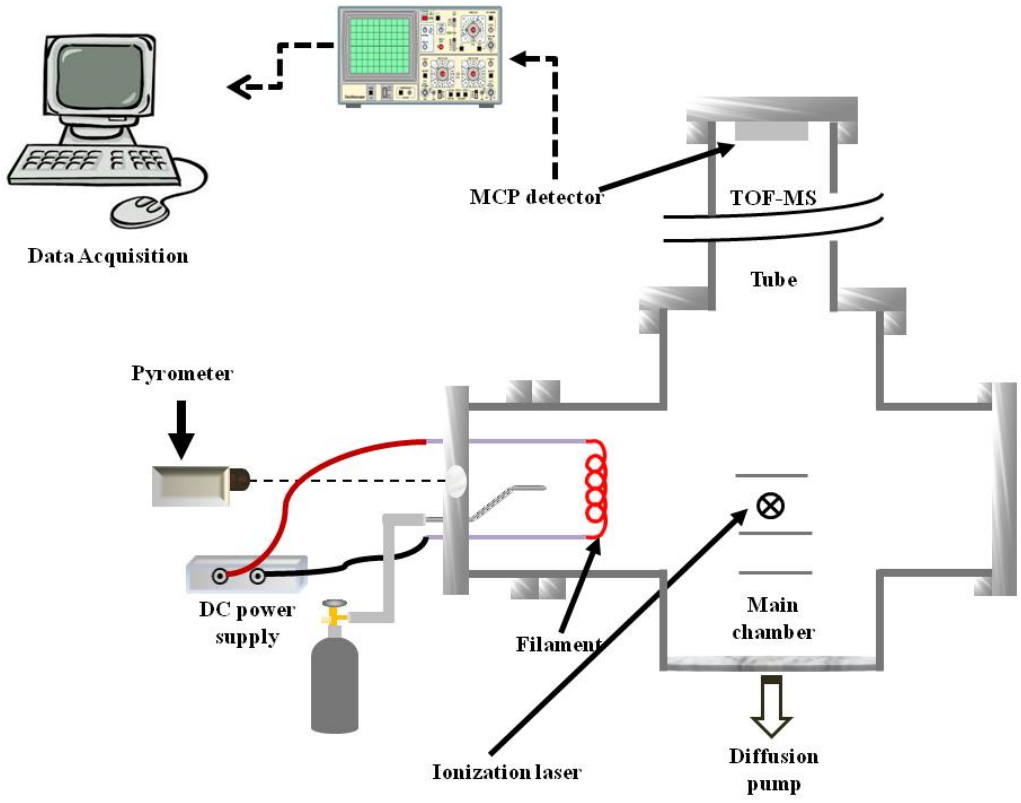


Figure 2-1: A schematic of the experimental setup for laser ionization mass spectrometric measurements

The main chamber is a six-way stainless steel cross (10 inch diameter). The top port of the chamber is coupled with the flight tube (1 m length) of the TOF mass spectrometer (R.M. Jordan Inc.), and the bottom port is connected to a diffusion pump (VHS-6, Varian) through a gate valve. An Ar/Xe gas cell, where the 118 nm laser is generated, is attached to the front port. A quartz window is placed in the center of the flange mounted onto the back port to avoid the electron emission as a result of the laser beam striking on the metal surface. The port on the right is connected to a mechanical pump which acts as both the roughing pump for the chamber and the backing pump for the diffusion pump, while the port on the left is connected with the HWCVD source, which will be described in detail below.

2.1 HWCVD Sources

To detect gas-phase species formed directly from the decomposition of source gases on a hot filament and those from secondary gas-phase reactions, two different setups were used as HWCVD sources, *i.e.,* a collision-free setup and a reaction chamber.

2.1.1 A Collision-Free Setup to Detect Decomposition Species on the Filament

The collision-free setup was used for detection of species produced directly from the hot filament. In this setup, a W or Ta filament (10 cm length, 0.5 cm diameter) was placed directly in the main chamber through two copper feedthroughs as shown in Figure 2-2. The filament was resistively heated by a DC power supply and its temperature was measured by a two color pyrometer (Chino Works) through an IR-grade quartz window. In addition, a stainless steel plate of about 18 cm in diameter with a hole in the centre (D

= 1.0 cm) was placed between the filament and the ion optics of the TOF mass spectrometer as a shield to prevent the electrons generated from the hot filament from interfering with the electric fields in the ion optics of the TOF MS. Source gases were introduced through a ¼ inch stainless steel tubing whose outlet was positioned 5 cm from the filament.

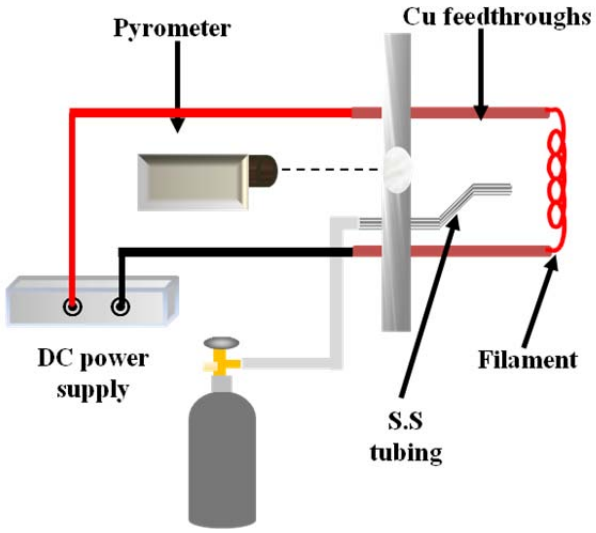


Figure 2-2: A schematic of the HWCVD collision-free flange for detection of direct hot-wire decomposition products. (S.S = stainless steel)

The base pressures in the main chamber and the TOF tube were maintained at $l.0 \times l0^{-7}$ Torr and $l.0 \times l0^{-8}$ Torr, respectively, by a diffusion pump and a turbo pump. During the experiment, the operating pressure was ~ 1.0×10^{-5} Torr in the main chamber and ~ $l.0 \times l0^{-6}$ in the TOF tube, respectively. Under this experimental condition, a collision-free condition was maintained; therefore, the secondary gas-phase reactions were avoided.

2.1.2 A Reactor Setup to Detect Species from Secondary Gas-phase Reactions

To detect species formed from secondary gas-phase reactions, a HWCVD reactor (inner diameter of 15 cm) was attached to the main chamber. A schematic diagram of the HWCVD reactor is illustrated in Figure 2-3. The reactor and main chamber were connected through a pinhole (0.15 mm diameter) drilled in the bottom plate of the reactor. The distance between the filament and the pinhole was held at 5 cm. This is the typical distance between the filament and substrate for the thin film deposition. The pressure in the reactor was maintained at 12 Torr using a mass flow controller (MKS, 1179A) and was monitored by a capacitance manometer (MKS Baratron, type 626 A). This gives a partial pressure of the methyl-substituted silane precursor of 120 mTorr if a 1% methyl-substituted silane /He mixture is used. The operating pressures in the main chamber and flight tube were maintained at 1.0-2.0 × 10^{-5} Torr and 1.0-2.0 × 10^{-6} Torr, respectively.

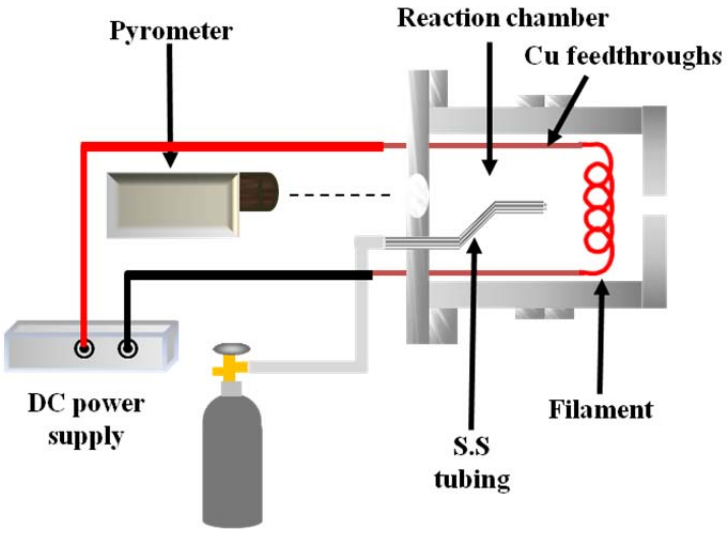


Figure 2-3: A schematic the HWCVD reactor for detection of secondary gas-phase products. (S.S = stainless steel)

Under the relatively high pressures of 12 Torr in the reactor, secondary gas-phase reactions are expected to occur. The products of these reactions were sampled through the pinhole into the main chamber, and the gas stream exiting the reactor formed an effusive molecular beam. Upon exposure to the low pressures in the main chamber, it is anticipated that all further gas-phase reactions cease, and therefore the detected species by TOF MS represent those from the gas-phase reactions in the HWCVD reactor. The molecular beam was oriented at right angles to the laser beam. The TOF mass spectra were collected at different filament temperatures ranging from 900 to 2000 ^{o}C with an increment of 100 ^{o}C. At each temperature, a mass spectrum was recorded every five minutes for one hour.

2.2 Ionization Sources

In this work, two ionization sources, including SPI and a dual SPI/LIEI sources were employed to detect the products generated from the hot wire decomposition of the source gas or the secondary gas phase reactions. The SPI technique is used to detect species with an IE below the energy of a single 118 nm photon (10.5 eV). The dual SPI/LIEI source is applied to simultaneously observe signals of species ionized by both SPI and LIEI, *i.e.*, species with an IE below and above 10.5 eV.

2.2.1 The Single Photon Ionization (SPI) Source

In the SPI technique, the 118 nm VUV photon is produced by non-resonant frequency tripling the 355 nm UV output from a commercially available Nd:YAG laser (Spectra-Physics, LAB-170-10) operating at a 10 Hz repetition rate. The 355 nm output

was attenuated to a constant energy of 20 mJ per pulse by the combination of a half-wave plate and a Glan laser polarizer. The laser was then focused into a gas cell by a quartz lens (f = 20 cm). The gas cell was filled with 210 Torr of a 10:1 Ar:Xe gas mixture, [116, 117] which was found to be the optimum pressure to produce the maximum intensity of VUV radiation. A lithium fluoride (LiF) lens was inserted into the optical path after the gas cell to focus the 118 nm light directly into the center of the space between the repeller plate and extraction grid in the TOF ion optics, while the fundamental UV beam was caused to diverge in the same region due to the difference in the refractive indices at two different wavelengths, as shown in Figure 2-4.

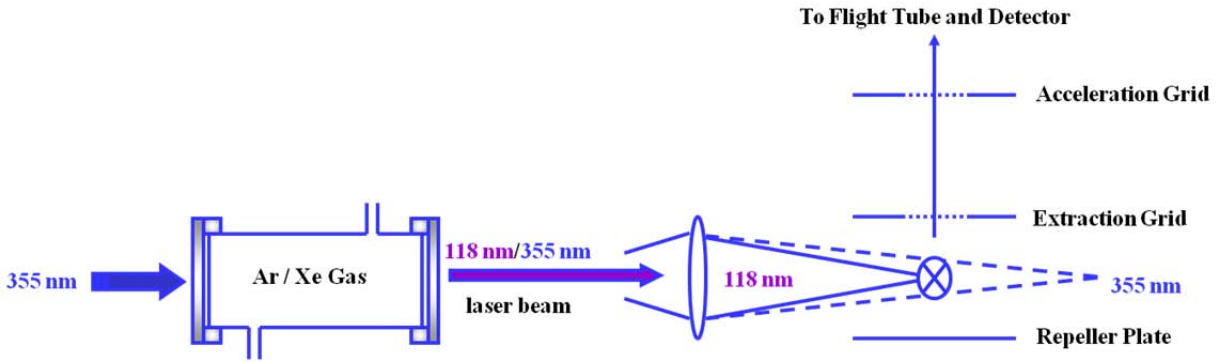


Figure 2-4: A schematic diagram of the single photon ionization (SPI) source.[118] (Adapted with permission from Springer Science and Business Media, Journal of the American Society for Mass Spectrometry, 18, 2007)

2.2.2 The Dual Single Photon Ionization and Laser Induced Electron Ionization (SPI/LIEI) Source

In addition to the above mentioned SPI techniques, a dual ionization source consisting of SPI and laser induced electron impact ionization (SPI-LIEI), developed in our laboratory[118] was employed in this work. In this source, the LiF lens after the gas cell

was removed, allowing both VUV (118 nm) and UV (355 nm) radiations to diverge and the path of the laser was adjusted in a way that the laser beam was aimed at the repeller plate of the TOF at a shallow angle, as illustrated in Figure 2-5. The 355 nm UV light scattered from the repeller plate generated photoelectrons from nearby metal surfaces, which were subsequently accelerated by the strong electric fields present in the ionization region. These high-energy photoelectrons led to the ionization of the sample species. In the dual ionization source, both 118 nm and 355 nm radiations are present simultaneously in the laser beam, resulting in the co-existence of both SPI and LIEI processes. This technique is versatile and capable of ionizing all species of interest. In addition, it is achieved in one source, without the need to switch between the SPI and LIEI modes.

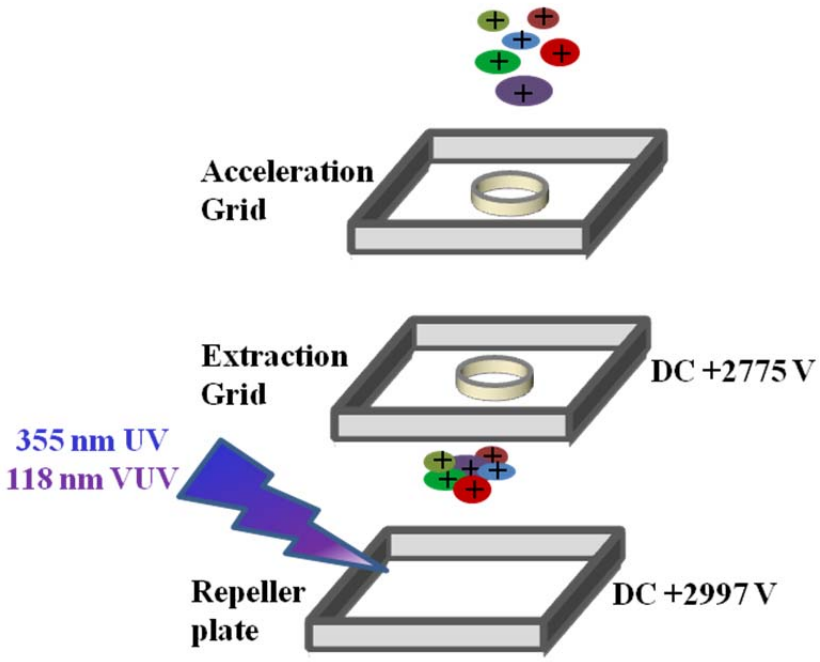


Figure 2-5: A schematic diagram the dual SPI/LIEI source.

2.3 TOF Mass Spectra Collection

In this work, the TOF MS system used is of the design proposed by Wiley and McLaren[119] and consists of a two-stage ion extraction system. In this design, an ionization region with modest electric field strength and an acceleration region with significantly stronger field strength are used. The boundaries of these regions are defined by the three metal plates: the repeller plate, the extraction grid, and the acceleration grid. Ions produced were first extracted from the ionization region by the DC electric field between the repeller and the extraction grid, and then accelerated into the field-free drift region of the TOF mass spectrometer. A schematic of Wiley-McLaren TOF-MS is shown in Figure 2-6.

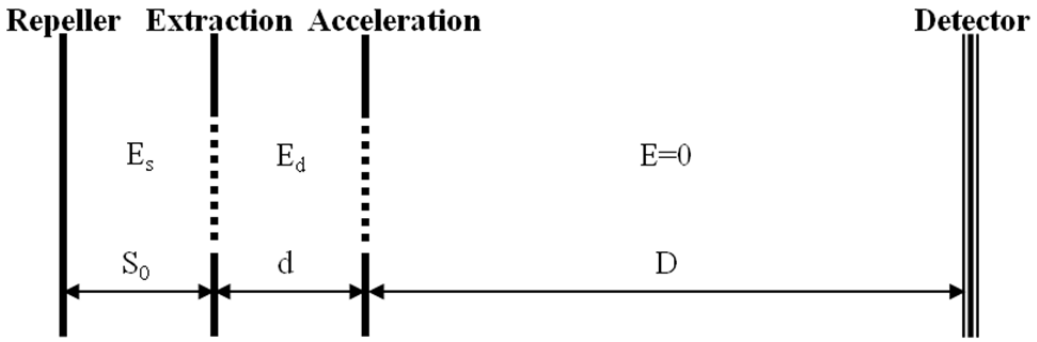


Figure 2-6: A schematic diagram of the Wiley-McLaren TOF mass spectrometer with a two-stage ion extraction optics configuration.

The ionization region experiences the field with a strength of E_s, and the acceleration region experiences the field with a strength of E_d. The drift region of length D is field free. The distance between the repeller and the extraction grid is S_o, and the one between the extraction grid and the acceleration grid is d. Wiley and McLaren has shown

that the location at which maximum resolution can be obtained is described by Equation (2-1):[119]

$$D = 2s_0 k_0^{3/2} \left(1 - \frac{1}{k_0 + k_0^{1/2}} \frac{d}{S_0} \right) \tag{2-1}$$

where k_0 is defined by:

$$k_0 = \frac{s_0 E_s + d E_d}{s_0 E_d} \tag{2-2}$$

The values for E_s and E_d must be determined experimentally, and in this work were found to be optimally defined at E_s = 175 V · cm^{-1} and E_d = 2185 V · cm^{-1}, which corresponds to a repeller voltage of 2997 V, an extraction grid voltage of 2775 V, and the acceleration grid voltage at ground potential. The distance between the plates was 1.27 cm for both the E_s and E_d regions. These values were determined for a length of the drift region D being fixed at 1 m.

Ions produces from VUV SPI or SPI/LIEI sources were detected by a micro-channel plate (MCP) detector at the end of the flight tube. Signals were preamplified using a preamplifier (SRS, SR445A) and displayed on a 300 MHz digital oscilloscope (Tektronics, TDS 3032B). Signals were averaged over 512 laser pulses before being saved into a computer using e-Scope.

Initially, the TOF mass spectra obtained from the computer were recorded in units of time-of-flight. A conversion from times-of-flight (t) values to mass-to-charge ratio

(*m/z*) was obtained by using known *m/z* values and their corresponding time-of-flight. The calibration was accomplished by fitting the known data to the following equation:

$$(m/z)^{1/2} = At + B \tag{2-3}$$

where A and B are the slope and y-intercept, respectively, from the linear fit. The calibration was performed for every collected TOF spectrum.

2.4 Synthesis of MMS-d_3, DMS-d_2 and TriMS-d_1

Four methyl-substituted silane molecules were studied in this work. They are TMS (99.9+%, NMR grade, Sigma-Aldrich), TriMS (UHP grade, 99.99% (volume), Voltaix Inc.), DMS (ABCR, 97 %), and MMS (Gelest, 99.9%). They were used without further purification. To confirm the mechanisms proposed for the primary decomposition and secondary gas-phase reactions, their corresponding isotopomers, MMS-d_3 (CH_3SiD_3), DMS-d_2 ($(CH_3)_2SiD_2$), and TriMS-d_1 ($(CH_3)_3SiD$), were used. These isotopomers are not commercially available and were synthesized following an established method by Tannenbaum *et al.*[120] and Sidorov *et al.*[121]. In this method, the corresponding chlorosilanes were reduced by an excess of lithium aluminum deuteride, $LiAlD_4$. For example, the reduction of dimethyldichlorosilane follows Equation (2-4).

$$2(CH_3)_2SiCl_2 + LiAlD_4 \xrightarrow{(n\text{-}C_4H_9)_2O} 2(CH_3)_2SiD_2 + AlCl_3 + LiCl \tag{2-4}$$

The experimental apparatus for the synthesis is shown in Figure 2-7.

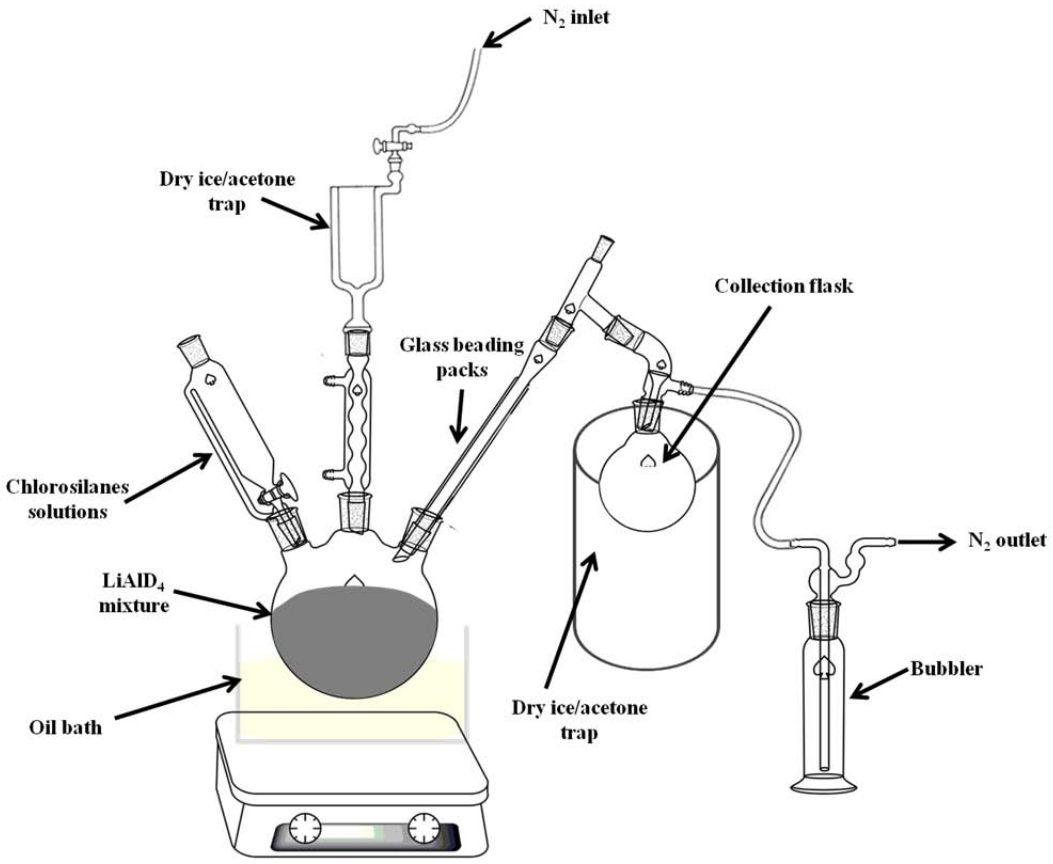


Figure 2-7: Experimental apparatus for the synthesis of deuterated methyl-substituted silane molecules.

For the synthesis of DMS-d_2, $(CH_3)_2SiCl_2$ (98%, Sigma Aldrich) (5.0 mL, 0.038 mol), was added from an additional funnel to a mixture of $LiAlD_4$ (98 atom % D, CDN Isotopes) (2g, 0.048 mol) in dibutylether (99.3%, Sigma Aldrich) (40 mL) in a 100 mL three-neck round-bottom flask. A still head cooled with dry ice/acetone slush was mounted atop of the reflux condenser on a round-bottom flask. Due to the air sensitivity of the reaction, a nitrogen (99.999%, Praxair) atmosphere was maintained at all times in the reactor. The mixture was stirred for 2 hours and brought to reflux at room temperature. As the product was formed, it was distilled from the reaction mixture with a

dry ice/acetone cold trap. Due to the high volatility of the product, its purity was examined mainly with our own mass spectrometer. The data obtained from our in-situ analysis of the room-temperature mass spectra of DMS-d_2 showed that the intensity ratio of the molecular ion peak of DMS (*m/z* 60) to that of DMS-d_2 (*m/z* 62) is 4.21 ± 0.01% indicating an isotope purity of 96% for our synthesized DMS-d_2 sample.

Following the same procedure, the synthesis of TriMS-d_1 was accomplished by the reaction between trimethylchlorosilane, $(CH_3)_3SiCl$ (98%, Sigma-Aldrich), and $LiAlD_4$. $(CH_3)_3SiCl$ (3.4 mL, 0.027 mol) was added from an additional funnel to a mixture of $LiAlD_4$ (2 g, 0.048 mol) in toluene (30 mL) in a 100 mL three-necked round bottom flask placed in an oil bath to maintain the temperature of the reaction at 80 ^oC. A reflux condenser on the round bottom flask was connected to a dry ice/acetone cold trap, where the product was collected. Since both reactants and product are air sensitive, the synthesis was carried out under inert atmosphere using N_2. The addition of the reactants lasted for about 1 hour. The purity of the sample was examined mainly with our mass spectrometer. The data obtained from our in-situ analysis of the room-temperature mass spectra showed that the intensity ratio of TriMS (*m/z* 74) to that of TriMS-d_1 (*m/z* 75) is 5.14 ± 0.02% resulting in an isotope purity of 95%.

Similarly, the synthesis of MMS-d_3, CH_3SiD_3, proceeded by the reduction reaction of methyltrichlorosilane, CH_3SiCl_3, (99%, Sigma Aldrich) by $LiAlD_4$. The synthesis apparatus consisted of 100 mL three-necked round bottom flask containing a mixture of $LiAlD_4$ (2.5 g, 0.06 mol) in dibutylether (50 mL). The side necks of the flask provided an opening for a dropping funnel, a condenser and a collection flask. A still head cooled with dry ice/acetone slush was mounted atop the condenser. Due to the air

sensitivity of the reactants and products, N_2 atmosphere was maintained in the reactor at all times. The mixture in the round bottom flask was stirred for 30 min at room temperature before CH_3SiCl_3 (5.5 mL, 0.047 mol) was added at a slow rate over a period of 1 hour. As the product is formed, it was distilled from the reaction mixture with a dry ice/ethanol cold trap. Similarly, the purity of the synthesized sample was extracted using our mass spectrometer. Due to the low molecular ion peak intensity for MMS-d_3, as well as the convolution of the peaks, the determination of the isotope purity was not conclusive. The success of the synthesis was confirmed by examining the observed peaks patterns in the collected TOF mass spectra.

2.5 Sample Preparation and Introduction

In the part of work where the formation of methyl radical (Chapter 3) and H_2 molecule (Chapter 4) from the decomposition of methyl-substituted silane molecules was investigated, TMS, TriMS, DMS and MMS were diluted in He (99.999%, BOC Gases) to prepare the 11%, 27%, 40%, and pure methyl-substituted silane molecules/He mixtures. For example, the 40% of TriMS in He mixture was prepared by first introducing 600 Torr of TriMS vapour into a 2.25 L stainless steel cylinder, and then balancing with He to a total pressure of 200 kPa. When a liquid precursor, *i.e.*, TMS, was used, the sample was first degassed by several cycles of freeze-pump-thaw. The room-temperature vapor was then diluted in He to give a mixture with desired concentration. Table 2-1 summarizes the composition of the mixtures prepared in this part of the work presented in Chapter 3 and 4.

Table 2-1 Composition of methyl-substituted silane/He mixtures studied in Chapters 3 and 4

Mixtures	*P(methyl-substituted silanes) (Torr)*	*P(total) (Torr)*
10.7%	160	1500
20.7%	400	1500
40%	600	1500
pure	Depends on the gas used	$P_{(\text{methyl-substituted silanes})}$

In the study of secondary gas-phase reactions of DMS (Chapter 5) and MMS (Chapter 6), 1%, 4% and 10% mixtures were prepared by diluting MMS and DMS samples in He in a 2.25 L stainless steel sample cylinder with He to a total pressure of 200 kPa. To confirm the proposed mechanism, 4% DMS-d_2/He and 4% MMS-d_3/He mixtures were also prepared in a 2.25 L sample cylinder. Before the preparation of each mixture, the cylinder was flushed three times with high pressure helium. The resultant mixtures were then introduced into the main chamber or the HWCVD reactor through a mass flow controller. The mixtures studied in Chapter 5 and 6 are listed in Table 2-2. Under collision-free conditions, the filament was etched between each run of experiments by heating the filament to 2000 °C for 2 hours using a 10% of H_2 in He mixture under a total pressure of $1x10^{-5}$ Torr. For the reactor experiment, the filament was changed for every new sample.

Table 2-2 Composition of methyl-substituted silane/He mixtures studied in Chapters 5 and 6

Mixtures	*P(methyl-substituted silanes) (Torr)*	*P(total) (Torr)*
1%	15	1500
4%	60	1500
10%	150	1500

To study the trapping of the active intermediates, gaseous mixtures were prepared using either MMS or DMS, trapping agents including NH_3 (BOC gases, 99.999%) and 1,3-butadiene (Air Liquide, 99.0%), and ultra-high purity He (99.995%, Praxair). The composition of the trapping mixtures studied in this work is shown in Table 2-3. All the mixtures were balanced with He to a total pressure of 200 kPa. 1:8 ratio trapping mixture was chosen following the previous pyrolysis studies.[94, 105, 122-124]

Table 2-3 Composition of methyl-substituted silane molecules /trapping agent mixtures studied in this work

Mixtures (P(methyl-substituted silanes) : P(trapping agent)	***P(methyl-substituted silanes) (Torr)***	***P(trapping agent) (Torr)***
1% DMS : 8% 1,3-butadiene	15	120
1% DMS : 8% NH_3	15	120
4% MMS : 32% 1,3-butadiene	60	480
4% MMS : 32% NH_3	60	480

2.6 Computational Methods

In this thesis, *ab initio* calculations were performed to study the various mechanism for the formation of hydrogen molecule during the primary decomposition of methyl-substituted silane molecules using the second-order Møller-Plesset (MP2) perturbation theory[125] and coupled cluster methods with single, double and perturbative triple excitations (CCSD(T)).[126] All calculations were performed using the Gaussian 03 program.[127] The reactions of interest involved the 1,1- and 1,2-H_2 elimination from MMS, DMS and TriMS by either a concerted or a stepwise mechanism. For each reaction, the transition state was located and the activation energy barrier was computed.

In addition, reaction enthalpies, Gibbs free energies and entropies were calculated in order to provide a thermochemical understanding of the reactions studied.

In our study, the geometries of all the reactants, products and transition states were optimized using the MP2 method and 6-311++G(d,p) basis set. The transition states (TS) were located by performing a TS search followed by geometry optimization and vibration frequency calculation. The TS was identified by the number of imaginary vibration frequency and verified by performing the intrinsic reactions coordinate (IRC) for each reaction to confirm that each TS certainly connected the two desired minima. The energies for all the reactants, products, and transition states were computed using the CCSD(T)/6-311++G(3d,2p) on the MP2/6-311++G(d,p) geometries. Zero-point energies (ZPE) were determined at the MP2/6-311++G(d,p) level of theory and were scaled by a factor of 0.9748, as proposed by Scott and Radom[128] for the MP2-fc/6-311G(d,p) level of theory. In addition, thermochemical analysis was explored at 0 K and room temperature of 298 K. In this part, enthalpies at 298 K (H_{298}) were obtained by adding the quantity (H_{298}-H_0) to the enthalpies at 0 K (H_0). The quantity (H_{298}-H_0) was computed by subtracting the unscaled ZPE from the thermal correction to enthalpy. Gibbs free energies at 298 K (G_{298}) was also obtained following the same procedure using the thermal correction to the Gibbs free energy. Entropy values at 298 K (S_{298}) were calculated from the values of enthalpy and Gibbs free energy at 298 K.

Chapter Three: Formation of Methyl Radicals from Decomposition of Methyl-substituted Silanes over Tungsten and Tantalum Filaments

3.1 Motivations

As stated in Chapter 1, methyl-substituted silanes ($(CH_3)_{4-x}SiH_x$, x =0-3), including monomethylsilane (MMS),[66, 129, 130] dimethylsilane (DMS),[131, 132] trimethylsilane (TriMS),[71, 133] and tetramethylsilane (TMS),[75, 134] have been widely used as single-source precursors in various CVD processes, including HWCVD,[31, 32, 135, 136] to form silicon carbide thin films. Despite these numerous studies, only few discuss the radical formation and detection with methyl-substituted silanes. Zaharias *et al.*[61] detected Si and methyl radicals as the two primary products during the decomposition of MMS, DMS, TriMS, TMS, and DMSCB on W and Re filaments. They have also determined the apparent activation energy for the formation of Si radical, which was found to increase with higher methyl substitution in methyl-substituted silanes. The activation energy for the methyl production was not determined in their work.

Recently, our group has examined the gas-phase reaction chemistry involved in using organosilicon compounds, including TriMS,[67] TMS,[89] HMDS,[82] 1-methyl-1-silacyclobuatne,[137] DMSCB,[138] and 1,1,3,3-tetramethyl-1,3-disilacylobutane,[92] in the HWCVD process. For all the studied precursors, the formation of methyl radical has been found to be a common step in their primary decomposition on the W filament. The activation energy for the methyl formation has been determined for all the above precursors except for TMS.

Methyl radicals are important growth intermediates in diamond thin film formation using CVD. Initially, it was believed that both acetylene and methyl were the two major key players in the diamond deposition process.[139] Further research carried out using kinetic modeling[140, 141] and experiments[142-145] has led several researchers to claim that methyl radicals are the dominant growth species in the CVD diamond formation process. The role of $^{\bullet}CH_3$ in the deposition of SiC thin films is currently unclear. Our previous study on the gas-phase reaction chemistry using organosilicon compounds[67, 82, 89, 92, 137, 138] in HWCVD has shown that the formation of $^{\bullet}CH_3$ from their hot-wire decomposition initiates a short chain reaction in the gas phase. Furthermore, $^{\bullet}CH_3$ can also serve as an excellent carbon source to carburize the heated tungsten filament used in hot-wires CVD.[146, 147]

This work reports a systematic study on the formation of methyl radical from MMS, DMS, TriMS, and TMS from their decomposition on W and Ta filament surfaces. The decomposition products are detected using laser ionization MS. The effect of filament temperature on the $^{\bullet}CH_3$ production is studied by examining its intensity profile at different temperatures. From the Arrhenius behavior in the temperature-dependent evolution of $^{\bullet}CH_3$ radical, the apparent activation energies were obtained. The effect of molecular structure, filament material, and sample pressure on the activation energy is also explored, which sheds lights onto the mechanism of the methyl radical formation on the metal filament surfaces.

3.2 The Intensity Profile of Methyl Radical on W Filament

The room-temperature 10.5 eV SPI mass spectra of TMS,[89] TriMS and DMS[67] have been presented in previous work. For MMS, the fragment peak of $HSiCH_3^+$ (*m/z* 44) dominates the room-temperature mass spectra. Other fragment peaks observed include SiH_x^+ (x = 0-3), $SiCH_3^+$, and $H_2SiCH_3^+$. The intensity ratios of the peaks at *m/z* 28, 29, 30, 31, 43, and 45 to that at *m/z* 44 are 0.340 ± 0.058, 0.228 ± 0.023, 0.316 ± 0.033, 0.246 ± 0.030, 0.501 ± 0.038, and 0.848 ± 0.069, respectively. The peak at *m/z* 46, which is the parent ion peak, is also observed with an intensity 35.9 ± 3.9% that of the peak at *m/z* 44, which is greater than the combined contributions of the isotopes from $HSiCH_3$ and H_2SiCH_3. Therefore, part of the peak intensity at *m/z* 46 comes from the parent ion of MMS.

In determining the primary decomposition products of these four methyl-substituted silane molecules on the filament, a new mass peak at *m/z* 15, representing methyl radical, appeared after the filament was turned on for all the chemicals tested. This is shown in Figure 3-1, where it illustrates the mass spectra collected at 2000 ^oC on a W filament temperature for a pure mixture in the mass region of 5-20 amu. Figure 3-2 shows the distribution of the normalized intensity of this peak as a function of filament temperature for all four molecules in their pure forms using W as a filament. The normalized intensity is obtained by multiplying the intensity of CH_3^+ at one specific temperature by the ratio of the intensity of the base peak or parent ion peak at room temperature to that at the same temperature. For MMS and TriMS, the base peaks at *m/z* 44 and 73, respectively, are used. The parent ion peaks at *m/z* 60 and 88, respectively, are used for DMS and TMS. The intensity of CH_3 radical increases with temperature for all

four chemicals, suggesting that a common decomposition channel exists to break the Si-CH_3 bond on the W filament.

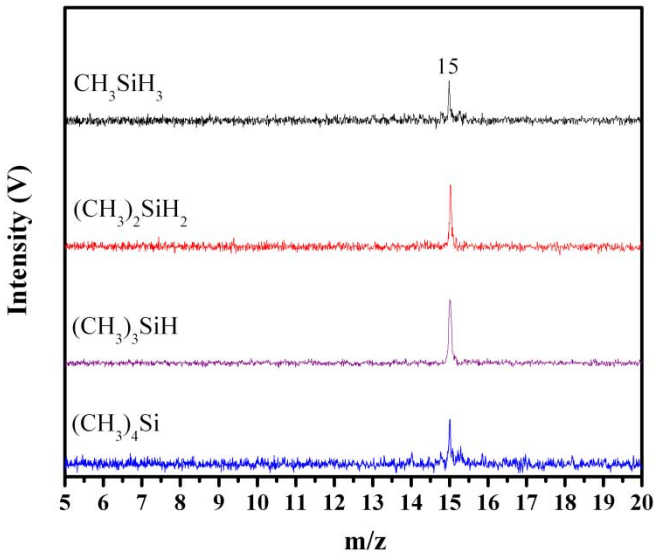


Figure 3-1: 10.5 eV VUV SPI TOF mass spectra of TMS, TriMS, DMS and MMS exposed to a W filament heated to 2000°C at a chamber pressure of ~1 × 10^{-5} Torr.

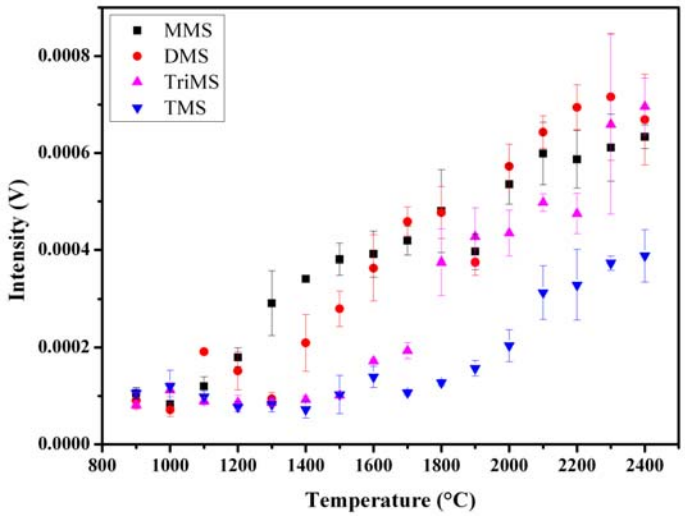


Figure 3-2: The normalized peak intensity of *m/z* 15 (CH_3^+) as a function of the filament temperature for pure MMS, DMS, TriMS, and TMS samples on a W filament at a chamber pressure of 1×10^{-5} Torr.

To further confirm the occurrence of the Si-CH_3 bond cleavage, the intensity ratio of the corresponding complementary peak ($[M\text{-}CH_3]^+$) relative to the respective parent ion peak (M^+) were examined. The intensity ratios of I(*m/z* 31)/I(*m/z* 46) from MMS and I(*m/z* 45)/I(*m/z* 60) from DMS as a function of W filament temperature, shown in Figure 3-3, revealed an increase of the ratio with temperature. The I(*m/z* 59)/I(*m/z* 74) for TriMS and I(*m/z* 73)/I(*m/z* 88) for TMS also showed the same behavior, as have been investigated in our previous work[67, 89] and also confirmed in this work. All these observations suggest that the methyl-substituted silane molecules decompose on the heated W filament to produce methyl radicals according to the following equation:

$$H_xSi(CH_3)_{4-x} \longrightarrow H_x\dot{S}i(CH_3)_{3-x} + \dot{C}H_3 \qquad (4\text{-}1)$$

As shown in Figure 3-2, a common feature for all four precursor molecules is that the intensity of the methyl radical increases with increasing filament temperature to around 2000 - 2100 ^oC and the production of the methyl radical begins to saturate beyond this temperature. Such behaviour has been rationalized by the transition in the rate-limiting step from surface reaction to mass transport. At low filament temperatures, the reaction at the filament surface to form radicals is slow and rate-limiting. As the temperature is increased the surface reaction starts to occur at a faster rate and the transport of the precursor gas to the surface becomes the limiting factor. The same behavior was observed for hot-wire decomposition of silane [129-131] and methyl-substituted silanes [132] to form Si radical.

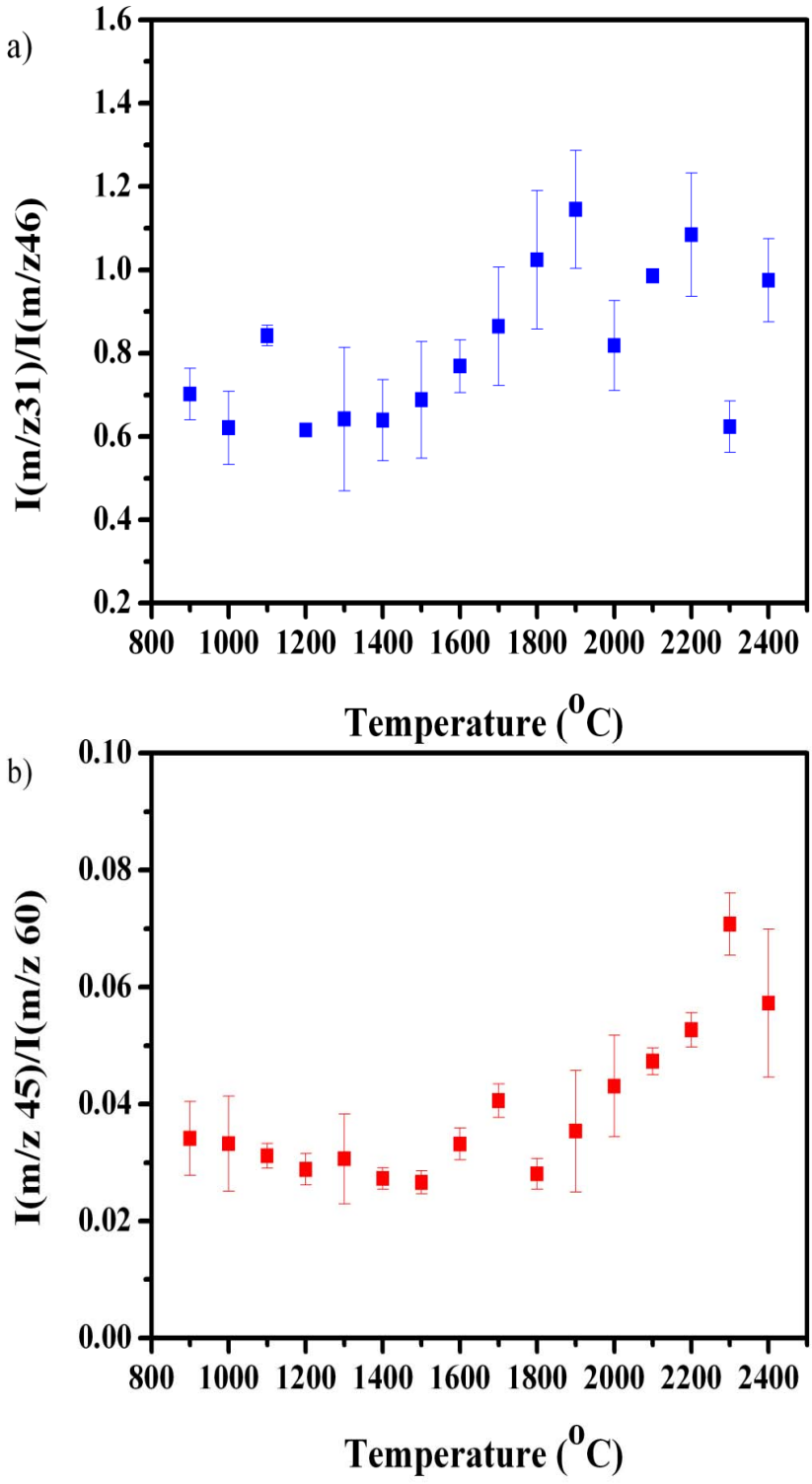


Figure 3-3: The intensity ratio of a) *m/z* 31 to *m/z* 46 for 8% MMS in He, and b) *m/z* 45 to *m/z* 60 for pure DMS samples as a function of W filament temperature at a chamber pressure of 1×10^{-5} Torr.

A comparison of the intensity profile for methyl radicals, when using the four methyl-substituted silane molecules in Figure 3-2, shows that TMS produces the least amount of methyl radicals. The intensity profiles for the $^{\bullet}CH_3$ radical peak are quite similar for MMS, DMS and TriMS. This is different from the perspective that the intensity of $^{\bullet}CH_3$ radical would be higher as the number of methyl groups present in the precursor increases. Our results are in good agreement with a previous study by Zaharias *et al.*[61] From the intensity profile shown in Figure 3-2, it is further observed that with increasing number of methyl group in the precursor compounds the temperature at which the methyl peak start to increase is shifted to the high temperature value. For MMS, the peak at *m/z* 15 started to appear at around 1200 ^{o}C, whereas this temperature was 1500 - 1600 ^{o}C for TMS. For DMS and TriMS, the observation of an increase in methyl peak intensity started at filament temperatures of 1300 - 1400 ^{o}C.

It should be mentioned that for MMS, 1% of benzene (98%, Sigma Aldrich) was added to each sample mixtures as an internal standard for optimum laser ionization conditions. The effect of benzene on the formation of methyl radicals was investigated by comparing the intensity profile of methyl peaks obtained from pure MMS samples mixed with benzene and in the absence of benzene. It is found that the presence of benzene had negligibly affected the intensity of methyl peak as both intensity profiles follow the same trend and the difference in intensity is minimal. Furthermore, the apparent activation energy for the formation of methyl radical was determined to be 51.4 ± 2.8 kJ·mol^{-1} and 50.5 ± 2.8 kJ·mol^{-1}, respectively, for samples without and with benzene. Therefore, the presence of benzene did not affect the apparent activation energy for the formation of

methyl radicals. As a result, the data obtained in the presence of 1% of benzene are used for MMS in the remaining discussions.

3.3 The Activation Energy of Forming Methyl Radicals on W - Effect of Molecular Structures

The temperature dependence of the normalized intensity of CH_3^+ peak shows an Arrhenius behavior in the region where there is a monotonic increase. From this, the apparent activation energy (E_a^{app}) for the formation for $^{\bullet}CH_3$ was determined. Similar to the results from our previous study on TriMS,[67] using mixtures of different concentrations of the same molecule resulted in comparable E_a^{app} values. The averaged E_a^{app} value from all tested mixtures for each precursor was found to be 51.1 ± 4.0, 61.0 ± 4.9, 78.8 ± 4.2, and 84.7 ± 4.0 kJ · mol^{-1} for MMS, DMS, TriMS and TMS, respectively. This is illustrated in a bar diagram in Figure 3-4. A comparison of the determined E_a^{app} values and the Si-CH_3 bond dissociation energy (BDE) in methyl-substituted silanes[37] demonstrates the catalytic nature of the formation of methyl radicals from their decomposition on the W filament.

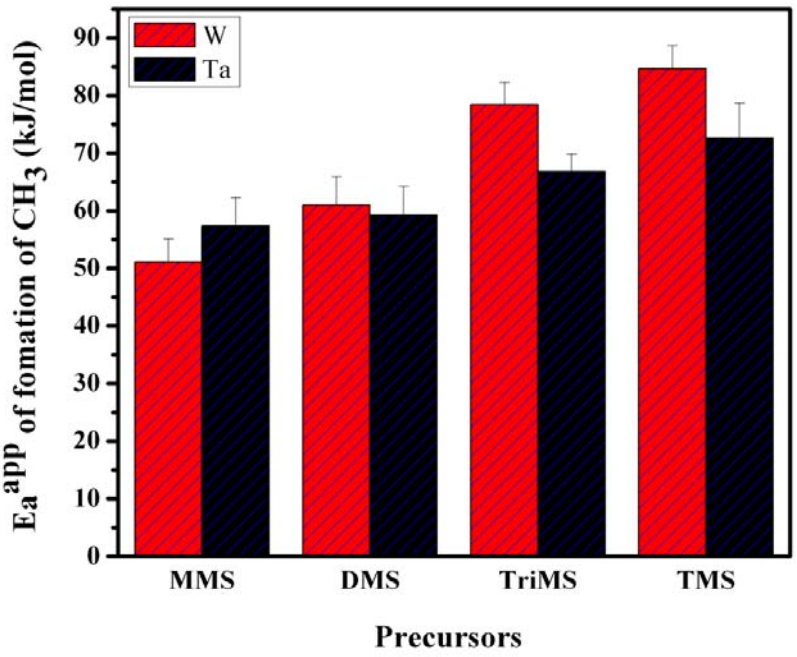
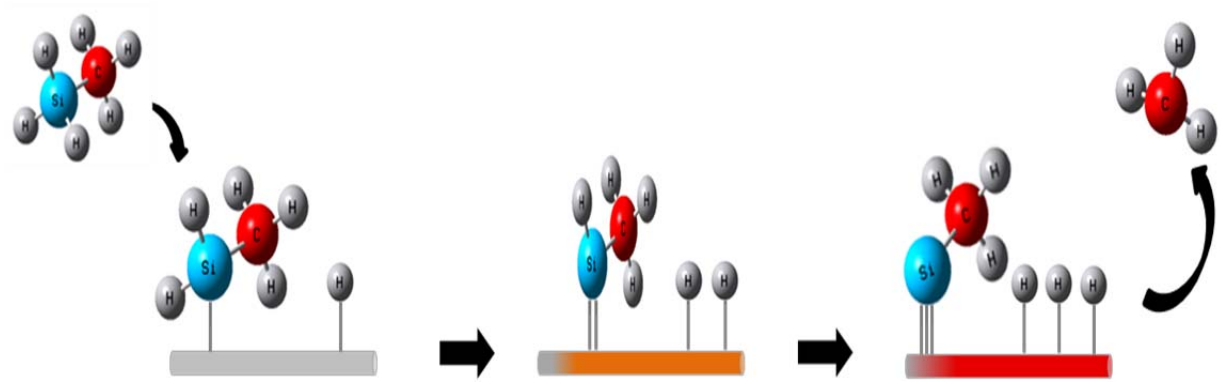


Figure 3-4: Apparent activation energy for methyl radical formation from the four methyl-substituted silanes over the surface of tungsten and tantalum surfaces.

Figure 3-4 also shows a clear trend in the activation energy when using the four methyl-substituted silane molecules to form methyl radicals. The E_a^{app} values increase with the increasing number of methyl substitution in the molecule. This is in good agreement with the results from a previous study[61] where it was found that the E_a^{app} for the Si radical formation when using the same four precursors increases in the order of MMS, DMS, TriMS and TMS. Extensive studies have been dedicated to understand the adsorption and decomposition of methyl-substituted silanes, among which MMS has been studied the most, on various metal surfaces, including W.[61, 148-151] Despite the fact that the bond strength of Si-H is ~ 8 kcal/mol (*i.e.*, a ~ 33 kJ/mol) higher than that of Si-C in methyl- substituted silanes,[152, 153] temperature programmed desorption and spectroscopic studies have unambiguously demonstrated that MMS adsorbs

dissociatively by Si-H bond cleavage. Similar results were obtained when studying the bond scission in ethane hydrogenolysis on various metal surfaces[154] which showed that C-H bonds are more reactive than C-C bonds although the latter are weaker by ~ 10 kcal/mol (*i.e.*, a ~ 42 kJ/mol). The nature of the final products of the dissociation of MMS depends on its surface coverage. In a study on the reactions of primary organosilanes on transition metal surfaces, Hostetler *et al.*[148] found that at low coverage of MMS, methylsilylyne ($CH_3Si\equiv$) is the predominant species bound to the Pt surface. As the coverage increases and approaches saturation, the presence of methylsilylyne starts to diminish, while at the same time methylsilylene ($CH_3HSi=$) and methylsilyl (CH_3H_2Si-) start to appear. Several groups have studied the surface reactions of MMS on the Si (100) surface and it was again found that the cleavage of Si-H is the initial step in the adsorption and favored over that of Si-C bonds.[155-157] Therefore, it is believed that the dissociation of the methyl-substituted silanes on W surfaces is mainly activated by the presence of the Si-H bond and is initiated by the Si-H bond cleavage resulting in the formation of methyl-substituted silyl/silylene/silylyne and hydrogen adsorbates. The mechanism is illustrated in scheme 3-1. The cleavage of all Si-H bonds in the molecules is followed by Si-C bond cleavage as the temperature is raised.



Scheme 3-1 Adsorption and decomposition of monomethylsilane on a W or Ta surface

For molecules not containing Si-H bonds, such as TMS, the only bonds that can possibly be broken are the Si-CH_3. Due to the absence of Si-H bond in the molecule, TMS becomes less susceptible to decompose on the heated wire, leading to the highest activation energy value as determined in this work. This also explains why TMS produces the least amount of $^{\bullet}CH_3$ radicals even though it has the greatest number of methyl substituent in the molecule.

The ejection of methyl radicals from surface-bound methyl-substituted silyl/silylene /silylyne or TMS adsorbates occurs by Si-CH_3 bond scission. According to Lin and Bent[158] in their work on the thermal decomposition of CH_3I on a Cu (111) surface, there are two pathways to form $^{\bullet}CH_3$ radicals. The first is to generate free $^{\bullet}CH_3$ radicals in the gas-phase with I bound concurrently to the Cu surface, and the second is the formation of adsorbed $^{\bullet}CH_3$ group followed by their desorption. Although the binding energy of CH_3-W is unknown, theoretical and experimental data on the binding energy of $^{\bullet}CH_3$ with various other transition metal surfaces is available.[154, 159, 160] These range from 26.7 to 53.8 kcal/mol (*i.e.*, a 111.7 – 225.1 kJ/mol), which is much higher than the Ea

value determined from our work. This strongly suggests that Si-CH_3 bond scission does not form surface-bound $^{\bullet}CH_3$ groups. As mentioned before, the obtained activation energy for forming $^{\bullet}CH_3$ radicals from this work is much lower than the Si-CH_3 bond dissociation energy. This indicates that the ejection of CH_3 radicals follows the first pathway where the bond cleavage is accompanied by the formation of a Si moiety bound to the W surface. Our results are in excellent agreement with Lin and Bent's work where they determined that the activation energy is low at 8.5 kcal/mol (*i.e.*, a 35.6 kJ/mol).

In a theoretical study on the effect of the electronic structure of substituent at the silicon atom on the structure and bond energies of methylhydrosilanes and silenes, Gusel'nikov *et al.*[153] have concluded that the Si-X (X=H and CH_3) bond becomes shorter and stronger with an increase in the electronegativity (χ) of the substituent. Considering that the χ for methyl and H substituent is 2.5 and 2.2, respectively, both Si-C and Si-H bonds are the strongest for TMS and weakest for MMS. They have found that the Si-C bond strength increased by 0.9 kcal/mol (*i.e.*, a 3.8 kJ/mol) per additional methyl. Casserly and Gleason[152] computed the Si-H and Si-C BDE of methyl-substituted silane molecules using density functional theory. They have found that the BDE was increased per additional methyl substitution by *ca.* 0.6 and 0.9 kcal/mol (*i.e.*, a 2.5 – 3.8 kJ/mol), respectively, for Si-H and Si-C bond. These data support the observed trend for the Ea values obtained in this work. The strengthening in both Si-C and Si-H bonds due to the increasing number of methyl group attached to the Si atom results in an increase in the energy required to form $^{\bullet}CH_3$ radicals.

3.4 Effect of Filament Material - W vs Ta

The primary decomposition of the four methyl-substituted silane molecules was also studied on different filament materials including W and Ta to gain a better insight into the process. Initially, the effect of filament materials was studied by comparing the methyl radical intensity profile from these two filaments. Figure 3-5 shows the normalized intensity of the methyl radicals as a function of the filament temperature from 900 °C to 2400 °C generated on both W and Ta when using MMS, DMS, TriMS and TMS samples, respectively. One difference between these two filaments is the temperature profile in the high-temperature region for MMS, DMS, and TriMS. A gradual decrease in the methyl intensity after reaching the optimum temperature was observed when Ta was used, whereas the intensity reached a plateau with W. This is explained by the tendency of the filament to release H and the number of available active sites at the filament surface. It has been demonstrated that both Ta and W filaments can generate H atoms by dissociating H_2 on the hot filament surface.[161, 162] Comerford *et al.*[161] has demonstrated that H atom formation involves a two-step chemisorption/desorption mechanism where 1) H_2 is dissociatively adsorbed on the filament surface to give a hydrogenated surface sites (H-*); and 2) atomic H is desorbed from the H-* to give a bare surface dangling bond -*. As shown in Scheme 3-1, the decomposition of MMS, DMS and TriMS all leads to the formation of hydrogenated surface sites H-*. As the temperature is increased, desorption of the H atom from surface starts to take place resulting in the presence of the dangling bond (active site) at the surface, which is followed by the adsorption of methyl radicals on the filament surface, hence reducing the intensity of methyl radicals detected in the gas-phase. Van der Werf *et*

al.[162] showed the amount of H atoms produced from Ta is twice that from W from H_2 dissociation. Therefore, Ta is more efficient in releasing H atoms from the surface, leaving more active sites on the surface for the adsorption of methyl radicals. The negative apparent activation energy values obtained in the high temperature range of 1700 - 2400 °C strongly support that this is an adsorption process. The E_a^{app} values are determined to be -104.2 ± 5.0 kJ/mol, -113.2 ± 7.6 kJ/mol, and -137.7 ± 7.8 kJ/mol for MMS, DMS, and TriMS, respectively. These values should be the binding energy of $\cdot CH_3$ species on the Ta metal surface. For W filaments, not enough active surface sites are available; therefore, mass transport is still the limiting step, leading to a plateau region. In the TMS molecule, there is no Si-H bond, consequently, no hydrogenated surface sites exist. Therefore, the methyl radical intensity did not decrease at the high-temperature end with Ta, and the intensity profiles are quite similar for the two filaments when TMS is used (Figure 3-5d). When comparing the methyl radical intensities for the four methyl-substituted silane molecules with the same Ta filament, the same trend as that with W (MMS ~ DMS ~ TriMS > TMS) has been found. TMS is the least efficient in producing $^{\bullet}CH_3$ radicals on the Ta filament. The other three molecules produce similar amount of radicals but MMS has the lowest activation energy.

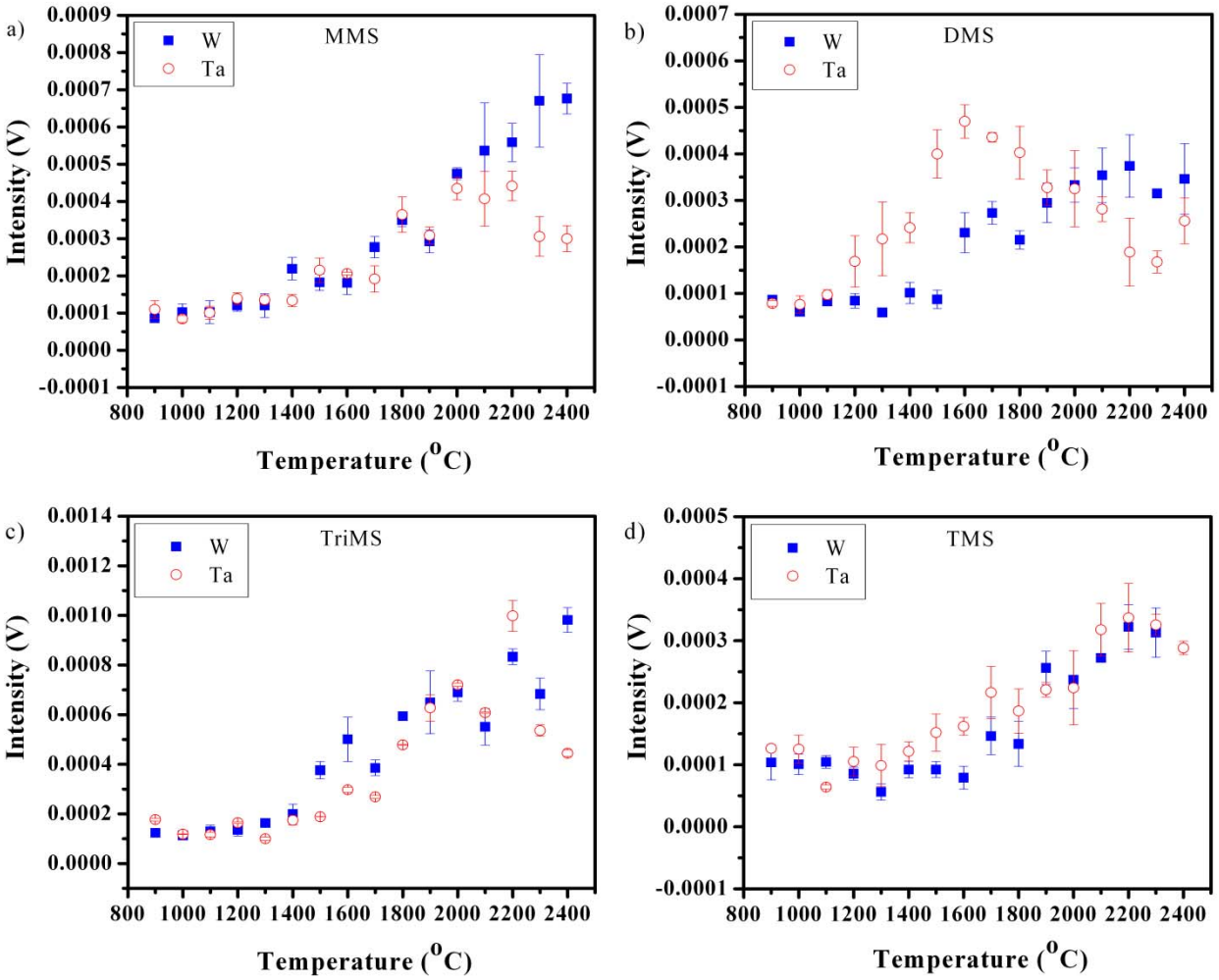


Figure 3-5: Temperature profiles of the normalized intensity of methyl radical from W and Ta filaments during the dissociation of a) MMS, b) DMS, c) TriMS, and d) TMS samples.

Similar to the W filament, the apparent activation energy for methyl radical formation from the dissociation of the four methyl-substituted silane molecules on the Ta filament can be obtained from the region where the methyl intensity increases with temperature. The E_a^{app} value averaged from all tested mixtures of MMS, DMS, TriMS and TMS, respectively, was determined to be 57.3 ± 5.0, 59.2 ± 5.0, 66.8 ± 3.1, and 72.7

± 6.0 kJ/mol. They are shown in a bar diagram in Figure 3-4, for a comparison with the values obtained with W. The usage of Ta filament during the dissociation of methyl-substituted silanes resulted in the E_a^{app} values in the similar range to those for W. This suggests that the formation of methyl radicals follows the same mechanism on both Ta and W, as described before. In addition, similar to W, the E_a^{app} values on Ta filaments increase with increasing number of methyl substitution in the methylsilene molecules.

3.5 Summary

All four methyl-substituted silane molecules, *i.e.*, MMS, DMS, TriMS, and TMS, decompose on the W and Ta metal filaments to form methyl radicals. The temperature distributions of the methyl radical intensities show different behavior on W and Ta filaments. When using W, due to a transition in the rate-limiting step from surface reaction to mass transport, the intensity of the methyl radical increases with increasing filament temperature to around 2000 - 2100 ^oC and reaches a plateau beyond. For the Ta filament, the methyl radical intensity initially increases with temperature. However, a gradual decrease in the intensity was observed after reaching the optimum temperature when using MMS, DMS, and TriMS. This is explained by the fact that Ta is more efficient in releasing surface-bound H and forming active sites on the metal surface, leading to the adsorption of methyl radicals on the surface at the high-temperature regions. The negative apparent activation energy values obtained in the monotonic decrease regions strongly support this conclusion.

For both W and Ta filaments, the apparent activation energy for methyl radical formation from the dissociation of the four methyl-substituted silane molecules increases

with the increasing number of methyl substitution. The dissociation of the methyl-substituted silanes on W and Ta surfaces to form methyl radicals is believed to be initiated by the Si-H bond cleavage resulting in the formation of methyl-substituted silyl/silylene/silylyne and hydrogen adsorbates and followed by Si-CH_3 bond cleavage. The obtained low activation energy values for methyl radical formation in the range of 51.1 – 84.7 kJ · mol^{-1} suggests that the ejection of CH_3 radicals is accompanied by the formation of a Si moiety bound to the metal surface. Overall, TMS produces the least amount of methyl radicals on both filaments with the highest activation energy. The amount of methyl radicals produced when using MMS, DMS, and TriMS are similar but MMS gives the lowest activation energy.

Chapter Four: Study of Hydrogen Elimination from the Decomposition of Methyl-Substituted Silanes over Tungsten and Tantalum Filament Surfaces

4.1 Motivations

Several studies have found that hydrogen plays a crucial role during diamond CVD.[163, 164] These investigations revealed that atomic hydrogen are perhaps the most critical determinants of the quality and growth rate of CVD diamond. The major importance of H_2 during diamond CVD is to prevent surface graphitization by etching the graphite layer co-deposited with the diamond.[165-168] In addition to diamond CVD, several studies reported the effect of hydrogen on the properties of silicon thin films. In a study carried out by Ciffre *et al*.[169] on the deposition of polycrystalline silicon (pc-Si) films using HWCVD, they found that the dilution of silane mixture with H_2 resulted in the formation of pc-Si film in comparison to amorphous Si film when pure silane was used. The obtainment of such polycrystalline films in a HWCVD system provides the possibility of fabricating efficient polycrystalline solar cells of low cost and large area that can be extended to application of optoelectronic devices and photovoltaic solar cells. To better understand the role of H_2 during the deposition of silicon films, Pant *et al*.[45] have studied the effect of process condition during the deposition of pc-Si films by monitoring the morphology of the films while increasing the concentration of hydrogen. Their results showed that with an increase in hydrogen dilution, the crystallinity of the deposited film increases. This enhancement is explained by the more efficient conversion of silane by hydrogen abstraction reaction in the gas phase leading to the deposition of pc-Si films. The same conclusion was reached by this group when the pressure of pure

silane in the reactor was increased, since this led to higher production of H_2 in the gas phase.

Furthermore, during the deposition of a-Si:H or SiC thin films in a HWCVD system, the silicidation of the used filaments is unpreventable and this filament poisoning will result in the deposition of poor-quality thin films.[12, 170, 171] This problem was overcome by exposing the filament to hydrogen, which reacted with the silicide on the surface of the filament and etched it.[162, 172, 173] These issues can also be extended to the deposition process of a-SiC:H, one form of SiC materials.[174, 175] Hence, it is critical to understand the process for the production of H_2 in order to relate it to the properties of the a-SiC:H thin films. One type of precursor suitable for the deposition of these films is methyl-substituted silane since they contain the three elements needed for the deposition of a-SiC:H films.

In several studies carried out on the pyrolysis of MMS[94, 176-178] and DMS[95, 179], it has been suggested that the formation of H_2 occurs via molecular elimination, and that both 1,1- and 1,2-hydrogen eliminations exist during the decomposition of theses precursors, with the 1,1- process being more dominant. Sawrey *et al.*[122-124] estimated the yield for the primary dissociation process for MMS under static conditions to be $\varphi_{1,1} \cong 0.7$ for the 1,1-H_2 elimination and $\varphi_{1,2} \cong 0.16$ for the 1,2-H_2 elimination. To gain further insight into the reactions involved in the primary decomposition of MMS, Gordon *et al.*[180] presented a theoretical study on eight competing primary decomposition reactions for MMS using full fourth-order Møller-Plesset (MP4) perturbation theory and the combined McLean-Chandler/6-311G basis set, augmented by polarization functions on

all atoms. From the calculations, this group concluded that, besides the homolytic cleavage of Si-C and Si-H, 1,1-H_2 elimination and methane formation required less amount of activation energy than the 1,2- H_2 elimination reaction, even though these reactions appeared to be thermodynamically competitive. Kinetically, they have found that the activation energy for the 1,2-H_2 elimination is nearly 25 kcal/mol (*i.e.*, a 105 kJ/mol) greater than that for the 1,1-H_2 elimination reaction. This group has concluded that silylene extrusion reaction is kinetically more favourable than the 1,2-H_2 elimination, which is in agreement with the study of Sawrey *et al.*[122] and O'Neal *et al.*[176] Unlike MMS and DMS, the formation of H_2 molecules during the decomposition of TriMS is believed to take place via a radical chain reaction, as proposed by Davidson *et al.*[181, 182] and supported by various other pyrolysis studies.[183, 184] Therefore, from these various studies, the formation of H_2 molecule can be categorized into two groups: molecular elimination for MMS and DMS, and radical chain reactions for TriMS. The interest in studying the formation of H_2 from the decomposition of methyl-substituted silanes has continued and expanded to the HWCVD technique in order to bring some insights on these dissociation steps in the presence of a metal surface.

In a HWCVD system, the presence of a metal filament is crucial in studying the gas-phase chemistry; however, its role is still unclear. In the hope to provide an understanding on the reaction of the precursor molecules on metal surface, several research groups studied the adsorption and decomposition of methyl-substituted silanes on various metal surfaces.[148-151] Bradshaw *et al*. examined the adsorption process of MMS on Au and Mo,[185] as well as on W, Ni and Rh.[150] From both studies, they have found that hydrogen and methane evolved upon the exposure of the metal surfaces to

MMS. Tounderstand the mechanism by which these two species are formed, they have carried out the same study using deuterated sample and their results showed that adsorption occurred through the silicon atom and the evolution of H_2(g) was due to dehydrogenation from the Si atom rather than the methyl moiety.

The decomposition of TMS over W and Fe surfaces was investigated by Roberts *et al*.[151] and they found that TMS is irreversibly and rapidly adsorbed on the W surface at 293 K. Gaseous hydrogen and methane were detected, which were desorbed upon heating the surface up to 420 K. They have concluded that the presence of H_2(g) and CH_4(g) is a clear evidence for the cleavage of C-H and C-Si bond. Similarly, Dubois and Zegarski[186] examined the low-temperature decomposition and adsorption of methyl-substituted silanes of the formula $SiMe_nH_{4-n}$ ($1 \leq n \leq 4$) as well as hexamethyldisilane (HMDS) using temperature programmed desorption (TPD) and Auger electron spectroscopy (AES) on Ni(1 0 0) surface. They have found that species with $n \leq 3$ underwent substantial decomposition accompanied with significant amount of H_2 being released in the gas phase while for both TMS and HMDS, where the molecule becomes so sterically hindered that bonding to the surface is weakened, only methyl desorption was observed indicating that radical desorption predominated at low temperature. Their TPD experiments indicated that methyl-substituted silanes adsorbed dissociatively with the cleavage of Si–H bonds. The common finding extracted from these studies is the dominance of the formation of gaseous hydrogen during the decomposition of methyl-substituted silanes via Si-H bond cleavage as an initial step for species containing Si-H bond within their frame, and for species lacking this bond their dissociation is initiated by the rupture of the Si-C bond followed by the cleavage of C-H bond.

In this work, we examined the primary decomposition of TMS, TriMS, DMS, and MMS on a heated W and Ta filament in a HWCVD process using laser ionization MS. The main focus of this chapter is to examine the formation of H_2 molecule from the decomposition of these precursor molecules on a heated W and Ta filament. The production of H_2 is detected using both SPI and dual SPI/LIEI ionization sources. To determine the process leading to the formation of H_2, experiments with the isotopomers, MM-d_3, DMS-d_2, and TriMS-d_1, were carried out under the same experimental conditions using the dual SPI/LIEI source. The effect of filament temperature on H_2 production is studied by evaluating its intensity profile at different temperatures. From the temperature-dependent study, the apparent activation energy is extracted. In addition, the effect of filament material, molecular structure, and sample pressure on the formation of H_2 and its activation energy is explored, which provides an understanding on this process and a mechanism for the production of H_2 on a metal filament surface.

4.2 Comparison of the Two Ionization Sources

In the current study, two complementary ionization sources, *i.e.*, non-resonant SPI using a VUV wavelength at 118 nm and dual SPI/ LIEI, were employed to study the formation of hydrogen via the decomposition of MMS, DMS, TriMS and TMS. The SPI source has been proven to ionize mainly species that have an IE below 10.5 eV and had uniform detection sensitivity for these compounds. The dual ionization source is effective in detecting all possible decomposition products with IE below and above 10.5 eV. It is worth noting that in pure SPI mode, the EI contribution from the photoelectrons is still present but minimal. Despite the fact that, in this mode, the 118 nm laser beam is focused

into the ionization region, the possibility of the scattered UV or VUV radiation striking either the repeller plate or the extraction grid in the TOF optics is inevitable. Therefore, this generates a minimal contribution from the LIEI. In order to quantify the EI contribution, an intensity ratio of the peak at *m/z* 4 representing He^+, which is caused by EI contribution since the IE of He is greater than 10.5 eV, to the base peak at *m/z* 73 in TriMS, which is originated from SPI, is computed and found to be only 0.036%. Similar ratio with a value of 0.034% was obtained with respect to the base peak at *m/z* 73 in TMS. Therefore, these values suggest that the contribution from UV photon-induced EI is minor when using the pure SPI source. The advantages and disadvantages of using these two ionization techniques were demonstrated by comparing the mass spectra collected during the decomposition of DMS samples on a heated W filament when using these two modes. DMS has an IE value of 11.2 eV.[187]

Figure 4-1 shows the mass spectra of pure DMS in the mass region between 0 and 20 amu at a filament temperature of 2000 ^oC and a chamber pressure of 1.0×10^{-5} Torr using SPI and dual SPI/LIEI modes. After the filament was turned on, two new peaks appeared at *m/z* 2 and 15 corresponding to H_2^+ and CH_3^+, respectively. Comparison of the two spectra in Figure 4-1 demonstrates the impact of the LIEI source on the mass spectra. The employment of LIEI significantly enhances the signal intensity of H_2^+, which has an IE of 15.4 eV,[188] at an expense of a lower resolution. The mass resolution ($m/\Delta m$) of the H_2^+ peak observed with LIEI source is found to be around 103, which is lower than the mass resolution for the He^+ peak recorded using SPI method, where a value of 145 was calculated. This is because the electrons produced during the LIEI process are not spatially controlled, and it is expected that peaks from the produced signals are broadened

as compared to those of the SPI signals generated from a tightly focused laser beam. The enhancement in the intensity for H_2^+ and He^+ peaks is indicative of the dominance of the electron ionization in the dual mode, where the LiF lens was pulled out and the laser beam was guided to the repeller plate. This difference in the H_2^+ intensity from the two sources is more clearly illustrated by Figure 4-2, where the intensity profile of the peak at *m/z* 2 is plotted at various filament temperatures.

As mentioned in Section 2.5, the filament was etched with 10% H_2/He for two hours between each run of experiment. In order to eliminate the contribution of this etching process to H_2 formation during the decomposition of methyl-substituted silanes, a control experiment was carried out to heat the etched filament in vacuum from 900 to 2400 ^oC. The analysis of this control experiment revealed the absence of any H_2 gas being desorbed from the surface of the filament. In addition, another control experiment was carried out with DMS sample after etching the filament with pure He instead of 10% H_2/He. It was found that the evolution of H_2 from the filament etched with He was comparable to the one obtained from the actual experiment. This suggests that the filament etching with 10% H_2/He does not contribute to the intensity of H_2 molecule formed during the decomposition of methyl-substituted silane molecules.

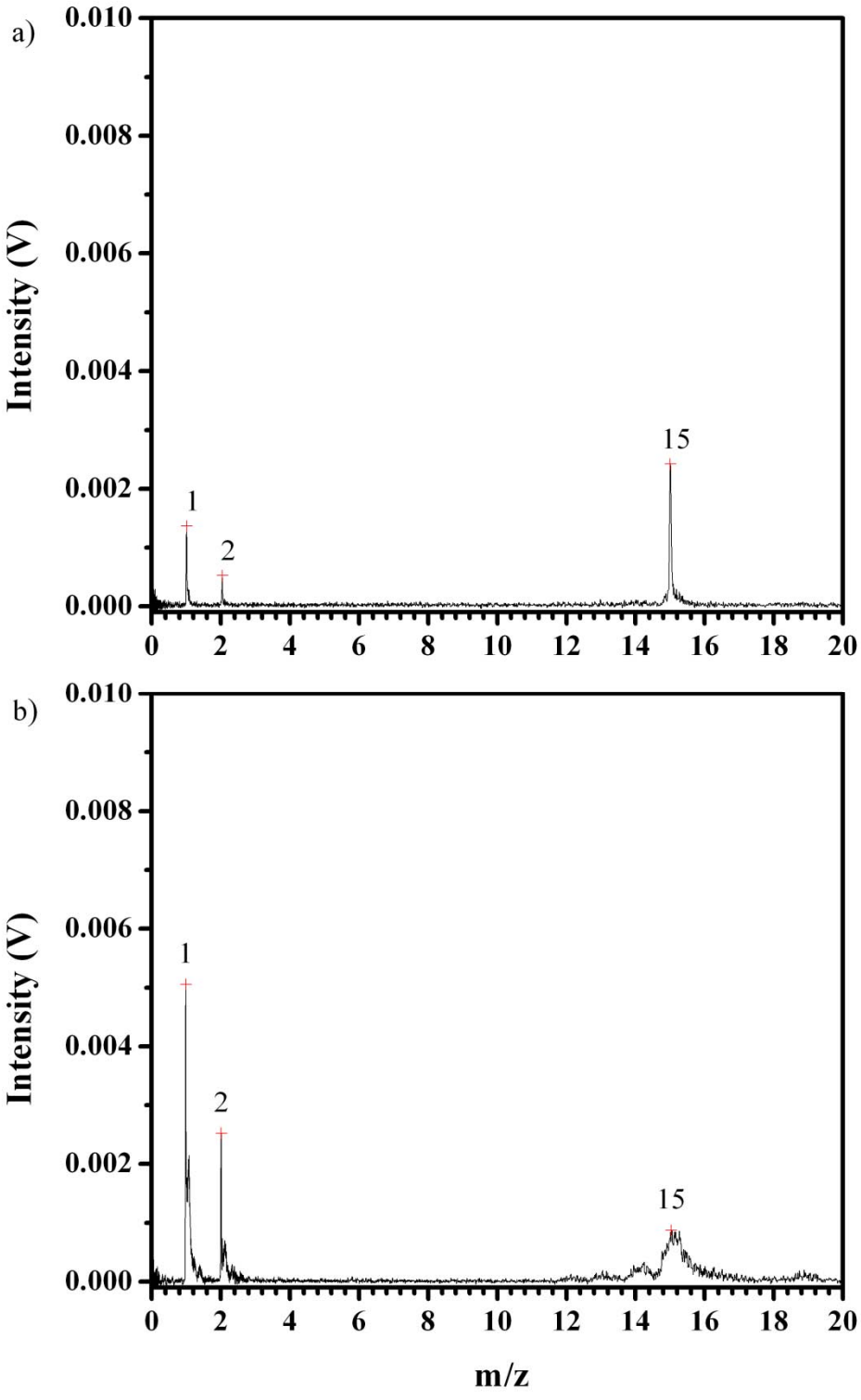


Figure 4-1: Mass spectra of pure DMS taken at a filament temperature of 2000 ^{o}C and a chamber pressure of 1 × 10^{-5} Torr using a) SPI mode and b) LIEI-SPI mode in the mass region between 0 and 20 amu.

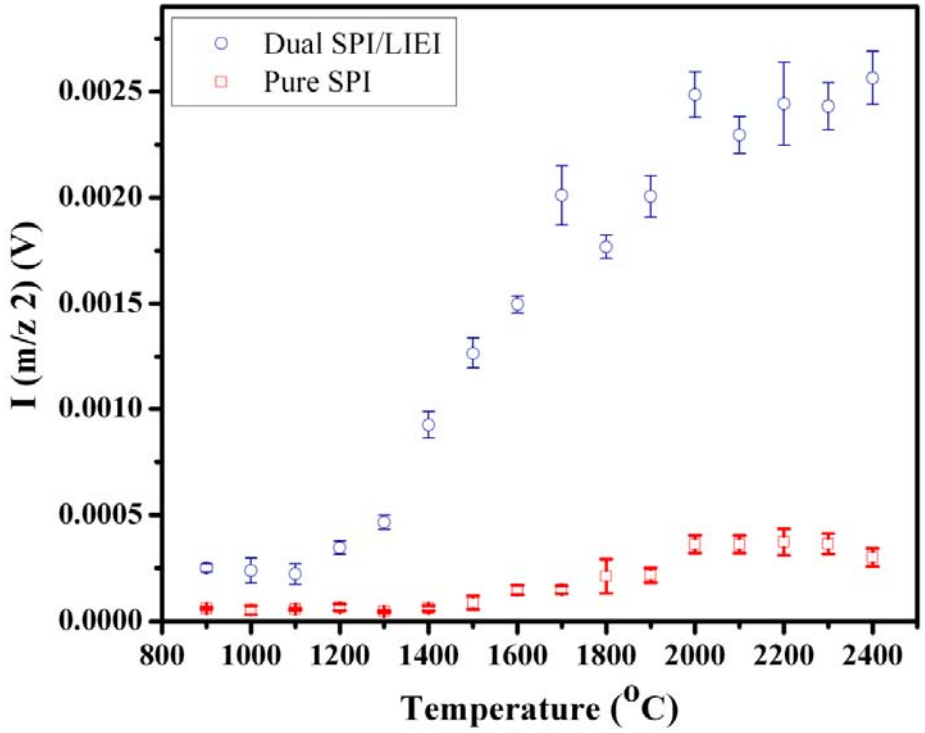


Figure 4-2: The intensity of the peak at *m/z* 2 at different W filament temperatures for pure DMS sample using the pure SPI and dual SPI/LIEI ionization sources.

In contrast to the intensity of the H_2^+ peak, as seen in Figure 4-1, the intensity of the CH_3^+ peaks, which has an IE of 9.84 eV,[189] was reduced from 2.4 mV with SPI to 0.88 mV with the dual ionization source. In SPI mode, the 118 nm VUV light is tightly focused resulting in the intensity of 10.5 eV radiations to be high, whereas it is divergent in the dual SPI/LIEI mode. This entails that the intensity of any peak representing a species with an IE below 10.5 eV will be reduced with the dual ionization source. However, with SPI mode, any species that cannot be ionized by 10.5 eV photons would give a relatively weak intensity, which originated from the ionization by the photoelectron as stated earlier. Evidently, any species with IE < 10.5 eV have enhanced signal intensities when SPI is used, and those with IP > 10.5 eV can only be effectively

ionized by the LIEI process. This comparison confirms the complementary nature of the two ionization sources under our experimental conditions. In this work, both ionization sources are used to study the decomposition of methyl-substituted silanes. The pure SPI source was used as a common ionization source for all of the performed experiments, whereas the dual SPI/LIEI source was employed as a confirmation tool for the primary decomposition products and in the experiments using the corresponding isotopomers.

4.3 H_2 Formation during the Decomposition of Methyl-Substituted Silanes on a Heated W Filament

The primary decomposition of TMS, TriMS, DMS and MMS on a hot W filament was studied under collision-free conditions. In studying the primary decomposition of these four methyl-substituted silanes, a new peak at *m/z* 2, corresponding to the formation of hydrogen molecule, appeared after the filament was turned on for MMS, DMS and TriMS while using the pure SPI source. This peak was absent when TMS was used. This behavior is illustrated in Figure 4-3a, showing mass spectra in the mass region of 1.5 - 4 amu collected during the decomposition of these precursors at a W filament temperature of 2000 ^{o}C using SPI mode. The detection of the peak at *m/z* 2 using SPI is due to the presence of photoelectrons generated from the scattered UV radiation striking the ion optics in the TOF mass spectrometer. For TMS, the lack of this peak is due to the possibility that this molecule produces insignificant amount of H_2 that cannot be detected. This, combined with the minor contributions of EI in the pure SPI mode, explains the difficulty associated in observing the peak at *m/z* 2 with TMS. In order to validate the formation of H_2, the mass spectra were collected during the decomposition of the same

four molecules using the dual SPI/LIEI source, as shown in Figure 4-3b. As noted from this figure, when switching to the dual ionization source, the intensity of the peak at *m/z* 2 is significantly enhanced for all methyl-substituted silane molecules, including TMS.

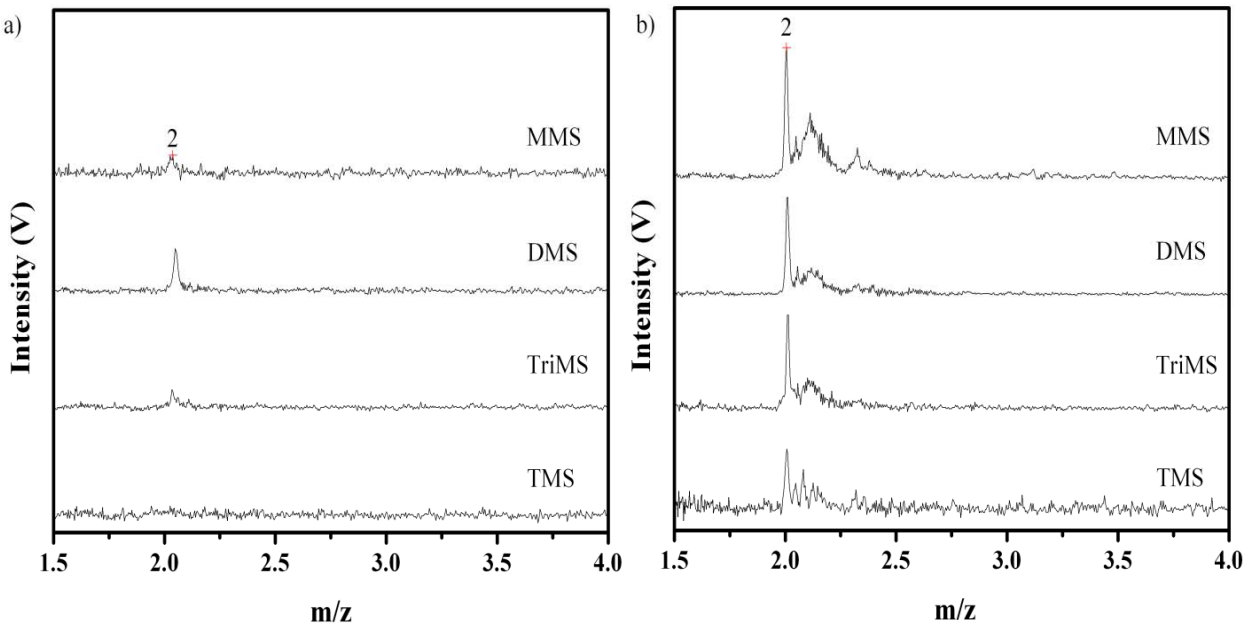


Figure 4-3: The mass spectra in the region between *m/z* 1 and *m/z* 4 for MMS, DMS, TriMS and TMS at a filament temperature of 2000 °C and a chamber pressure of 1 × 10^{-5} Torr using a) SPI mode and b) dual SPI/LIEI source.

Figure 4-4a shows the distributions of the normalized intensity of the peak at *m/z* 2 as a function of filament temperature for pure MMS, DMS and TriMS samples using pure SPI mode. The normalized intensity is obtained by multiplying the intensity of H_2^+ at one specific temperature by the ratio of the intensity of the base peak or parent ion peak at room temperature to that at the same temperature. For MMS and TriMS, the base peaks at *m/z* 44 and 73, respectively, are used, whereas for DMS and TMS the parent ion peaks at *m/z* 60 and 88, respectively, are employed. The intensity of H_2^+ increases with

temperature for all three chemicals, indicating that H_2 molecule is indeed being formed during their decomposition on a W filament.

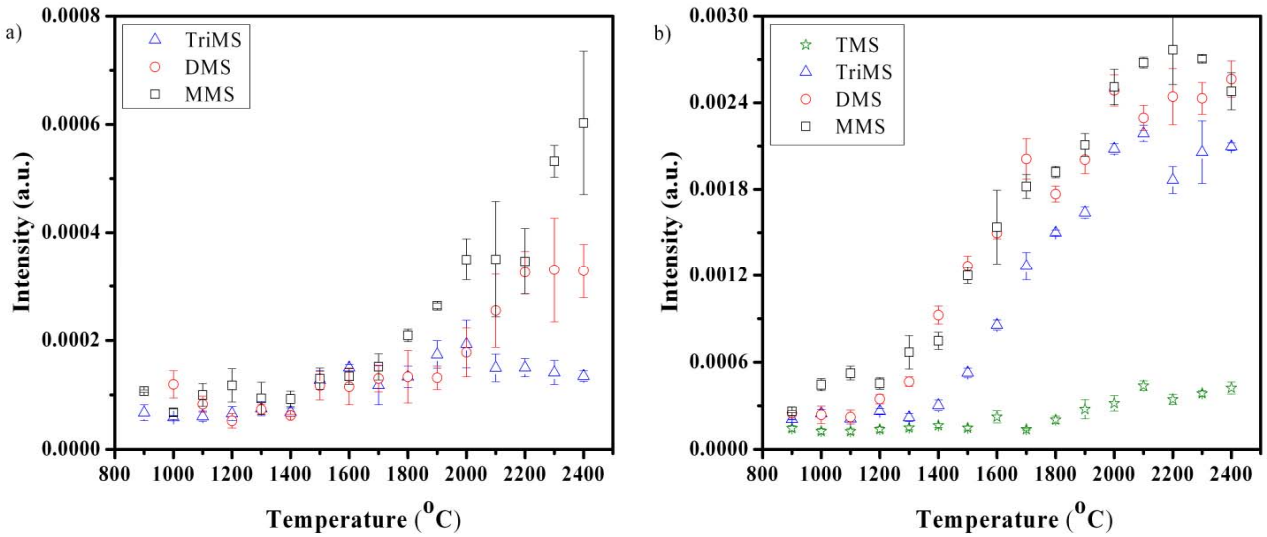


Figure 4-4: The intensity distributions of the peak at *m/z* 2 at different W filament temperatures for MMS, DMS, TriMS and TMS precursors using a) SPI mode, and b) dual SPI/LIEI ionization mode at a chamber pressure of 1×10^{-5} Torr.

As mentioned earlier, since the IE value of H_2 at 15.4 eV[188] is higher than the photon energy in the SPI mode, the decomposition of MMS, DMS, TriMS and TMS were repeated using the dual SPI/LIEI method under the same collision-free conditions to, first of all, confirm the occurrence of this reaction, and secondly to obtain a better indication of the amount of H_2 produced in our system. Figure 4-4b illustrates the temperature evolution of the peak at *m/z* 2 from these methyl-substituted silane samples using the dual SPI/LIEI source. As expected, the intensity of this peak increased with increasing filament temperature, and its intensity was higher compared to those obtained using the SPI method. In addition, the evolution of H_2 from the dissociation of TMS on W can

clearly be seen from Figure 4-4b. Therefore, it was further confirmed that hydrogen molecule was produced during the decomposition of MMS, DMS, TriMS and TMS on a heated filament in a HWCVD process.

As shown in Figure 4-4, a comparison of the intensity profile for H_2 production from the four precursors showed that the intensity of hydrogen molecule increased with increasing filament temperature to around 2000 – 2100 ^{o}C and beyond this temperature, the production of the H_2 molecule from these molecules started to plateau. This behaviour is explained by the transition in the rate-limiting step from surface reaction to mass transport.[36] At low filament temperatures, the reactions at the surface of the filament is dominating and occurring at a lower rate, and as the temperature is increased these surface reaction starts to occur at a faster rate and the transport of the gas to the surface becomes the limiting factor. This behavior was also observed in the study on Si radical formation during the hot-wire decomposition of silane[42, 81] and methyl-substituted silanes[77, 129] as well as for methyl radical formation from these precursors, as explained in Chapter 3.

Additionally, the examination of the intensity profiles in Figure 4-4 reveals that among the four methyl-substituted silane molecules, TMS produces the least amount of hydrogen molecule, while the intensity distribution for the H_2 molecule peak is the highest with MMS, followed by DMS and then TriMS. It is also noticed from this figure that with increasing methyl substitution in the molecule, the temperature at which the peak at *m/z* 2 starts to appear is shifted to a higher value. For MMS and DMS, the peak at *m/z* 2 starts to appear at around 1400 ^{o}C, whereas this temperature was shifted to 1800 ^{o}C for TMS. The formation of H_2 molecules started at 1500-1600 ^{o}C for TriMS.

In addition to the W filament, the primary decomposition of MMS, DMS and TriMS was also studied on a Ta filament. The effect of filament material on the decomposition was illustrated by comparing the H_2 molecule intensity profile from these two filaments as a function of filament temperature from 900 to 2400 ^{o}C, as shown in Figure 4-5. It was found that the intensity profile of H_2 evolution from both filaments is comparable to each other. For both filaments, the intensity of H_2 increased with increasing filament temperature until reaching a plateau at higher temperatures. This suggests that both filaments are equally efficient in forming H_2 molecule. In addition, the hydrogen molecule intensities for the three methyl-substituted silane molecule from the Ta filament has the same trend, *i.e.*, MMS > DMS > TriMS, as the one from W.

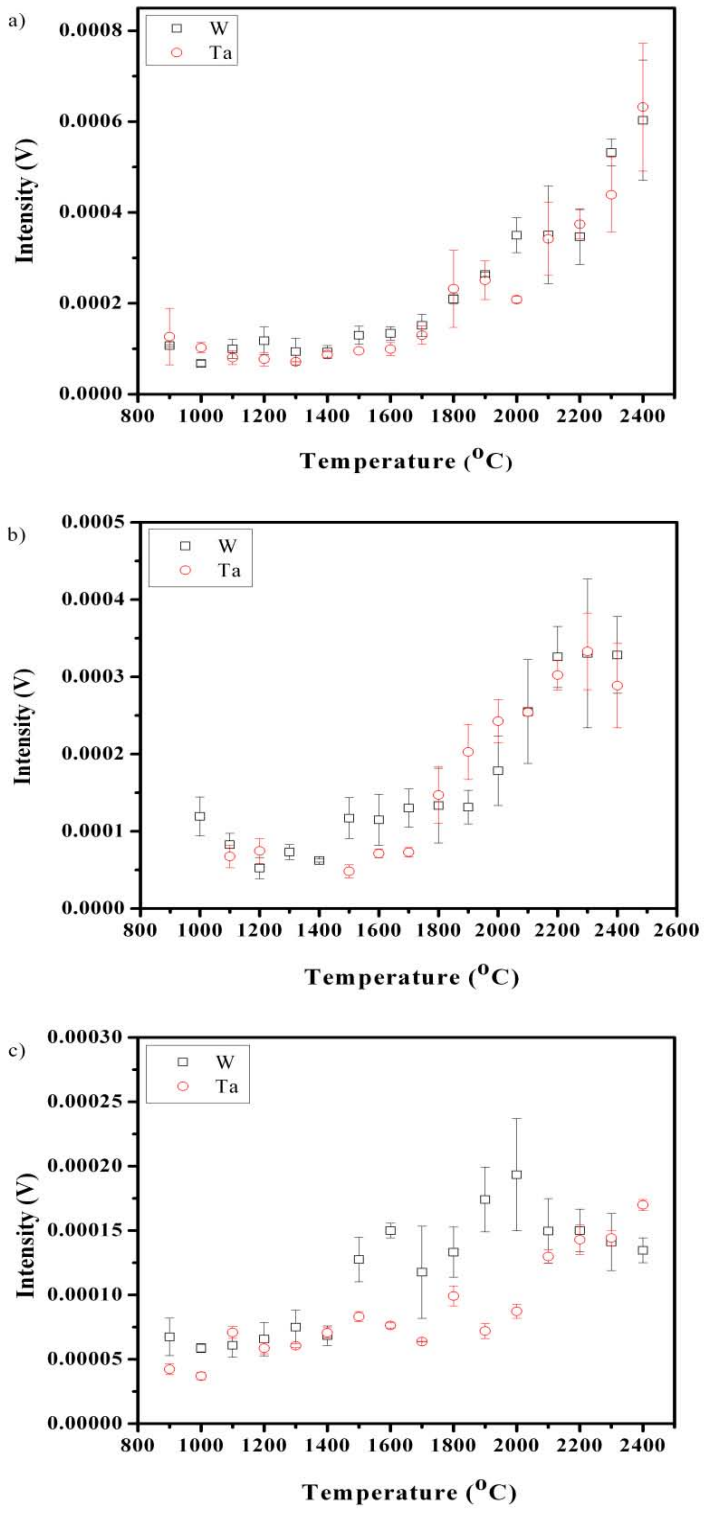


Figure 4-5: Temperature profiles of the normalized intensity of H_2^+ using SPI mode from W and Ta filaments during the dissociation of a) MMS, b) DMS, and c) TriMS samples.

Furthermore, the cleavage of the Si-H bond in MMS, DMS and TriMS, is also believed to occur, as established in several pyrolysis studies on MMS,[178] DMS,[190, 191] and TriMS.[192, 193] Under our experimental conditions, a relatively strong background peak at *m/z* 1 is present in all of the mass spectra, which presents a difficulty in determining the nature of this peak. However, a careful examination of the temperature distribution of this peak revealed that the intensity of the peak at *m/z* 1 increased with increasing W filament temperature, as shown in Figure 4-6. This indicates that H radical is also produced during the dissociation of the four methyl-substituted silane molecules on a heated W filament.

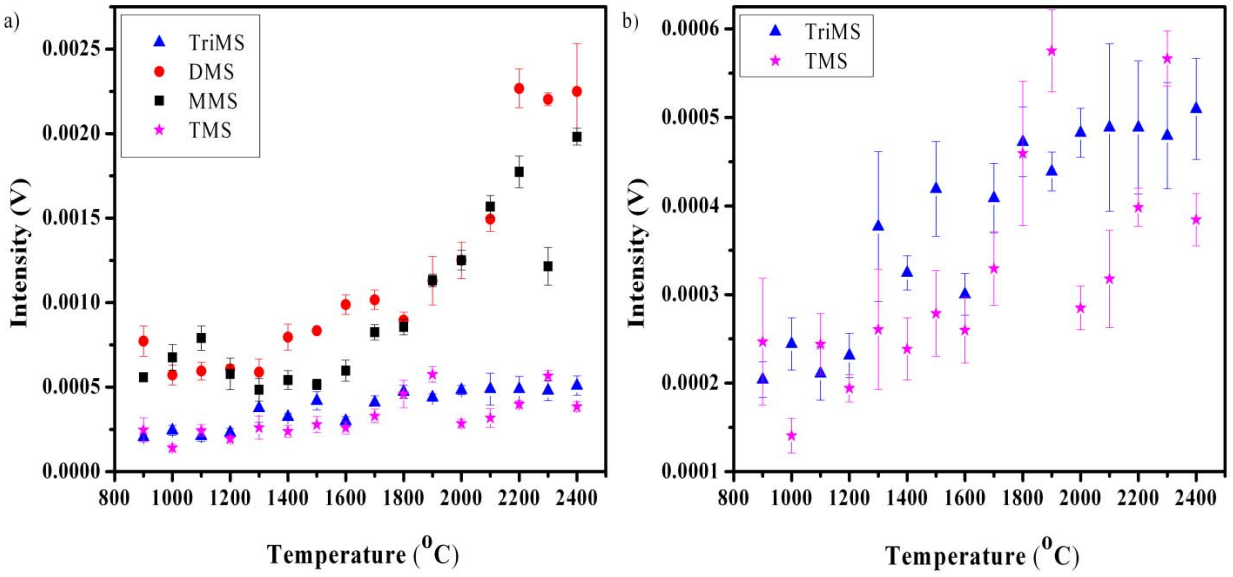


Figure 4-6: a) The intensity evolution of the peak at *m/z* 1 as a function of W filament temperatures for MMS, DMS, TriMS and TMS precursors using SPI ionization source at a chamber pressure of 1×10^{-5} Torr, and b) an enlarged plot for the peak 1 evolution from TriMS and TMS samples.

The observation of the peak at *m/z* 1 has two origins. It can either originate from the ionization of H atom desorbed from the filament surface or the dissociative ionization

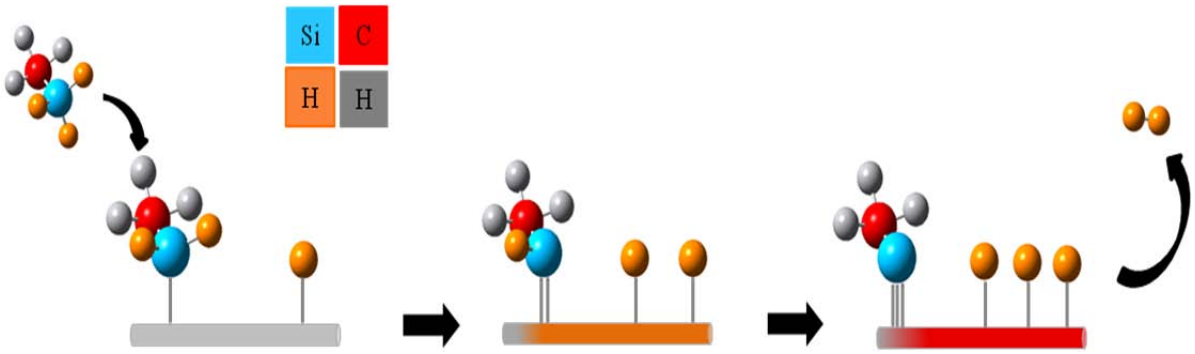
of the formed H_2 molecule. These two possible mechanisms are indicated by the Equation (4-1) and (4-2), respectively.

$$e^- + H \longrightarrow H^+ + 2e^- \quad (4\text{-}1)$$

$$e^- + H_2 \longrightarrow H + H^+ + 2e^- \quad (4\text{-}2)$$

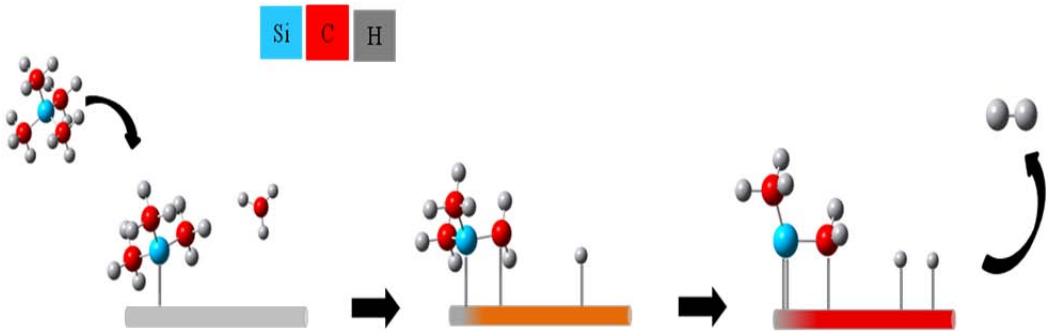
In order to distinguish between these two origins, examination of the ratio of the peak at *m/z* 1 with respect to one for H_2^+ molecule indicated that this ratio actually decreased with increasing filament temperature. With DMS as a precursor, this ratio varied from 8.9 at 900 ^oC to 3.1 at 2400 ^oC. Similar values were obtained from TriMS and MMS. The decrease in the ratio suggests that less amount of H^+ species are produced in the gas phase with increasing temperature as compared to H_2. Since the value of the ratio was not constant, it was concluded that H radical formation proceed via Equation (4-1), which represents the direct ionization of the desorbed H species.

From the results obtained in Chapter 3, it was concluded that the dissociation of methyl-substituted silanes molecules containing Si-H bond on a metal surface proceeds via the breakage of Si-H bond. This initial bond rupture results in the formation of methyl-substituted silyl/silylene/silylyne and hydrogen adsorbates. As the filament surface is covered with hydrogen moieties and the temperature of the filament is increased, desorption of H_2 molecule from the surface takes place. The mechanism is illustrated in scheme 4-1, with MMS as a precursor. This process is found to follow the Langmuir-Hinshelwood mechanism.[194]



Scheme 4-1 Chemisorption and decomposition of MMS on a metal surface

The detection of H_2 molecule during the decomposition of TMS on a heated W filament indicates that C-H bond in CH_3 is broken, since TMS does not contain Si-H bonds in its structure. Roberts *et al.*[151] found that at low coverage weakly adsorbed methyl-substituted silyl species exist together with reversibly adsorbed hydrogen on tungsten at 293 K, but with an increased coverage only reversible hydrogen exists together with irreversibly adsorbed carbon- and silicon-containing species. Therefore, the dissociation of TMS on W surface proceeds via the cleavage of Si-CH_3 bond and C-H bond resulting in the formation of methyl-substituted silyl/silyl-CH_2(ads)/silylene-CH_2(ads), and hydrogen adsorbates. The mechanism is illustrated by scheme 4-2.



Scheme 4-2 Chemisorption and decomposition of TMS over a metal surface

Hence, it is believed that, unlike the pyrolysis studies, the H_2-elimination process of methyl-substituted silanes in the HWCVD process takes place on the surface of the filament rather than in the gas phase. This mechanism is further supported by the experiments performed using the isotopomers under the same experimental conditions, which is discussed in the next section.

4.4 Experiments with MMS-d_3, DMS-d_2 and TriMS-d_1

To better understand the mechanism involved in the H_2-elimination process, experiments with the deuterated isotopomers, including TriMS-d_1, DMS-d_2 and MMS-d_3, were carried out using the dual SPI/LIEI ionization source. After turning the W filament on, a careful examination of the mass spectra in the low mass region revealed the appearance of new mass peaks at *m/z* 2, 3 and 4 for MMS-d_3 and DMS-d_2 samples, and peaks only at *m/z* 2 and 3 for TriMS-d_1. Figure 4-7a shows the mass spectra for MMS-d_3 where it presents the evolution of these new peaks at different filament temperatures. Similar mass spectra were collected for DMS-d_2 (Figure 4-7b) and TriMS-d_1 (Figure 4-7c). The peaks at *m/z* 2, 3 and 4 are associated with the formation of D, HD and D_2 species, respectively, during the decomposition of MMS-d_3, DMS-d_2 and TriMS-d_1 on a W filament, and their intensities were plotted at different filament temperatures, as illustrated in Figure 4-8. From the intensity profiles, it was noticed that the intensity of the peaks at *m/z* 2, 3 and 4 increased with increasing filament temperature.

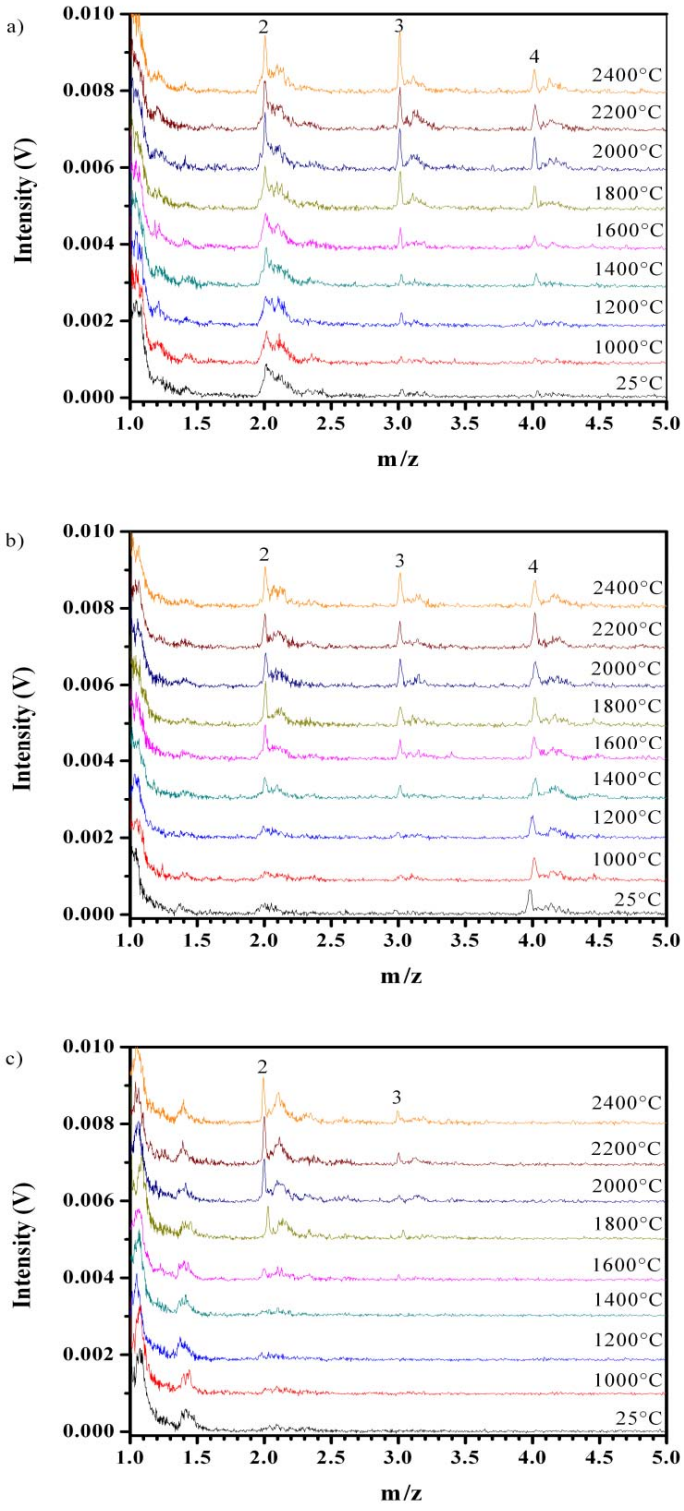


Figure 4-7: SPI/LIEI TOF mass spectra of pure a) MMS-d_3, b) DMS-d_2 and c) TriMS-d_1 in the mass region 1 - 5 amu at filament temperatures ranging from 25 °C - 2400 °C and a chamber pressure of 1×10^{-5} Torr.

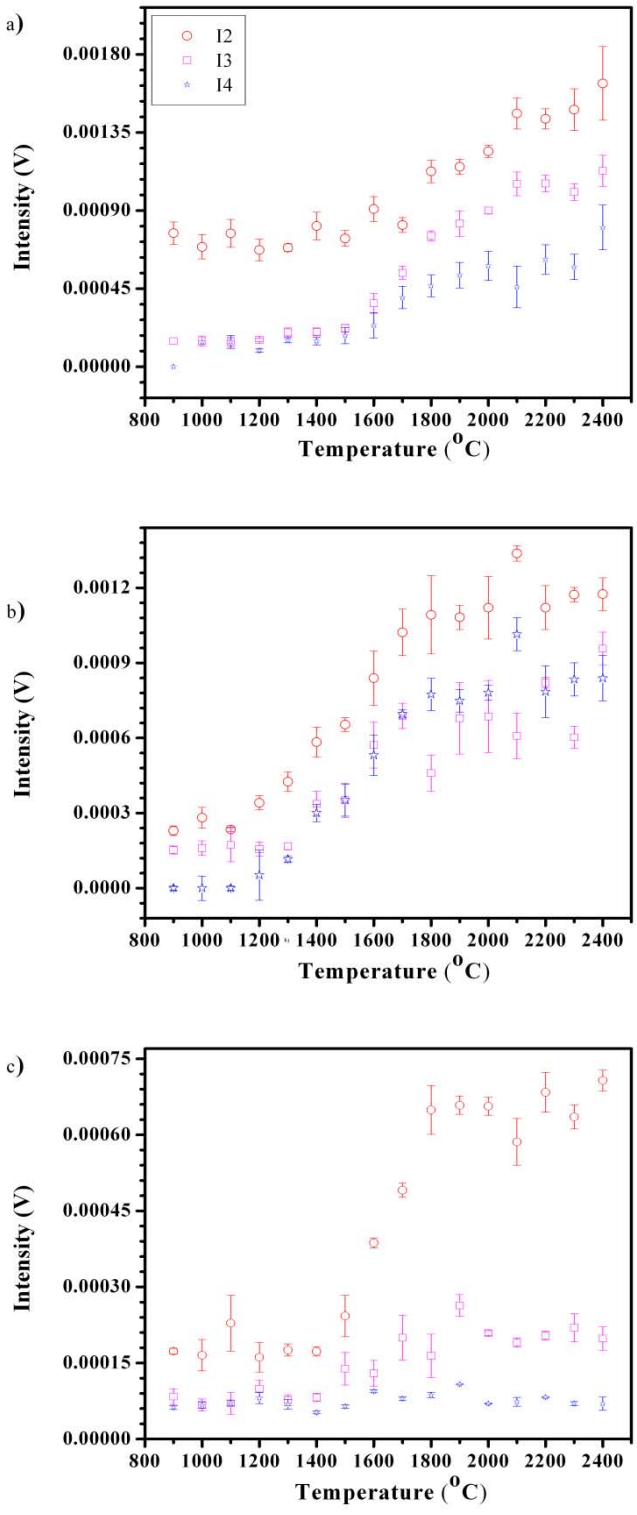
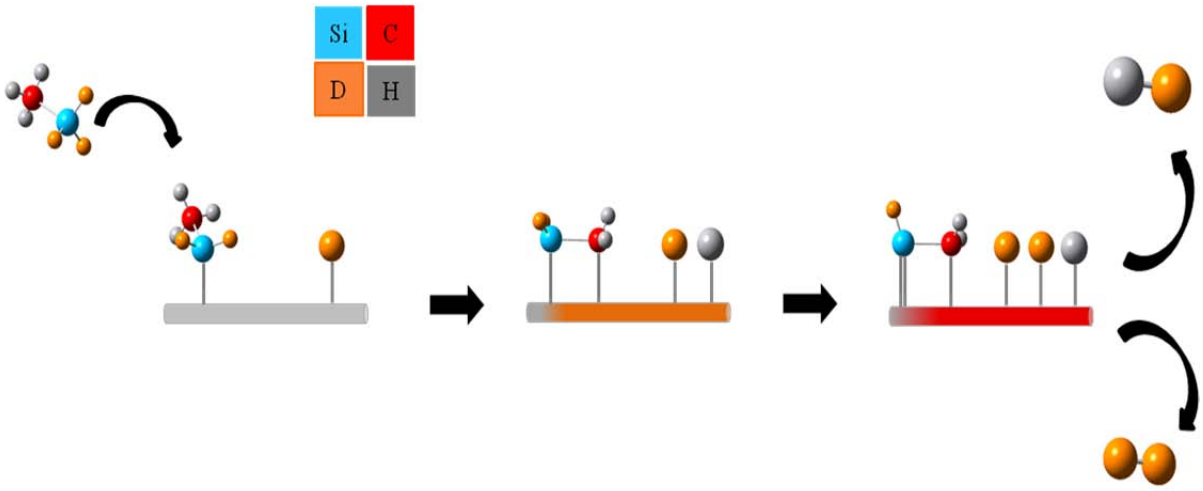


Figure 4-8: The intensity evolution of the peaks at *m/z* 2, 3 and 4 at different W filament temperatures for a) MMS-d_3, b) DMS-d_2, and c) TriMS-d_1 precursors using the dual SPI/LIEI ionization source.

As it has been demonstrated in section 4.3 and in our study on methyl formation in Chapter 3, the primary decomposition of MMS, DMS, and TriMS occurs on the surface of the heated metal filament and is initiated by the cleavage of the Si-H bond. This bond cleavage is confirmed by the appearance of a peak at *m/z* 2 which represents the rupture of the Si-D bond in all the corresponding isotopomers of the three molecules resulting in the formation of the D atom and methyl-substituted silyl adsorbates. The observation of peak *m/z* 4, representing D_2^+, confirms the occurrence of Langmuir-Hinshelwood mechanism, in which two atomic hydrogen adsorbates combine to form hydrogen molecules. Similarly to H_2 formation, this process is initiated by the rupture of Si-D bond resulting in the presence of methylsilyl and D adsorbates on the surface of the filament. As the temperature is raised, a high surface coverage is achieved, consequently desorption of D(ads) to form D_2 occurs. This mechanism is illustrated by scheme 4-3. Therefore, despite the fact most of the pyrolysis studies[94, 177, 180, 191, 195-198] claim that the formation of H_2 takes place via molecular elimination mechanism, it is believed that, in this current study, the formation of H_2 follows Langmuir-Hinshelwood mechanism rather than a molecular elimination mechanism.



Scheme 4-3 Chemisorption and decomposition of MMS-d_3 on a metal surface

For the peak at *m/z* 3, its detection is explained by the existence of C-H bond cleavage resulting in the presence of H and D moieties on the surface of the filament. Previous studies of the adsorption of methyl-substituted silanes on metal surfaces have demonstrated that they are dissociatively chemisorbed on the surface.[150, 151] In a study on the reactions of MMS at the surface of Ni, Rd and W, Bradshaw *et al.*[150] have found that a slight exchange between the deuterium and hydrogen atoms evolved from dehydrogenation of the methyl group as the temperature is increased. Based on the results obtained for TMS in this current study and also from a previous study,[151] the cleavage of C-H bond in MMS-d_3, DMS-d_2, and TriMS-d_1 is probable in addition to the rupture of the Si-D bond. Hence, the observation of the peak at *m/z* 3 indicates that during the decomposition of methyl-substituted silanes a dehydrogenation from methyl groups under our experimental conditions is also occurring. This mechanism is also illustrated by scheme 4-3. The occurrence of this process can further be confirmed by examining the intensity profile of this peak, shown in Figure 4-9. From the results obtained for TMS, H_2

molecule started to be formed at a temperature around 1600-1800 ^{o}C. This temperature is indicative of C-H bond rupture taking place. By examining the temperature profile of peak at *m/z* 3 for the three deuterated methyl-substituted silanes, it was noted that this peak started to appear within the similar temperature range, which coincides with C-H bond cleavage. Hence, this observation confirms that during the decomposition of methyl-substituted silane molecules, the rupture of the C-H bond is also taking place during the HWCVD process

In addition to obtaining an understanding of the mechanism involved in the process of hydrogen elimination, the dominance of bond cleavage of Si-H (Si-D) versus C-H is also examined. An analysis of the intensity profile of the peaks at *m/z* 2, 3 and 4 obtained in our system, shown in Figure 4-8, revealed that the rupture of Si-D bond, which was represented by a peak at *m/z* 2, was the major initiation step occurring during the decomposition of MMS, DMS and TriMS on a heated W filament, assuming the ionization cross sections for peaks at *m/z* 2, 3 and 4 are the same. Therefore, the presence and the dominance of the peak at *m/z* 2, representing deuterium atom, from the isotopomer experiments suggest that under our experimental conditions H_2 formation proceeds in a stepwise mechanism by the formation of hydrogen adsorbates on the metal filament surface. This adsorption process is in agreement with the previous studies on the exposure of the metal surface to methyl-substituted silanes.[156] As the temperature of the filament is increased, a recombination reaction between adjacent H atoms takes place releasing H_2 molecule to the gas phase, following Langmuir-Hinshelwood mechanism. In addition, the observation of peak at *m/z* 3 suggests the occurrence of C-H bond cleavage in methyl-substituted silane molecules in a HWCVD process.

4.5 The Activation Energy of Forming H_2 Molecules on W and Ta

Under the collision-free conditions, where the gas flow rate is constant, the detected hydrogen molecule intensity shown in Figure 4-4 is proportional to the net production rate of the hydrogen molecule.[199] An examination of the temperature evolution for the formation of H_2 during the decomposition of TriMS, DMS and MMS under collision-free conditions revealed an Arrhenius behaviour.

From the plotted data, the apparent activation energy (E_a^{APP}) of H_2 production from W filament was extracted and found to be 70.7 ± 7.4 kJ · mol^{-1} for TriMS, 68.1 ± 5.8 kJ · mol^{-1} for DMS, and 55.4 ± 5.4 kJ · mol^{-1} for MMS in the filament temperatures ranging from 1200 - 1500 ^{o}C to 2200 - 2400 ^{o}C. This is illustrated in a bar diagram in Figure 4-9. These values are significantly lower than their respective Si-H bond dissociation energies (BDE) which are 374.89, 374.05, and 377.82 kJ · mol^{-1} for MMS, DMS and TriMS, respectively.[37] This comparison indicates that the elimination of H_2 during the decomposition of MMS, DMS and TriMS on a heated filament is a catalytic process. For TMS, the H_2^+ peak intensity was extremely weak so that it was not possible to extract meaningful activation energies values.

An examination of E_a^{app} values in Figure 4-9 revealed that the apparent activation energy for the formation of H_2 molecules increased with increasing methyl group present in the precursor molecule. This trend implies that the decrease in the number of methyl group and the corresponding increase in the number of H atoms results in a lowering in the apparent energy barrier required for the cleavage of the Si-H bond. This is in good agreement with the results from the previous study[61] where it was found that the E_a for the Si radical formation when using the same four precursor increases with increasing

methyl substitution in the precursor molecules. This finding is also in agreement with the results obtained in Chapter 3 regarding the activation energy of forming methyl radicals. As explained in Chapter 3, the increase of methyl substitution on the Si atom will result in strengthening of Si-H bond, yielding a higher energy that is required to cleave this bond.

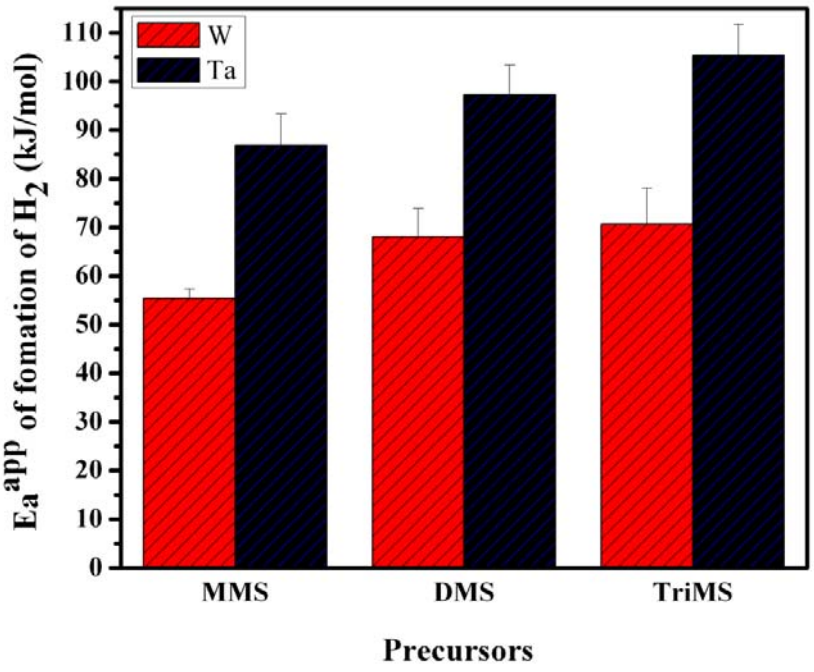


Figure 4-9: Apparent activation energy for hydrogen molecule formation from MMS, DMS and TriMS on the two filaments of tungsten and tantalum.

In addition, the effect of filament material was investigated by comparing the E_a^{app} values for H_2 formation during the decomposition of pure samples of MMS, DMS and TriMS on a W and Ta filament. Figure 4-9 shows the comparison of the apparent activation energy for H_2 on the two filaments. As noted from the bar graphs, the usage of a Ta filament resulted in higher E_a^{app} values. This observed behaviour is attributed to the

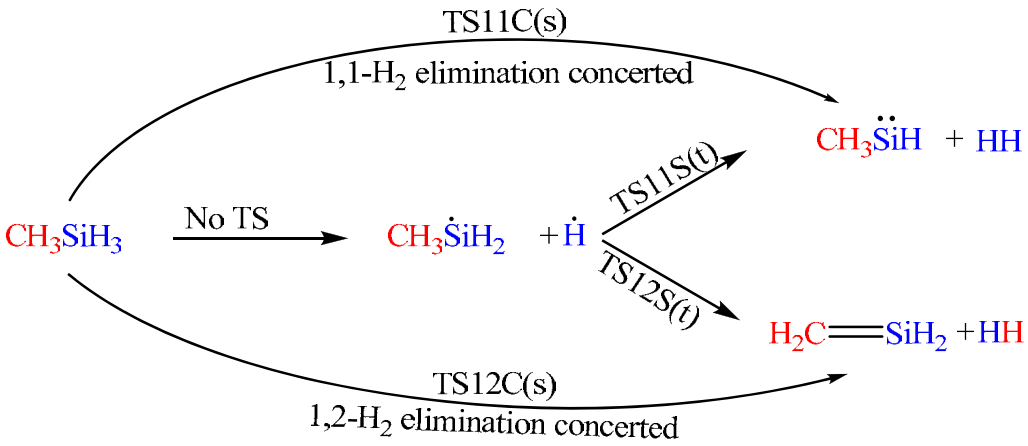
different strength of the binding energy of H atom to either of the metal surfaces. Both theoretical[200] and experimental[201] studies have stated that the binding energy of H on Ta has a value of 93 – 99 kcal/mol (*i.e.*, a 389 – 414 kJ/mol) and 75 – 76 kcal/mol (*i.e.*, a 314 – 318 kJ/mol)on W. This explains the difference in E_a^{app} values obtained under our experimental conditions. In a way, it will require more energy to break the bond between H and Ta than the H-W bond. Additionally, the value of desorption energy of H_2 from a metal surface was examined. It was found that the desorption energy from W varies from 1.7 to 2.0 eV (*i.e.*, *a* 164.0 – 190.0 kJ/mol), and from Ta this value was between 2.9 and 3.1 eV (*i.e.*, *a* 279.8 – 299.1 kJ/mol).[202] A comparison between these values showed that the obtained E_a^{app} values for the formation of H_2 molecules under our experimental conditions is much lower than both the H_2 desorption energy and relevant bond breaking energy. These lower energy values are attributed to the formation of Si-X (X= W or Ta) bond occurring concurrently with Si-H bond scission, resulting in the lowering of the energy barrier.[158] The same conclusion was obtained for methyl radical formation, as explained in Chapter 3.

4.6 1,1-H_2 and 1,2-H_2 Elimination: A Theoretical Study

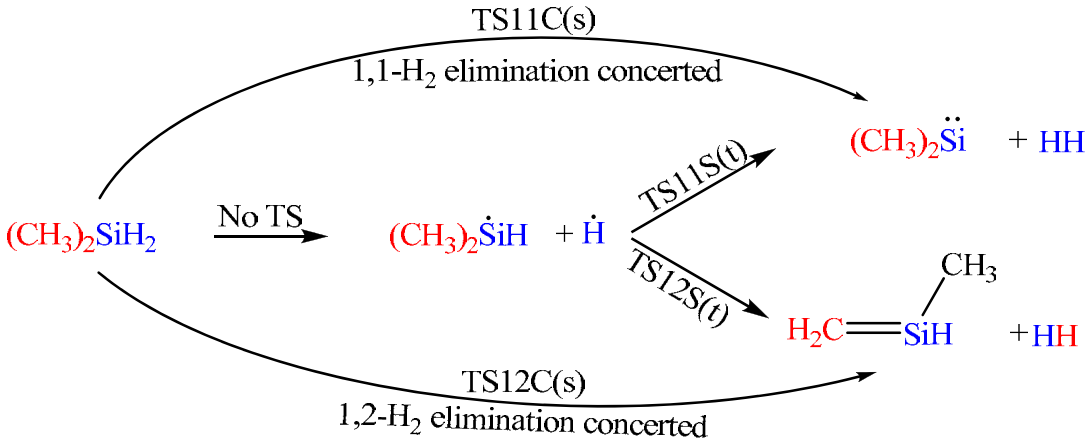
From the previous discussions, it was demonstrated that the process of hydrogen formation during the decomposition of methyl-substituted silane molecules in a HWCVD system occurs at the surface of the heated metal filament and follows the Langmuir-Hinshelwood mechanism. However, the results from pyrolysis studies in the literature claim that the evolution of H_2 proceeds via molecular elimination process. To confirm the role of the metal surface, *ab initio* calculations on the formation of H_2 in the gas phase

and on the surface were planned. As a first step, the reactions in the gas phase were investigated. To our knowledge, there have been no reports on a systematic study on the decomposition of these methyl-substituted silanes using the *ab initio* methods. In this work, the competition between 1,1- and 1,2-H_2 elimination is explored for MMS, DMS and TriMS using the second-order Møller-Plesset (MP2) perturbation theory[125] and coupled cluster methods with single, double and perturbative triple excitations (CCSD(T)).[126] The reactions of interest involved the 1,1- and 1,2-H_2 elimination from MMS, DMS and TriMS by either a concerted or a stepwise mechanism. For each reaction, the transition state was located and the activation energy barrier was computed. In addition, reaction enthalpies, Gibbs free energies and entropies were calculated in order to provide a thermochemical understanding of the reactions studied.

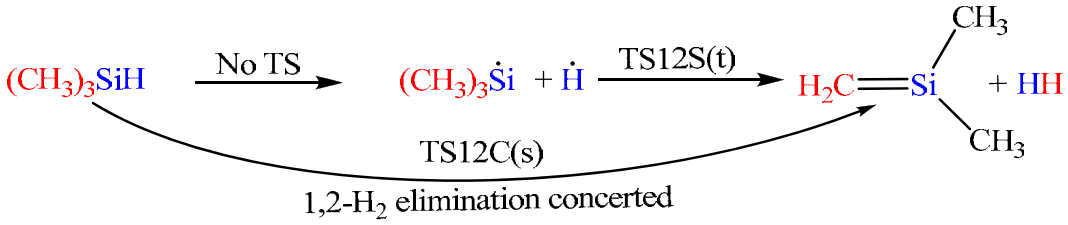
Schemes 4-4, 4-5, and 4-6 illustrate both the concerted and stepwise routes for 1,1- and 1,2-H_2 elimination reactions of MMS, DMS and TriMS, respectively. Aside from H_2, the concerted 1,1-, and 1,2-H_2 eliminations produced various silylene and silene intermediates, respectively.



Scheme 4-4 Stepwise and concerted 1,1- and 1,2-H_2 elimination reactions for MMS



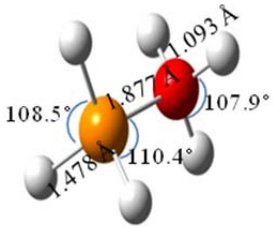
Scheme 4-5 Stepwise and concerted 1,1-, and 1,2-H_2 elimination reactions for DMS



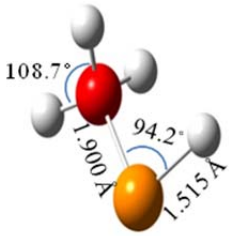
Scheme 4-6 Stepwise and concerted 1,2-H_2 elimination reactions for TriMS

The optimized structures for each of the reactants and products involved in each of the mechanisms for the three molecules are shown in Figures 4-10 to 4-12. The geometry parameters for the parent molecules are consistent with the experimental values obtained by Bond *et al*. using the electron-diffraction method.[203]

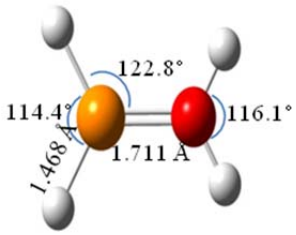
a) Monomethylsilane



b) Methylsilylene



c) Silene

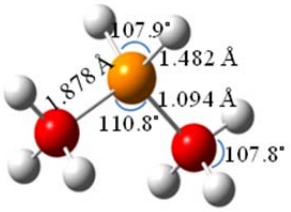


d) Methylsilyl

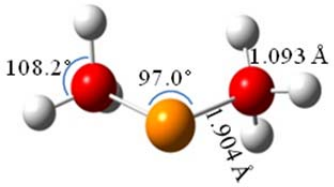


Figure 4-10: Optimized structures of a) monomethylsilane, b) methylsilylene, c) silene, and d) methylsilyl involved in the concerted and stepwise 1,1-, and 1,2-H_2 elimination mechanism of MMS.

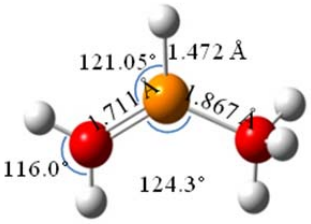
a) Dimethylsilane



b) Dimethylsilylene



c) Methylsilene



d) Dimethylsilyl

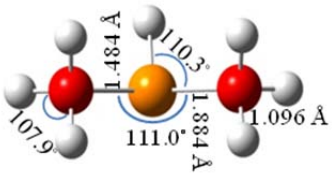
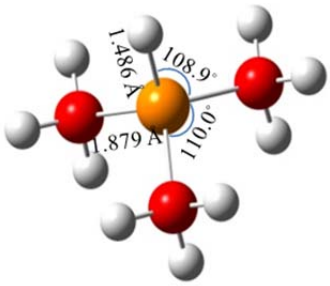
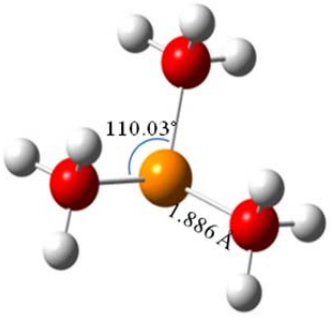


Figure 4-11: Optimized structures of a) dimethylsilane, b) dimethylsilylene, c) methylsilene, and d) dimethylsilyl involved in the concerted and stepwise 1,1-, and 1,2-H_2 elimination mechanism of DMS.

a) Trimethylsilane



b) Trimethylsilyl



c) Dimethylsilene

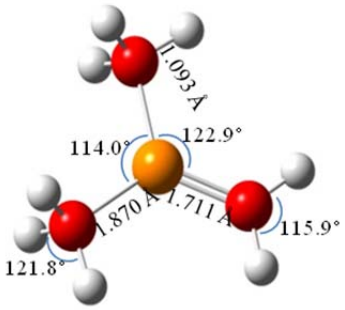


Figure 4-12: Optimized structures of a) trimethylsilane, b) trimethylsilyl, and c) dimethylsilene involved in the concerted and stepwise 1,1-, and 1,2-H_2 elimination mechanism of TriMS.

For the stepwise processes, the reaction starts with the Si-H bond cleavage to form a methyl-substituted silyl and H radicals. Then, the H radical captures a second H bonded to either Si resulting in 1,1-H_2 elimination, or a neighbouring C atoms leading to 1,2-H_2 elimination, along with the corresponding co-products. It should be noted that the final products from the stepwise mechanism are the same as the concerted ones. In the stepwise mechanism, the rate-determining step, which is the first step involving the homolytic cleavage of the Si-H generating methylsilyl and hydrogen radicals, was found to proceed without a transition state.

The corresponding transition states for the concerted steps have been located, and are labeled TS11C and TS12C. Those for the second steps in the stepwise process have also been located, and are labeled as TS11S and TS12S for the 1,1- and 1,2-H_2 eliminations, respectively. The optimized structures for these four transition states involved in the H_2 eliminations from each of MMS, DMS and TriMS are shown in Figures 4-13 to 4-15. The transition states in the stepwise mechanisms were optimized on a triplet surface since the singlet TS could not be located at the MP2 level.

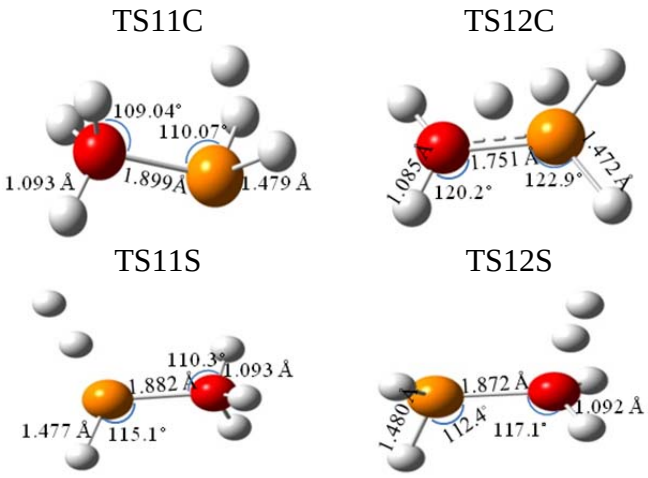


Figure 4-13: Optimized structures of the transition states for the concerted and stepwise H_2 elimination processes from MMS.

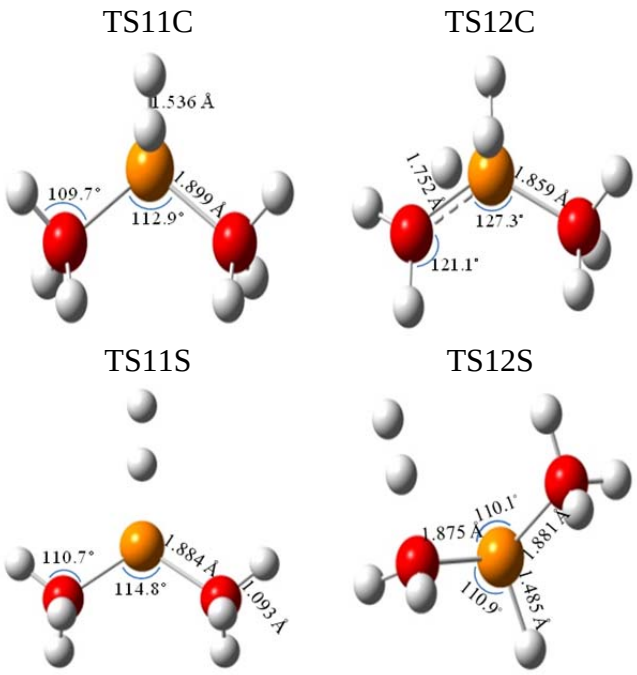


Figure 4-14: Optimized structures of the transition states for the concerted and stepwise H2 elimination processes from DMS.

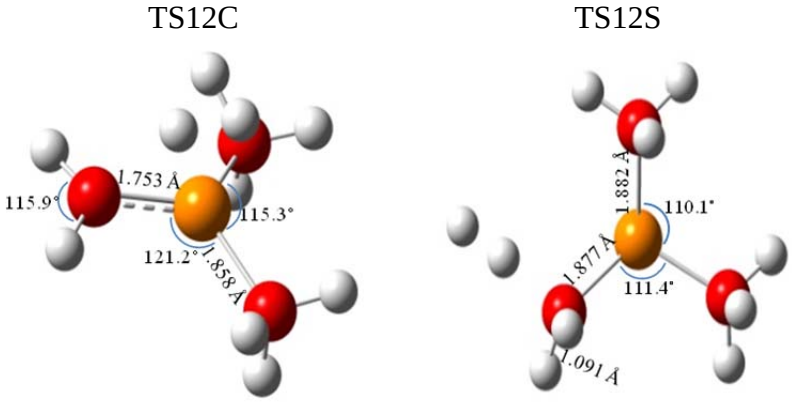


Figure 4-15: Optimized structures of the transition states for the concerted and stepwise H2 elimination processes from TriMS.

The energy level diagrams for all of the reactions under study for each of the three molecules were shown in Figures 4-16 to 4-18. From these diagrams, it was concluded

that all of the studied reactions were endothermic. The concerted mechanism for all of the studied reactions produces singlet products, whereas the ones from the stepwise mechanism are in the triplet state. A comparison of the energy of the final products produced from concerted and stepwise mechanism revealed that the ones generated following the stepwise mechanism have a higher energy. For example, with MMS, the products from the concerted 1,1-process have an energy value of 52.1 and 49.1 kcal/mol (*i.e.*, a 217.9 – 205.4 kJ/mol) for singlet silylene and silene, respectively, and the corresponding ones in the triplet state have an energy of 74.9 and 100.1 kcal/mol (*i.e.*, a 313.4 – 418.8 kJ/mol). This comparison is also valid for DMS and TriMS. Hence, it can be concluded that the products from concerted reactions are thermodynamically more favourable for all of the molecules. The energy values for the various methyl-substituted silylene and silene species from 1,1- and 1,2-H_2 eliminations are summarized in Table 4-1 and 4-2. When comparing the total energy of the products from MMS, DMS, and TriMS decomposition, it was noticed that their energies decreased with methyl substitution, suggesting that the increase of methyl groups in silene or silylene species stabilizes them energetically. This is in agreement with the literature.[204] Furthermore, from this table, it can be noticed that methyl-substituted silene are more stable than their corresponding silylene species in the singlet state. Examination of the energies of these species at the triplet state revealed that methyl-substituted silylene are the ones energetically more stable.

Table 4-1 Total energies of singlet silene and methylsilylene species and corresponding zero point energies (ZPE) in Hartee's at CCSD(T)/6-311++G(d,p) level

State	*Silene(s)*			*Methylsilylene(s)*		
	Energy	ZPE	$\mathbf{E_{Total}}$	Energy	ZPE	$\mathbf{E_{Total}}$
Singlet	-329.3974	0.0402	**-329.3572**	-329.3949	0.0425	**-329.3524**
	Methylsilene(s)			Dimethylsilylene(s)		
	Energy	ZPE	$\mathbf{E_{Total}}$	Energy	ZPE	$\mathbf{E_{Total}}$
Singlet	-368.6361	0.0699	**-368.5662**	-368.6349	0.0719	**-368.5630**
	Dimethylsilene(s)					
	Energy	ZPE	$\mathbf{E_{Total}}$			
Singlet	-407.8753	0.0990	**-407.7763**			

Table 4-2 Total energies of triplet silene and methylsilylene species and corresponding zero point energies (ZPE) in Hartee's at CCSD(T)/6-311++G(d,p) level

State	*Silene(t)*			*Methylsilylene(t)*		
	Energy	ZPE	$\mathbf{E_{Total}}$	Energy	ZPE	$\mathbf{E_{Total}}$
Triplet	-329.3111	0.0362	**-329.2749**	-329.3594	0.0434	**-329.3160**
	Methylsilene(t)			*Dimethylsilylene(t)*		
	Energy	ZPE	$\mathbf{E_{Total}}$	Energy	ZPE	$\mathbf{E_{Total}}$
Triplet	-368.5766	0.0687	**-368.5079**	-368.5939	0.0733	**-368.5206**
	Dimethylsilene(t)					
	Energy	ZPE	$\mathbf{E_{Total}}$			
Triplet	-407.7929	0.0995	**-407.6934**			

A comparison between the two concerted reactions shows that the 1,1-H_2 elimination reactions occurring via TS11C for both MMS and DMS require less energy barrier with respect to the 1,2-H_2 elimination via TS12C. The energy barrier for concerted

1,1-H_2 elimination was 62.0 kcal/mol (*i.e.*, a 259.4 kJ/mol) for MMS and 66.3 kcal/mol (*i.e.*, a 277.4 kJ/mol) for DMS. The corresponding value for concerted 1,2-H_2 elimination was 92.9 kcal/mol (*i.e.*, a 388.7 kJ/mol) for MMS and 89.5 kcal/mol (*i.e.*, a 374.5 kJ/mol) for DMS. The activation energy values for the concerted H_2-elimination process with MMS are in reasonable agreement with those obtained by Gordon *et al.* [180], which were determined to be 65.6 and 100.9 kcal/mol (*i.e.*, a 274.5 and 422.2 kJ/mol) for 1,1- and 1,2-H_2 elimination, respectively.

For the stepwise mechanism, the energy needed in the cleavage of the Si-H bond in the first step, generating two radicals, was calculated to be 88.6 kcal/mol (*i.e.*, a 370.7 kJ/mol) for MMS, 89.5 kcal/mol (*i.e.*, a 374.5 kJ/mol) for DMS, and 90.2 kcal/mol (*i.e.*, a 377.4 kJ/mol) for TriMS. These determined Si-H bond energy values were in agreement with the previous *ab initio* calculation[205] as well as the experimental values.[206] In the second step of the stepwise mechanism in the MMS decomposition, an energy barrier of 4.6 and 11.5 kcal/mol (*i.e.*, a 19.3 and 48.1 kJ/mol) was needed to reach the transition state for the 1,1- and 1,2-elimination processes, respectively. From DMS, the energy required to overpass the respective barriers was 4.8 and 11.1 kcal/mol (*i.e.*, a 20.1and 46.4 kJ/mol) in the 1,1- and 1,2-eliminations. During the dissociation of TriMS, the energy barrier for the second step was 10.9 kcal/mol (*i.e.*, a 45.6 kJ/mol) from the trimethylsilyl and hydrogen radicals. Hence, as illustrated by the energy diagrams, it can be concluded that among all of the reactions studied for MMS and DMS, the concerted 1,1-H_2 elimination mechanism occurred with the lowest activation barrier. The energy barriers for concerted 1,2-H_2 elimination and the rate-determining step in the stepwise mechanism are comparable for all three molecules.

The activation energy for H_2 formation was found to be 68.0 kcal/mol[94] (*i.e.*, a 285.0 kJ/mol) and 64.8 kcal/mol[94, 176, 177] (*i.e.*, a 271.1 kJ/mol) from the pyrolytic decomposition of DMS and MMS, respectively. These values represent the apparent energy barriers for H_2 elimination as a whole, since it was not possible to distinguish between the two mechanisms experimentally. However, a comparison between these experimental values and the ones obtained computationally in this work showed that the experimental data are comparable to the activation barriers for concerted 1,1-H_2 elimination process for DMS and MMS. Therefore, our calculation results are in agreement with the observation that 1,1-H_2 elimination mechanism is the favoured and dominant pathway for the formation of H_2 molecule during the pyrolysis of MMS and DMS. For TriMS, the absence of 1,1-elimination pathway and the comparable activation barrier for concerted and stepwise 1,2-elimination may provide an explanation of a mechanism switch in the H_2 formation mechanism. As mentioned before, Davidson *et al*.[192, 207] have shown that, during the pyrolysis of TriMS, H_2 production involved a stepwise process where the H radical is first produced and then abstract the hydrogen atom from the parent molecule.

It is worth noting the difference between the E_a^{app} obtained under HWCVD conditions in section 4-5 and the *ab initio* calculations presented here. A comparison of these values revealed that the experimental E_a^{app} values were significantly lower than the calculated ones for all molecules. This observation was expected, since the theoretical study carried out is on the decomposition processes in the gas phase, whereas experimentally, there is the presence of a metal surface, which serves as a catalyst and results in lower Ea values.

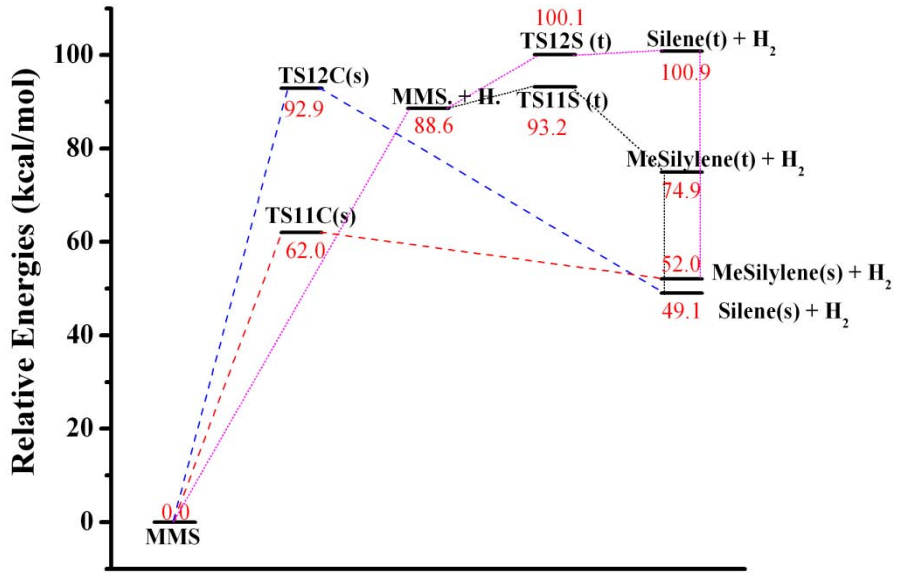


Figure 4-16: Energy level diagrams for the 1,1-, and 1,2- H_2 elimination pathways of MMS. For each pathway, both stepwise and concerted mechanisms were investigated. Energy values represent the relative enthalpies in kcal/mol at 0 K (ZPE corrections included).

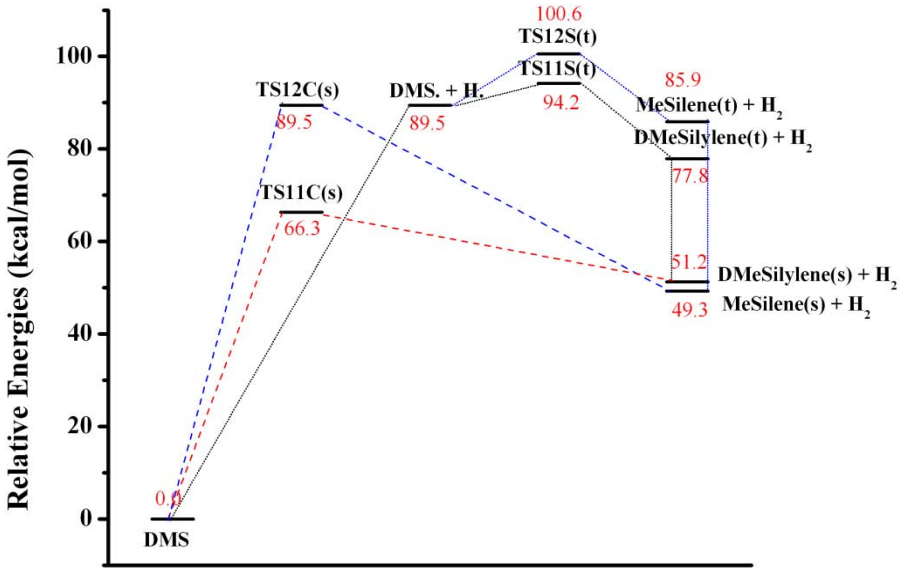


Figure 4-17: Energy level diagrams for the 1,1-, and 1,2- H_2 elimination pathways of DMS. For each pathway, both stepwise and concerted mechanisms were investigated. Energy values represent the relative enthalpies in kcal/mol at 0 K (ZPE corrections included).

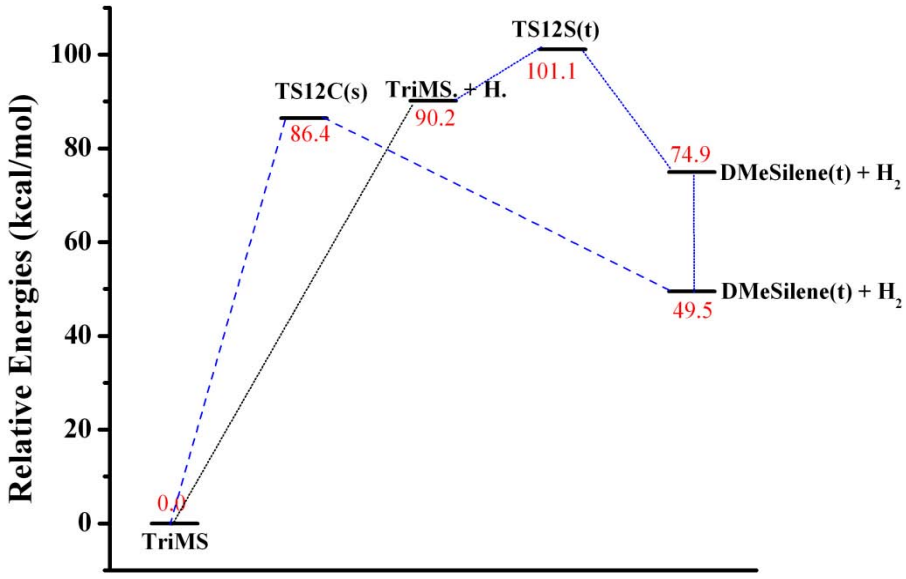


Figure 4-18: Energy level diagrams for the 1,2- H_2 elimination pathways of TriMS. For each pathway, both stepwise and concerted mechanisms were investigated. Energy values represent the relative enthalpies in kcal/mol at 0 K (ZPE corrections included).

In addition, a thermochemical study was carried out for the various decomposition pathways of DMS and MMS represented in Scheme 4-4 and 4-5 using CCSD(T)/6-311++G(3d,2p)//MP2/6-311++G(d,p). Table 4-3 and 4-4 list, respectively, the values of activation enthalpies ($\Delta H_0^{\neq}$) and reaction enthalpies (ΔH_0) for these reactions. The subscript 0 indicates values obtained at 0 K.

Table 4-3 Activation enthalpies, entropies, and Gibbs free energies for the various decomposition pathways of MMS and DMS

	Reaction	Transition state	$\Delta H_0^{\neq}$ *(kcal/mol)*	$\Delta H_{298}^{\neq}$ *(kcal/mol)*	$T\Delta S_{298}^{\neq}$ *(kcal/mol)*	$\Delta G_{298}^{\neq}$ *(kcal/mol)*
MMS (Scheme 4-4)	Concerted 1,1-H_2 elimination	TS11C	62.0	62.0	0.7	61.3
	Concerted 1,2-H_2 elimination	TS12C	92.9	93.0	0.8	92.2
	Stepwise 1,1- / 1,2-H_2 elimination		88.5	88.5	8.6	79.9
DMS (Scheme 4-5)	Concerted 1,1-H_2 elimination	TS11C	66.3	66.3	0.4	65.9
	Concerted 1,2-H_2 elimination	TS12C	89.4	89.4	0.3	89.1
	Stepwise 1,1- / 1,2-H_2 elimination		89.4	89.3	8.5	80.8

Table 4-4 The reaction enthalpies, entropies, and Gibbs free energies for the various decomposition pathways of MMS and DMS

		Products	ΔH_0 *(kcal/mol)*	ΔH_{298} *(kcal/mol)*	$T\Delta S_{298}$ *(kcal/mol)*	ΔG_{298} *(kcal/mol)*
MMS (Scheme 4-4)	1,1-Concerted	Methylsilylene(s) + H_2	52.0	54.0	9.6	44.4
	1,1-Stepwise	Methylsilylene(t) + H_2	74.9	76.8	10.3	66.6
	1,2-Concerted	Silene(s) + H_2	49.0	50.9	8.8	42.1
	1,2-Stepwise	Silene(t) + H_2	100.8	102.7	10.4	92.4
DMS (Scheme 4-5)	1,1-Concerted	Dimethylsilylene(s) + H_2	51.2	53.2	9.6	43.6
	1,1-Stepwise	Dimethylsilylene(t) + H_2	77.8	79.8	10.6	69.2
	1,2-Concerted	Methylsilene(s) + H_2	49.2	51.0	9.1	41.9
	1,2-Stepwise	Methylsilene(t) + H_2	85.8	87.7	9.6	77.9

As shown in the tables, the concerted 1,1-H_2 elimination had the lowest energy barrier for both molecules followed by the stepwise mechanism with an energy barrier of

88.5 kcal/mol (*i.e.*, a 370.3 kJ/mol) for MMS and 89.4 kcal/mol (*i.e.*, a 374.1 kJ/mol) for DMS. Interestingly, the concerted mechanism for the 1,2-H_2 elimination resulted in the highest activation barrier of 92.9 and 89.4 kcal/mol (*i.e.*, a 388.7 and 374.1 kJ/mol) for MMS and DMS, respectively. Examination of the reaction enthalpy for the same reactions revealed that the endothermicity of the concerted reactions was comparable, with the 1,2-H_2 elimination forming silene molecules slightly less endorthermic than the respective 1,1-H_2 elimination process.

The effect of temperature change on the activation and reaction enthalpy ($\Delta H^{\neq}$, ΔH), entropy ($\Delta S^{\neq}$, ΔS) and Gibbs free energy ($\Delta G^{\neq}$, ΔG) was also examined by calculating these parameters at a room temperature of 298 K. Tables 4-3 and 4-4 also list the thermochemical and kinetic parameters obtained at 298 K. As noted in these tables, all of the entropies of activations are positive. This observation is explained by the fact that the reactions involved in Scheme 4-4 and 4-5 are decomposition reactions. For both molecules, the concerted mechanism showed lower $\Delta S^{\neq}_{298}$ value in comparison to the stepwise mechanism. The magnitude of entropy values is believed to be related to the transition state structure. If $\Delta S^{\neq}_{298}$ is relatively high, this indicates a loose structure of the transition state; and if $\Delta S^{\neq}_{298}$ is relatively low, the structure of the transition state is considered to be tight in nature.[208] Furthermore, it was noted that the increase of temperature from 0 to 298 K did not exert any effect on the sequence of either the reaction enthalpy or activation enthalpy for both molecules. In terms of the Gibbs free energies of activation, it was concluded that the enthalpy term is the major contributor by comparing the values of $\Delta H_{298}^{\neq}$ with $T\Delta S^{\neq}_{298}$. Among all of the reactions studied, the

concerted 1,1-H_2 elimination process provided the lowest $\Delta G_{298}^{\neq}$ value for both molecules.

A comparison of the values of entropy of activation $\Delta S_{298}^{\neq}$ and reaction entropy ΔS_{298} showed that the latter was higher. This is attributed to the fact that in the overall reactions one reactant molecule decomposes to form two different species as products, thus increasing the reaction entropy. The increased difference between ΔG_{298} and ΔH_{298} is indicative that the reaction entropy started to contribute more to the Gibb free energy. This contribution is expected to increase significantly with further increase in temperature. Based on the *ab initio* calculations, increasing the temperature to 298 K did not affect the preference towards the concerted 1,1-H_2 elimination process, which is the most kinetically and thermodynamically favourable.

To better understand the process of H_2 formation and relate it to our experimental results, the thermochemical study was also performed at a temperature range between 298 K to 2000 K. Figure 4-19 and 4-20 illustrate the temperature distribution of Gibbs free energy of activation ($\Delta G^{\neq}$) for the concerted and stepwise H_2 elimination processes from DMS and MMS decomposition. From these two Figures, it was noticed that the increase in the temperature only affected majorly the stepwise mechanisms due to the significant contributions of the entropy term to the Gibbs free energy term. Examining the entropy values in Table 4-3, it was noticed that at 298 K this term is in the range of 0.4 to 0.8 kcal/mol for the concerted mechanism and for the stepwise mechanism this value is increased to 8.5 and 8.6 kcal/mol. This difference is further enhanced with increasing temperature. The energy for the concerted pathway is relatively constant throughout the entire temperature range. As demonstrated previously, the concerted

mechanism was more favourable than the stepwise one at 0 K and 298 K, with 1,1-process being the most favourable of all. However, as indicated in Figures 4-19 and 4-20, when the temperature is increased to 800 K the stepwise pathway became kinetically more favourable. Similarly, the effect of temperature on Gibbs free energy of activation (ΔG) for the same reaction pathways was examined and shown in Figure 4-21 and 4-22. As noted from these plots, for both reaction mechanisms, the value of ΔG decreased with increasing temperature. For ΔG, the entropy term is comparable for both concerted and stepwise mechanism (Table 4-4), whereas the enthalpy term has approximately doubled in value when comparing the concerted and stepwise pathways. This implies that the enthalpy term is the major contributor to the ΔG term. Hence, it can be concluded from this examination that the concerted 1,1- and 1,2-H_2 elimination mechanism is still thermodynamically more favourable than the stepwise pathway.

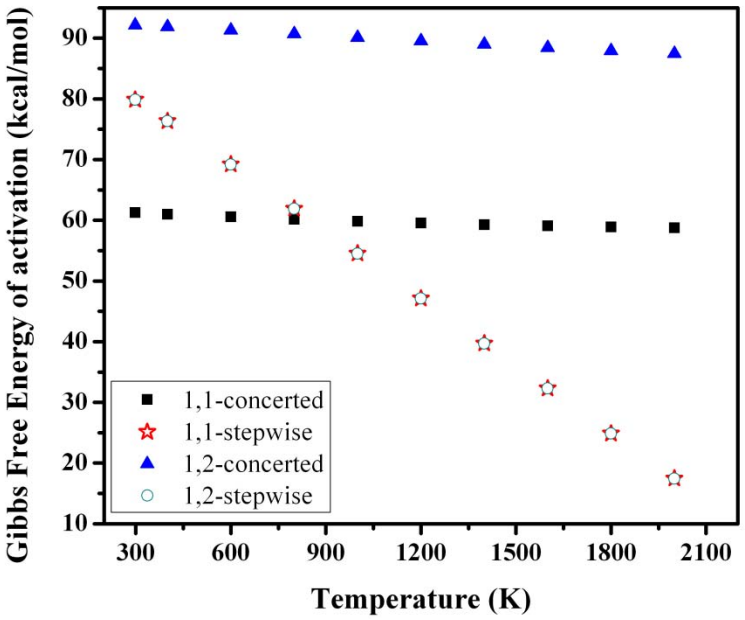


Figure 4-19: Temperature distribution of Gibbs free energy of activation ($\Delta G^{\neq}$) for the 1,1-, and 1,2- H_2 elimination pathways of MMS. For each pathway, both stepwise and concerted mechanisms were investigated. (ZPE corrections included)

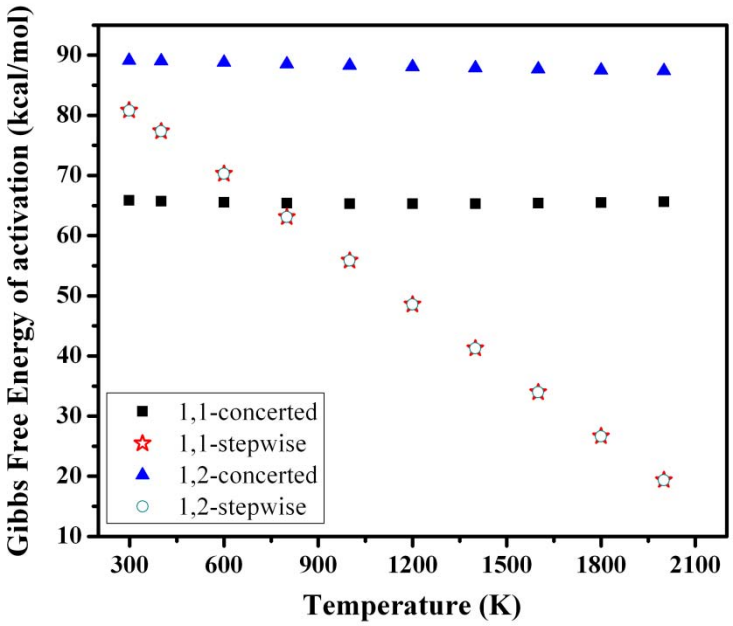


Figure 4-20: Temperature distribution of Gibbs free energy of activation ($\Delta G^{\neq}$) for the 1,1-, and 1,2- H_2 elimination pathways of DMS. For each pathway, both stepwise and concerted mechanisms were investigated. (ZPE corrections included)

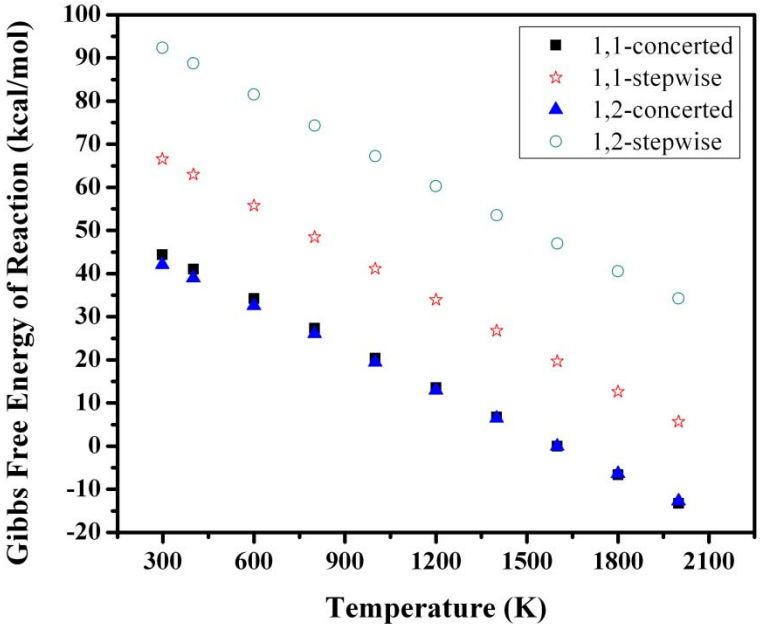


Figure 4-21: Temperature distribution of Gibbs free energy of reaction (ΔG) for the 1,1-, and 1,2- H_2 elimination pathways of MMS. For each pathway, both stepwise and concerted mechanisms were investigated. (ZPE corrections included)

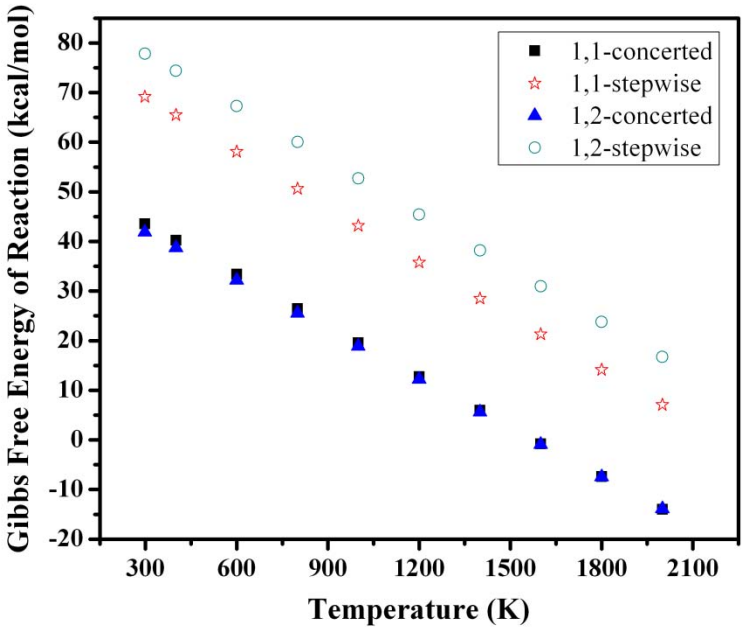


Figure 4-22: Temperature distribution of Gibbs free energy of reaction (ΔG) for the 1,1-, and 1,2- H_2 elimination pathways of DMS. For each pathway, both stepwise and concerted mechanisms were investigated. (ZPE corrections included)

4.7 Summary

The catalytic decomposition of four methyl-substituted silane molecules, including MMS, DMS, TriMS, and TMS, on a heated W and Ta filament was investigated in this work using laser ionization coupled with TOF MS in a HWCVD process. Two ionization methods, *i.e.,* SPI and dual SPI/ LIEI sources, were employed. The former is used as a universal technique to ionize species with an IE below 10.5 eV, while the latter is a complementary technique that ionizes species with an IE above and below 10.5 eV. Comparison of the two ionization sources has shown that species with an IE below 10.5 eV exhibit stronger peaks in the mass spectra recorded using SPI. On the other hand, peaks representing products with an IE above 10.5 eV, such H_2 and He, display an enhancement in their intensities when the dual ionization source is utilized.

The study on the decomposition of these methyl-substituted silane molecules on a heated W and Ta filament showed the formation of H_2 molecules. For both filaments, it was noted that the intensity of hydrogen molecule increases with increasing filament temperature to around 2000 - 2100 ^{o}C and reaches a plateau beyond. This behaviour signifies the transition from surface reaction rate limitation to mass transport limitation. Additionally, the temperature dependence study on the production of H_2 revealed an Arrhenius behaviour from which the apparent activation energy for the formation of H_2 was extracted. The examination of the activation energy values revealed an increase with increasing methyl substitution on the parent molecule. The difference in binding energy between the H and the metal surface as well as the desorption energy of H_2 from these surfaces explained the difference in apparent activation energy for the formation of H_2 from a W and Ta filament.

It was also demonstrated that the dissociation of these methyl-substituted silanes on W and Ta surfaces is initiated by the Si-H bond cleavage, and as the temperature is raised, C-H bond is also ruptured. The cleavage of these two bonds resulted in the presence of H adsorbates on the filament surface. The recombination reaction of two adsorbed H atoms leads to the formation H_2 molecule, following the Langmuir-Hinshelwood mechanism. This mechanism has been confirmed using the isotopomer of MMS, DMS and TriMS where the formation of the peaks at *m/z* 3 and 4, representing HD and D_2, is observed.

Ab initio calculations on the possible H_2 elimination pathways using MMS, DMS, and TriMS were also carried out. Both concerted and stepwise 1,1- and 1,2-H_2 elimination mechanisms were explored using *ab initio* methods at the CCSD(T)/6-311++G(3d,2p)//MP2/6-311++G(d,p) level of theory. The results from theoretical calculations suggest that the concerted 1,1-H_2 elimination is the most kinetically favorable of all pathways for MMS and DMS. The activation barriers for concerted 1,2-H_2 elimination and the rate-determining step in the stepwise mechanism are comparable for all three molecules. Thermodynamically, the concerted mechanism is favourable. A detailed thermodynamic and kinetic study was performed by examining the enthalpy ($\Delta H^{\neq}$), entropy ($\Delta S^{\neq}$), and Gibbs free energy ($\Delta G^{\neq}$) of activation along with reaction enthalpy (ΔH), entropy (ΔS), and Gibbs free energy (ΔG) at both 0 K and 298 K. The concerted 1,1- H_2 elimination was found to be the most kinetically and thermodynamically favourable route for the formation of H_2 during the decomposition of MMS and DMS at both temperatures.

Chapter Five: Role of Free-Radical and Methylsilene/Dimethylsilylene in the Reaction Chemistry of Dimethylsilane in a Hot-Wire Chemical Vapour Deposition Process

5.1 Motivations

There have been several studies on the gas-phase chemistry during the pyrolysis of dimethylsilane (DMS). Ring *et al.*[176] studied the pyrolysis of DMS in a continuous flow reactor and proposed that the decomposition of this precursor is initiated by either molecular elimination to produce silylene (R_2Si:)/silene ($CH_2=SiR_2$) or bond cleavage to produce free radicals. The major primary dissociation reactions are represented by Equations (5-1) to (5-4).

$$(CH_3)_2SiH_2 \longrightarrow (CH_3)_2Si: + H_2 \quad (5\text{-}1)$$

$$(CH_3)_2SiH_2 \longrightarrow CH_2=SiHCH_3 + H_2 \quad (5\text{-}2)$$

$$(CH_3)_2SiH_2 \longrightarrow CH_4 + :SiHCH_3 \quad (5\text{-}3)$$

$$(CH_3)_2SiH_2 \longrightarrow \dot{C}H_3 + CH_3\dot{S}iH_2 \quad (5\text{-}4)$$

Rickborn *et al*.[95] studied the shock-induced pyrolysis of DMS at 1135-1290 K and concluded that the secondary reactions involved both free radical and silylene chain reactions, with the latter being the dominant participant even when trapping agents are added. Under stirred flow conditions, they found that the major products are monomethylsilane and trimethylsilane with traces of ethene and acetylene. It has been suggested that the two major products are the results of both dimethylsilylene ($(CH_3)_2Si$:) and free radical reaction, while the minor ones come mainly from dimethylsilylene decomposition through the intermediacy of a silirane and silacyclopropene. They also

concluded that the main primary dissociation reactions of DMS are H_2 and methane elimination, with methane elimination accounting for about 17% of the total primary dissociation. The major involvement of silylene chemistry during the decomposition of DMS was also supported by the study carried out by O'Neal and Ring.[179] Their mechanism is based on unimolecular and bimolecular reaction of silylene intermediates, which explains the production of the complex linear and cyclic carbosilane products observed during their study.

Despite its simple structure, DMS has received less attention than the other methyl-substituted silanes as a possible precursor for the deposition of SiC thin films. In an attempt to study the influence of filament materials, Nakayama *et al.*[60] used DMS as a source gas to prepare $Si_{1-x}C_x$ thin films using Cat-CVD with four different filaments: W, Ta, Mo and Pt. They found that filament materials affected the film composition. The composition ratio C/Si in Si–C alloy films showed the maximum content for Pt. Additionally, the growth rate was also found to depend on the filament materials; among all filaments studied, W showed the maximum growth rate. Their results also showed the activation energy to break the Si-C bond on W filament surface to be 3.89 eV, which is lower than the Si-C bond dissociation energy of 4.68 eV. They concluded that the W filament acted as a catalyst to lower the dissociation energy of Si-C bond through the dissociation /adsorption processes. Furthermore, under conditions similar to the one used in this thesis, Zaharias *et al.*[61] identified the filament decomposition products of several single source precursors, including MMS, DMS, TriMS and TMS. The major decomposition products released from W or Re filaments with all of these precursors were found to be Si and CH_3. C and H radicals were also expected to be produced but

could not be detected. To correlate the gas-phase chemistry with deposited thin films using the same precursors, Zaharias *et al*. collected infrared spectra of the grown films and observed the presence of CH_3 symmetric and antisymmetric stretching modes along with a broad band assigned to SiH_2. This silicon hydride was only detected in the films grown from MMS, DMS and TriMS, and its origin is related to the hydrogenation of the Si radicals, which were found to be the dominant species in the gas phase. They also postulated that H radical, which is an important species in the film growth, is also produced during the hot-wire decomposition of these precursors. The deposition mechanism of SiC thin films with these single-source gases is not clear so far.

To gain better insights into the deposition chemistry of DMS in HWCVD, the decomposition and secondary gas-phase reaction chemistry using DMS with both W and Ta filaments has been studied in this work. Here, detection of decomposition products released directly from the hot filament made of either W or Ta was carried out under collision free-conditions for filament temperatures ranging from 900 °C to 2400 °C. Mixtures with various concentrations of 1%, 4 %, and 10% DMS seeded in He were used for the detection of gas-phase reaction products with a total gas pressure of 12 Torr in the HWCVD reactor. Both W and Ta were used as filament materials. The filament temperatures tested varied from 900 °C to 1800 °C. In order to confirm the assignments of the mass peaks detected using DMS, spectra were also collected using a 4% DMS-d_2/He mixture. Several trapping agents, including 1,3-butadiene and ammonia, were used to trap silylene and silene intermediates, as stated in Chapter 1. This serves to provide a better understanding of the reaction mechanism and help confirm the involvement of silene and silylene intermediates.

5.2 Primary Decomposition on Ta and W Filament

As described in a previous publication,[67] the room-temperature TOF mass spectra with DMS show predominantly two peaks at *m/z* 58 ($Si(CH_3)_2^+$) and 60 (parent $H_2Si(CH_3)_2^+$), with an intensity ratio of I(*m/z* 58)/I(*m/z* 60) = 2.13 ± 0.09. It is noted that the parent ion peak intensity was much higher than the combined isotope contribution from the peaks at *m/z* 58 and 59. In determining the primary decomposition products of DMS, it was found that a new mass peak at *m/z* 15, assigned to methyl radical, appeared after the filament was turned on for both W and Ta filaments. The mechanism for the formation of this species is discussed in details in Chapter 3. It has been shown in Chapter 3 that DMS dissociates on the hot W and Ta filament to methylsilyl and methyl radicals, as represented by Equation (5-4).

In addition, we have demonstrated in Chapter 4 that DMS dissociates to form H radical and also H_2 molecule. The formation of H radicals via Si-H bond cleavage, as represented by Equation (5-5), has been observed in previous pyrolysis studies[95, 176, 177, 179, 183, 192, 207, 209] and during HWCVD processes.[67, 89]

$$(CH_3)_2SiH_2 \longrightarrow (CH_3)_2\dot{S}iH + \dot{H} \qquad (5\text{-}5)$$

The presence of the complementary fragment, *i.e.*, dimethylsilyl radical ($(CH_3)_2SiH^{\bullet}$), was confirmed by examining the ratio of this peak with respect to the parent ion peak ($[M]^+$), shown in Figure 5-1a. This ratio increased with filament temperature, indicating the presence of dimethylsilyl radical in the gas phase.

The H_2 formation from the hot-wire decomposition of DMS follows the Langmuir-Hinshelwood mechanism, as discussed in Chapter 4. Figure 5-1b shows the plot of the intensity ratio of the fragment peak ($[M-2]^+$) with respect to the parent ion

peak ($[M]^+$). Examination of this ratio revealed that it also increased with filament temperature, suggesting that the co-products of H_2 formation in the gas phase are possibly dimethylsilylene and methylsilene (both having a mass of 58 amu), as represented by Equations (5-1) and (5-2).

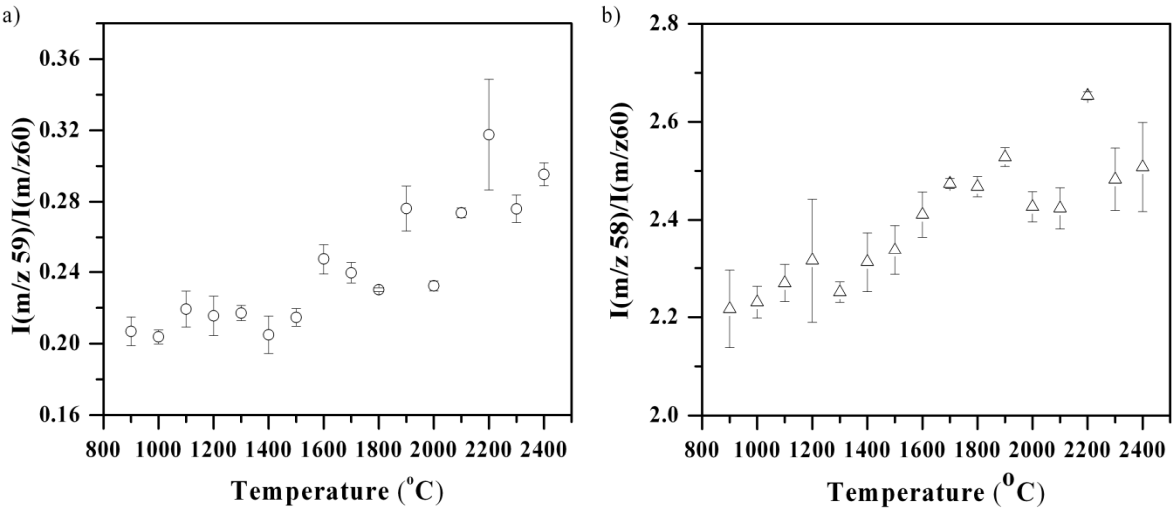


Figure 5-1: The Intensity ratio of a) $(CH_3)_2SiH^+$ (*m/z* 59) to that of the parent of $(CH_3)_2SiH_2^+$ (*m/z* 60), and b) $(CH_3)_2SiH^+$ (*m/z* 58) to that of the parent of $(CH_3)_2SiH_2^+$ (*m/z* 60) for pure DMS versus the filament temperature at a chamber pressure of 1×10^{-5} Torr.

5.3 Secondary Gas-Phase Reactions on a Ta Filament

The chemical products generated from the secondary gas-phase reactions between the primary decomposition intermediates on the filament and the parent DMS molecule were studied by monitoring the species exiting from the HWCVD reactor. The TOF mass spectra were collected at different filament temperatures ranging from 900 to 1800 ^oC with an increment of 100 ^oC. At each temperature, a mass spectrum was recorded every five minutes for one hour. Three mixtures with different concentrations at 1%, 4% and 10% of DMS seeded in He were studied. This provides a DMS partial pressure of 0.12,

0.48, and 1.2 Torr, respectively, when using a total pressure of 12 Torr. The discussions in this section are mainly based on the results of using 1% DMS/He mixture on Ta filament.

Most of the studies using methyl-substituted silane precursors in a HWCVD setup opt for a W filament due to its high melting point and low vapour pressure. However, a W filament suffers from a short lifetime, especially at lower filament temperatures. Several studies have shown the susceptibility of the W filament to this drawback.[34, 40, 210, 211] In contrast, Ta filament has a longer lifetime due to the less amount of silicide formed on its surface.[40] Despite this fact, little is known on the gas-phase chemistry of these precursor molecules in HWCVD using Ta as a filament. Therefore, we have studied the gas-phase chemistry of DMS on a Ta filament, and the results are presented in this section. A comparison of the effect of different filament materials on the gas-phase chemistry is discussed in section (5.5).

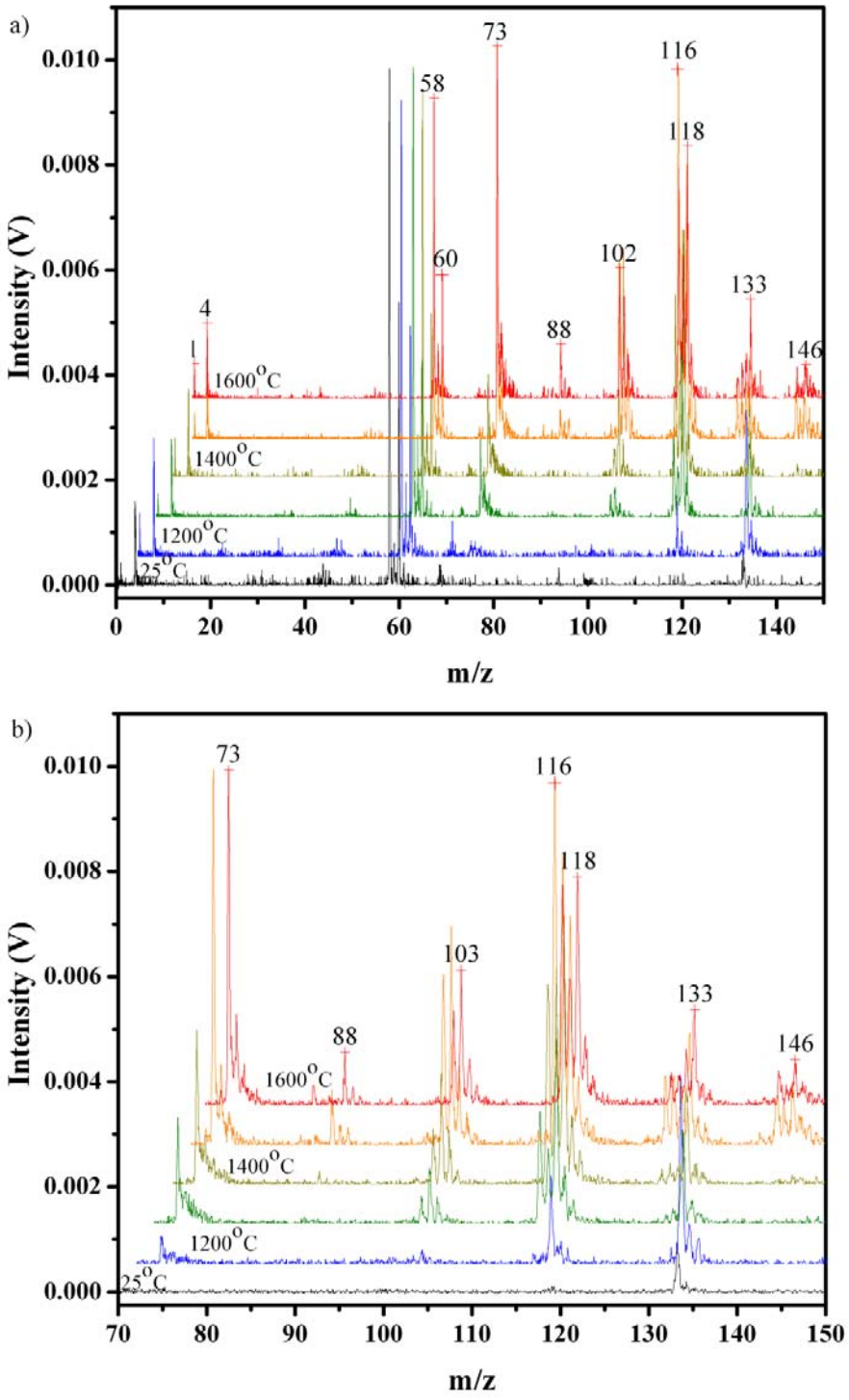


Figure 5-2: a) 10.5 eV SPI TOF mass spectra of 12 Torr 1% DMS/He in the reactor at filament temperatures between 1200 and 1600 ^{o}C. The spectrum at 25 ^{o}C is recorded when the filament is off; b) enlarged spectra in the mass regions of 70-150 amu.

Figure 5-2 shows the TOF mass spectra recorded for 12 Torr of 1% DMS/He sample at different temperatures ranging from 1200 and 1600 ^{o}C at a filament-on time of 10 minutes. After the filament was turned on, the parent and its photofragment ion peak [$Si(CH_3)_2^+$ (*m/z* 58)], dominated in the room-temperature mass spectrum of DMS decreased with increasing filament temperature, indicating that the parent DMS molecules were decomposed on the filament and consumed in secondary gas-phase reactions in the reactor. This decrease was observed to start at ~1200 ^{o}C, which was lower than those for TMS[89] and HMDS,[82] but higher than the lowest decomposition temperatures when using two four-membered-ring compounds, *i.e.*, silacyclobutane[90] and 1,1-dimethyl-1-silacyclobutane.[91] When the intensity of the parent molecule decreased, a variety of new mass peaks appeared after the filament was turned on, *e.g.*, those at *m/z* 73, 88, 103, 116, and 118.

In order to closely examine the extent to which the intensity of the $Si(CH_3)_2^+$ peak decreased relative to that of parent $SiH_2(CH_3)_2^+$, the intensity ratio of peak at *m/z* 58 to that at *m/z* 60 was calculated and plotted versus the filament-on time for different filament temperatures. This plot is illustrated in Figure 5-3. As noted in the graph, the intensity ratio was found to be higher than that for filament off (2.13 ± 0.09) at the decomposition temperature of 1200 ^{o}C, and the increase of the ratio is more accentuated as the filament temperature is increased. This suggests that other sources than the photofragmentation of DMS contribute to the peak at *m/z* 58. This will be discussed in later sections.

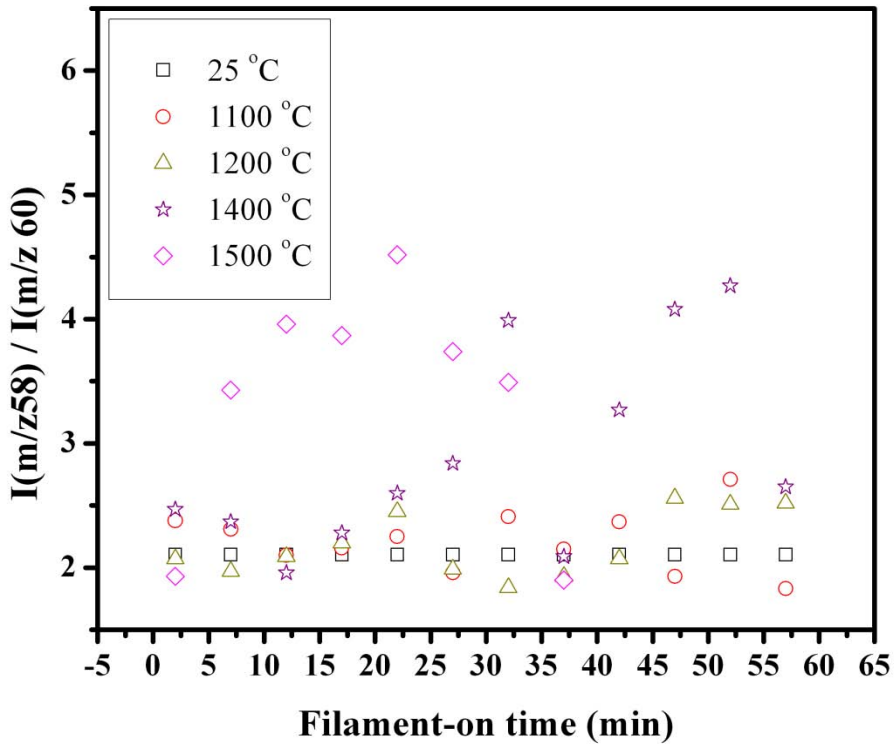


Figure 5-3: The intensity ratio of the peak at *m/z* 58 to the parent ion peak at *m/z* 60 from 12 Torr of 1% DMS/He as function of filament-on time over the temperature range of 1100 to 1700 °C.

5.3.1 Possible Secondary Reactions

5.3.1.1 Hydrogen Abstraction and Biradical Recombination Reactions

From the previous study of TMS,[89] HMDS,[82] and TriMS,[67] it was discussed that the radicals produced from the primary decomposition will react with each other or with the parent molecule in the HWCVD reactor. Under collision-free condition, the decomposition of DMS resulted in the formation of methylsilyl ($CH_3SiH_2^{\bullet}$), dimethylsilyl ($(CH_3)_2SiH^{\bullet}$), methyl, and hydrogen radicals. Among all of the four radical intermediates, the methyl radical has been demonstrated to be the main chain propagator in the chain reaction mechanism involved in the secondary gas-phase reactions, using TMS,[89]

HMDS[82] and TriMS[212] in a HWCVD reactor. The low strength of Si-H bond formed in comparison to the C-H bond makes methyl-substituted silyl radicals a poor hydrogen abstractor. Therefore, the H abstraction reactions involving these intermediates do not occur in the reactor.

If the same chain reaction mechanism occurs with DMS, CH_3 radical will react with the parent DMS molecule by abstracting H atoms according to Equation (5-6). This reaction leads to the formation of methane and dimethylsilyl radical, $(CH_3)_2SiH^{\bullet}$.

$$\dot{C}H_3 + (CH_3)_2SiH_2 \longrightarrow (CH_3)_2\dot{S}iH + CH_4 \quad (5\text{-}6)$$

This can then be followed by several biradical combination reactions shown below:

$$\dot{C}H_3 + (CH_3)_2\dot{S}iH \longrightarrow \underset{74\ amu}{(CH_3)_3SiH} \quad (5\text{-}7)$$

$$2\,(CH_3)_2\dot{S}iH \longrightarrow \underset{118\ amu}{(CH_3)_2SiHSiH(CH_3)_2} \quad (5\text{-}8)$$

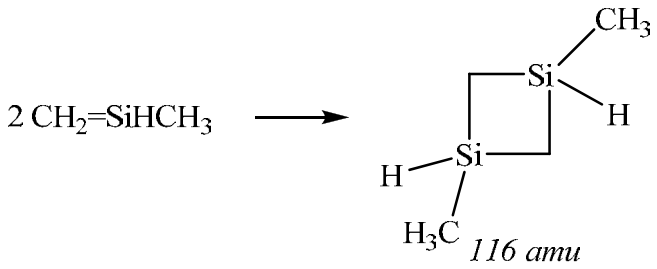
$$2\,CH_3\dot{S}iH_2 \longrightarrow \underset{90\ amu}{CH_3SiH_2SiH_2CH_3} \quad (5\text{-}9)$$

$$(CH_3)_2\dot{S}iH_2 + CH_3\dot{S}iH_2 \longrightarrow \underset{104\ amu}{(CH_3)_2SiHSiH_2CH_3} \quad (5\text{-}10)$$

5.3.1.2 Reactions Involving Silene and Silylene Intermediates

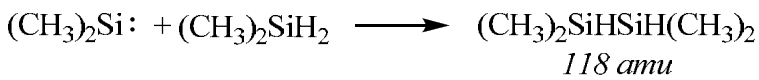
It is noted from section 5.2 that the co-products to the hydrogen molecule during the H_2 elimination from the decomposition of DMS on the Ta filament could be methylsilene ($CH_3SiH{=}CH_2$) and dimethylsilylene ($(CH_3)_2Si$:). Methylsilene intermediate is known to be unstable and tend to undergo rapid cyclodimerization[110, 111 110] resulting in

the formation of 1,3-dimethyl-1,3-disilacyclobutane (DMDSCB) as indicated by Equation (5-11).



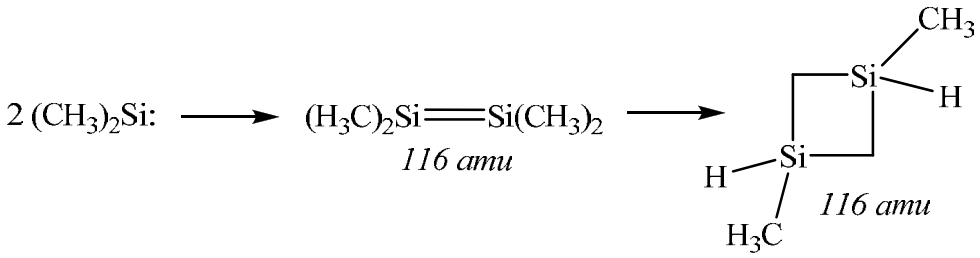
(5-11)

The reactive intermediate, dimethylsilylene, is known to undergo insertion reactions into a variety of chemical bonds including Si-H bond. Under our experimental conditions, where the pressure in the HWCVD reactor is 12 Torr, there is an abundant source of parent DMS molecules. Therefore, dimethylsilylene species react with them by inserting into its Si-H to form 1,1,2,2-tetramethyldisilane, which is represented in Equation (5-12).



(5-12)

Dimethylsilylene can also dimerize forming 1,1,2,2-tetramethyldisilene, which in turn undergoes rearrangement to produce DMDSCB, as represented by Equation (5-13).



(5-13)

5.3.2 Formation of the Main Products

As shown in Figure 5-2, the new peaks after the filament was turned on when using DMS in the HWCVD reactor are predominantly those at *m/z* 73, 116, and 118. Figure 5-4 shows the intensity distribution of these three main peaks at different filament temperatures. Both filament-on time and filament temperatures play a role in determining the relative intensity of these peaks. At 1200 ^{o}C, the peak at *m/z* 118 is dominating at $t \leq$ 30 min, beyond this time, there is an increase in the peak intensity at *m/z* 73. As the filament temperature is increased to 1300 and 1400 ^{o}C, the time when the peak at *m/z* 118 is dominant is shortened to 25 min and 10 min, respectively. The peaks at *m/z* 73 and 116 become more important beyond. A detailed discussion on the formation of these main products is presented in the following sections.

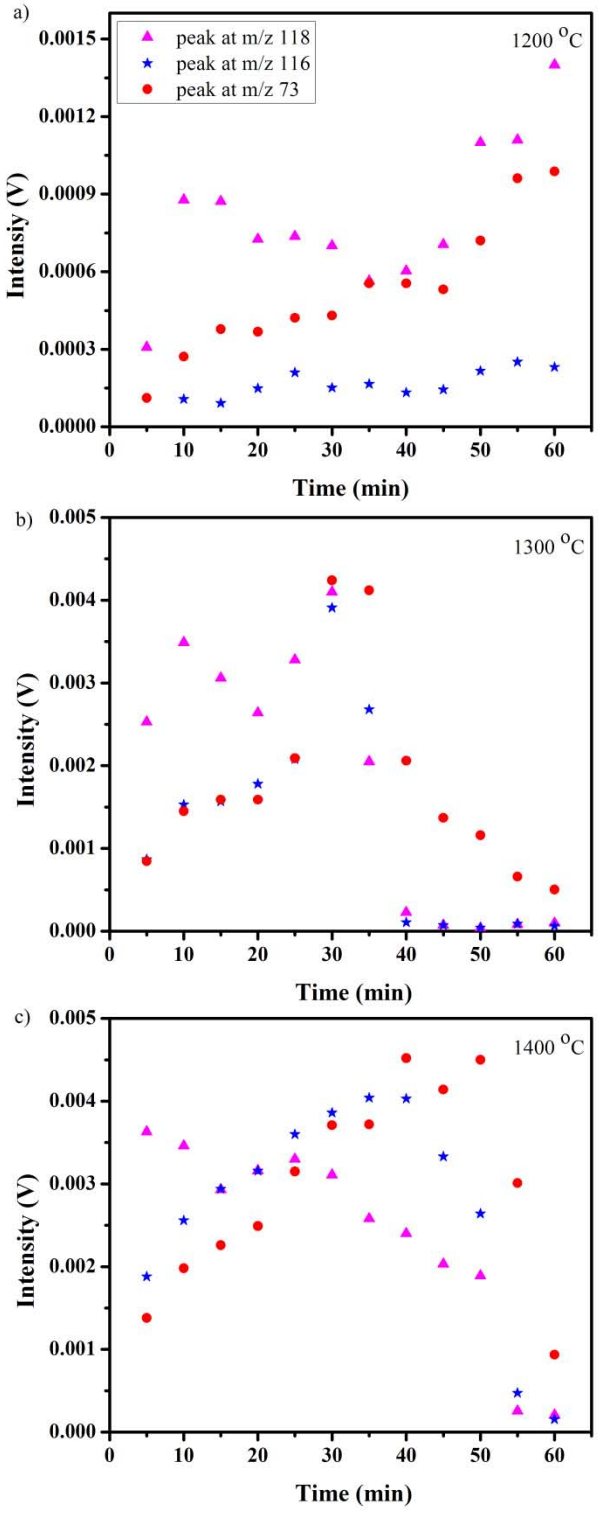
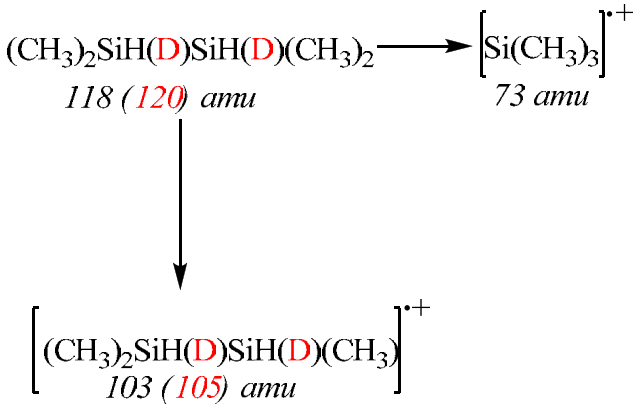


Figure 5-4: Intensity distribution of peaks at *m/z* 73, 118 and 116 when using 12 Torr of 1% DMS/He and at a filament temperature of a) 1200 °C, b) 1300 °C, and c) 1400 °C.

5.3.2.1 Formation of 1,1,2,2-Tetramethyldisilane at Low Filament Temperatures

The gas-phase chemistry of DMS was dominated by the peak at *m/z* 118 at a relatively low filament temperature and a short filament-on time. Based on the proposed reaction mechanism (Section 5.3.1) and the mass, this peak was assigned to 1,1,2,2-tetramethyldisilane (TMDS). To confirm the nature of this peak being TMDS, the mass spectrum of 1% DMS/He at 1200 ^{o}C was compared to the room-temperature mass spectrum of an authentic TMDS sample purchased from Santa Cruz Biotechnology, as illustrated in Figure 5-5. From the authentic TMDS sample, two photofragment ions, *i.e.*, $Si(CH_3)_3^+$ (*m/z* 73) and $Si_2H_2(CH_3)_3^+$ (*m/z* 103), were observed. The intensity ratios of I(*m/z* 73)/I(*m/z* 118) and I(*m/z* 103)/I(*m/z* 118) were found to be 0.31 ± 0.01 and 0.039 ± 0.003, respectively. These ratios were similar in values to those obtained from the experiments using 0.12 Torr of DMS after the filament was turned on, hence confirming the nature of the peak at *m/z* 118 as being 1,1,2,2-tetramethyldisilane.

In addition, the nature of this peak was further confirmed by performing the same experiment using the deuterated isotopomer, DMS-d_2. Figure 5-6 shows the mass spectrum of 12 Torr of 4% DMS-d_2/He mixture recorded at a Ta filament temperature of 1200 ^{o}C. When DMS-d_2 was used, the peak at *m/z* 118 was clearly shifted to *m/z* 120, and the dominance of the peak at *m/z* 120 is preserved in the spectra in the mass regions beyond 62 amu after turning the filament on. The corresponding two photofragment ions from TMDS are now shifted to *m/z* 73 and *m/z* 105, as explained in scheme 5-1. This clearly demonstrates that the peak at *m/z* 118 is indeed originated from 1,1,2,2-tetramethyldisilane.



Scheme 5-1 Photofragmentation mechanism of 1,1,2,2-tetramethyldisilane.

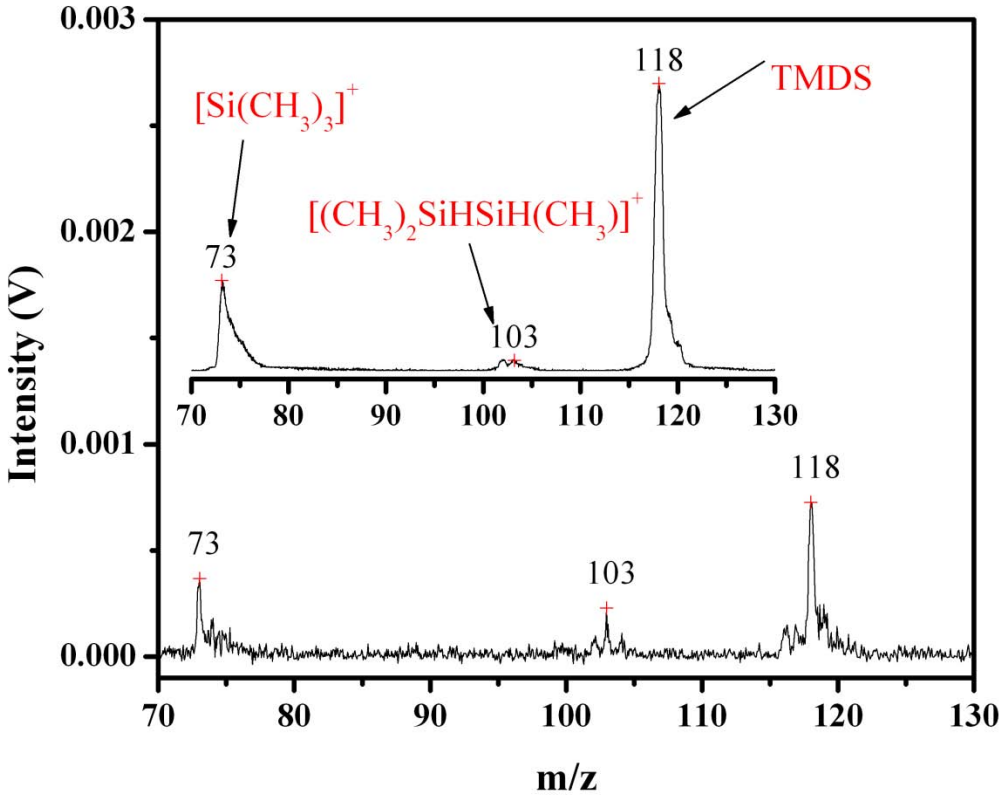


Figure 5-5: 10.5 eV SPI TOF mass spectrum of 0.12 Torr of DMS sample in the reactor at a filament temperature of 1200 ^{o}C in the mass region of 70 - 130 amu. The inset is a mass spectrum of an authentic TMDS sample recorded at room temperature.

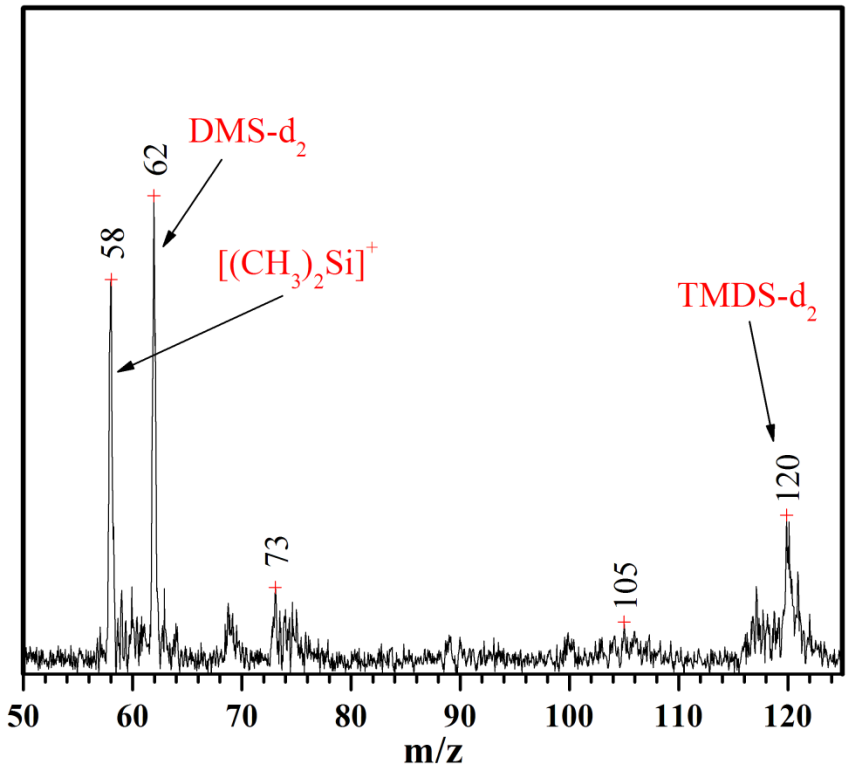


Figure 5-6: 10.5 eV SPI TOF mass spectrum of 12 Torr of 4% DMS-d_2/He mixture recorded 10 minutes after the filament was turned on at 1200 °C.

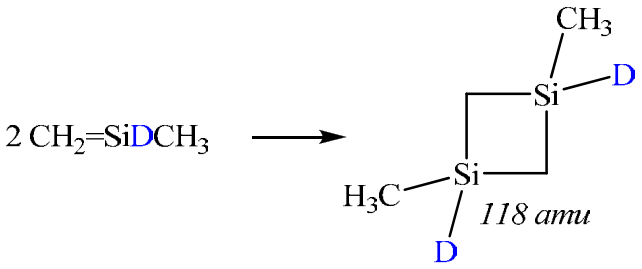
As discussed in section 5.3.1, the formation of TMDS can proceed via two pathways, either radical recombination reaction (Equation (5-8)) or silylene insertion reaction (Equation (5-12)). Upon the usage of the deuterated sample, both reaction mechanisms will yield the same product, as shown by Equation (5-14).

$$\left.\begin{array}{l} 2\ (CH_3)_2\dot{S}iD \\ (CH_3)_2Si: \ + \ (CH_3)_2SiD_2 \end{array}\right\} \rightarrow \underset{\textit{120 amu}}{(CH_3)_2SiDSiD(CH_3)_2} \qquad (5\text{-}14)$$

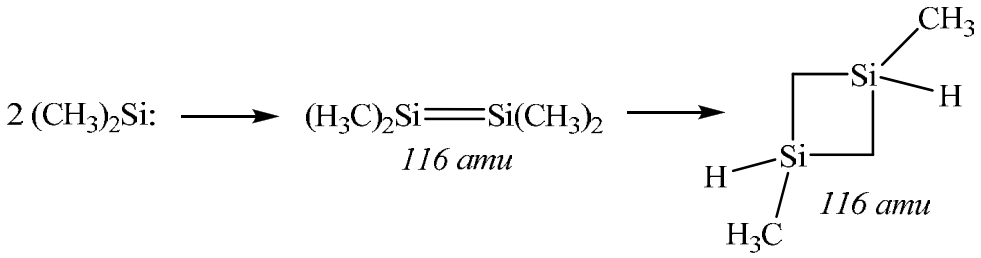
Hence, the exact mechanism for the formation of this product cannot be easily determined clearly when using the deuterated DMS-d_2 sample. In order to identify the mechanism responsible for the production of TMDS, chemical trapping experiments of the active intermediates using 1,3-Butadiene were carried out and the results are presented in section (5.3.4).

5.3.2.2 Formation of 1,3-Dimethyl-1,3-disilacyclobutane at High Filament Temperatures

When the filament temperature was increased to 1300 ^{o}C and higher, the peak at *m/z* 116 appeared and predominated the gas-phase chemistry. This peak is assigned to 1,3-dimethyl-1,3-disilacyclobutane (DMDSCB). The formation of this peak can occur via the dimerization reactions of either methylsilene or dimethylsilylene, as described by Equation (5-11) and (5-13), respectively. The use of isotopomer DMS-d_2 would result in different mass shift in DMDSCB if it were to be formed by the two different mechanisms. As illustrated in Equations (5-15) and (5-16), a mass shift from *m/z* 116 to 118 would be observed for the cyclodimerization reaction of methylsilene, whereas the mass of DMDSB from the dimerization reaction of dimethylsilylene would remain at *m/z* 116.



(5-15)



(5-16)

Figure 5-7 illustrates a comparison between the mass spectra recorded with 12 Torr of 4% DMS/He sample and 12 Torr of 4% DMS-d_2 sample in the HWCVD reactor at a filament temperature of 1400 ^{o}C in the mass region of 110 - 125 amu.

It can be noticed that the dominance of the peak at *m/z* 116 is preserved when using DMS-d_2, but shifted by 2 amu to a peak at *m/z* 118. To better illustrate this preservation of dominance, an intensity distribution of peaks at *m/z* 116, 118 and 120 originated from DMS-d_2 is plotted and compared to the one for the peaks at *m/z* 116 and 118 obtained from 4% DMS. They are shown in Figure 5-8. The intensity of the peak at *m/z* 116 is higher than the one for the peak at *m/z* 118 when using DMS. The same trend is observed when the isotopomer was used where the peak at *m/z* 118 is dominating over the one at *m/z* 120. It should be noted that the peak at *m/z* 116 did not disappear when DMS-d_2 was used, indicating the occurrence of dimethylsilylene dimerization.

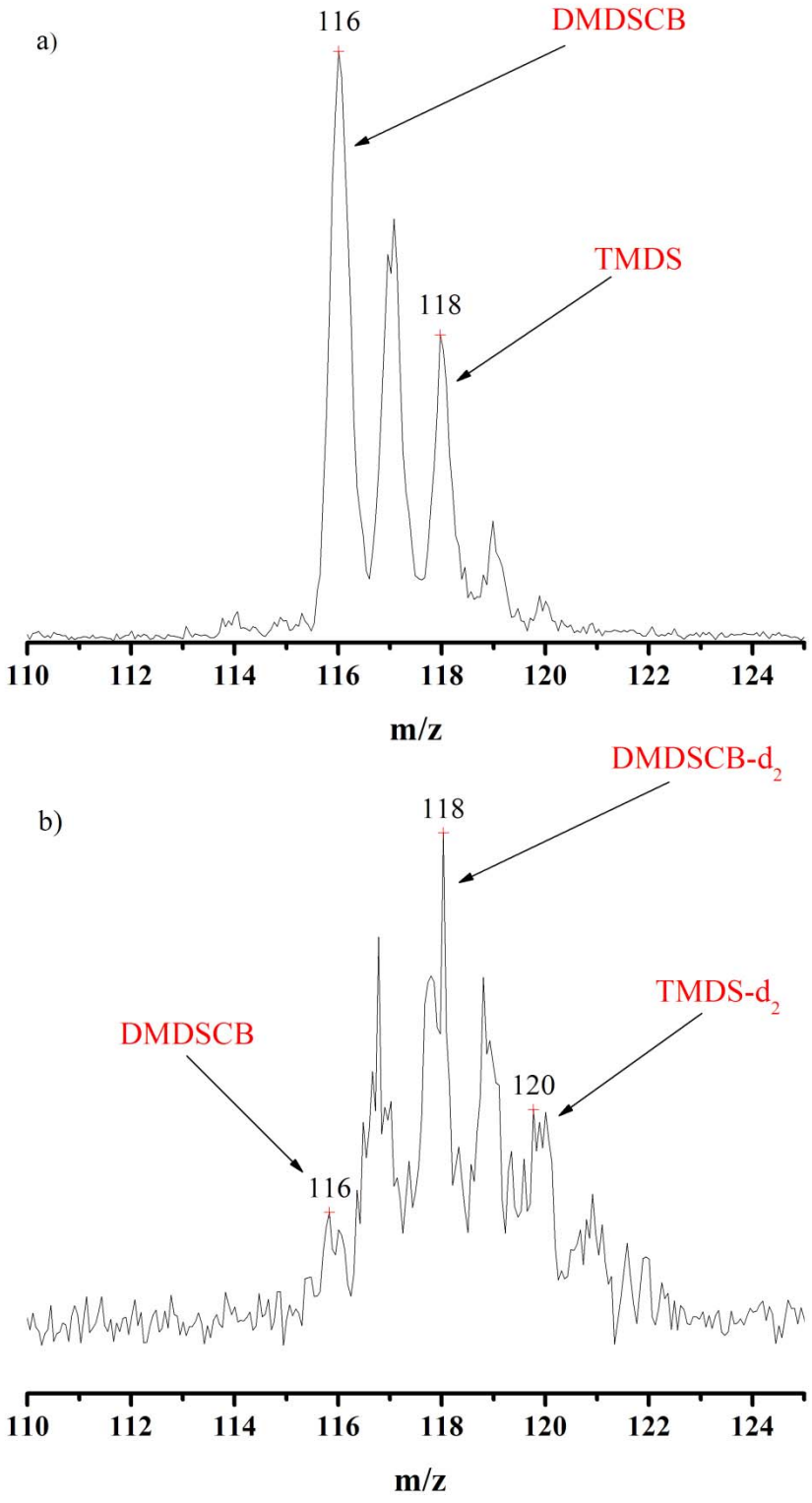


Figure 5-7: 10.5 eV SPI TOF mass spectra of a) 12 Torr of 4% DMS/He, and b) 12 Torr of 4% DMS-d_2/He in the reactor at a filament temperature of 1400 ^{o}C.

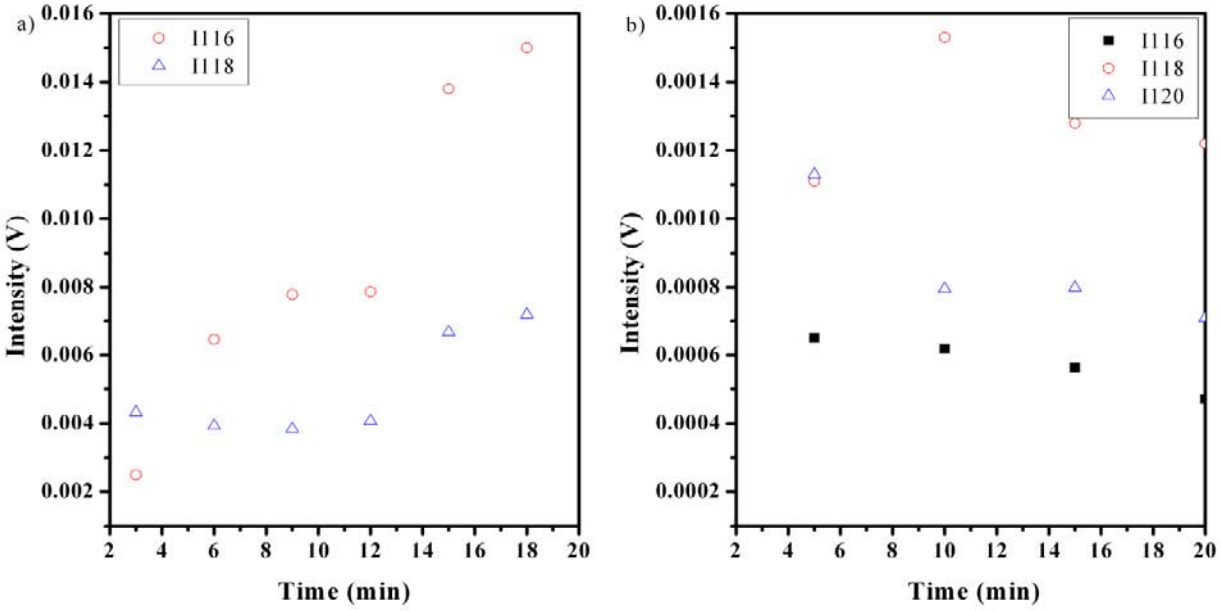


Figure 5-8: Intensity distribution of the peaks at a) *m/z* 116 and 118 originated from 4% DMS/He and b) *m/z* 116, 118 and 120 produced from 4% DMS-d_2/He at a filament temperature of 1400 ^{o}C.

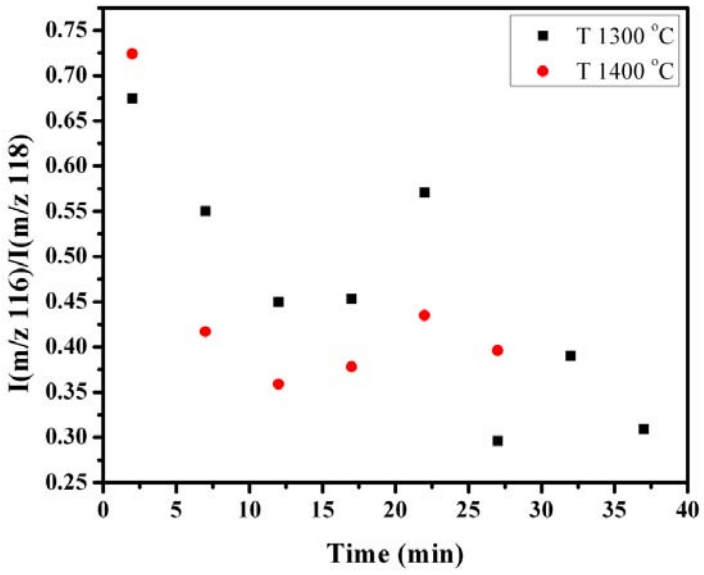


Figure 5-9: Comparison of the intensity ratio of the peak at *m/z* 116 to the one at *m/z* 118 from the 12 Torr 4% DMS-d_2/He mixture versus filament-on time at 1300 and 1400 ^{o}C.

Figure 5-9 shows the intensity ratio of I(*m/z* 116)/I(*m/z* 118) with the DMS-d_2 sample. The ratio ranges from 0.30 to 0.72. Therefore, it can be concluded that both silene cyclodimerization and silylene dimerization reactions contribute to the appearance of DMDSCB molecule. Since the intensity ratio of I(*m/z* 116)/I(*m/z* 118) is less than 1, silene contribution dominates. To clearly identify the mechanism accountable for the formation of DMDSCB, trapping experiments with 1,3-butadiene and ammonia were carried out and the results are presented in section (5.3.3).

5.3.2.3 Formation of Trimethylsilane and Tetramethylsilane at High Filament Temperatures

After the filament was turned on when using DMS is the reactor, a distinct increase in the peak intensity at *m/z* 73 was observed at higher temperatures. Figure 5-10 shows the mass spectrum of 1% DMS/He at 1300 ^{o}C after thirty minutes of reaction time.

At this temperature, the peak at *m/z* 73 surpasses those at *m/z* 116 and 118, and becomes the dominant peak in the mass region above 60 amu. Along with it, the increase in the peak intensity at *m/z* 58 was also observed. The intensity of the peak at *m/z* 73 increased with increasing filament temperature, as shown in Figure 5-11a. The peak at *m/z* 73 started to appear at 1200 ^{o}C and at this temperature, as discussed earlier, this peak has a contribution from the photofragment of TMDS (*m/z* 118). An examination of the ratio of the peak at *m/z* 73 to the one for *m/z* 118 showed that it varied from 0.29 to 1.19 at 1200 ^{o}C. The lower value of the ratio is comparable to one obtained from TMDS authentic sample. After one hour of reaction time, the ratio reached its maximum value of 1.19. This increase in the value indicates that additional factors are contributing to the

intensity of this peak. From our previous study on TriMS,[67] it is known that its room-temperature mass spectrum is dominated by two mass peaks at *m/z* 58 and 73 with an intensity ratio of 0.35 ± 0.01. The increase in the peak intensity at *m/z* 58 accompanying the one at *m/z* 73 strongly indicates that the peak at *m/z* 73 observed in our experiment is likely originated from trimethylsilane. Its formation involves radical recombination reaction between methyl and dimethylsilyl radicals formed from the hot wire activation, as illustrated by Equation (5-7).

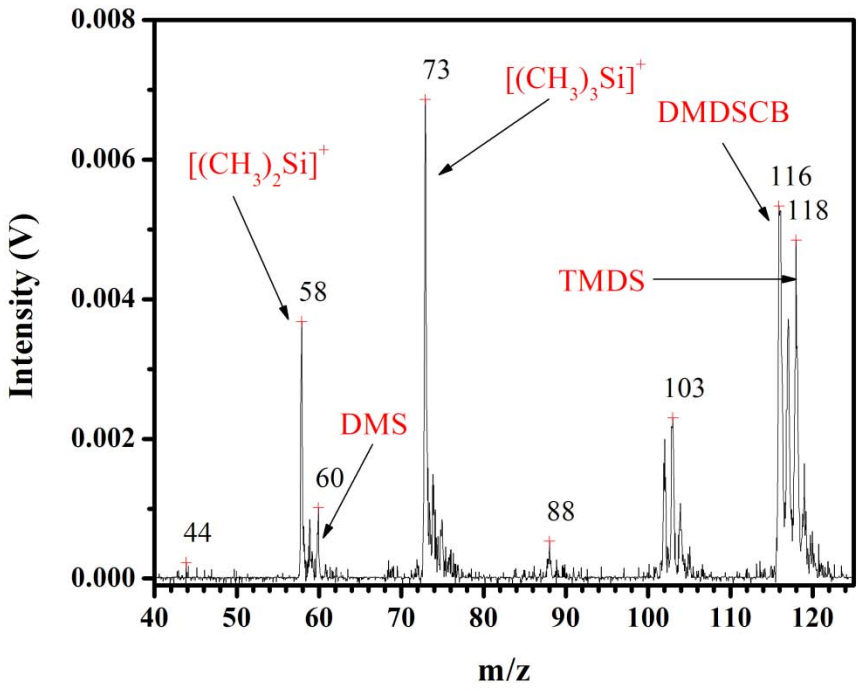


Figure 5-10: 10.5 eV SPI TOF mass spectra of 12 Torr 1% DMS/He in the reactor at filament temperature of 1300 °C.

The gas-phase chemistry from using TriMS predominantly produced two major product, i,e,, TMS (*m/z* 88) and HMDS (*m/z* 146). Both of these peaks were observed in

our experiments with DMS. The detection of these two peaks presents a further confirmation on the production of TriMS in our current experiment.

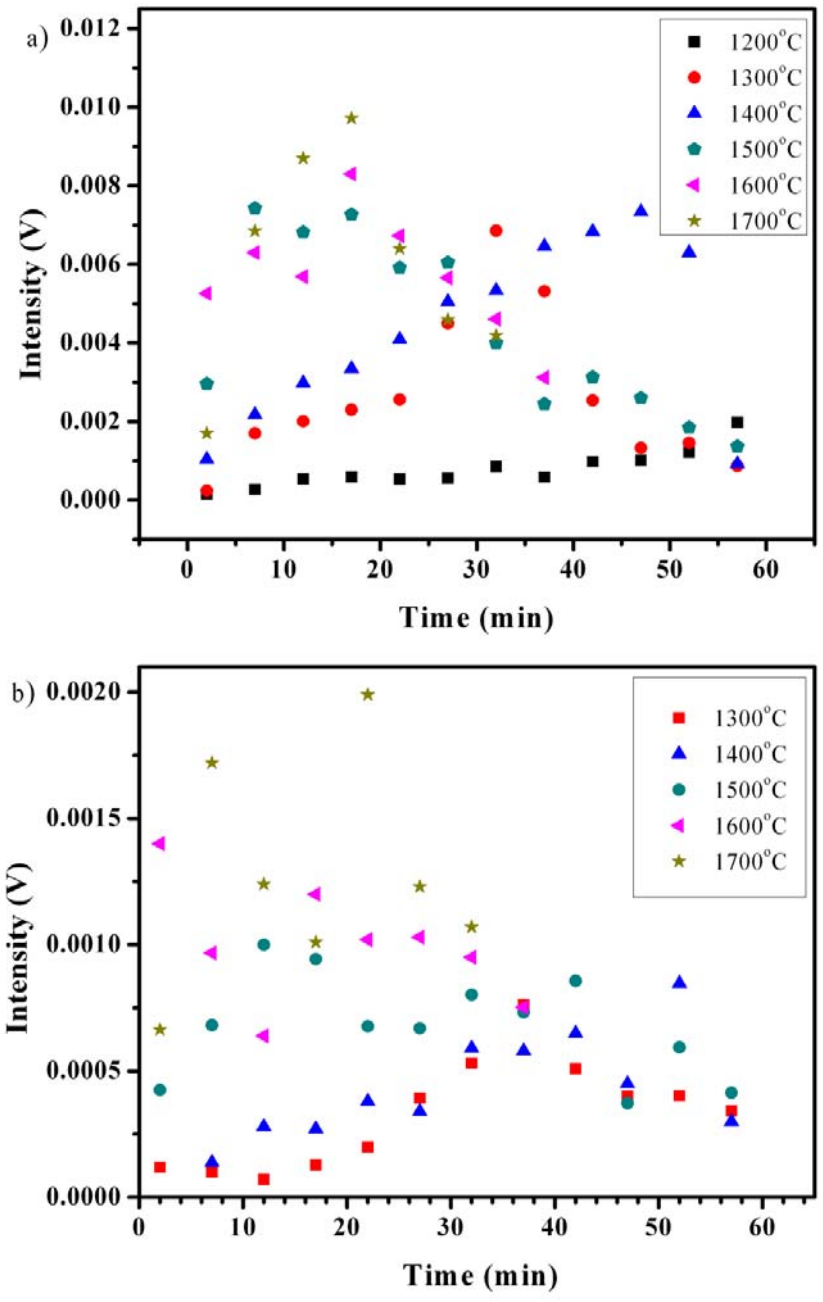


Figure 5-11: Intensity distribution of the peak at a) *m/z* 73, and b) *m/z* 88 as a function of filament-on time over a temperature range of 1200 to 1700 °C.

The weak intensity of the peak at *m/z* 88 is due to the fact that TMS is a product from TriMS chemistry rather from DMS precursor. The formation of TMS from TriMS is further confirmed by examining the intensity distributions of the TMS peak at *m/z* 88 shown in Figure 5-11b and by comparing them with those of the peak at *m/z* 73 (Figure 5-11a). TMS started to form at 1300 ^{o}C and its intensity reached a maximum after 35 minutes of reaction time. This time coincided with the decrease in the intensity of the peak at *m/z* 73, which is indicative that TriMS is decomposing and undergoing secondary gas-phase reactions.

From our current and previous studies, it is known that the contribution to the intensity of the peak at *m/z* 73 comes from the photofragmentation of more than one molecule. Aside from TriMS and TMS, 1,1,2,2-tetramethyldisilane (*m/z* 118) was also produced in a significant amount when using DMS in the reactor. As shown in Figure 5-5 and discussed previously, TMDS photo-fragments to produce a peak at *m/z* 73 with an intensity ratio of I(*m/z* 73)/I(118) to be equal to 0.32. The only characteristic photofragment peaks of TMS from 118 nm VUV SPI TOF is at *m/z* 73 and the intensity ratio of the peak at *m/z* 73 to the parent TMS ion peak at *m/z* 88 is 4 : 1[89] when the filament is off.

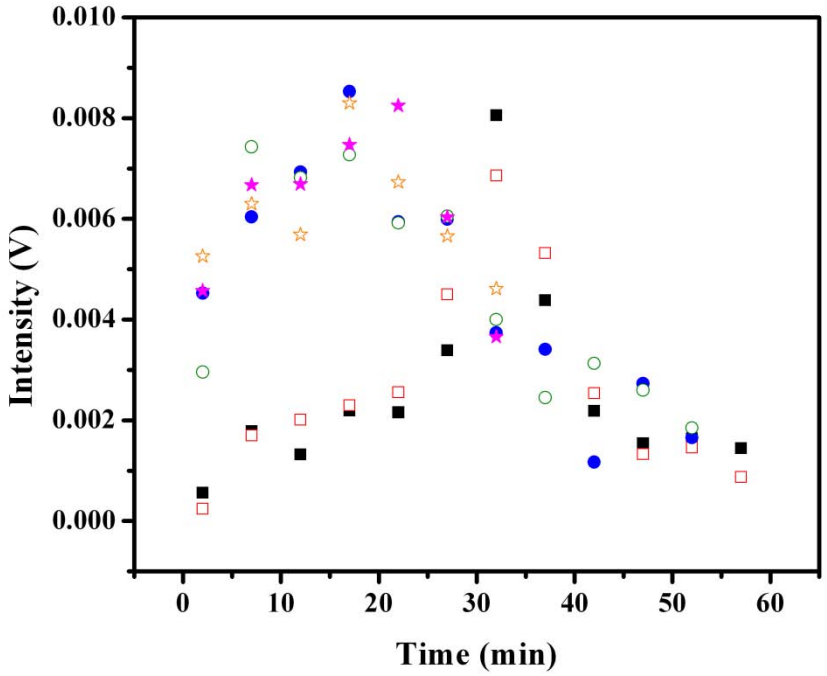


Figure 5-12: Intensity of the peak at *m/z* 73 observed with 12 Torr of 1% DMS/He mixture at 1300 °C (□), 1500 (○), and 1600 °C (☆). The contribution to the peak intensity from the photofragmentation of TriMS, TMS, and TMDS combined at 1300 (■), 1500 (●) and 1600 °C (★) is shown for comparison.

Figure 5-12 illustrated the intensity distribution of the peak at *m/z* 73 observed from the experiments using 12 Torr of 1% DMS in the reactor at filament temperatures of 1300, 1500 and 1600 °C as a function of filament-on time. The combined contributions to the intensity of the same peak from the 118 nm VUV photofragmentation of TriMS, TMS, and TMDS were computed based on the observed intensity at *m/z* 58, 88, and 118 at each temperature and filament-on time and using the respective intensity ratio in the room-temperature mass spectra. They are shown in the same figure for comparison. It is worth noting that for the peak at *m/z* 58 the contribution of the photofragment from DMS was subtracted from the observed intensity during the experiment. The close resemblance

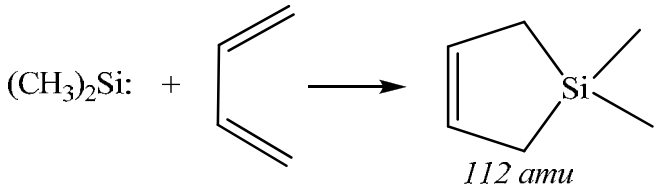
of observed intensities with those from calculations strongly that both TriMS and TMS were produced in our HWCVD reactor when using DMS as a source gas.

5.3.3 Trapping of Active Intermediates

From the above discussions, it was demonstrated that three major products, *i.e.*, 1,1,2,2-tetramethyldisilane (TMDS, *m/z* 118), 1,3-dimethyl-1,3-disilacyclobutane (DMDSCB, *m/z* 116), and trimethylsilane (TriMS, *m/z* 74), were formed during the secondary gas-phase reactions of DMS. However, the formation of these major products involved more than one possible mechanism. In order to have a better understanding on the identity of the mechanism responsible for the formation of these products, trapping experiments with 1,3-butadiene (BTD) and ammonia (NH_3) were carried out to trap the intermediates involved in these mechanisms. These experiments were performed by mixing DMS with 8-fold of trapping agents at a filament temperature of 1200 and 1400 ^{o}C. The reason behind the choice of temperature is due to the difference in behaviour of the gas-phase chemistry of DMS. As discussed earlier, the peak at *m/z* 118 was predominantly present at 1200 ^{o}C, whereas the peak at *m/z* 116 was dominating along with the one at *m/z* 73 at a filament temperature of 1400 ^{o}C. The trapping experiments were performed in the HWCVD reactor. For each temperature a mass spectrum was collected every five minutes for one hour. Prior to each trapping experiment, a control experiment with 1% DMS/He and trapping agents, respectively, was done separately as a reference under the same experimental conditions.

5.3.3.1 Trapping Experiment with 1,3-Butadiene

As discussed in earlier sections, the formation of TMDS was found to proceed via two mechanisms, either radical recombination reaction (Equation (5-8)) or silylene insertion reaction (Equation (5-12)). To identify the origin of its production, trapping experiments with 1,3-butadiene was carried out. Figure 5-13 shows the TOF mass spectrum of 12 Torr of 8% BTD : 1% DMS in helium recorded at a Ta filament temperature of 1200 ^{o}C after one hour of reaction time. 1,3-Butadiene is known as an excellent silylene trapping agent,[179, 213, 214] It reacts with silylene species to form a five-membered-ring adduct. The reaction between dimethylsilylene and BTD is illustrated in Equation (5-17), leading to an adduct product with a mass of 112 amu.



(5-17)

Upon the addition of the trapping agent, the peak at *m/z* 118 was completely suppressed and a new peak representing the trapping adduct at *m/z* 112 appeared instead. In the absence of BTD, the intensity of the peak at *m/z* 118, shown in Figure 5-4a, increased with reaction time at the same temperature. To confirm the role of the trapping agent, an intensity distribution of these peaks at *m/z* 112 with filament-on time at a filament temperature of 1200 ^{o}C is plotted and illustrated in Figure 5-14. As shown in this plot, the intensity of this peak increased with increasing reaction time indicating that the trapping of dimethylsilylene by BTD was effective. This has led us to conclude that

the molecule 1,1,2,2-tetramethyldisilane is originated mainly from the insertion reaction of dimethylsilylene into the Si-H bond in the parent DMS molecule.

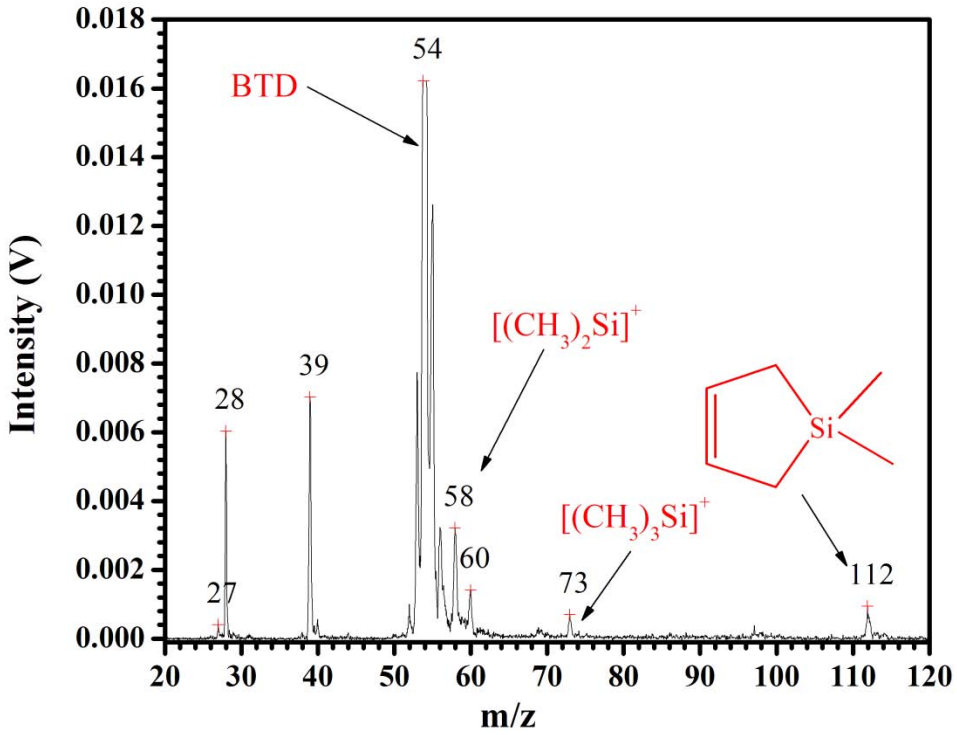


Figure 5-13: 10.5 eV SPI TOF mass spectra of 12 Torr 1% DMS + 8% BTD in He in the reactor at filament temperature 1200 ^{o}C after one hour of turning the filament on.

In addition, the peak at *m/z* 73 is still present and part of its intensity is believed to originate from radical recombination reaction as illustrated by Equation (5-7). This indicates that BTD does not react with the free radicals. The intensity profile of the peak at *m/z* 73 in the presence of BTD is also plotted in Figure 5-14. These intensities increased with reaction time and were comparable to those obtained in the absence of BTD. This suggests that the peak at *m/z* 73 originated mainly from radical recombination

reactions and that the addition of 1,3-Butadiene to the mixture did not affect the occurrence of the radical chain reactions during the gas-phase chemistry of DMS.

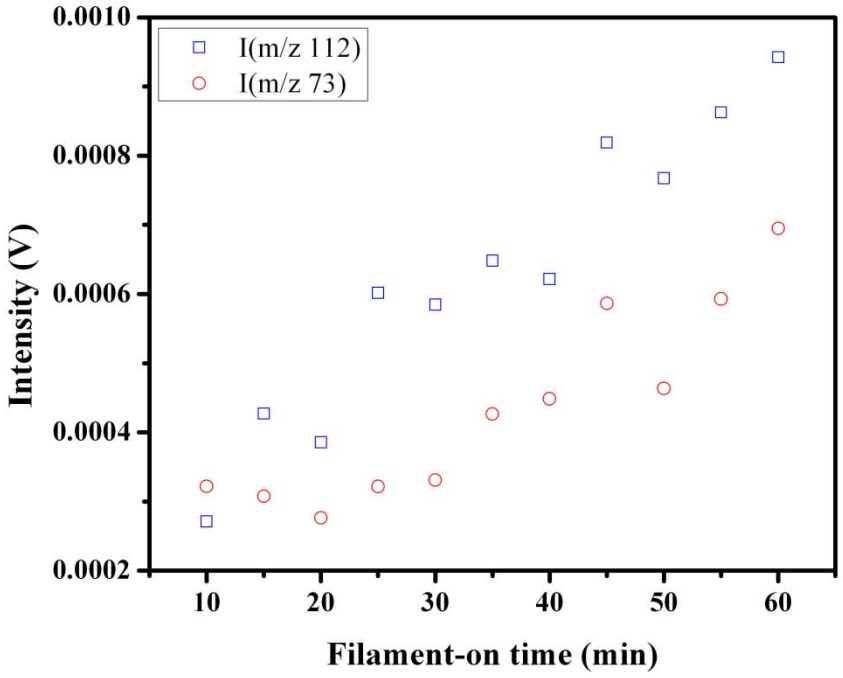


Figure 5-14: Intensity of peak at *m/z* 112 and 73 from 12 Torr 8% BTD + 1% DMS/He versus filament-on time at a filament temperature of 1200 ^{o}C.

In order to differentiate between the peaks generated from the chemical trapping reactions and the decomposition of 1, 3-butadiene itself, a control experiment using 8% BTD was performed under the same experimental conditions. The collected mass spectrum is shown in Figure 5-15. The room-temperature SPI TOF mass spectrum of 8% BTD/He is dominated by the parent ion peak at *m/z* 54 and its photofragment ion peaks at *m/z* 28 [$(C_2H_4)^+$] and 39 [$(C_3H_3)^+$]. The examination of the mass spectrum of BTD at a filament temperature of 1200 ^{o}C revealed the absence of any new peaks produced, as

illustrated in Figure 5-15b, suggesting that at this temperature this molecule is relatively stable and does not decompose or undergo gas-phase reactions.

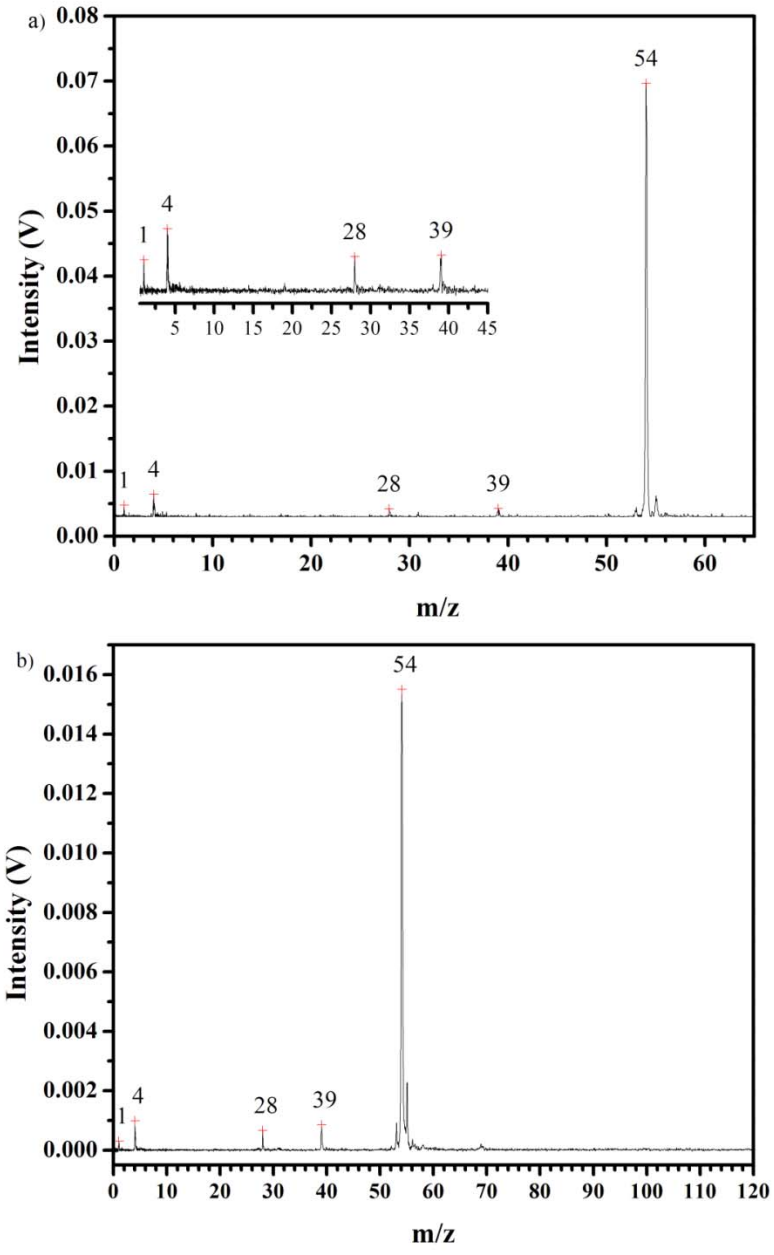
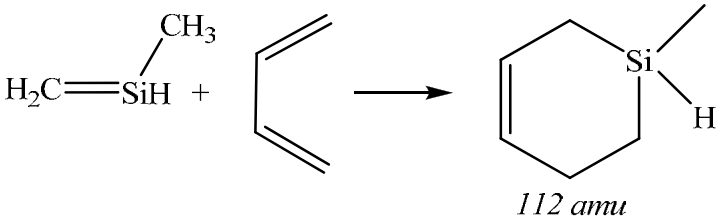


Figure 5-15: 10.5 eV SPI TOF mass spectrum of a) 1,3-Butadiene at room-temperature (Inset: an enlarged picture in the mass region of 0-45 amu), b) 12 Torr of 8% BTD/He mixture recorded 10 minutes after the filament was turned on at 1200 °C.

The trapping experiment with BTD was repeated at a higher temperature of 1400 ^{o}C to confirm that the formation of DMDSCB involves silylene and silene species. In addition to the reaction with a silylene species as shown in Equation (5-17), BTD is also known to react with silene to form a six-membered-ring compound. Equation (5-18) shows such a reaction between BTD and methylsilene, forming an adduct with a mass of 112 amu.



(5-18)

Figure 5-16 illustrates the mass spectrum recorded at a filament temperature of 1400 ^{o}C using the mixture of 8% BTD + 1% DMS/He. Both peaks at *m/z* 118 and 116 that were present in the absence of BTD disappeared upon the addition of BTD. Along with it, the peak at *m/z* 112 representing the trapping adduct was observed. The appearance of the adduct peak is indicative that DMDSCB is originating from silene/silylene chemistry, not from reactions involving free radicals. It is worth mentioning that at this high temperature, the control experiment with 8% BTD showed the appearance of new peaks at *m/z* 40, 66, 68, 70, 78, 80, 81, 92, 95 and 110 resulting from the secondary gas-phase reaction of BTD at 1400 ^{o}C. These peaks did not overlap with any of the peaks related to DMS chemistry.

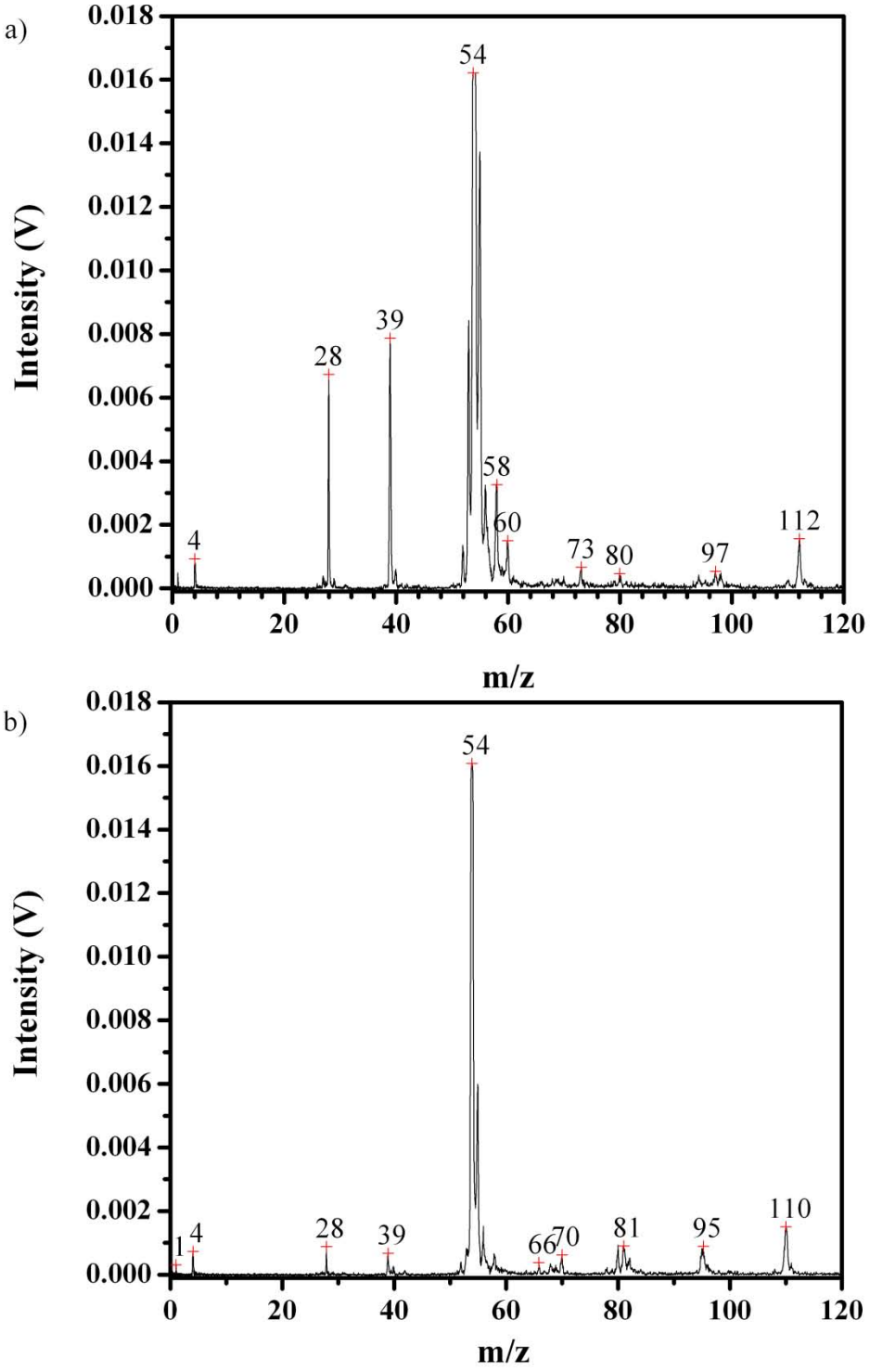
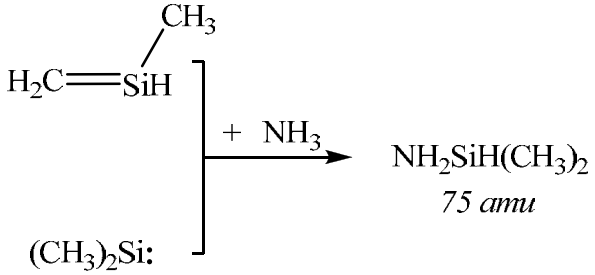


Figure 5-16: a) 10.5 eV SPI TOF mass spectra of 12 Torr 1% DMS + 8% BTD in He in the reactor at filament temperature 1400 ^{o}C (Note the peak at *m/z* 54 is overloaded), b) 10.5 eV SPI TOF mass spectra of 12 Torr of 8% BTD in He in the reactor at filament temperature 1400 ^{o}C after 30 min of reaction time.

The reactions between the trapping agent BTD and methylsilene/dimethylsilylene intermediates result in the formation of two different adducts with the same mass, as represented by Equations (5-17) and (5-18). Therefore, the usage of BTD did not help in differentiating between the two routes responsible for the formation of DMDSCB. This has compelled us to investigate additional trapping agents that will enable us to distinguish between the two routes.

5.3.3.2 Trapping Experiments with Ammonia

The reactions of ammonia with either intermediate lead to the formation of dimethylsilylamine with a mass of 75 amu, as represented by Equation (5-19).



(5-19)

The mass spectrum collected during the experiment of 1% DMS + 8% NH_3/He in the HWCVD reactor at a filament temperature of 1300 ^oC is presented in Figure 5-17 along with the mass spectrum obtained in the absence of ammonia. The peak of the trapping adduct at *m/z* 75 overlaps with the isotope peak for the one at *m/z* 73 originating from TriMS. A comparison of the intensity ratio of I(*m/z* 75)/I(*m/z* 73) using the two mixtures in the presence and absence of the ammonia is shown in Figure 5-18. The ratio obtained in the presence of the trapping agent at a filament temperature of 1300 ^oC was, in general, higher than the one obtained from the control experiment in the absence of

NH_3. This increase in the ratio confirms that ammonia did indeed trap $CH_3SiH{=}CH_2$ and $(CH_3)_2Si$: intermediates responsible for the formation of DMDSCB.

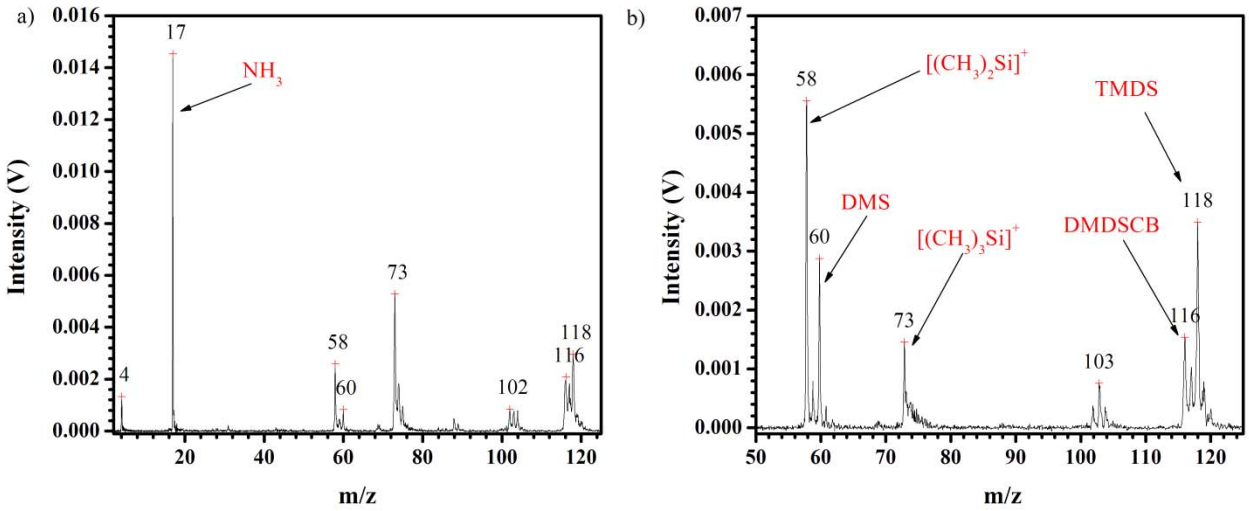


Figure 5-17: 10.5 eV SPI TOF mass spectra of a) 12 Torr of 1% DMS + 8% NH_3 in He, and b) 12 Torr of 1% DMS/He in the reactor at filament temperature 1300 ^{o}C and after five minutes of turning the filament on.

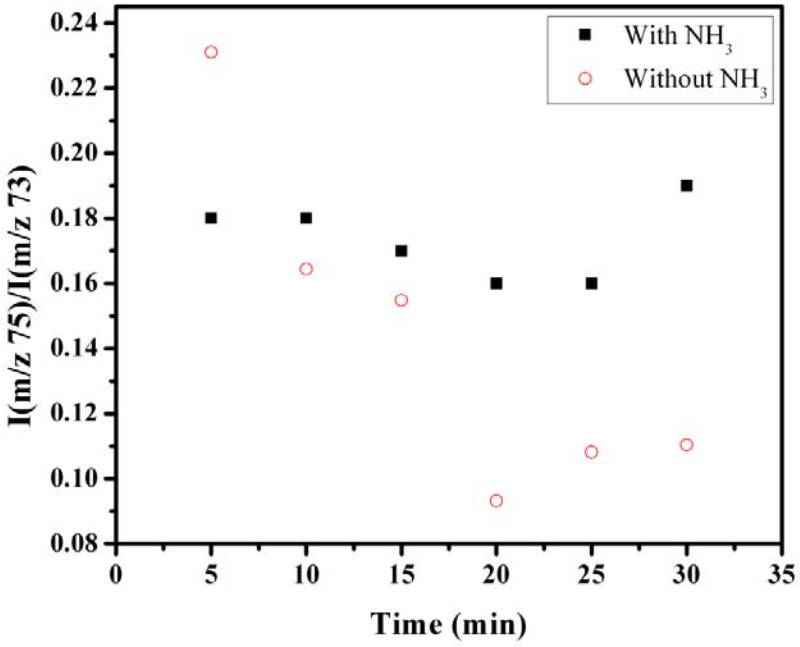


Figure 5-18: Comparison of the intensity ratio of the peak at *m/z* 75 to the one at *m/z* 73 in the presence and absence of ammonia versus filament-on time at 1300 ^{o}C.

At this temperature, as elucidated by Figure 5-17b, the peak at *m/z* 116 starts to appear and with increase in reaction time will dominate over the peak at *m/z* 118. Upon the addition of the trapping agent, the intensities of these two peaks were both reduced, which was expected since NH_3 will react with the precursor intermediates for these two products. In order to obtain a better understanding on the relative efficiency of NH_3 to trap methylsilene and dimethylsilylene, the intensity ratio of the peak at *m/z* 116 to the one at *m/z* 118 with and without NH_3 is plotted in Figure 5-19. The ratio is found to decrease in value upon the addition of ammonia. This signifies that NH_3 traps methylsilene (precursor for the formation of the peaks at *m/z* 116) more effectively than dimethylsilylene (precursor involved in the mechanism for peak at *m/z* 118). This behaviour was also observed at filament temperature of 1400 ^{o}C.

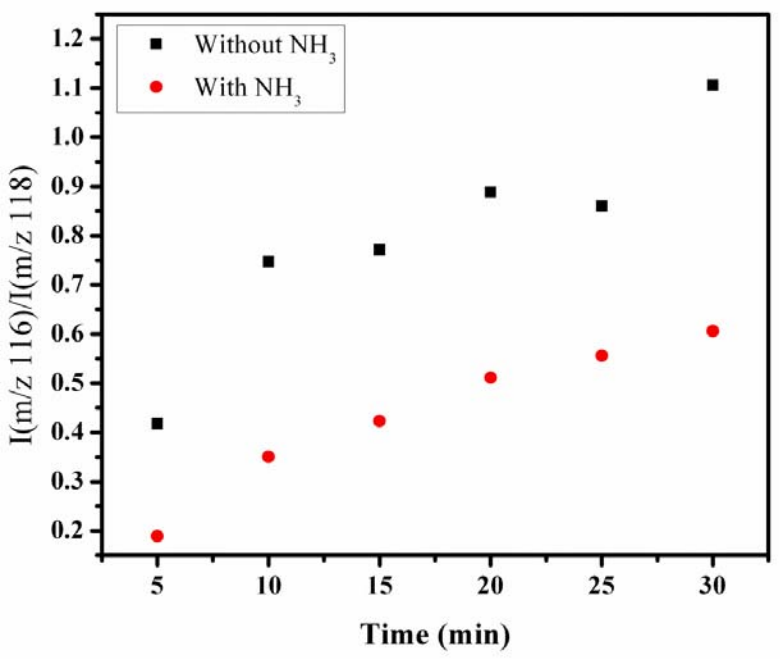


Figure 5-19: Comparison of the intensity ratio of the peak at *m/z* 116 to the one at 118 in the presence and absence of ammonia at 1300 ^{o}C.

To further examine the reactions of NH_3 with the two active intermediates, methylsilene and dimethylsilylene, *ab initio* calculations were carried out on the two reactions using Gaussian 09 at the CCSD(T)/6-311++G(3d,2p)//MP2/6-311++G(d,p) level of theory. The energy level diagram for both reactions is shown in Figure 5-20. All energies include the ZPE corrections. The values represent relative Gibbs free energy at 298 K.

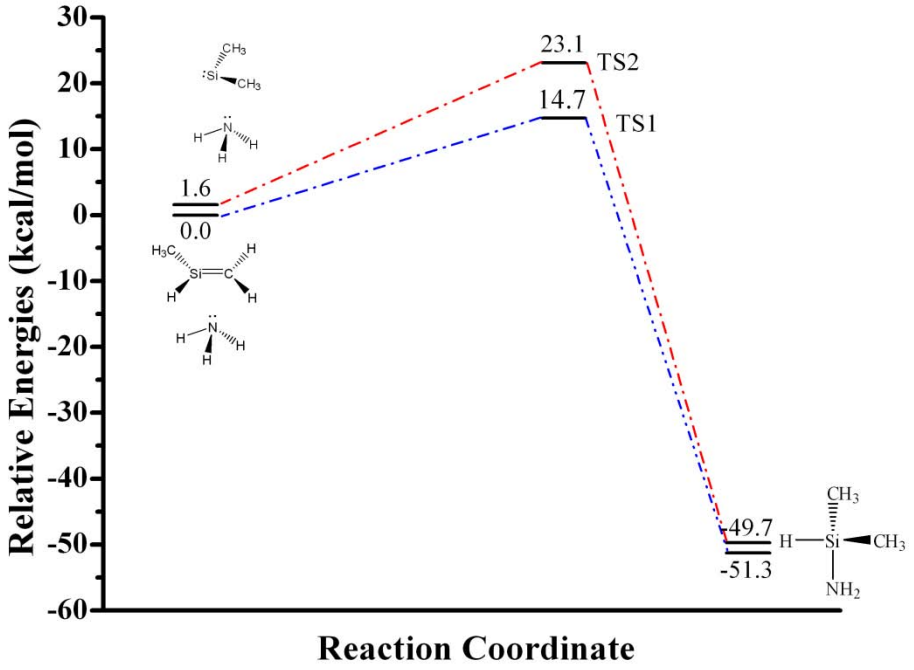


Figure 5-20: Energy level diagrams for the addition reactions of ammonia to methylsilene and dimethylsilylene species. Energy values represent the relative Gibbs free energy in kcal/mol at 298 K (ZPE corrections included).

As shown in the energy diagram, the addition reaction of ammonia to either species to form dimethylsilylamine is exothermic by ~ 50 kcal/mol (*i.e.*, a ~ 209 kJ/mol). The energy barrier for the addition to methylsilene is computed to be 14.7 kcal/mol (*i.e.*,

a 61.5 kJ/mol), whereas the one for the addition to dimethylsilylene is found to be 23.1 kcal/mol (*i.e.*, a 96.7 kJ/mol) at room temperature. These values indicate that the reaction of ammonia with methylsilene is kinetically favoured over the one with dimethylsilylene. In addition, the bimolecular rate constants for both reactions are computed using $k_{bimol} = e^2\left(\frac{k_B T}{h}\right) e^{\Delta S^{\neq}/R} e^{-Ea^{\neq}/RT}, Ea^{\neq}_{bimol} = \Delta H^{\neq} + 2RT$. The value was determined to be 96.5 $M^{-1} s^{-1}$ and 6.6×10^{-5} $M^{-1} s^{-1}$ for the reaction of ammonia with methylsilene and dimethylsilylene, respectively. As these values indicate, the reaction of ammonia with methylsilene is significantly faster than the addition of ammonia to the silylene intermediate. This agrees with our experimental observations.

In summary, the involvement of free radicals and silene/silylene intermediates in the gas-phase chemistry of DMS is portrayed by the presence of the peaks at *m/z* 73, 118 and 116. As it was demonstrated, the gas-phase chemistry of DMS is dominated by the peak at *m/z* 118, representing 1,1,2,2-tetramethyldisilane, at low filament temperatures. With the help of trapping experiments with 1,3-butadiene, it was confirmed that the origin for the formation of this molecule involves the insertion reaction of dimethylsilylene into Si-H bond of the parent molecule. As the temperature is increased to 1300 ^{o}C and higher, the peaks at *m/z* 73 and 116 predominate. The peak at *m/z* 73 was assigned to trimethylsilane, arisen from radical recombination reaction between methyl and dimethylsilyl radicals. The detection of the peak at *m/z* 116 indicate the formation of 1,3-dimethyl-1,3-disilacyclobutane. From the isotope experiment as well as the trapping experiment with 1,3-butadiene and ammonia, it was concluded that the formation of this

peak proceeds via both methylsilene cyclodimerization reaction and dimethylsilylene dimerization reaction, with the former being more important.

5.4 Effect of Precursor Gas Pressure on DMS Gas-Phase Chemistry

In the deposition process using HWCVD, the precursor pressure is considered as an important factor that can influence the properties of the deposited thin film. Several studies were carried out to explore the correlation between the precursor pressure and deposited film properties. For instance, Pant *et al*.[45] have found that an increase in silane pressure resulted in a transition from amorphous to polycrystalline silicon films. The same conclusion was reached by Zhao *et al*.,[215] who showed that the crystallinity of the deposited SiC thin films was improved upon the usage of a higher total gas pressure with a mixture composed of SiH_4, CH_4, and H_2.

In this study, the effect of the precursor pressure on the secondary gas-phase reactions is explored by studying the intensity distributions of the main product peaks using 1.2 Torr of DMS and comparing with the ones obtained with 0.12 Torr. With increasing pressure, the intensity of the parent ion peak at *m/z* 60 ($(CH_3)_2SiH_2^+$) and its photofragment at *m/z* 58 ($(CH_3)_2SiH_2^+$) was noticed to decrease at a filament temperature of 1100 ^oC after the filament was turned on when 1.2 Torr of DMS was used. This temperature was slightly lower than the one obtained using 0.12 Torr of DMS. Along with the decrease of the parent ion peak, two new peaks appeared at *m/z* 73 and 118 at the same temperature. As it has been described previously, the peaks at *m/z* 73 and 118 have been assigned to trimethylsilane (TriMS) and 1,1,2,2-tetramethyldisilane (TMDS), respectively.

To illustrate the effect of the DMS pressure, Figure 5-21 shows a comparison between the mass spectra recorded using 12 Torr of 1% DMS/He sample (p(DMS) = 0.12 Torr) and 12 Torr of 10% sample (p(DMS) = 1.2 Torr) in the HWCVD reactor at a filament temperature of 1300 ^{o}C. The increase of the precursor pressure resulted in a greater number of products as indicated by the increase in the number of mass peaks. In addition, at this temperature, the secondary gas-phase reaction was dominated by the formation of TMDS (*m/z* 118 and its photofragment ions at *m/z* 103 and 73) resulted from silylene insertion reaction when using 0.12 Torr of DMS. When the DMS pressure was increased 10 fold, the chemistry became dominated by TriMS (*m/z* 73) formed by a free-radical recombination reaction and DMDSCB (*m/z* 116) generated from silene/silylene dimerization reactions. This change in dominant peaks with an increase in pressure is also observed when using 12 Torr of 4% DMS/He (p(DMS) = 0.48 Torr).

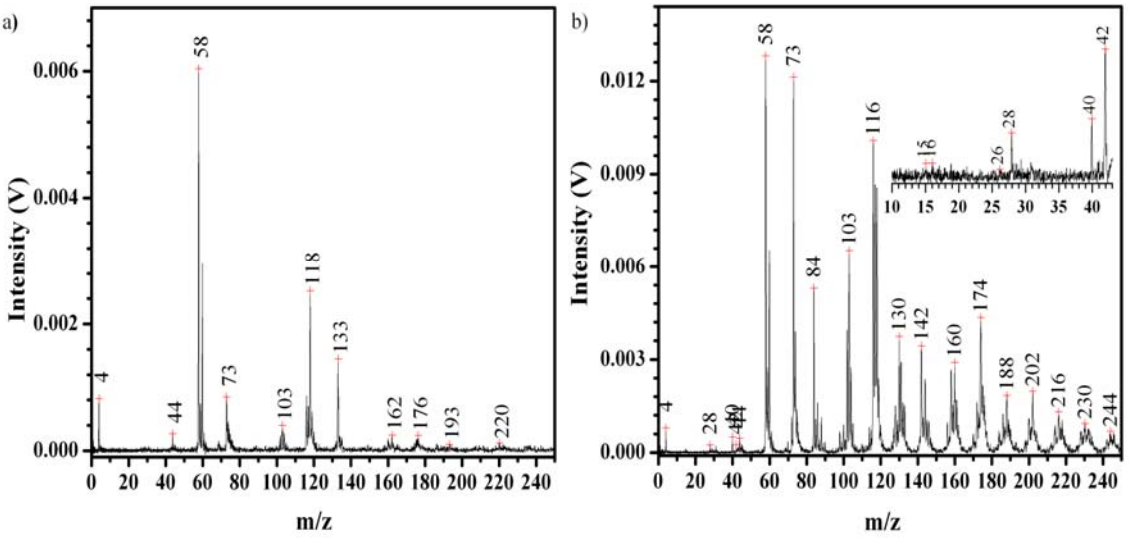


Figure 5-21: 10.5 eV SPI TOF mass spectra of a) 12 Torr of 1% DMS/He, and b) 12 Torr of 10% DMS/He in the reactor at a filament temperature of 1300 ^{o}C. (Inset: an enlarged spectrum in the mass region of 10-45 amu).

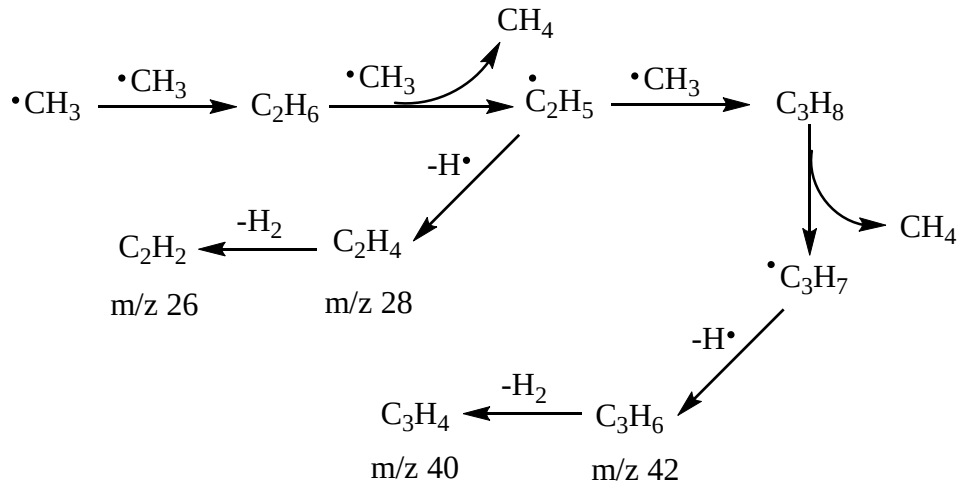
Table 5-1 summarizes the intensity ratios of each of the mass peaks at *m/z* 73, 116, 118 to that of the parent ion peak at *m/z* 60 for two filament temperatures of 1300 ^{o}C and 1400 ^{o}C when using 0.12 and 1.2 Torr of DMS. Examination of these ratios obtained under different sample pressures showed that the ratios generally increased with increasing pressure at the initial stages of the reaction. This indicates that the amount of products represented by the peaks at *m/z* 118, 73 and 116 increases when using a high pressure of DMS. As the reaction progresses, all the ratios experience a decrease in their values. The reason responsible for this behaviour will be described later.

Table 5-1 Summary of the intensity ratios of each of the peaks at *m/z* 73, 116, and 118 to that of the parent peak at *m/z* 60 when using 0.12 Torr and 1.2 Torr of DMS in HWCVD reactor at filament temperatures of 1300 and 1400 ^{o}C

Intensity ratio	0.12 Torr of DMS		1.2 Torr of DMS	
	1300 ^{o}C	1400 ^{o}C	1300 ^{o}C	1400 ^{o}C
I(73 amu) /I(60 amu)	0.051- 32.93	0.28-10.88	0.71-11.62	3.29-11.87
I(116 amu)/I(60 amu)	0.045-5.43	0.37-5.72	0.39-3.49	1.76-4.53
I(118 amu)/I(60 amu)	0.056-4.96	0.84-3.92	0.57-1.49	0.85-1.83

Furthermore, it was noticed that the increase in the pressure of DMS resulted in the formation of small hydrocarbons at 1300 ^{o}C, which were absent with 0.12 Torr of DMS, as illustrated in Figure 5-21. With 1.2 Torr of DMS, new peaks at *m/z* 28, 40, and 42 appeared and were assigned to ethene, propyne and propene, respectively. The confirmation of the identity of these peaks was obtained by comparing with the room-temperature mass spectra of the authentic samples. It should be noted that two very weak

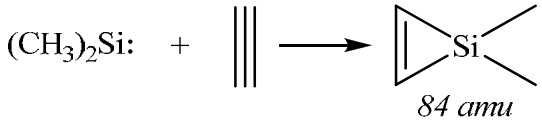
peaks at *m/z* 16 and 26, representing methane and acetylene, were also observed. The weakness of these peaks is related to their high ionization energy of 12.68 eV[216] for methane and 11.42 eV[217] for acetylene. These values are higher than the photon energy (10.5 eV) used for ionization. A potential formation pathway of these small hydrocarbons is described in Scheme 5-2 and involves radical recombination reactions between methyl moieties as well as H abstraction reaction, as suggested by the previous study by Taylor and Milazzo.[218]



Scheme 5-2 Formation of small hydrocarbons

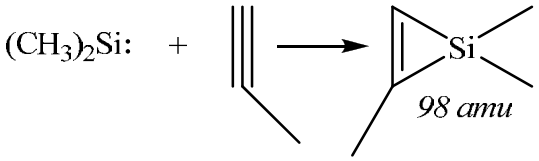
In the experiment with 1.2 Torr of DMS for temperatures of 1300 and 1400 ^{o}C, the intensity ratio of ethene/propene was found to range from 0.30 to 1.37. Taking into consideration the differences in the ionization cross sections, the formation of ethene is favored over propene as a hydrocarbon product from the secondary gas-phase reactions with a ratio ranging from 10.8 : 1 to 49.2 : 1.

The presence of these hydrocarbons during the secondary gas-phase reactions with DMS as a precursor gas is believed to behave as trapping agents and reacts with silylene intermediates, which in turn affects the formation of products generated from these intermediates. Acetylene molecules, produced in-situ, is a well-known trapping agent for silylene species.[122, 176, 219] One of the characteristic reaction of silylene is to react with CC double and triple bond through π-type addition reaction.[220] Hence, the dimethylsilylene intermediate reacts with acetylene yielding 1,1-dimethylsilacyclopropene with a mass of 84 amu, as illustrated by Equation (5-20).



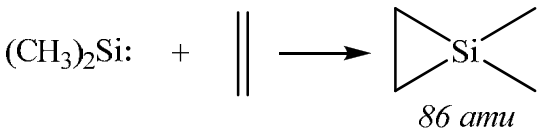
(5-20)

Similarly, dimethylsilylene (:Si$(CH_3)_2$) can react with propyne (*m/z* 40), producing 1,1, 2-trimethylsilacyclopropene (*m/z* 98) (Equation (5-21)).



(5-21)

Several studies have claimed that ethene traps efficiently methylsilyl radicals,[94, 122, 176, 221, 222] , however, it is believed that this molecule will also react with silylene intermediates. The reaction is represented by Equation (5-22).



(5-22)

To confirm the occurrence of the reactions of ethene with both silylene and silyl species, a trapping experiment with 8 fold of ethene was conducted and the collected mass spectrum is presented in Figure 5-22. The reaction of ethene with dimethylsilylene and dimethylsilyl radical will yield the formation of 1,2-dimethylsilacyclopropane (*m/z* 86) and 1-dimethylethylsilane (*m/z* 88), respectively. As shown in Figure 5-22, these two peaks were observed. A comparison of the intensity distributions of the main product peaks at *m/z* 73, 116, and 118 from using DMS showed that their intensities were reduced in the presence of ethene, indicating that this trapping agent reacts with both dimethylsilyl radical and dimethylsilylene intermediates. In order to elucidate the trapping efficiency of either intermediate by ethene, the intensity ratio of the respective peaks in the presence and absence of ethene was examined. Table 5-2 lists these intensity ratios. All of the obtained ratios were less than 1, which confirms that ethene trapped dimethylsilyl radical and dimethylsilylene species. The ratio obtained with the peak at *m/z* 118, which originated from dimethylsilylene insertion reaction, was the lowest among the three. This signifies that ethene trapped more efficiently dimethylsilylene intermediates, which contradicts with the literature[94, 122, 176, 221, 222] claiming that ethene scavenges mainly methylsilyl radicals.

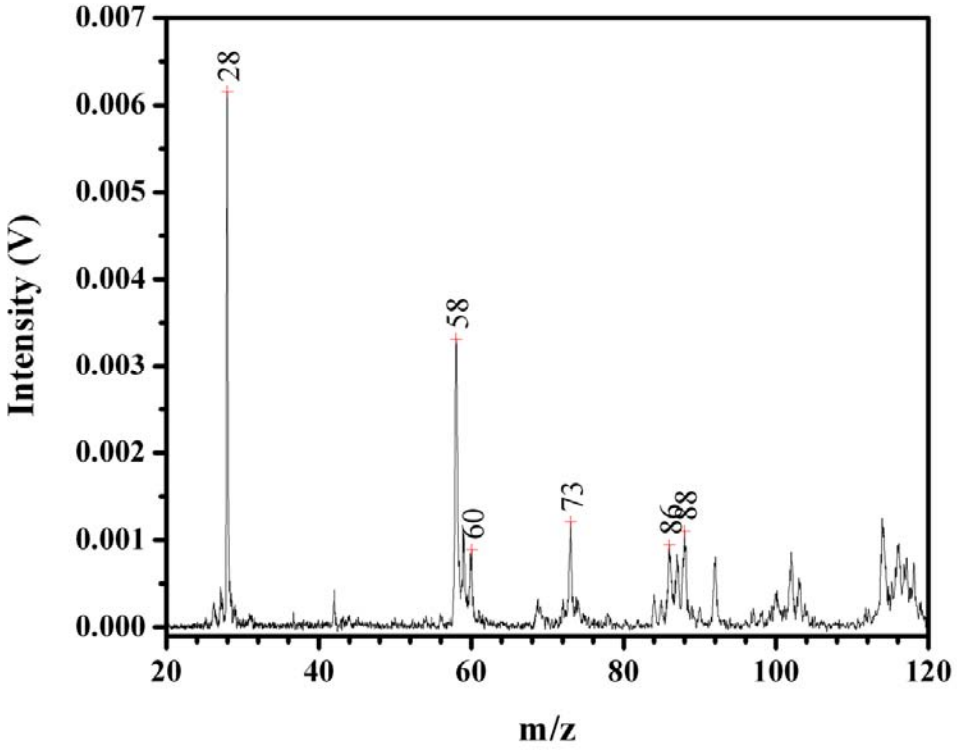


Figure 5-22: 10.5 eV SPI TOF mass spectra of 12 Torr of 1% DMS + 8% ethene in He in the reactor at filament temperature 1300 ^{o}C.

Table 5-2 Comparison of the intensity ratios of each of the peaks at *m/z* 73, 116, and 118 in the presence and absence of ethene ((') indicates the ones with ethene)

I(73)'/I(73)	I(116)'/I(116)	I(118)'/I(118)
0.20 – 0.90	0.28 – 0.97	0.15 – 0.43

Figure 5-23 shows the intensity distribution of peaks at *m/z* 26, 28, 40, 84, 86 and 98 as a function of filament-on time for a filament temperature of 1300 ^{o}C with 1.2 Torr of DMS in the reactor. The detection of peaks at *m/z* 84, 86 and 98 strongly suggests that ethene, acetylene and propyne were produced and in-situ trapping of dimethylsilylene took place during the secondary gas-phase reactions of 12 Torr of 10% DMS in the in the

HWCVD process. Comparison of Figure 5-23a and b also demonstrates that the peaks at 84, 86, and 98 appear strongly only when there is a significant amount of hydrocarbons formed.

As it has been mentioned before, with an increased in the DMS pressure from 0.12 Torr to 1.2 Torr, a switch in the dominance in the peaks at *m/z* 73, 116, and 118 was observed. This behavior is illustrated in Figure 5-24, where it shows a comparison of the intensity profiles of the three major products at *m/z* 73, 118 and 116 at the filament temperature of 1300 ^{o}C for the different DMS pressure of 1.2 Torr (Figure 5-24a) and 0.12 Torr (Figure 5-24b). As noticed from this comparison, the formation of TMDS (*m/z* 118) was favoured at the lower precursor pressure up to $t \leq 25$ min; however, with increasing pressure, this product had the weakest intensity of all. For the same temperature, the peak at *m/z* 73 was found to dominate the gas-phase chemistry when 1.2 Torr of DMS was used throughout the entire reaction time, whereas at the lower pressure the dominance of this peak was only accentuated after 30 minutes of turning the filament on. Similar behaviour can be observed for the peak at *m/z* 116. The intensity profile of these peaks at the higher pressure of 1.2 Torr and a filament temperature of 1300 ^{o}C resembled the one obtained at a higher temperature of 1500 ^{o}C (Figure 5-24c) using 0.12 Torr of DMS in a way that the intensity of these major peaks increased in the first few minutes after turning the filament on, followed by a decrease.

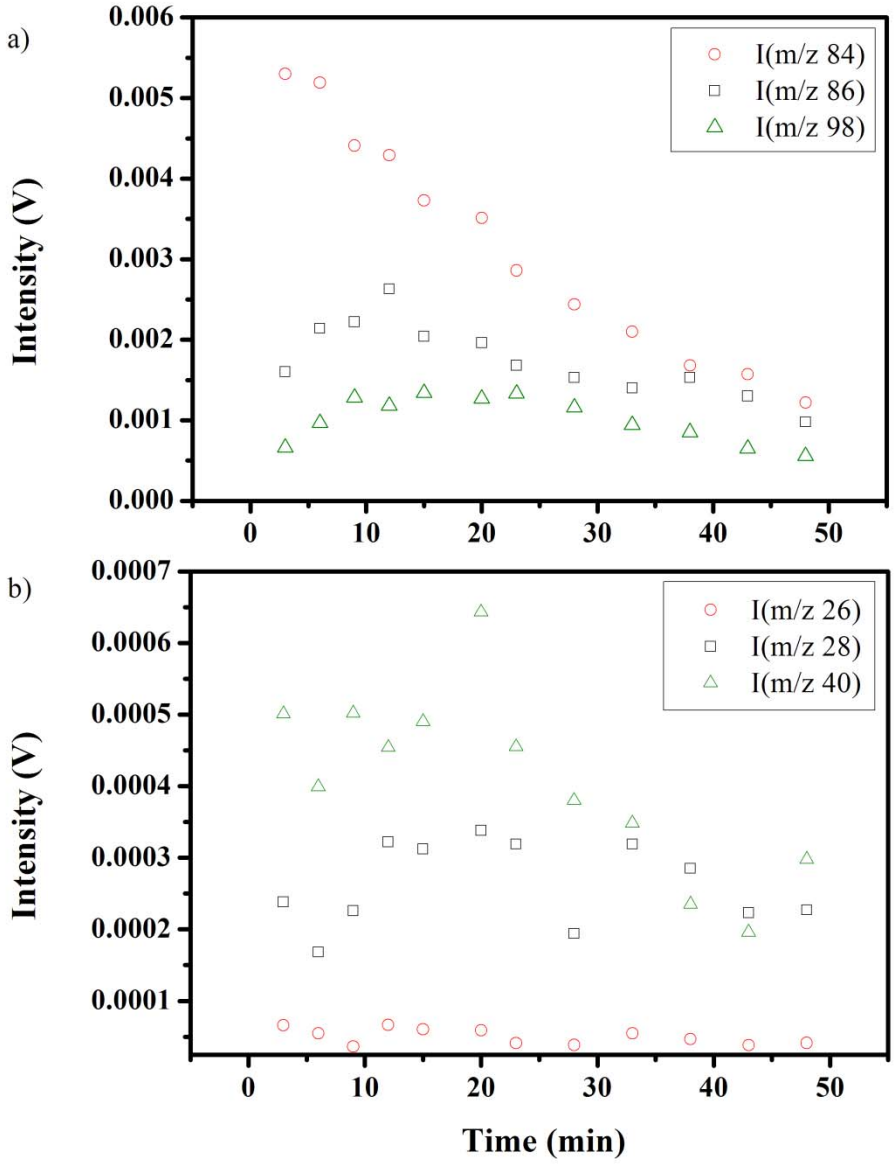


Figure 5-23: Comparisons of the intensity of the peaks at a) *m/z* 86, 84, 98 and b) *m/z* 26, 28, 40 versus filament-on time at 1300 ^{o}C observed with 1.2 Torr of DMS.

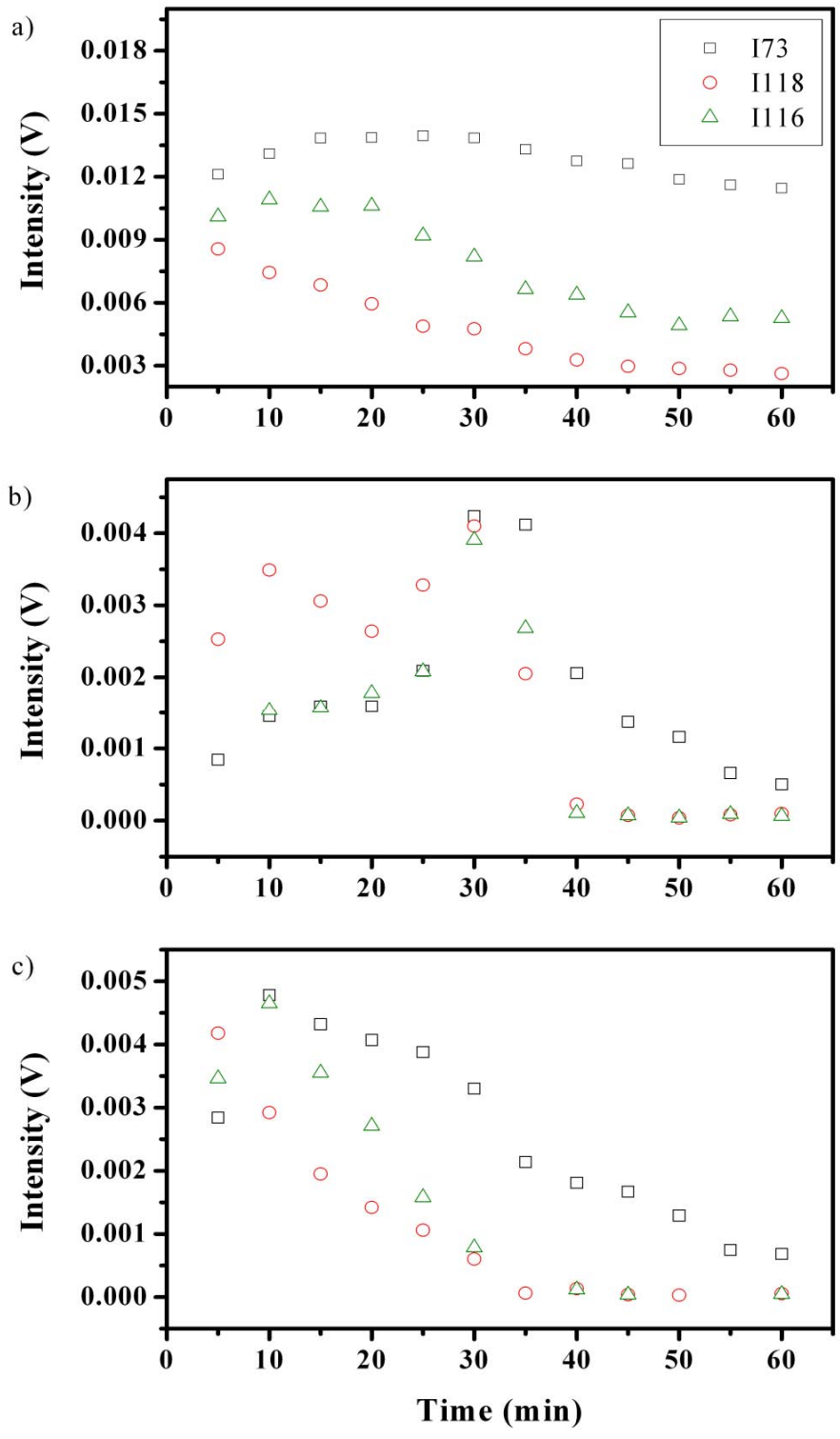


Figure 5-24: The intensity of the peaks at *m/z* 73, 118, and 116 versus filament-on time observed with a) 1.2 Torr of DMS at 1300 ^{o}C, b) 0.12 Torr of DMS at 1300 ^{o}C, and c) 0.12 Torr of DMS at 1500 ^{o}C.

The change in trend in the evolution of these peaks suggests a competition between free-radical reactions and silylene chemistry. As it has been previously discussed, the usage of high precursor pressure resulted in the production of several small hydrocarbon molecules, including methane, ethene, acetylene, propene, and propyne. Acetylene[122] has been known to react with silylene species, while ethene[94, 122] and propene[122] was claimed to react mainly with free radicals. Therefore, their presence during the secondary gas-phase reactions of DMS will affect the formation of all the products involving these intermediates. This effect is reflected on the intensity profile of the peak at *m/z* 118, which was observed to decrease when these hydrocarbon were simultaneously formed. From Figure 5-23, it can be seen that the peaks 26, 28 and 40 representing acetylene, ethene and propyne, reached their maximum intensity at 25 min. This time also coincides with the formation of the trapping products with *m/z* 84 and 98 amu. Therefore, before 25 min, the amount of hydrocarbon produced was not significant to react with dimethylsilylene. The observed increase in the intensity of the peak at *m/z* 118 when comparing both Figures 5-24a and 5-24b within the first 25 min of reaction time is due to the significant abundance of dimethylsilylene intermediate when the precursor pressure is increased. When the trapping reactions between silylene species and the various hydrocarbons started to take place at $t \geq 25$ min, a decrease in the formation of TMDS (*m/z* 118) was observed (Figure 5-24a). This explanation can be extended to explain the behaviour for the other two peaks. As it can be noted from Figure 5-24, the intensity profile of peaks at *m/z* 73 and 116 showed an increase when switching from low to high precursor pressure in the 30 minutes of reaction time. As the reaction progresses and a good amount of hydrocarbon is present, a decrease in the intensity of these peaks is

observed due to the trapping of the corresponding intermediates by the hydrocarbon molecules. Furthermore, the presence of the hydrocarbon molecules at high precursor pressure did not affect the formation of the major peaks to the same extent. As stated earlier, the intensity of the peak at *m/z* 118 was the lowest of all with increasing precursor pressure. This is due to the fact that the mechanism of this peak involves solely dimethylsilylene species, which is consumed by the various hydrocarbon molecules, hence, reducing its participation in the formation of TMDS. On the other hand, the major contributor to the peak at *m/z* 73 is dimethylsilyl radical recombination reaction with methyl radical. Among all of the hydrocarbons produced, only ethene and propene would have an effect on the production of trimethylsilane by reacting with dimethylsilyl radical. For the formation of DMDSCB (*m/z* 116), aside from dimethylsilylene, there is an additional contribution from methylsilene. The formed hydrocarbons would only react with dimethylsilylene moieties, while not affecting methylsilene. Therefore, the peak at *m/z* 118 is affected the most by the production of small hydrocarbons with the increase in the DMS pressure.

In summary, the increase in the sample pressure has yielded the formation of small hydrocarbons including methane, ethene, acetylene, propene and propyne. This leads to a switch from silylene dominant chemistry to a free-radical dominant chemistry with the increase in the sample pressure at a low filament temperature of 1200 ^{o}C. At the low pressure, the formation of 1,1,2,2-tetramethyldisilane (*m/z* 118) by dimethylsilylene insertion reaction into Si-H bond in the DMS molecule was favoured over trimethylsilane (*m/z* 73) produced from a free-radical recombination reaction. However,

when the pressure is increased by 10 times, the gas-phase chemistry was dominated by the formation of trimethylsilane. This is explained by the trapping of the corresponding active intermediates by the small hydrocarbons, ethene, propyne and acetylene produced in-situ.

5.5 Effect of Filament Material on DMS Gas-Phase Chemistry

The nature of the filament material is believed to play a role in the decomposition of the gas precursors in the HWCVD system. In the study of the influence of filament material on the deposition of polycrystalline silicon thin films, it was found that thin films grown by HWCVD using W and Ta as filament materials show different material properties, and this difference is caused by the different surface reaction and catalytic properties of the filament material.[40] In addition, Duan *et al*.[36] has studied the effect of filament material on the decomposition of silane by monitoring the production of Si radical from W, Re, Mo and Ta filaments. Their results showed that the different material provided different apparent activation energy values for Si formation, suggesting that different mechanisms may be active. Additionally, in a study carried out to examine the effect of filament material including W, Ta, Mo and Pt on the deposition of SiC thin films using dimethylsilane, Nakayama *et al*.[60] found that among all chosen filaments, W was the most effective catalyzer with the highest growth rate. It was also shown that Mo and Pt produced large precursors leading to high carbon content in the film, while W and Ta decomposed DMS to form small precursors, reducing the carbon composition in the film.[60] Hence, as the key component in HWCVD is the filament at which the catalytic decomposition of the source gas occurs, the possible use of different materials is

investigated. In this study, the gas-phase chemistry of dimethylsilane was examined on a W filament using 12 Torr of 1% DMS/He and 10% DMS/He mixtures, and the results were compared those obtained with the Ta filament.

From the previous discussions, it was concluded that the secondary gas-phase reactions of DMS on Ta filament are dominated by three major products, *i.e.*, trimethylsilane at *m/z* 73, 1,1,2,2-tetramethyldisilane at *m/z* 118, and 1,3-dimethyl-1,3-disilacyclobutane at *m/z* 116. From the examination of the gas-phase reaction chemistry with W filament, it was found that the same gas-phase species have been detected. However, the effect of the filament material is determined based on which product is formed initially and the temperature at which the gas-phase chemistry becomes active. Figure 5-25 shows two mass spectra collected for 12 Torr of 1% DMS/He mixture under the same conditions using W and Ta filaments. As noted from this figure, when the W filament was used, a peak at *m/z* 73 appeared first, whereas, with Ta filament, the peak at *m/z* 118 was detected initially.

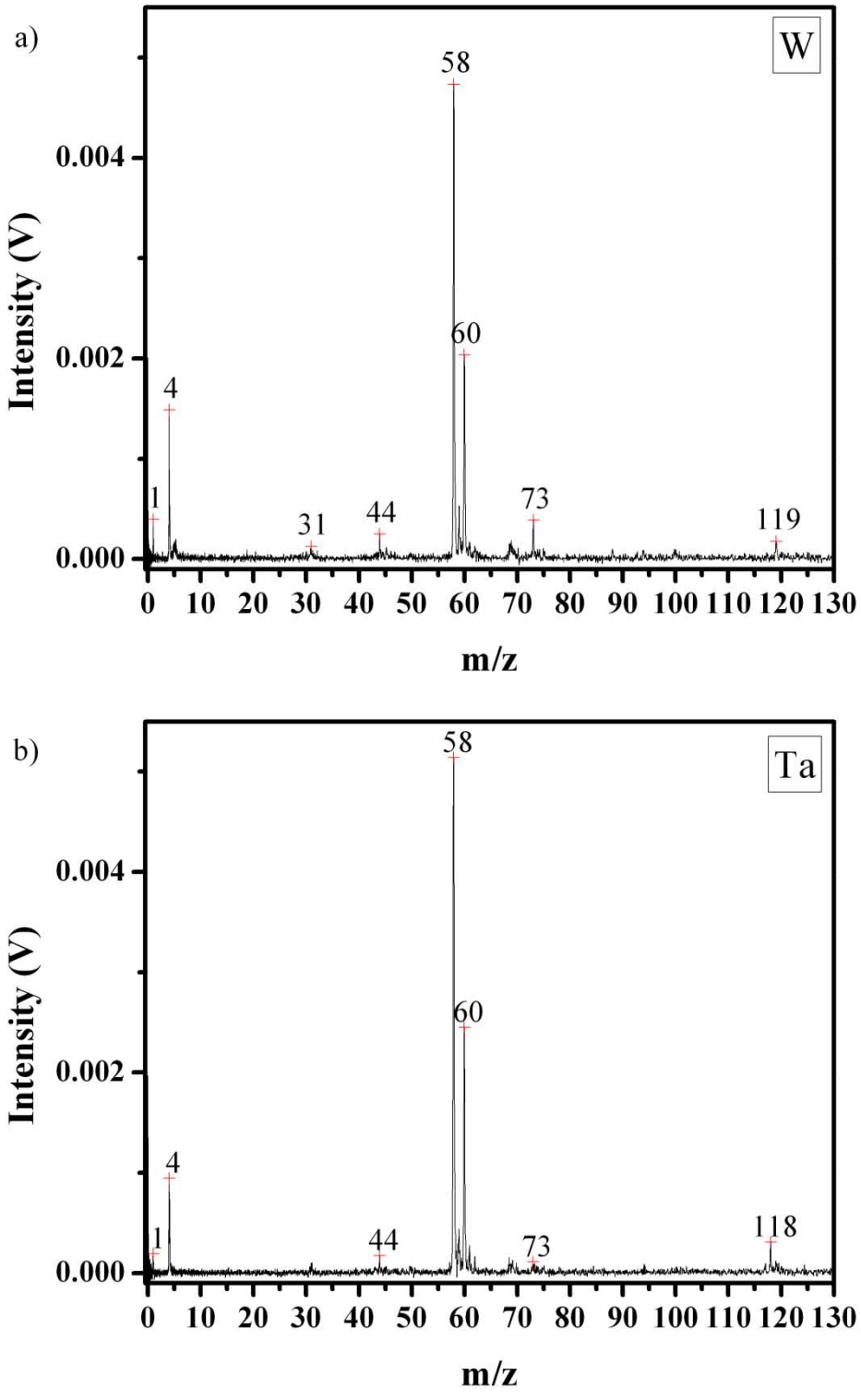


Figure 5-25: 10.5 eV SPI mass spectra using a) W filament and b) Ta filament for 12 Torr of 1% DMS/He at filament temperature of 1200 °C and filament-on time of 5 min.

In order to better illustrate the effect of filament material, the intensity profiles of the major peaks at *m/z* 73, 118 and 116 as a function of filament-on time are plotted for W filament at a filament temperature of 1200 ^{o}C. This plot is shown in Figure 5-26. At 1200 ^{o}C, the gas-phase chemistry was dominated by the peak at *m/z* 73 followed by the peak at *m/z* 118 when using W filament. DMDSCB (*m/z* 116) is still not formed at this low W filament temperature. This behaviour is reversed when Ta filament is employed, as shown in Figure 5-4a, the formation of TMDS at *m/z* 118 is favoured over that of TriMS at *m/z* 73. The DMDSCB product at *m/z* 116 was also produced but in a small amount. This observed difference is related to the origin of the formation of these species. As it has been discussed in previous sections, TMDS is originating from silylene insertion reaction into Si-H bond of the parent molecule, whereas TriMS is formed by the recombination reaction between methyl and dimethylsilyl radicals. The difference is also related to the decomposition mechanism occurring at the filament surface. It has been discussed previously that the decomposition of methyl-substituted silanes on a metal surface is initiated by the cleavage of the Si-H bond resulting in the occupation of the majority of the catalytic sites by H atom and Si moiety.[61, 148, 202] As the filament temperature is increased the Si-CH_3 bond is ruptured resulting in the release of the methyl group into the gas phase. The formation of H_2 occurs by the recombination reaction between two H adsorbates, following Langmuir-Hinshelwood mechanism.

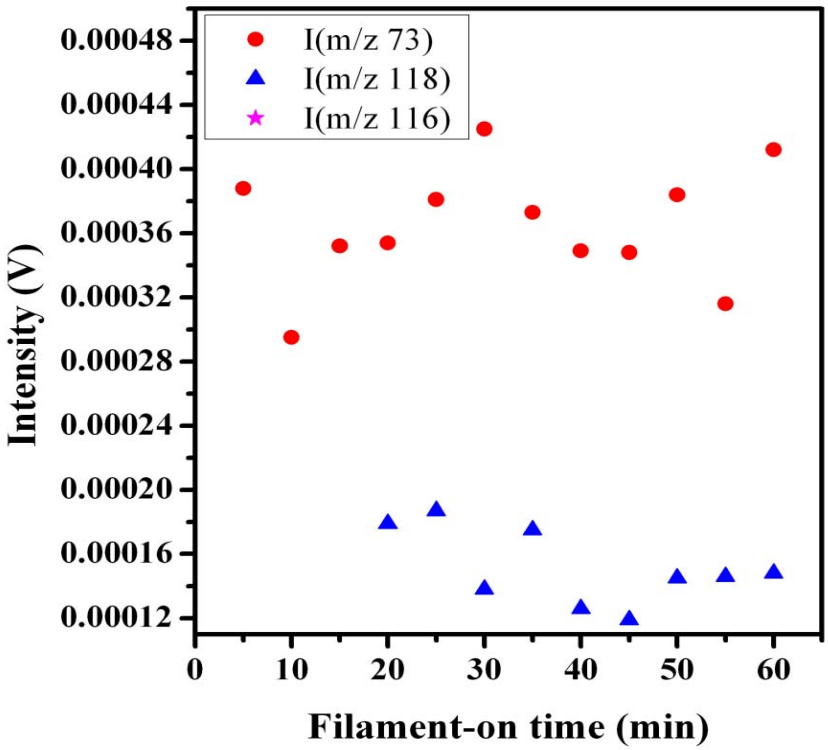


Figure 5-26: Intensity distribution of peaks at *m/z* 73, 116 and 118 generated from W filament when using 12 Torr of 1% DMS/He at a filament temperature of 1200 ^{o}C.

It has been shown that Ta produces H_2 molecule more efficiently.[223, 224] The production of H_2 molecule is accompanied by the formation of silylene and silene reactive species. Therefore, the employment of Ta filament favours the formation of products involving the silylene intermediates at lower temperatures, whereas, on the W wire, the gas-phase chemistry seems to be leaning towards radical recombination reactions. Figure 5-27 shows the intensity profiles of the main products at a higher temperature of 1400 ^{o}C. At this temperature, the chemistry on W and Ta is comparable and is both dominated by the formation of trimethylsilane at *m/z* 73. Hence, it is concluded that, at a low filament temperature of 1200 ^{o}C, W and Ta filaments display different capabilities in generating different radicals thus influencing the subsequent

secondary gas-phase chemistry. This difference no longer exists with increasing temperatures.

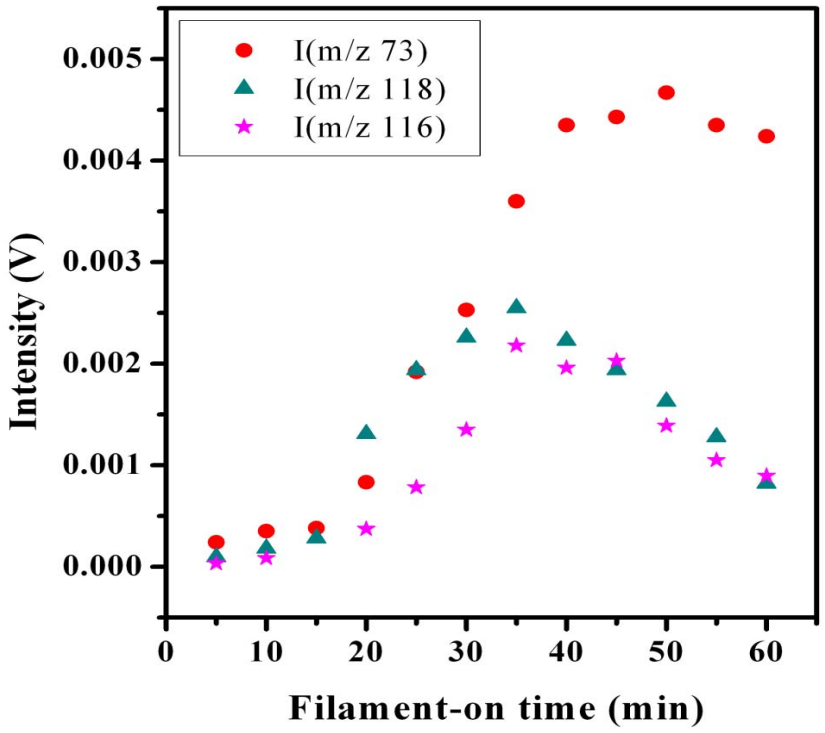


Figure 5-27: Intensity distribution of peaks at *m/z* 73, 116 and 118 generated from W when using 12 Torr of 1% DMS/He and at a filament temperature of 1400 ^{o}C.

5.6 Summary

In this study, the decomposition of dimethylsilane (DMS) on a hot W and Ta filament was explored using laser ionization mass spectrometry. The decomposition of DMS on a W and Ta filament under collision-free conditions proceeds via two major pathways, *i.e.*, methyl and methylsilyl radical ($^{\bullet}CH_3SiH_2$) formation, and elimination of H_2 yielding dimethylsilylene ($(CH_3)_2Si$:) and methylsilene ($(CH_3)HSi=CH_2$).

Under a DMS partial pressure of 0.12 Torr in the HWCVD reactor, secondary gas-phase reactions are dominated by silylene insertion reaction into Si-H bond of the parent molecule at low temperatures, illustrated by the appearance of 1,1,2,2-tetramethyldisilane at *m/z* 118. As the filament temperature is increased, the secondary gas-phase chemistry is governed by the H abstraction reaction between methyl radicals and the parent DMS molecules, followed by radical combination reactions. This is indicated by the detection of peak *m/z* 73 assigned to trimethylsilane. It has also been demonstrated that 1,1-dimethyl-1,3-disilacyclobutane (*m/z* 116) is produced in the reactor when using DMS as a source gas. This species is believed to be formed from the cyclodimerization reactions of methylsilene and also from dimethylsilylene dimerization. The mechanism for the formation of the major products were confirmed by using the deuterated isotopomer, DMS-d_2, as well as chemical trapping with 1,3-butadiene and ammonia. Our study of the reaction chemistry of DMS has shown that both free radicals and silenes/silylenes intermediates play important roles in the gas-phase chemistry. The competition between these two types of intermediates depends heavily on the filament temperature.

The effect of source gas pressure on the gas-phase chemistry has been studied by investigating the behavior of two mixtures of DMS in He with different DMS concentrations. It is found that with a decrease in DMS partial pressures, less gas-phase reaction products were detected, due to less efficient collisions between the source gas molecules and the filament and between species in the gas-phase. As the precursor pressure is increased, small hydrocarbons, including methane, ethene, acetylene, propene, and propyne were produced. The presence of these molecules affects the gas-phase

chemistry of DMS by switching from silylene dominant chemistry to free-radical dominant chemistry at a low filament temperature of 1200 ^{o}C. At low pressure regime and low filament temperature, *i.e.,* 0.12 Torr and 1200 ^{o}C, respectively, the gas-phase chemistry is dominated by TMDS formation. As the pressure is increased to 1.2 Torr, TriMS production predominates. This switch in chemistry is explained by the in-situ trapping of the various intermediates by the formed hydrocarbons molecules, specifically, ethene, acetylene, and propyne.

The comparison between DMS gas-phase chemistry obtained using W and Ta as the filament material shows that same gas-phase species have been detected with different filament material for 1% DMS/He. However, the formation of these species occurs at different filament temperature and reaction time. This indicates that the filament material influences its decomposition capability to form different species on the filament and affect the secondary gas-phase reactions in the HWCVD reactor. For Ta filament, the production of silylene species is favoured at a low temperature, whereas at the same filament temperature, W promotes radical formation.

Chapter Six: Gas-Phase Chemistry of Monomethylsilane in a HWCVD Reactor

6.1 Motivations

Several studies on the reaction kinetics and mechanism of the pyrolysis of monomethylsilane (MMS) are documented in the literature. The kinetics on the thermal decomposition of MMS were previously studied by Neudorfl and Strausz[94] in a conventional static system at 613 to 713 K, and by Davidson and Ring [177] in a low-pressure static system at 842 to 1000 K. From these studies, it has been found that the major products were hydrogen molecule (H_2), 1, 2-dimethyldisilane (DMDS), DMS and silane. DMDS was produced from silylene insertion reaction into the Si-H bond, while DMS and SiH_4 were postulated to arise from a free-radical chain reaction.

Sawrey *et al.*[122-124] revisited the decomposition of MMS in order to determine the nature and yields of the primary decomposition processes. They have carried out a study in a single-pulse shock tube at a total pressure of 4700 Torr in the temperature range of 1125-1250 K. They have determined, for the primary dissociations processes, the yield for the 1,1-H_2 elimination (a molecular elimination of H_2 with the formation of methylsilylene, $:SiHCH_3$, intermediate) to be $\varphi_{1,1} \cong 0.7$, for the 1,2-H elimination (a molecular elimination of H_2 with the formation of silene, $CH_2=SiH_2$, intermediate) to be $\varphi_{1,2} \cong 0.16$, and for the methane elimination to be $\varphi \cong 0.06$. Methane was not a reported reaction product by Neudorfl *et al.*[94] In addition to the primary dissociation processes, Sawrey *et al.* have examined the secondary reactions in order to isolate the primary mechanism for the formation of the major products. They have conducted their

experiments in the presence of various trapping agents, including ethene, propene, and acetylene. They have suggested that in the absence of trapping agents, the major products, silane and DMS, are produced by free radical processes. Upon the addition of olefins, a suppression of the concentration in free-radical products is observed due to the trapping of the free radical intermediates forming the corresponding adducts. Their results confirmed that the production of DMS and silane involved free radicals.

From all of the studies in the literature,[94, 122-124, 177, 197, 198, 225] several primary reactions have been predicted for initiating the decomposition of MMS as follows:

$$CH_3SiH_3 \longrightarrow CH_3SiH: + H_2 \qquad \Delta H = 60.1 \text{ kcal.mol}^{-1} (251.5 \text{ kJ.mol}^{-1}) \qquad (6\text{-}1)$$

$$CH_3SiH_3 \longrightarrow CH_2{=}SiH_2 + H_2 \qquad \Delta H = 46 \text{ kcal.mol}^{-1} (192 \text{ kJ.mol}^{-1}) \qquad (6\text{-}2)$$

$$CH_3SiH_3 \longrightarrow CH_4 + :SiH_2 \qquad \Delta H = 54.4 \text{ kcal.mol}^{-1} (227.6 \text{ kJ.mol}^{-1}) \qquad (6\text{-}3)$$

$$CH_3SiH_3 \longrightarrow CH_3\dot{S}iH_2 + \dot{H} \qquad \Delta H = 89.6 \text{ kcal.mol}^{-1} (374.9 \text{ kJ.mol}^{-1}) \qquad (6\text{-}4)$$

$$CH_3SiH_3 \longrightarrow \dot{C}H_3 + \dot{S}iH_3 \qquad \Delta H = 87.4 \text{ kcal.mol}^{-1} (365.7 \text{ kJ.mol}^{-1}) \qquad (6\text{-}5)$$

The first proposed decomposition reaction that leads to the formation of molecular hydrogen and methylsilylene is accepted by most research groups to be the dominant step. However, the occurrence of other steps differs from one study to another. The two other molecular elimination reactions (Equations (6-2) and (6-3)) are also considered to play a role in the decomposition chemistry of this precursor gas, and their occurrence was proven with the aid of the isotopomer, CH_3SiD_3 (MMS-d_3).[122-124, 176, 197] Regarding the two steps represented by Equations (6-4) and (6-5), the formation of methylsilyl radical and methyl radical through the cleavage of Si-H and Si-C bond,

respectively, was discounted on thermochemical grounds as indicated by the reaction enthalpy values.[94, 178] Under pyrolysis conditions, these two reactions would require high energy and it was proposed that these bond cleavage reactions might occur to a small extent in the presence of a highly active surface. Hence, free radicals formed during the decomposition of MMS are produced heterogeneously, whereas molecular elimination reactions involve homogeneous chemistry. Therefore, it is concluded that the primary process involved in the pyrolysis of MMS is the molecular elimination along with the generation of silylene or silene species.

Studies of homogeneous decomposition of MMS[122-124, 176, 178] have shown that the primary product is methylsilylene with yields ranging from 98% at 700 ^{o}C to 70% at 900 ^{o}C. Silene is also produced but its formation is relatively minor varying from about 1% to 15% over the same temperature range. Regarding the secondary gas-phase reactions, these studied have agreed that the formation of 1,2-dimethyldisilane, being one of the dominant products, involves mainly methylsilylene insertion reaction rather than radical recombination reaction. This conclusion is supported by the study carried out by Obi *et al.*,[226] where he examined the photolysis of MMS in the presence of nitric oxide, an efficient methylsilyl radical scavenger. They found that the concentration of DMDS was not affected upon the addition of NO. Despite the presence of the large number of studies on MMS, none of the studies mentioned the formation of 1,3-disilacyclobutane. Sawrey *et al.*[123] speculated its formation by the dimerization of dimethylsilylene and not silene cycloaddition.

MMS, the smallest open-chain methyl-substituted silane, was found to be a promising precursor for the deposition of SiC thin films with 1:1 Si to C ratio. MMS has

been used as a precursor for the deposition of SiC films by PECVD,[66, 227] LPCVD,[228] thermal CVD,[72, 229, 230] rapid thermal CVD (RTCVD)[231] and HWCVD.[31, 32, 61] From these studies, it was found that the deposited SiC film has a polymethylsilane structure. Recently, Lee *et al*.[31] have studied the bonding in SiC film grown by MMS in a HWCVD process. From the multiple internal reflection infrared spectroscopy study, they showed that the dominant species in the film are silicon hydrides (SiH, SiH_2 and SiH_3) and intact CH_3 groups. Under their experimental conditions, they have also found that the growth of the film network proceeds via Si-H bond rather than C-H bond breakage, and that the formation of polysilane-like material (Si-Si backbone) is favoured.

Although MMS has been used as a source gas in different CVD processes, the gas-phase chemistry involved in generating the precursors for the deposition of SiC films is not well understood. In this study, SPI with the 118 nm VUV wavelength in tandem with TOF MS is used to study MMS decomposition on hot W and Ta filaments. The mechanisms for the formation of secondary gas-phase reaction products, which are generated from the reactions between the species from the primary decomposition, are also investigated. The proposed mechanism is supported by the usage of the isotopomer, MMS-d_3, under the same experimental conditions, and chemical trapping experiments using 1,3-butadiene and ammonia.

6.2 Primary Decomposition of MMS on W and Ta Filaments

Under pyrolysis conditions, the decomposition of MMS (*m/z* 46) proceeds through the molecular elimination of H_2 as represented by Equations (6-1) and (6-2). As discussed in Chapter 4, the evolution of H_2 molecule was also observed during the

decomposition of this gas in the HWCVD process, and its formation took place over the surface of the filament. To examine the formation of the co-products of 1,1- and 1,2-H_2 elimination, the intensity ratio of I(*m/z* 44)/I(*m/z* 46) was calculated. This ratio is plotted in Figure 6-1. It is noticed that this ratio increases with temperature and its value can go as high as 7.2, which exceeds the filament-off ratio of 2.8. This suggests that MMS decomposes on a heated filament producing methylsilylene and silene species.

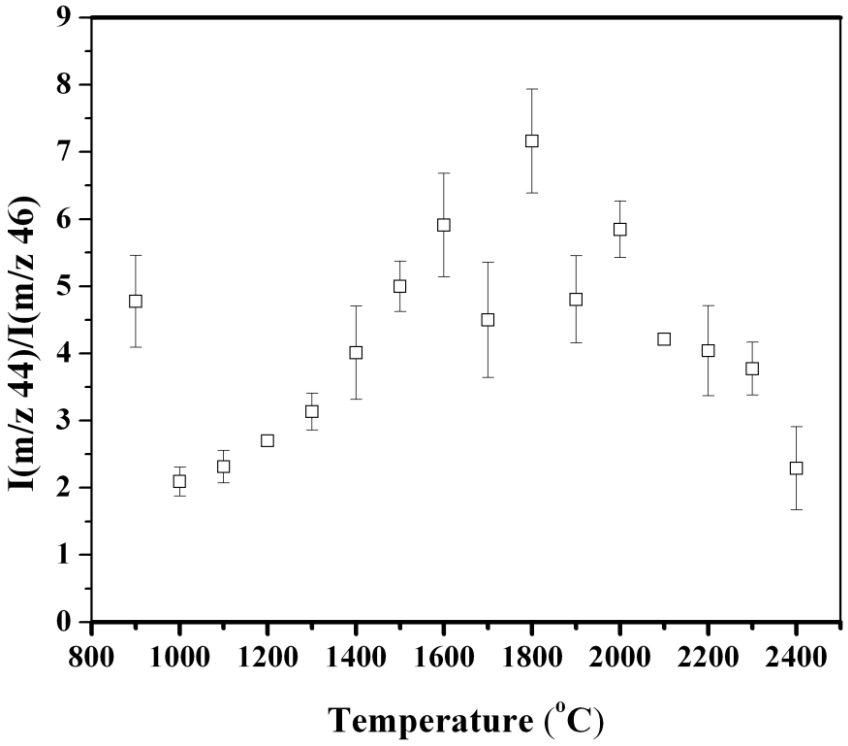


Figure 6-1: The intensity ratio of I(*m/z* 44)/I(*m/z* 46) versus the filament temperature for pure MMS sample at a chamber pressure of 1×10^{-5} Torr.

Aside from the H_2 elimination, MMS also decomposes to methyl and silyl radicals on the metal filaments. In our experiment, a new peak at *m/z* = 15 representing methyl radical was observed to come out after the filament was turned on, and its

intensity increased with increasing filament temperature. The mechanism for the formation of CH_3 radical is presented in details in Chapter 3. Based on the earlier discussion, it was concluded that MMS decomposes on the hot W and Ta filament to silyl and methyl radicals, according to Equation (6-5).

In addition, we have found that MMS also decomposes to methylsilyl and hydrogen radicals via the cleavage of the Si-H bond, as shown by Equation (6-4). The occurrence of this step is confirmed by examining the intensity ratio of *m/z* 45 ($CH_3SiH_2^+$) to *m/z* 46, as illustrated in Figure 6-2. The ratio increases with temperature, thus supporting the decomposition mechanism of MMS into methylsilyl and hydrogen radicals.

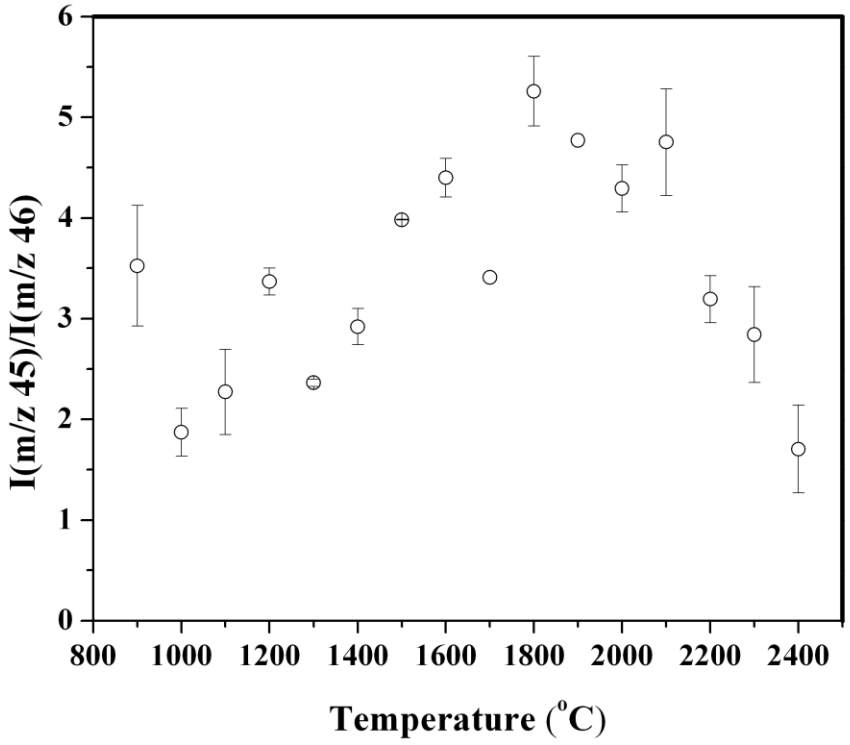


Figure 6-2: The intensity ratio of I(*m/z* 45)/I(*m/z* 46) versus the filament temperature for pure MMS sample at a chamber pressure of 1×10^{-5} Torr.

6.3 Secondary Gas-Phase Reaction of MMS in a HWCVD Reactor on Ta Filament

To study the secondary gas-phase reactions, 12 Torr of 4% MMS diluted in He was introduced in the HWCVD reactor, and the mass spectra were collected at different filament temperatures ranging from 900-1800 °C. For each temperature, a mass spectrum was recorded every two minutes for 60 minutes. Figure 6-3 shows the mass spectra recorded for 12 Torr of 4% MMS/He sample in the HWCVD reactor at different temperatures ranging from 900 to 1700 °C. As can be seen from Figure 6-3a, the intensity of the predominant fragment peak of the parent MMS at m/z 44 decreases with increasing filament temperatures. This indicates that the parent MMS molecules decompose on the filament and are consumed in the secondary gas-phase reactions in the HWCVD reactor. It was found that the intensity of the peak at *m/z* 44 started to decrease at a filament temperature of 1000 °C, and simultaneously two new peaks appeared at *m/z* =88 and 90, respectively. Compared to the lowest temperature of 1400 °C for the decomposition of TMS,[89] and 1200 ^{o}C for TriMS[67] and DMS, this temperature is indeed lower. This is probably due to the increase of the number of hydrogen bonds present in the molecule which facilitates the various bond rupture, producing the intermediates for the secondary gas-phase reactions. At temperatures higher than 1600 °C, all peaks including the base peak at *m/z* 44 disappeared as soon as the filament was turned on.

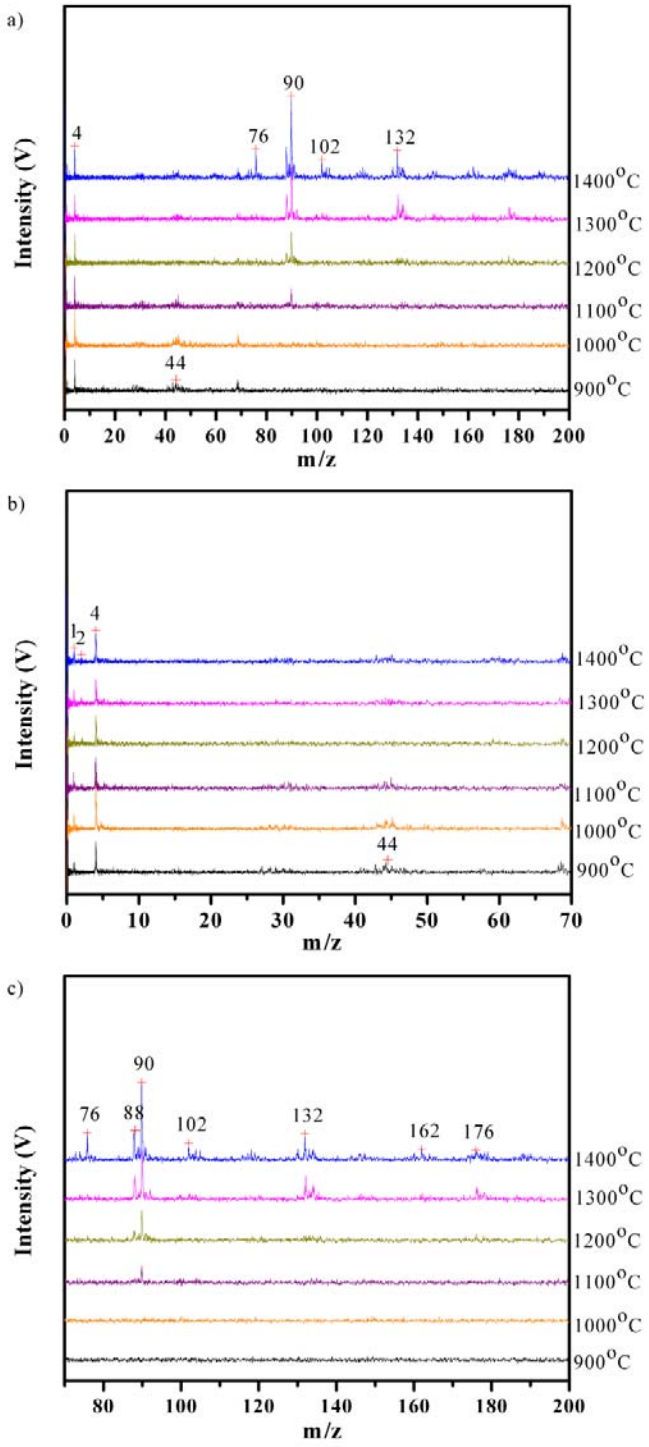


Figure 6-3: a) 10.5 eV SPI TOF mass spectra of 12 Torr of 4% MMS/He in the HWCVD reactor at filament temperatures ranging from 900-1400 °C at two minutes of reaction time, and enlarged spectra in the mass region of b) 0-70 amu, and c) 70-200 amu.

When the parent molecules decreased in intensities, new peaks at *m/z* =2, 76, 88 and 90 were observed with the one at *m/z* 90 being the dominant of all. From the enlarged mass spectra shown in Figure 6-3c and more clearly in Figure 6-4 at 1400 ^{o}C, other peaks at *m/z* = 102, 132, 134, 174, and 176 were also observed. These high mass peaks can be divided in two series. The first one includes peaks at *m/z* 90, 134, and 178 which have a mass difference of 44 amu between the neighbouring peaks. Similarly, the second one involves the ones at *m/z* 88, 132, and 176, with the same mass difference of 44 amu. Figure 6-5 shows the intensity distribution of the peaks in these two series with filament-on time at a filament temperature of 1200 ^{o}C. The plotted intensity distributions of the peaks in the same series follow the same trend, which is indicative that they come from the same origin.

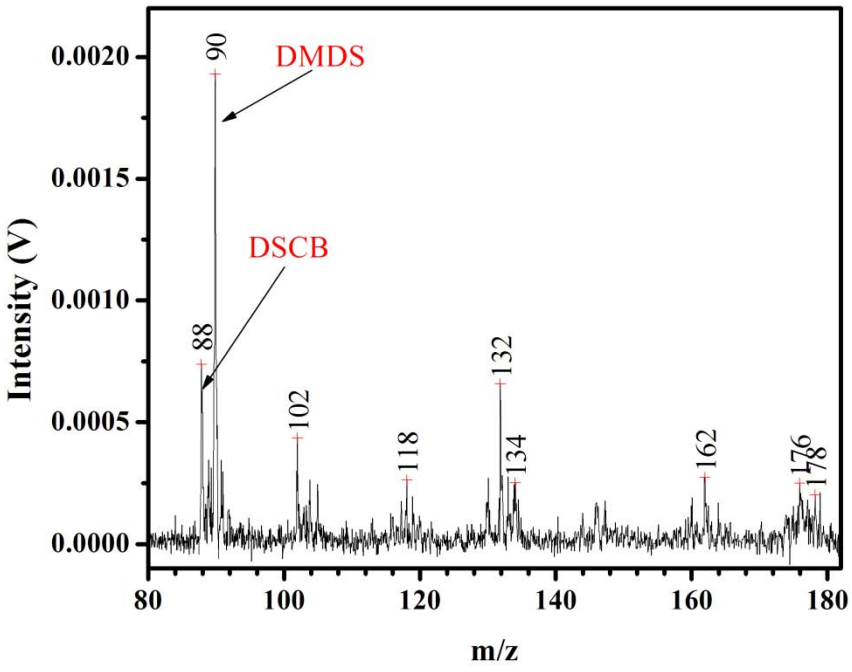


Figure 6-4:10.5 eV SPI TOF mass spectrum of 12 Torr of 4% MMS/He at the filament temperature of 1400 ^{o}C in the mass region between 80 and 180 amu.

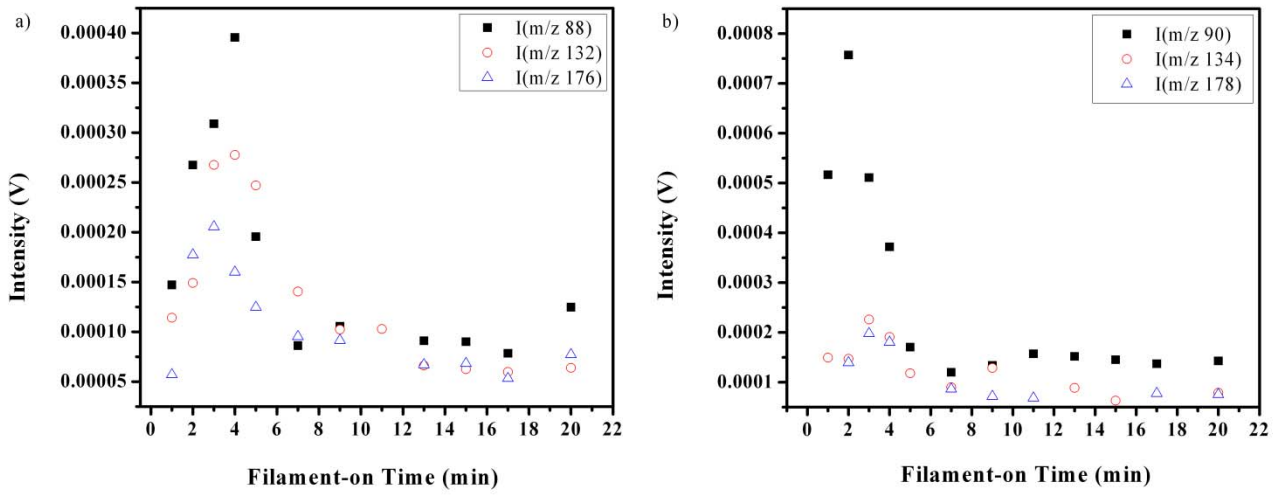


Figure 6-5: The peak intensity in the series of a) *m/z* 88 + n 44 and b) *m/z* 90 + n 44 from 12 Torr of 4% MMS/He as a function of filament-on time at a filament temperature of 1200 ^{o}C.

6.3.1 Possible Secondary Gas-phase Reactions

6.3.1.1 Hydrogen Abstraction Reactions and Biradical Combinations

As indicated previously, the primary decomposition reactions (6-4 and 6-5) of MMS on the filament produced methyl and silyl radicals along with methylsilyl and hydrogen radicals. In our HWCVD reactor, secondary reactions of $^{\bullet}CH_3$, $^{\bullet}SiH_3$, $^{\bullet}SiH_2CH_3$ and $H^{\bullet}$ radicals with the parent MMS molecule are likely to occur. As discussed in our experimental results with TriMS,[67] TMS[89] and HMDS,[82] following the decomposition of the source gas on the hot filament, the primary radicals produced will react with each other or with the abundant parent molecule in the reactor environment. When using MMS as a precursor in the reactor, it is expected that the methyl radical reacts with the parent MMS molecule by abstracting H atoms leading to the formation of methane and methylsilyl radicals according to Equation (6-6).

$$\dot{C}H_3 + CH_3SiH_3 \longrightarrow CH_3\dot{S}iH_2 + CH_4 \quad (6\text{-}6)$$

This can then be followed by several biradical combination reactions, as shown below:

$$\dot{C}H_3 + CH_3\dot{S}iH_2 \longrightarrow \underset{60\ amu}{(CH_3)_2SiH_2} \quad (6\text{-}7)$$

$$2\,CH_3\dot{S}iH_2 \longrightarrow \underset{90\ amu}{CH_3SiH_2SiH_2CH_3} \quad (6\text{-}8)$$

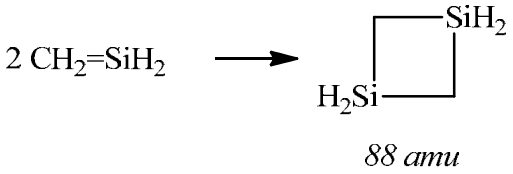
$$\dot{S}iH_3 + CH_3\dot{S}iH_2 \longrightarrow \underset{76\ amu}{CH_3SiH_2SiH_3} \quad (6\text{-}9)$$

The products from Equation (6-8) and (6-9), *i.e.*, 1-methyldisilane at *m/z* 76, and 1,2-dimethyldisilane at *m/z* 90, seemed to be observed experimentally. However, the signal of the stable product from Equation (6-6), methane, was not observed in our mass spectra due to its high IE of 12.6 eV, which is above the ionization wavelength of 10.5 eV. In addition, the product from Equation (6-7), DMS, was not observed in our mass spectra, indicated by the absence of a peak at *m/z* 60. This suggests that DMS was not produced when using MMS as a source gas in the reactor.

6.3.1.2 Reactions Involving Silene and Methylsilylene Intermediates

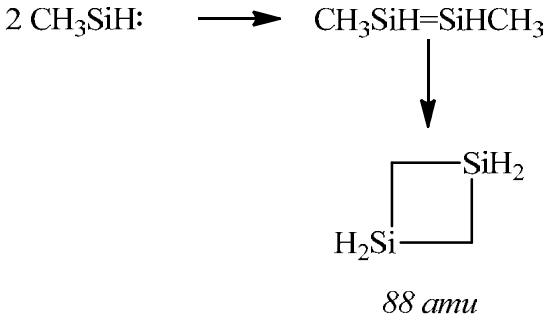
Silene (*m/z* 44) and methylsilylene (*m/z* 44) were formed under the collision-free conditions in our experiment as the co-products of H_2. Silene (CH_2=SiH_2), an unsaturated compound containing a silicon-carbon double bond, is considered to be short-lived and unstable.[232] Maier *et al.*[233] found that silene was stable only under argon matrix isolation at 10 K and it dimerized to 1, 3- disilacyclobutane upon thawing of the matrix at 35 K. In our experiment, a mass peak at *m/z* 88 was detected, which could be attributed to the 1,3-

disilacyclobutane (DSCB) resulting from the dimerization of the unsaturated silene molecule, as represented by Equation (6-10).



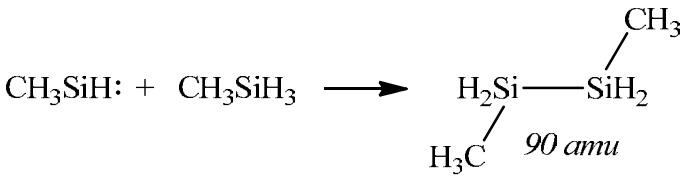
(6-10)

Additionally, DSCB can be formed by the dimerization of methylsilylene, producing 1,2-dimthyldisilene, which in turn undergoes rearrangement to produce the final product[234] according to Equation (6-11).



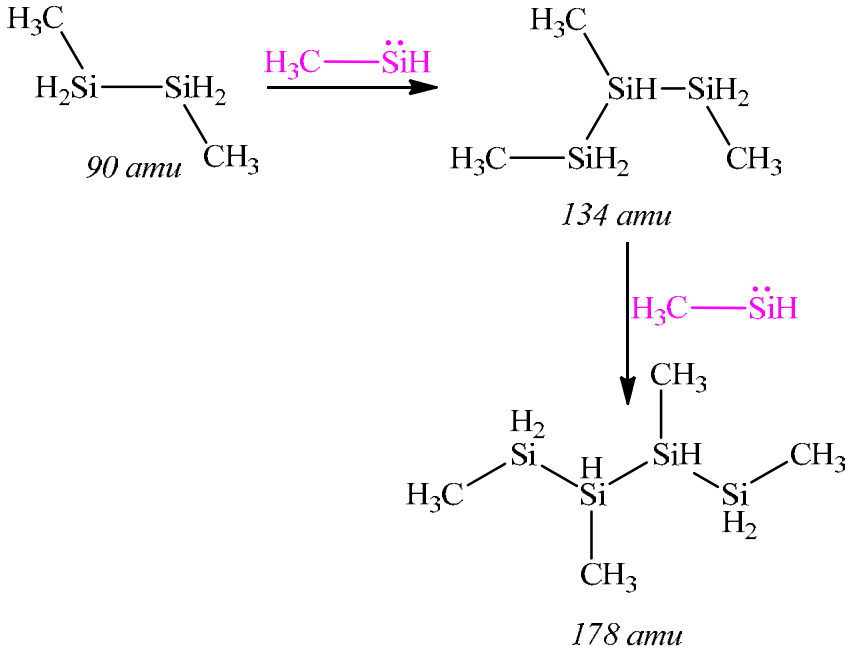
(6-11)

Methylsilylene (:$SiHCH_3$), a reactive intermediate, is known to undergo insertion reactions into a variety of chemical bonds including Si-H bond.[235] Under our experimental conditions, where the pressure in the HWCVD reactor is 12 Torr, there is an abundant source of the parent MMS molecules containing three Si-H bonds. Therefore, This intermediate would insert into the Si-H bond of the parent MMS molecule to form 1,2-dimethyldisilane (DMDS) with mass of 90 amu. This reaction is given by Equation (6-12).



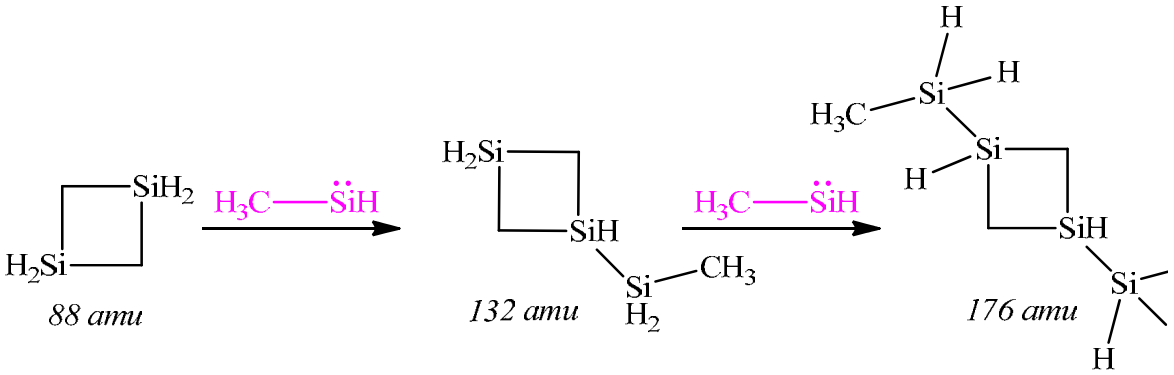
(6-12)

Since MMS has three Si-H bonds, up to three methylsilylene species can be inserted into the parent MMS molecule, as is shown in Scheme 6-1. This leads to the formation of the series of peak of 90, 134 and 178 with a mass difference of 44 amu.



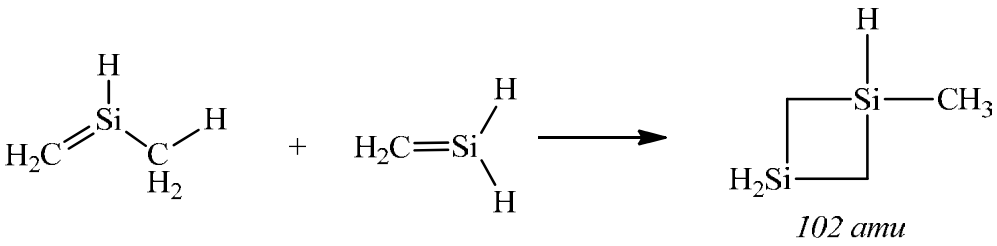
Scheme 6-1 Methylsilylene insertion reactions into Si-H bond of 1,2-dimethyldisilane

The formation of the second series of peak at *m/z* 88, 132 and 176 is also due to the existence of multiple Si-H bonds in DSCB. The insertion of methylsilylene into Si-H bonds in DSCB is illustrated in Scheme 6-2.



Scheme 6-2 Methylsilylene insertion reactions into Si-H bond of 1,3-disilacyclobutane

In addition to these peaks, the peak at *m/z* 102 was also observed. This peaks is believed to be the products of 1,3-disilacyclobutane undergoing decomposition followed by secondary gas-phase reactions similar to MMS. The formation of the peak at *m/z* 102 is proposed to be the product of cycloaddition reaction between methylsilene and silene molecules (Equation 6-13). This has been proved using an authentic DSCB sample.



(6-13)

6.3.2 Formation of the Main Products

As it was discussed in section 6-3, the secondary gas-phase reactions of MMS in the HWCVD process are dominated by the products represented by the peaks at *m/z* 90 and 88. Figure 6-6 shows the intensity distribution of the peaks at *m/z* 88 and 90 at

filament temperatures ranging from 1000 to 1300 ^{o}C. As can be seen from this Figure, the formation of these products

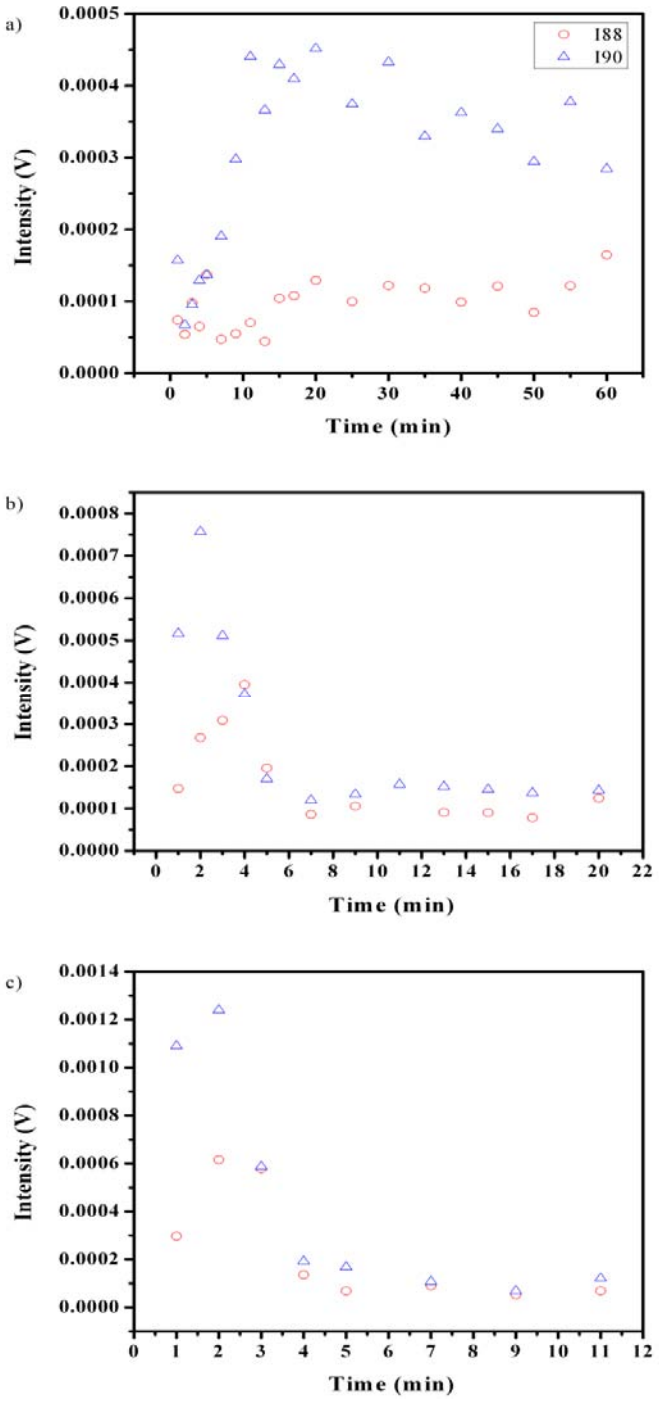


Figure 6-6: The intensity distribution of the peak at *m/z* 88, and 90 as function of filament-on time at filament temperatures a) 1000 °C, b) 1200 °C, and c) 1300 °C.

started as early at 1000 ^{o}C. At this temperature, the peak intensities first increase with time and reach a plateau at $t \geq 20$ min. As the filament temperature in increased, the intensity decreased after about one to three minutes of turning on the filament. This indicates that, once formed in the reactor, these species themselves can undergo primary decomposition and secondary gas-phase reactions, similar to the parent molecule MMS. A detailed discussion on the mechanisms for the formation of these two main products is presented in this section.

6.3.2.1 Formation of 1,2-Dimethyldisilane

The peak at *m/z* 90 is the dominant product throughout the entire temperature range and reaction time when using MMS in the reactor. This peak is assigned to 1,2-dimethyldisilane (DMDS). The mechanism for the formation of this product can occur either by biradical recombination reaction of methylsilyl radical as indicated by Equation (6-8) or by methylsilylene insertion reaction with the parent molecule as represented by Equation (6-12).

In order to isolate the mechanism responsible for its formation, experiments with the isotopomer, MMS-d_3, was carried out under the same experimental conditions. 12 Torr of 4% MMS-d_3 seeded in He was prepared and mass spectra were recorded every two minutes after the filament was turned on in the filament temperature range of 900 to 1500 ^{o}C. Figure 6-7 shows the mass spectrum of 12 Torr of 4% MMS-d_3/He mixture recorded at a filament temperature of 1300 °C after two minutes of reaction time. As above mentioned, with 4% MMS/He, the gas-phase chemistry was dominated by the peak at *m/z* 90. When MMS was replaced with MMS-d_3, the peak at *m/z* 90 was clearly shifted

to *m/z* 94, and the dominance of this peak is preserved in the spectra recorded after the filament was turned on at 1300 °C. The presence of the peak at *m/z* 94 indicated the formation of the isotopomer of 1,2-dimethyldisilane, DMDS-d_4, with a mass of 94 amu, and its formation is illustrated by Equation (6-14).

$$\left.\begin{array}{l} CH_3SiD_3 + CH_3SiD: \\ 2\,CH_3\dot{S}iD_2 \end{array}\right\} \rightarrow CH_3SiD_2SiD_2CH_3 \quad (6\text{-}14)$$

94 amu

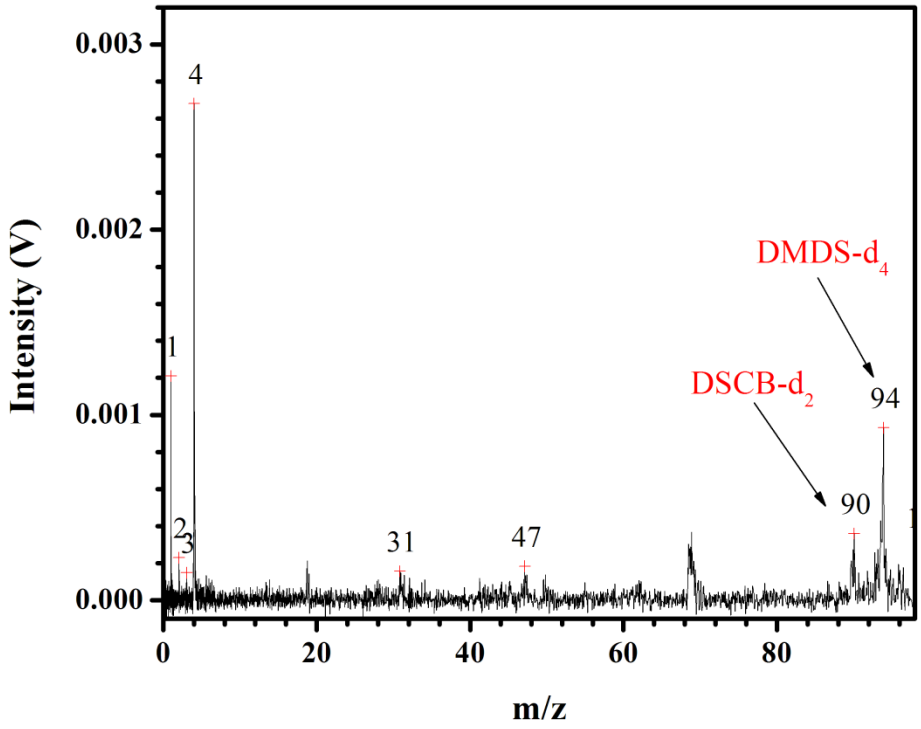


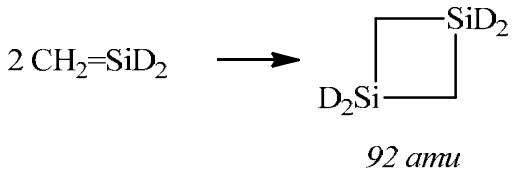
Figure 6-7: 10.5 eV SPI TOF mass spectra of 12 Torr of 4% CH_3SiD_3 in He mixture in the reactor at a filament temperature of 1300 °C in the mass region of 0-100 amu.

As shown by the above mechanism, the usage of the isotopomer was not helpful in determining the mechanism responsible for the formation of DMDS, since both pathways yielded the same deuterated product. Therefore, other methods needed to be

explored. In this study, trapping experiments of the active intermediates using 1,3-butadiene were carried out and the results will be presented in section 6.3.31.

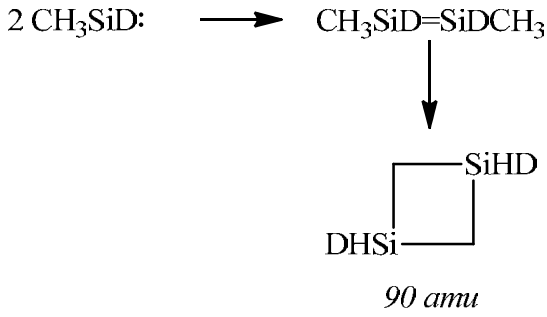
6.3.2.2 Formation of 1,3-Disilacyclobutane

The gas-phase chemistry of MMS is also represented by the peak at *m/z* 88, which was assigned to 1,3-disilacyclobutane (DSCB). This product can be formed by either silene dimerization (Equation (6-10)) or methylsilylene dimerization (Equation 6-11). If it were formed by silene dimerization, switching to MMS-d_3 should result in a mass shift of 4 amu and a mass peak at *m/z* 92 should be detected, as illustrated by Equation (6-15).



(6-15)

On the other hand, silylene dimerization reaction will result in the formation of a peak at *m/z* 90, when using MMS-d_3 precursor in the HWCVD reactor, as shown by Equation (6-16). As illustrated by the collected mass spectrum of 12 Torr of 4% MMS-d_3/He in Figure 6-7, the peak at *m/z* 90 was strongly detected, whereas the one at *m/z* 92 was barely discernible from the baseline.



(6-16)

Based on the results obtained using the isotopomer, it was concluded that dimerization reaction of methylsilylene is the major channel for the formation of DSCB molecule. The weakness in the peak at *m/z* 92 strongly suggests that the dimerization of methylsilene does not play a significant role in the formation of DSCB. In order to firmly confirm these statement, trapping experiment with 1,3-Butadiene and ammonia are carried out and the results are presented in section 6.3.3.

6.3.3 Trapping of Active Intermediates

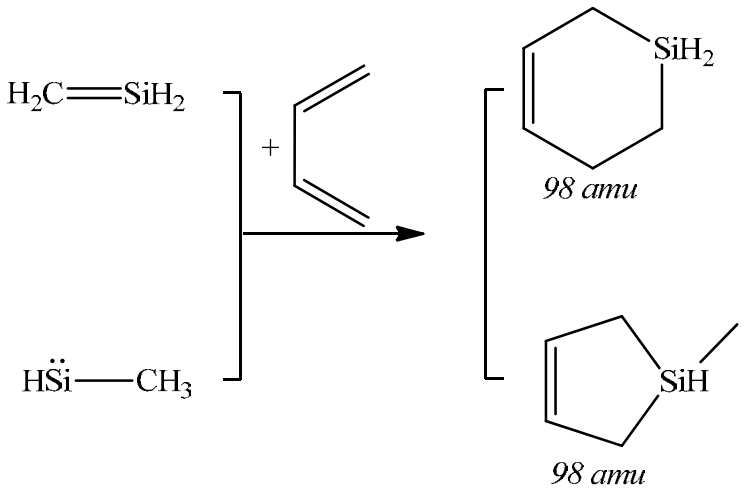
In order to verify the existence of silylene and better understand the proposed gas-phase reaction meachnism involving the chemistry of silylene species, experiments using different trapping agents are conducted. As it has been discussed in previous sections, the formation of the major products at *m/z* 88 and 90 can occur via two different routes. Therefore, in order to determine which mechanism is responsible for their formation, and to confirm the involvement of silylene, 1,3-butadiene and ammonia were used as chemical agents to trap the various intermediates.

6.3.3.1 Trapping Experiments with 1,3-Butadiene

In this work, a mixture of 4% MMS and 32% 1,3-butadiene (BTD) was prepared. The trapping experiments on the Ta filament were performed by monitoring the species exiting a HWCVD reactor as described in Chapter 2. Mass spectra for filament temperatures ranging from 1200 to 1400 °C were recorded. For each temperature, a mass spectrum was collected every two minutes for 30 minutes. Figure 6-8a and b shows the mass spectra collected from 12 Torr of 4% MMS: 32% BTD/He mixture at room

temperature and at a filament temperature of 1300 °C after the filament was on for 30 minutes, respectively. Figure 6-8c is a mass spectrum of a control experiment with 32% BTD at the same filament temperature after the filament was on for 15 min. The two peaks at *m/z* 28 and 39 are photofragments of BTD[236] and have appeared in the filament-off spectrum. The peaks at *m/z* 68 and 80 are secondary products of BTD after the filament was on, in addition to *m/z* 40, 66, 70, 78, 80, 81, 84, 92, 95 and 110, also observed at higher reaction time.

From the examination of the mass spectra collected during the trapping experiment with 1,3-butadiene, it was noticed that the peaks at 88 and 90 have disappeared with the appearance of a new peak at *m/z* 98. This peak is assigned to the adduct product resulted from the reaction between BTD (*m/z* 54) and silene (CH_2=SiH_2, *m/z* 44) and silylene (CH_3SiH:, *m/z* 44). These trapping reactions are represented by scheme 6-3.



Scheme 6-3 Reaction of 1,3-butadiene with methylsilylene and silene species.

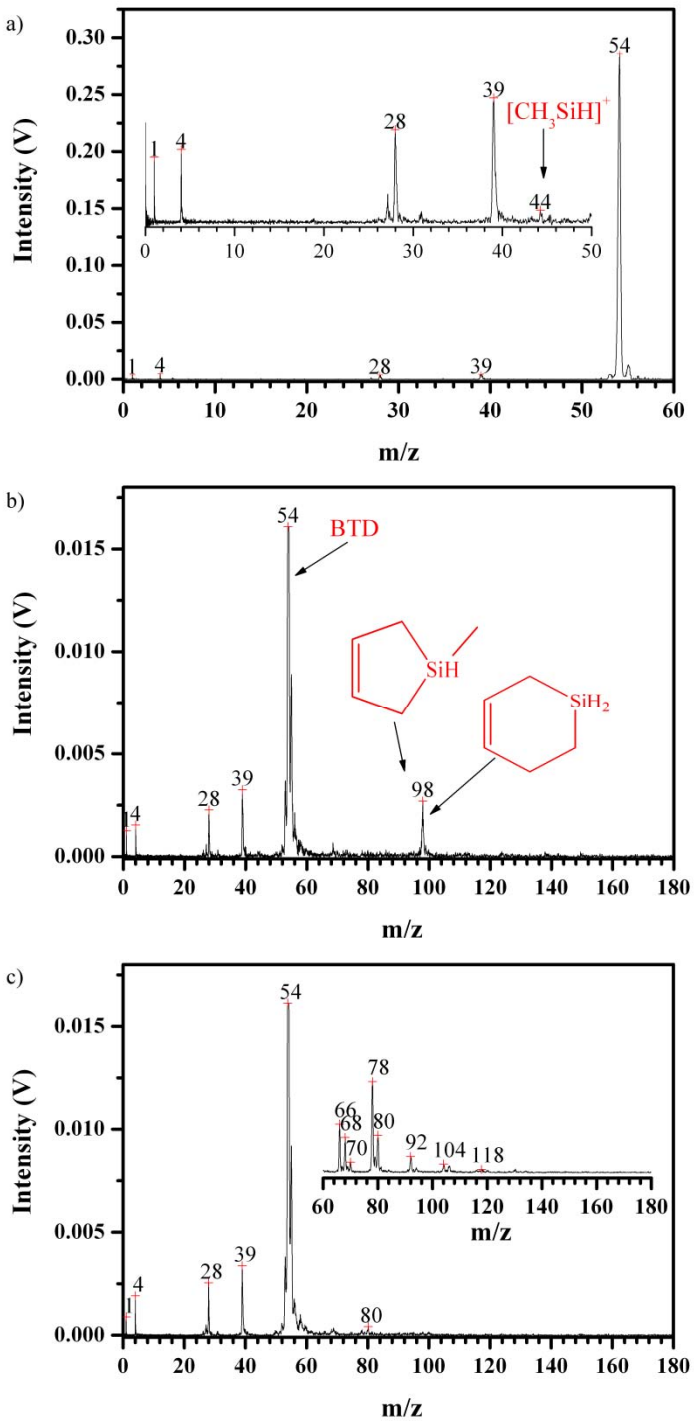


Figure 6-8: 10.5 eV SPI TOF mass spectra of a) 12 Torr of 4% MMS + 32% BTD in He mixture at room temperature (Inset: enlarged picture in the mass region of 0-50 amu); b) 12 Torr of 4% MMS + 32% BTD mixture in He in the reactor at filament temperature of 1300 ^{o}C; c) 12 Torr of 32% BTD in He mixture in the reactor at filament temperature of 1300 ^{o}C. The peak at *m/z* 54 is overloading.

As has been discussed earlier, DMDS (*m/z* 90) can be formed either from silylene insertion (Equation 6-12) or from radical recombination reaction (Equation (6-8)). Since 1, 3-butadiene can only react with silylene and silene moieties, not the free radicals, the complete absence of the peak at *m/z* 90 upon the addition of 1,3-BTD strongly suggests that DMDS is produced solely by methylsilylene insertion reaction into the parent molecule, not by the recombination reaction of methylsilyl radicals.

The absence of the peak at *m/z* 88 and the ones at higher mass, *e.g.*, those at *m/z* 132 and 176, in the mass spectra of 4% MMS + 32% BTD (Figure 6-8b) is indicative that their production entails silylene and silene intermediates, as predicted in earlier section. However, since BTD reacts with both silene and silylene intermediates, a differentiation between the two mechanisms is not possible when using this trapping agent.

6.3.3.2 Trapping Experiments with Ammonia

As demonstrated by the previous study on the trapping experiment with DMS in Chapter 5, ammonia was to react with both silene and silylene species, with a higher efficiency towards silene intermediates. In this work, a mixture of 4% MMS and 32% NH_3 was prepared and mass spectra were collected at filament temperatures ranging from 1200 to 1400 ^{o}C. Figure 6-9 shows the mass spectrum obtained during the trapping experiment with NH_3 at 1300 ^{o}C and after four minutes of turning the filament on.

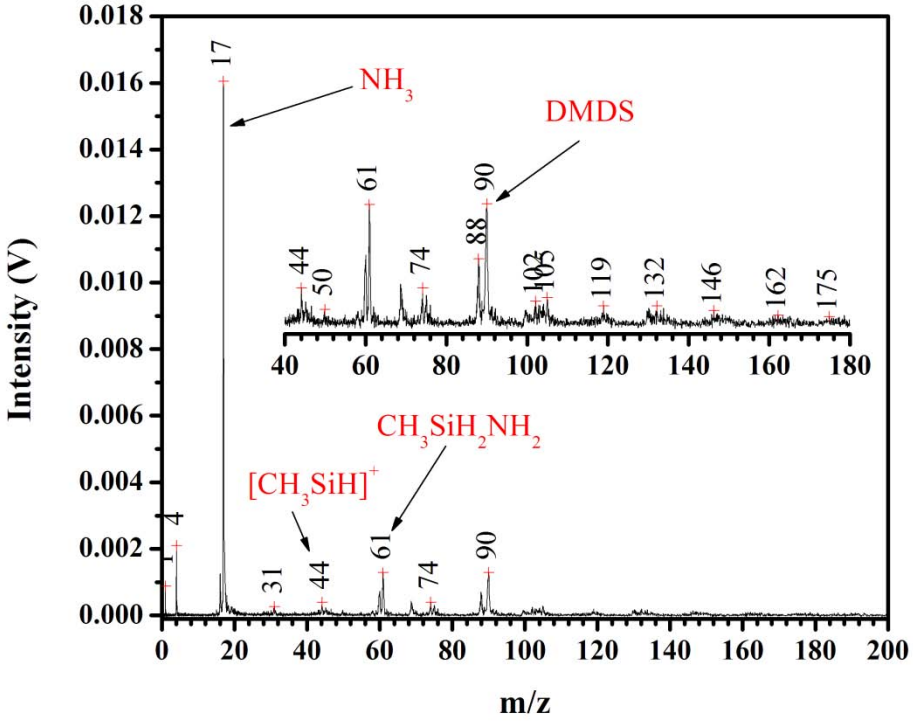
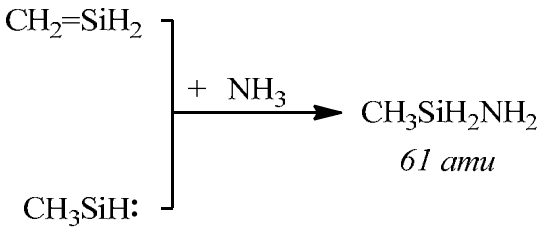


Figure 6-9: 10.5 eV SPI TOF mass spectra of 12 Torr 4% MMS + 32% NH_3 in He in the reactor at a filament temperature of 1300 ^oC after 4 minutes of turning the filament on. (Inset: an enlarged mass spectrum in the mass region of 40 to 180 amu.

The examination of the collected mass spectra showed the appearance of a new peak at *m/z* 61 and an enhancement in its intensity upon the addition of ammonia. The nature of this peak was attributed to the product formed from reactions between ammonia and silene or silylene, as shown by Equation (6-17).



(6-17)

From the analysis of the mass spectra in Figure 6-9, it was noted that both peaks at *m/z* 90 and 88 were still detected in the presence of NH_3. Figure 6-10 shows the intensity distribution of the peaks at *m/z* 61, 90 and 88 obtained using 4% MMS + 32% NH_3 mixture at a filament temperature of 1300 ^oC. For comparison, the intensity of the mass peaks at *m/z* 90 and 88 from the control experiment using 4% MMS/He sample is also plotted in the same figure. The adduct peak at *m/z* 61 increases with filament-on time and reaches a plateau at around seven minutes. At approximately the same time, the intensity of the peaks at *m/z* 90 and 88 started to decrease. This indicates that the trapping reaction between NH_3 and either silylene or silene intermediates is very active at this time when the intensity of the peaks at *m/z* 90 and 88 has reached its maximum.

Furthermore, the effect of the addition of NH_3 into the mixture on the overall gas-phase chemistry can also be deduced from Figure 6-10. This effect is obtained by comparing the intensity of the peak at *m/z* 90 and 88 in the presence and absence of the trapping agent, respectively. The formation of both of these peaks involves methylsilylene species. The peak at *m/z* 90 originated from insertion reaction of CH_3SiH:, whereas the one at *m/z* 88 is produced from the dimerization of the same intermediate. An examination of the intensity distribution in Figure 6-10 shows that in the first two minutes with the reaction with NH_3, the intensity of the peak at *m/z* 88 is lower than the one obtained in the absence of this trapping agent, whereas the intensity of the peak at *m/z* 90 is comparable. This implicates that the addition of NH_3 into the mixture lowered the rate of the dimerization reaction, while it did not affect the insertion reaction. A $t \approx 4$ min, the tertiary gas-phase reactions involving the formation of peaks at *m/z* 132 and 134 begins to occur, as indicated by the decrease in the intensity of the peaks at *m/z* 88 and 90

in the absence of NH_3. These reactions proceed via insertion reactions. It is observed that at this reaction time and in the presence of the trapping agent, the intensity of the peaks at *m/z* 90 and 88 is enhanced. This enhancement further confirms that NH_3 does not affect the rate of the insertion reactions. This is also reflected in the intensity profile of the peaks at *m/z* 132 and 176 produced from *m/z* 88 + n44 along with the ones at *m/z* 134 and 178 arisen from *m/z* 90 + n44 series shown in Figure 6-11 at a filament temperature of 1300 ^{o}C. After $t \geq 4$ min, the intensity of both peaks at *m/z* 88 and 90 present in the mixture with NH_3 started to decrease, implying their consumption in the gas phase, and the corresponding product started to be formed as illustrated in Figure 6-11. It can be concluded that the efficiency of the trapping reaction of NH_3 to methylsilylene is affected by the competition between various reactions involving this intermediate.

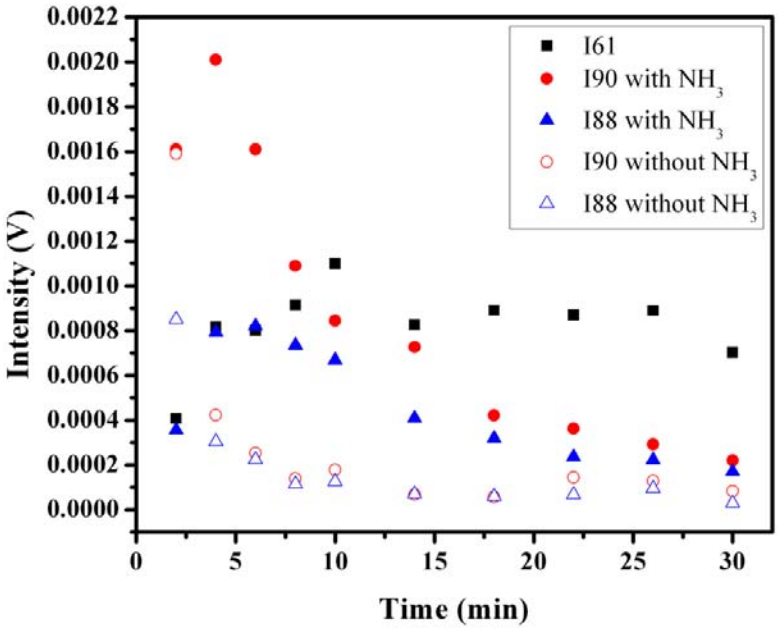


Figure 6-10: The intensity distribution of mass peaks at *m/z* 61 and 90 and 88 in the absence and presence of the trapping agent, NH_3, at a filament temperature of 1300 ^{o}C.

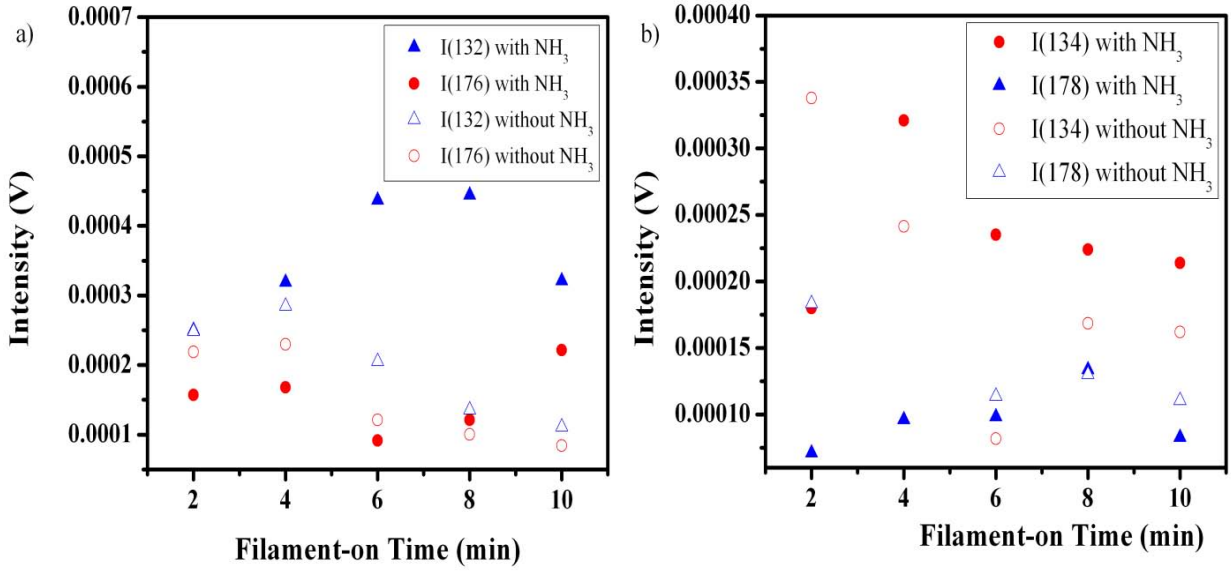


Figure 6-11: The peak intensities in the series of a) *m/z* 88 + n 44 and b) *m/z* 90 + n 44 as a function of filament-on time at a filament temperature of 1300 ^{o}C in the absence and presence of ammonia.

The purpose of using ammonia as a trapping agent was to facilitate the identification of the mechanism responsible for the formation of DSCB at *m/z* 88. From the experiments using the isotopomer MMS-d_3, it was deduced that the dimerization of methylsilylene reaction is the predominant contributor to the production of DSCB. In order to support this statement, an intensity ratio of the peak at *m/z* 90 over to the one at *m/z* 88 is plotted in Figure 6-12 in the presence and absence of the trapping agent, respectively, at a filament temperature of 1300 ^{o}C. The two ratios are similar, indicating that ammonia affected the formation of these two products to the similar extent. This implies that the same intermediate is responsible for the formation of the product peaks at *m/z* 90 and 88. From the experiment with 1,3-butadiene, it was concluded that DMDS at *m/z* 90 is solely produced from the insertion reaction of methylsilylene into the Si-H bond of the parent molecule. Therefore, the observation here suggests that methylsilylene is the

intermediate responsible from the formation of DSCB. This agrees with our experiment with MMS-d_3.

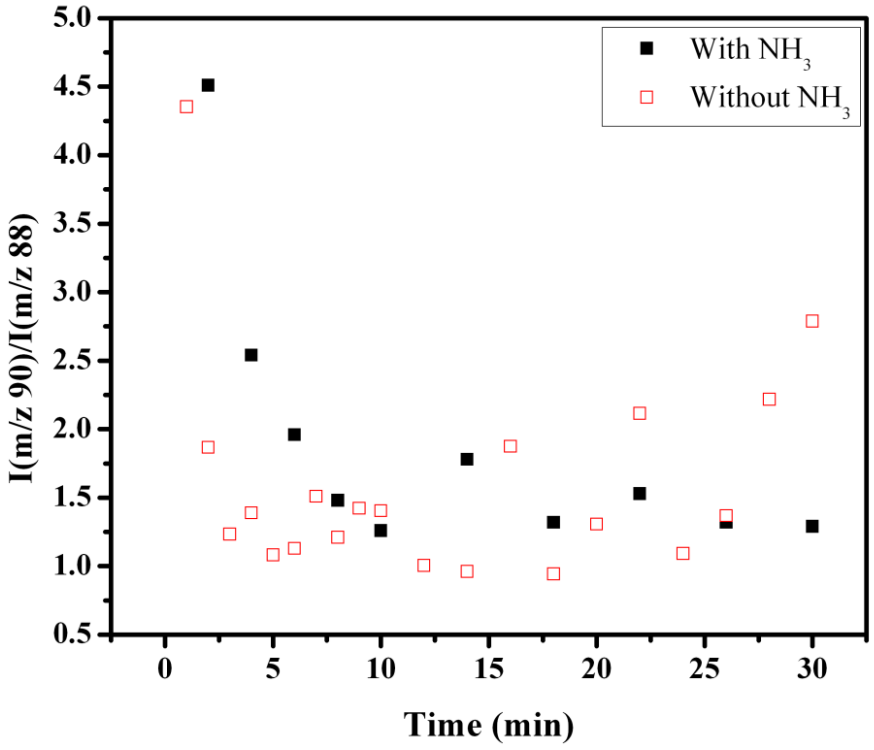


Figure 6-12: Comparison of the intensity ratio of the peak at *m/z* 90 to the one at *m/z* 88 as a function of filament-on time at a filament temperature of 1300 ^{o}C in the absence and presence of ammonia.

Therefore, unlike DMS, the gas-phase chemistry of MMS in HWCVD process involves exclusively silylene intermediates. The formation of DSCB is originating from the dimerization reaction of methylsilylene and that of DMDS proceeds by the insertion reaction of methylsilylene. It can be concluded that silene intermediate does not play a role in the gas-phase chemistry of MMS in HWCVD.

6.4 Effect of Filament Materials on MMS Gas-Phase Chemistry

Similar to DMS, the effect of filament materials on the gas-phase chemistry of MMS was also carried out in a HWCVD reactor with 12 Torr of 4% MMS/He on W and Ta. Figure 6-13a and b show the two mass spectra collected using this mixture under the same experimental conditions for W and Ta filaments at 1200 and 1300 ^{o}C, respectively. It is clear from this Figure that the same gas-phase species have been detected with different filament materials. This implies that, when using MMS as a precursor, the filament material does not affect the decomposition of source gas on the filament or the secondary gas-phase reaction pathways in the HWCVD reactor. Unlike DMS, whose chemistry involves both free radicals and silene/silylene intermediates as discussed in Chapter 5, MMS chemistry, as presented in previous sections in this chapter, involves exclusively silylene intermediates. Hence, the choice of filament material will not affect the gas-phase chemistry of MMS, as it is expected.

To further illustrate the effect of filament materials, the intensity distributions of the main peaks with different filament materials are plotted in Figure 6-14a and b, respectively, for a filament temperature of 1200 ^{o}C and 1300 ^{o}C. From the previous discussion on the gas-phase chemistry of MMS, it was concluded that its chemistry is dominated mainly by two peaks at *m/z* 90 and 88, representing 1,2-dimethyldisilane and 1,3-disilacyclobutane, respectively. At both temperatures, the peak at *m/z* 90 is dominating throughout the entire reaction time for both filaments. In addition, for all the peaks, the intensity profile followed the same trend, with an initial increase followed by a decrease. These observations further support the conclusion that with the involvement of only one intermediate, the effect of filament materials is negligible.

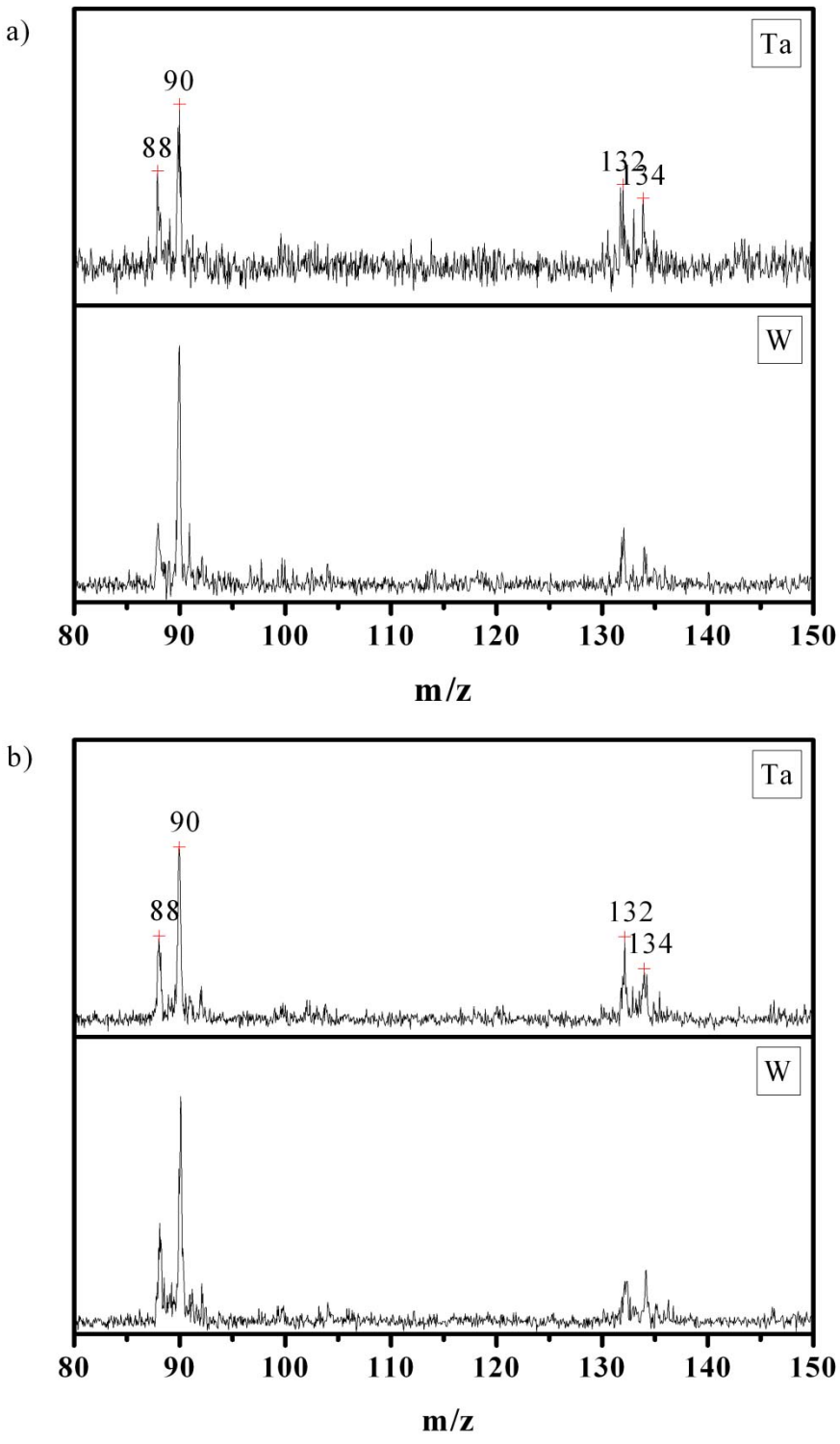


Figure 6-13: 10.5 eV SPI TOF mass spectra using W and Ta filament for 12 Torr of 4% MMS/He mixture at a filament temperature of a) 1200 ^{o}C, and b) 1300 ^{o}C and filament-on time of 3 min.

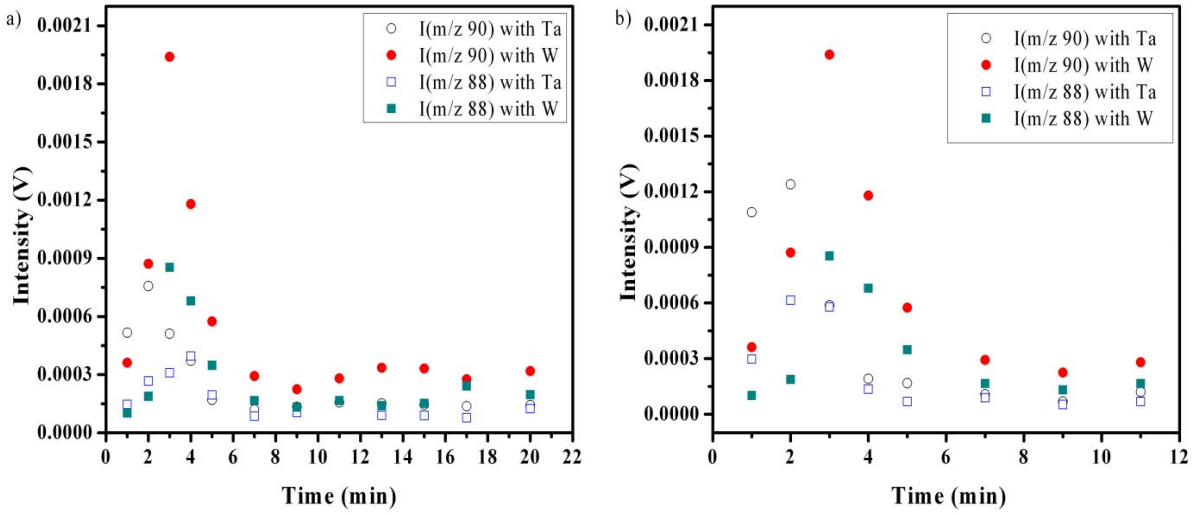


Figure 6-14: The intensity distribution of peaks at *m/z* 90 and 88 generated from W and Ta filaments when using 12 Torr of 4% MMS/He and at a filament temperature of a) 1200 ^{o}C, and b) 1300 ^{o}C.

6.5 Effect of Source Gas Pressure on MMS Gas-Phase Chemistry

Similar to the work done with DMS, the effect of source gas pressure is conducted by comparing the gas-phase chemistry of 12 Torr 10% MMS/He to the one of 12 Torr 4% MMS/He on Ta filament. The effect of source gas pressure is illustrated in Figure 6-15, where mass spectra recorded using 12 Torr of 4% MMS/He sample (p(MMS) = 0.48 Torr) and 12 Torr of 10% sample (p(MMS) = 1.2 Torr) in the HWCVD reactor at a filament temperature of 1300 ^{o}C are plotted. This comparison showed that, at both pressures, the gas-phase chemistry is still dominated by the peaks at *m/z* 90 and 88, formed from methylsilylene insertion and methylsilylene dimerization reactions, respectively. In addition, the increase in the precursor pressure did not alter the mechanisms occurring in the gas-phase chemistry. As it can be observed from this figure, the insertion reactions of methylsilylene into the Si-H bond of DMDS and DSCB

yielding the formation of the peaks at *m/z* 132, 134, 176 and 178 are still occurring with increase precursor pressure. Furthermore, the change in the pressure did not result in the formation of small hydrocarbon molecules, as it was the case with DMS. The lack of detecting hydrocarbon molecules with increasing the pressure of MMS is probably due to the fact that free radicals do not participate in the gas-phase chemistry of this specific molecule as discussed earlier.

Figure 6-16 shows the intensity distribution of the main peaks plotted for *p*(MMS) of 0.48 Torr and *p*(MMS) of 1.2 Torr at filament temperatures of 1200 and 1300 ^{o}C. The preservation of the chemistry can clearly be observed, since throughout the entire reaction time, the peak at *m/z* 90 is dominating over the one at *m/z* 88. Additionally, it can be noticed from this plot that the intensity distribution of these peaks followed the same trend at different precursor pressures. This further confirms that the change in the precursor pressure did not affect the gas-phase chemistry of MMS.

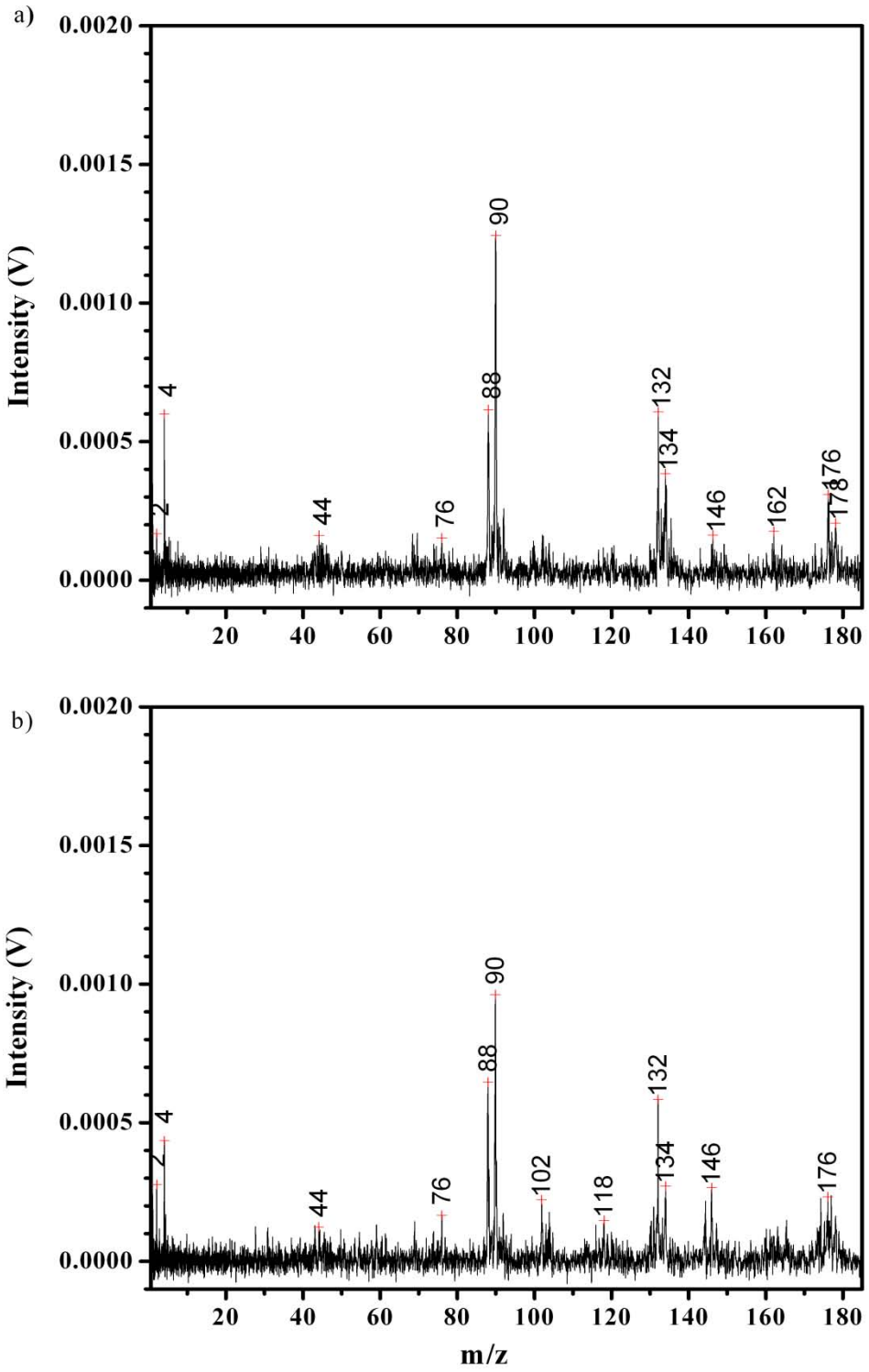


Figure 6-15: 10.5 eV SPI TOF mass spectra of a) 12 Torr of 4% MMS/He, and b) 12 Torr of 10% MMS/He in the reactor at a filament temperature of 1300 °C in the mass range of 0 to 200 amu.

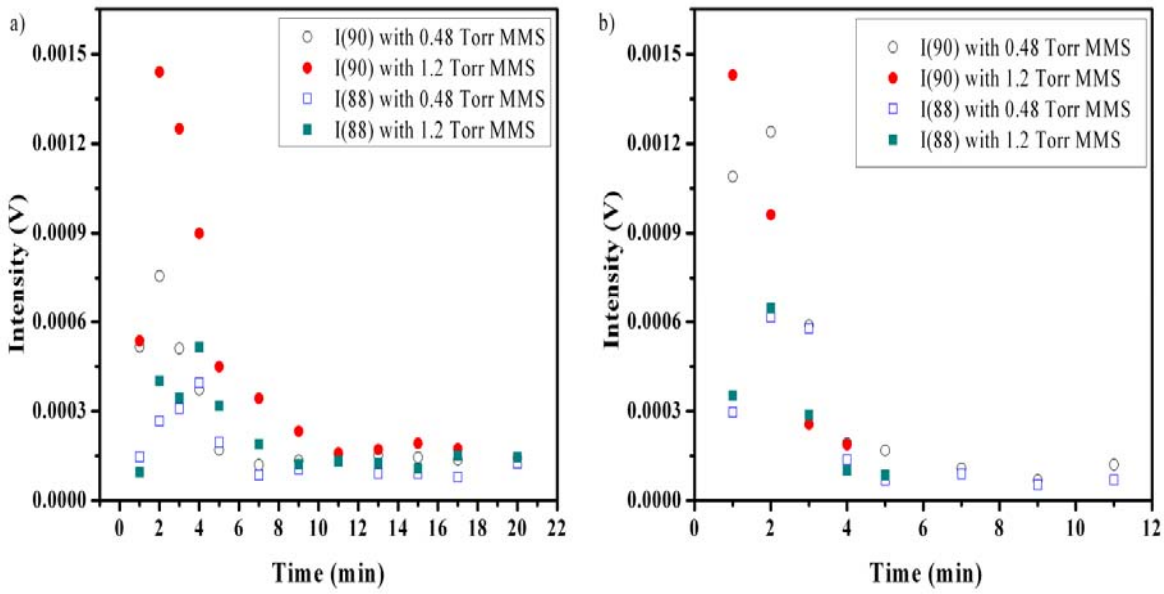


Figure 6-16: The intensity of the peaks at *m/z* 90, and 88 versus filament-on time observed with 0.48 Torr and 1.2 Torr of MMS at a) 1200 ^{o}C and b) 1300 ^{o}C.

6.6 Comparison of Gas-Phase Chemistry with Four Methyl-Substituted Silane Molecules

The knowledge of the gas-phase species formed during the gas-phase chemistry prior their deposition on a substrate surface helps in identifying the major contributor to the film growth as well as the properties of the deposited film. The Shi group has previously studied the primary decomposition and secondary gas-phase reactions of tetramethylsilane (TMS)[89] and trimethylsilane (TriMS).[67] It has been found that TMS decomposes to methyl and trimethylsilyl radicals, which react with the abundant parent molecules in the HWCVD reactor, producing secondary gas-phase products. H abstraction followed by self- and cross-combinations reactions of the primary and secondary radicals lead to the generation of small alkenes (C_nH_{2n}, $n \leq 4$), alkyl-

substituted silanes, and silyl-substituted alkanes. The study of TriMS revealed the effect of the Si-H on the gas-phase reaction products. It was found that TriMS decomposed into $(CH_3)_2HSi$, and CH_3 radicals. When using TriMS as a source gas in HWCVD reactor, the radical chain reactions were still the major pathway in the gas-phase chemistry. This is supported by the detection of TMS (*m/z* 88) and hexamethyldisilane (HMDS, *m/z* 146), which are considered the two major products formed from the radical recombination reactions in the termination steps. In addition, it is found that there is a more active, although minor, involvement of the reactive silene intermediates, based on the detection of three methyl-substituted disilacyclobutane molecules, *i.e.,* 1,3-dimethyl-1,3-disilacyclobutane,1,1,3-trimethyl-1,3-disilacyclobutane, and 1,1,3,3-tetramethyl-1,3-disilacyclobutane. This shows that upon the introduction of a Si-H bond into the molecule, the chemistry involving silene and silylene intermediates started to play a role in the gas-phase chemistry. This role is further enhanced when DMS and MMS are used as source gases. As discussed in Chapter 5, DMS chemistry is dominated by the formation of TriMS (*m/z* 73) via H-abstraction followed by radical recombination reaction, 1,1,2,2-tetramethyldisilane (*m/z* 118) and 1,3-dimethyl-1,3-disilacyclobutane (*m/z* 116), which are the products of silylene insertion and silene cycloaddition reactions, respectively. It has also been shown that at low filament temperatures, the peak at *m/z* 118 dominates the gas-phase chemistry of DMS. As the filament temperature is increased, the secondary gas-phase chemistry is governed by the formation of peaks at *m/z* 73 and 116. This clearly demonstrates the competitions between reactions involving free radicals and those with silene/silylene species. As the number of Si-H in the molecule is increased, the involvement of silene and silylene is more accentuated with

DMS than with TriMS or TMS. For MMS, as discussed in this chapter, it is found that the chemistry is exclusively controlled by silylene chemistry. This is concluded based on the fact that the major peaks, 1,2-dimethyldisilane (*m/z* 90) and 1,3-disilacyclobutane (*m/z* 88), come from methylsilylene insertion into Si-H bond of the parent molecule and dimerization reactions, respectively. Therefore, with the increase of Si-H bond in the source gas, a switch from radical-dominated chemistry to silylene-dominated chemistry takes place. This change should also be reflected in the structure of the deposited film.

The correlation between the gas-phase reaction chemistry and film structure can be investigated by examining the film structures deposited by Zaharias *et al*. [61] and Lee *et al*.[32] when using these methyl-substituted silane molecules. Lee *et al*. carried out a spectroscopic study using MMS, TriMS and TMS. The IR spectra of the films grown using MMS and TriMS showed the same C-H and Si-H absorption frequencies implying that the same functional groups are present in deposited films. The main difference between the films grown from these two precursors lies on the amount of Si-H and C-H bond which was obtained from the relative integrated area of SiH_x and CH_3 stretching modes. They have found that the concentration of methyl groups present in the film's network is two times more when using TriMS than MMS. In addition, they have confirmed that the Si-H bond cleavage is responsible for network propagation. The reactivity of TMS is found to be much lower than the other two precursors, and the film grown using TMS is mainly composed of CH_2 and CH_3 groups. Their results suggest that C-H bond cleavage is the major pathway to film growth when using TMS, which is less favourable than Si-H bond cleavage. These results were comparable to the ones obtained from Zaharias *et al.*, where they found that the concentration of SiH_x species present in

the grown films from these precursors increased with decreasing methyl group present in the precursor molecules. The structure of the grown films in these two studies clearly demonstrates the effect of Si-H bonds in the precursor molecule. As the number of Si-H bond is increased, the grown film switched from C-rich to Si-rich material, which is related to the intermediates produced in the gas phase. As stated earlier, with an increase in methyl substitution in the precursor molecule, there is a switch from silylene/silene dominated chemistry to free radical dominated one. This is reflected in the structures of the deposited films.

6.7 Summary

The decomposition of MMS and secondary gas-phase reactions in the HWCVD reactor when using W and Ta filaments were examined using laser ionization mass spectrometry. It is found that MMS decomposes on the metal filament to form methyl and silyl radicals. In addition, MMS decomposed to form short-lived methylsilylene and silene intermediates with H_2 as a concomitant product. Under a MMS partial pressure of 0.48 Torr in the HWCVD reactor, secondary gas-phase reactions are dominated by silylene insertion and dimerization reactions. These reactions lead to the formation of 1,2-dimethyldisilane (*m/z* 90) and 1,3-disilacyclobutane (*m/z* 88), as well as high-mass methyl-substituted disilanes (*m/z* 132, 134) and trisilanes(*m/z* 176, and 178). The decomposition temperature for MMS in the reactor is found to be as low as 1000 °C. The usage of the deuterated isotopomer, MMS-d_3, and chemical trapping with 1,3-butadiene and ammonia helps in confirming the pathways responsible for the formation of the major species. It is concluded that 1,2-dimethyldisilane originates from methylsilylene

insertion reaction into the Si-H bond of the parent molecule, while the formation of 1,3-dimethyl-1-disilacyclobutane involves the dimerization reaction of the same intermediate. This leads to the conclusion that in the gas-phase chemistry of MMS, free radical and silene intermediates do not play an important role.

In addition, the effect of filament materials on the gas-phase chemistry of MMS has been investigated. Since the gas-phase chemistry only involves one type of intermediates, silylene, the filament material is found not to be a factor. Study on the effect of precursor pressure shows that an increase in the pressure of MMS does not affect the gas-phase chemistry for the same reason.

Chapter Seven: Effect of Trimethylsilane Pressure on the Gas-phase Reaction Chemistry in the HWCVD process

7.1 Motivations

The mechanisms and kinetics of the pyrolysis of trimethylsilane (TriMS) have been well studied in the literature.[183, 184, 192, 207] Methane and hydrogen (H_2) were observed as the main products in all studies. It was believed that the formation of CH_4 and H_2 is initiated by the dissociation of Si- CH_3 and Si-H bond, respectively. The direct molecular elimination from TriMS was discounted as a possible channel to form these two molecules in pyrolysis. Other products in the TriMS pyrolysis include several methyl-substituted disilacylobutanes that are formed from the silicon- carbon double-bonded (silene) intermediates. Closed related to the pyrolysis of TriMS is its use in thermal chemical vapor deposition (CVD). Indeed, TriMS has been used as a single precursor with existing Si-C bonds in rapid thermal CVD[71, 237] for the deposition of silicon carbide films. In addition, it has also been employed for the same purpose in PECVD[70], atomic hydrogen-induced CVD[133, 238] and HWCVD.[32, 73]

In a previous study from our group,[67] the decomposition chemistry of TriMS on a hot W filament and secondary reaction chemistry in a hot-wire CVD reactor have been systematically investigated using laser ionization mass spectrometry. It is found that TriMS decomposes on the hot filament via Si-H and Si-CH_3 bond cleavages, forming CH_3, H, and methyl-substituted silyl radicals. In the reactor where the partial pressure of TriMS is 0.12 Torr, the major products in the gas-phase are found to be hexamethyldisilane (HMDS) and tetramethylsilane (TMS) formed from radical

recombination reactions. Cycloaddition reactions of methyl-substituted silene intermediates produce three disilacyclobutane molecules, including 1,3-dimethyl-1,3-disilacyclobutane (DMDSCB, *m/z* 116), 1,1,3-trimethyl-1,3-disilacyclobutane (TriMDSCB, *m/z* 130), and 1,1,3,3- tetramethyl-1,3-disilacyclobutane (TMDSCB, *m/z* 144), as the minor products. The formation of methane and H_2 was not examined in our previous study with 0.12 Torr of TriMS.

In this work, the effect of TriMS pressure in the hot-wire CVD process on the secondary gas-phase reactions is explored by examining the product distributions at an increased pressure of 4.0 Torr and comparing with those at 0.12 Torr. The formation of methane and hydrogen molecules was also investigated. The intensity distributions of the five major products observed in the hot-wire CVD reactor as a function of reaction time and filament temperature for both sample pressures were investigated. The reasons why different trends were observed for the five high-mass products were provided.

7.2 Gas-Phase Reaction Products from Trimethylsilane in a HWCVD Reactor

As has been described in our previous study,[67] the room-temperature 10.5 eV SPI TOF mass spectrum of TriMS is predominated by two photofragment ions at *m/z* 73 ($Si(CH_3)_3^+$) and 58 ($Si(CH_3)_2^{+\cdot}$). After turning the filament on, it was noticed that the intensity of these two photofragment ions started to decrease at a filament temperature of 1100 ^oC when using 4.0 Torr of TriMS and simultaneously two new peaks appeared at *m/z* 88 and 146. This temperature was comparable to the one obtained with 0.12 Torr of TriMS, which was ~ 1200 ^oC. Main contribution to the two new peaks at *m/z* 88 and 146 has been assigned, respectively, to TMS and HMDS, in our previous study.[67] To confirm

that it is TMS and HMDS that are produced with 4.0 Torr of TriMS, we have compared the intensity profile of the peak at *m/z* 73 versus the filament-on time obtained from the experiments with the calculated intensity considering the combined contributions to this peak from the 10.5 eV photofragmentation of TriMS, TMS and HMDS combined. Figure 7-1 shows the comparison at filament temperatures of 1300 and 1500 ^{o}C. The similar trend in the intensities obtained experimentally and those computed theoretically strongly suggests that the two new peaks at *m/z* 88 and 146 are from TMS and HMDS.

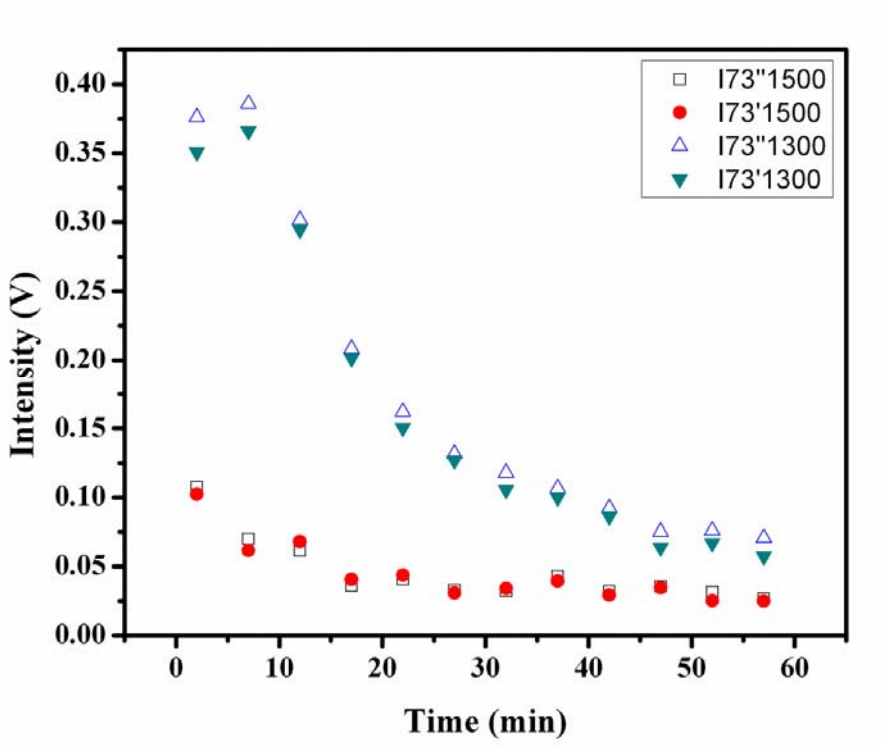


Figure 7-1: Intensity of the peak at *m/z* 73 (I73') observed with 20 Torr of 20% TriMS/He mixture at 1300 ^{o}C (▼) and 1500 ^{o}C ( ), compared with the calculated contribution to the peak intensity (I73'') from the photofragmentation of TriMS, TMS, and HMDS combined at 1300 ^{o}C (Δ), and 1500 ^{o}C (□).

To illustrate the effect of the TriMS pressure on the gas-phase reaction products, a comparison between the mass spectra recorded with 12 Torr of 1% TriMS/He sample (p(TriMS) = 0.12 Torr) and 20 Torr of 20% sample (p(TriMS) = 4.0 Torr) in the hot-wire CVD reactor at a filament temperature of 1300 ^{o}C is shown in Figure 7-2. At this temperature, the secondary gas-phase reactions using the 0.12 Torr TriMS sample is dominated by the formation of TMS (*m/z* 88) and HMDS (*m/z* 146 and its photofragment ion at *m/z* 131) resulted from the radical recombination reactions. The products from silene cycloaddition reactions are absent at 1300 ^{o}C. When the pressure of TriMS was increased to 4.0 Torr, a more active chemistry was observed under the same experimental conditions due to the presence of much more mass peaks as well as the early emergence of the peaks at *m/z* 116 (DMDSCB), 130 (TriMDSCB) and 144 (TMDSCB) evolved from silene chemistry.

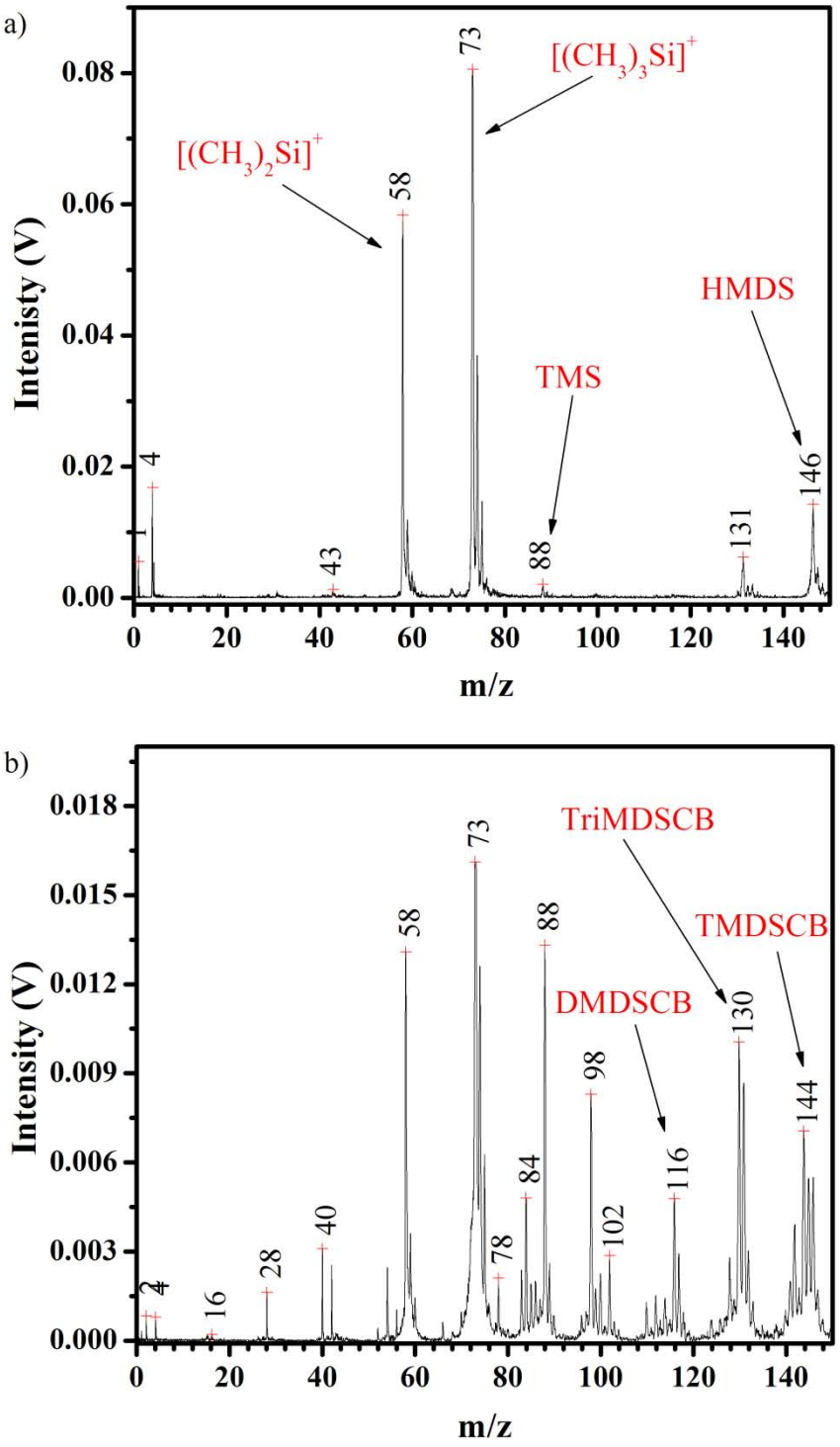


Figure 7-2: 10.5 eV SPI TOF mass spectra of a) 12 Torr of 1% TriMS/He and b) 20 Torr of 20% TriMS/He in the reactor at a filament temperature of 1300 ^{o}C.

Table 7-1 summarizes the intensity ratios of each of the mass peaks at *m/z* 88, 146, 116, 130, 144 to that of the peak at *m/z* 58 (the characteristic photofragment peaks from TriMS) for two filament temperatures of 1300 ^{o}C and 1500 ^{o}C when using 0.12 and 4.0 Torr of TriMS. Examination of these ratios obtained under different sample pressures showed that the ratios generally increased with increasing pressure except for the I(146 amu)/I(58 amu) which shows a significant decrease. This indicates that the amount of products represented by the peaks at *m/z* 88, 116, 130, and 144 increases when using high pressure of TriMS, whereas the amount of HMDS (*m/z* 146) decreased. The reason responsible for this behaviour will be described in section 7-5.

Table 7-1 Summary of the intensity ratios of each of the peaks at *m/z* 146, 116, 130, and 144 to that of the peak at *m/z* 58 when using 0.12 Torr and 4.0 Torr of TriMS in the hot-wire CVD reactor at filament temperatures of 1300 and 1500 ^{o}C

Intensity ratio	0.12 Torr TriMS		4.0 Torr TriMS	
	1300 ^{o}C	1500 ^{o}C	1300 ^{o}C	1500 ^{o}C
I(88 amu) / I(58 amu)	0.014-0.35	0.056-2.04	0.21-1.23	0.21-1.28
I(146 amu) / I(58 amu)	0.064-1.29	0.16-4.40	0.22-0.48	0.19-0.88
I(116 amu) / I(58 amu)	0.013-0.080	0.023-0.31	0.20 -0.50	0.22 -0.40
I(130 amu) / I(58 amu)	0.009-0.013	0.031-0.73	0.26 - 0.77	0.24 – 0.82
I(144 amu) / I(58 amu)	0.024-0.076	0.16-0.92	0.09 - 0.54	0.06 – 0.69

It should be noted that the peak at *m/z* 4 representing the helium ion was observed in both mass spectra in Figure 7-2, although the ionization energy (IE) of He is greater than 10.5 eV. The observation of this peak is attributed to electron impact ionization (EI)

due to small amount of photoelectrons caused by scattered UV radiation in the photoionization region. The intensity of the peak at *m/z* 4 from EI contribution was found to be only 0.14% that of the base peak at *m/z* 73 originating from SPI in the room-temperature mass spectra. Therefore, the contributions from UV photon-induced EI are minor in our experiments.

7.3 Formation of Methane and other Small Hydrocarbon Molecules

Furthermore, the increase in the pressure of the precursor gas resulted in the formation of small hydrocarbon molecules at 1300 ^{o}C, which was lacking when 0.12 Torr of TriMS is used. This is clearly seen in Figure 7-2. With 4.0 Torr of TriMS, new peaks at *m/z* 16, 28, 40, and 42 were observed. The confirmation of the assignment of peak at *m/z* 16 to methane was done by comparing the observed intensity profile from *m/z* 13 - 16 to the room-temperature mass spectrum of an authentic methane sample, as is illustrated in Figure 7-3. From the authentic methane sample, the intensity ratios of I(*m/z* 14)/I(*m/z* 16) and I(*m/z* 15)/I(*m/z* 16) are equal to 0.17 ± 0.01 and 0.84 ± 0.04, respectively. These ratios were comparable to those obtained from the experiments using 4.0 Torr of TriMS, thus confirming the nature of peak at *m/z* 16 as being methane. This is the first time the formation of methane has ever been confirmed when using open-chain methyl-substituted silanes[67, 82, 89] or four-membered-ring (di)silacyclobutanes[90-92, 137, 239] as precursor gases in the hot-wire CVD process.

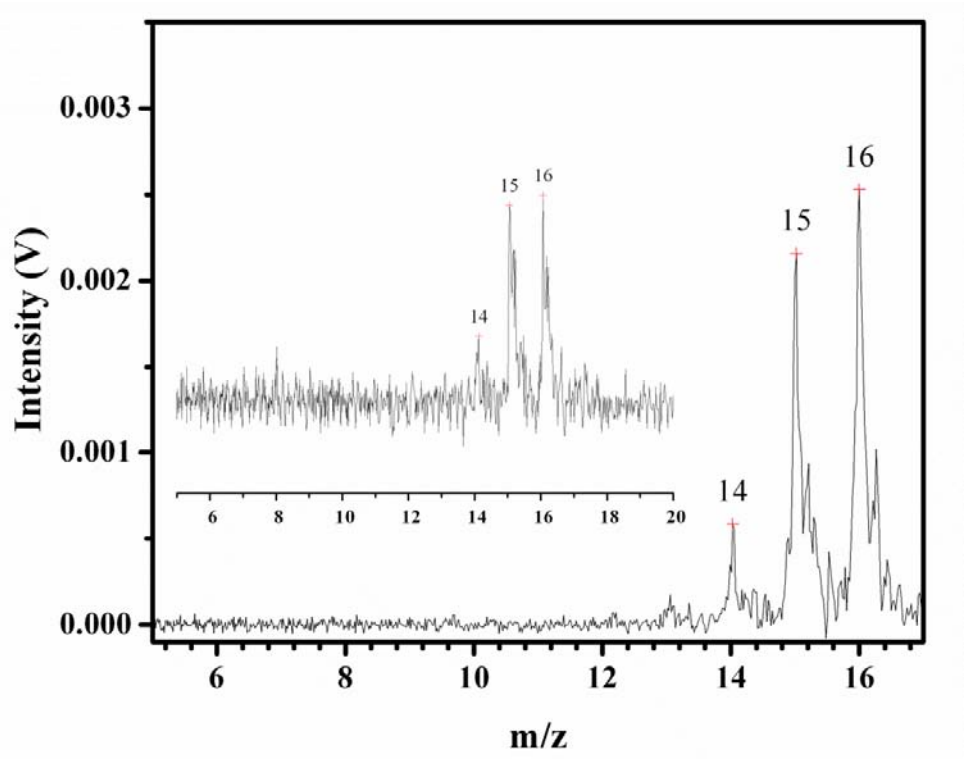


Figure 7-3: 10.5 eV SPI TOF mass spectrum of an authentic methane sample recorded at room temperature. The inset is a mass spectrum of 4.0 Torr of TriMS sample in the reactor at a filament temperature of 1300 ^{o}C in the mass region of 5 - 20 amu.

Similarly, the peaks at *m/z* 28, 40 and 42 are assigned to ethene, propyne, and propene, respectively, by comparing with the room-temperature mass spectrum of the authentic samples. It should be noted that a very weak peak at *m/z* 26 is also observed, indicating the formation of acetylene molecule. The weakness of the peak is due to the fact that the ionization energy of acetylene at 11.41 eV [217] is higher than the photon energy (10.5 eV) used for ionization. As illustrated in Scheme 5-2, the formation of these small hydrocarbons involved the recombination reactions between methyl radicals, the H abstraction, and the decomposition of alkyl radicals, according to the study by Taylor and Milazzo.[218]

In our experiments with 4.0 Torr of TriMS for the temperatures of 1300 - 1500 ^{o}C, the intensity ratio of ethene/propene was found to range from 0.59 to 1.90. Taking into consideration the difference in the ionization cross section,[89] the formation of ethene is found to be dominant over propene as a hydrocarbon product from the secondary gas-phase reactions with a ratio ranging from 21.2 : 1 to 68.4 : 1.

Methane has been found to be one of the main products in the pyrolysis of TriMS.[183, 184, 192, 207] The first-order rate constant for forming methane is determined to be $log_{10}k_{CH_4}/s^{-1} = (16.4 \pm 0.7) - (320 \pm 2)kJ.mol^{-1}/2.303RT$.[183, 192, 207] The close resemblance of the experimentally-determined activation energy with the bond dissociation energy D(Me_2HSi-Me) of 318 kJ/mol [240] leads to the conclusion that methane is formed by the following reactions (Equations (7-1) and (7-2)) initiated and rate-determined by the dissociation of Si-Me bond.

$$(CH_3)_3SiH \longrightarrow (CH_3)_2\dot{S}iH + \dot{C}H_3 \quad (7\text{-}1)$$

$$\dot{C}H_3 + (CH_3)_3SiH \longrightarrow (CH_3)_3\dot{S}i + CH_4 \quad (7\text{-}2)$$

Our previous study on the secondary gas-phase reactions of TriMS in the hot-wire CVD process[67] also suggested that the methane production involved the hydrogen abstraction by $^{\bullet}CH_3$ from the parent molecule. However, it has been shown that aside from the formation of trimethylsilyl radical by Equation (7-2), the H abstraction reaction to form methane also yields trimethylsilylmethyl radical as shown in Equation (7-3).

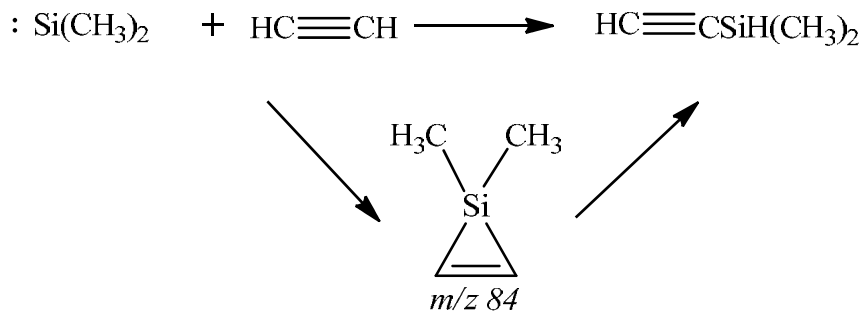
$$\dot{C}H_3 + (CH_3)_3SiH \longrightarrow \dot{C}H_2SiH(CH_3)_2 + CH_4 \quad (7\text{-}3)$$

Other possible pathway to form methane could be from the molecular elimination reaction, as illustrated by Equation (7-4).

$$(CH_3)_3SiH \longrightarrow :Si(CH_3)_2 + CH_4 \quad (7\text{-}4)$$

Although the formation of CH_4 via molecular elimination has never been reported in the pyrolysis of TriMS, it has been observed when using monomethylsilane [122-124, 177] and dimethylsilane [95, 176] in pyrolysis. The results from the pyrolysis of monomethylsilane showed that out of the three elimination channels, *i.e.*, 1,1-H_2, 1,2-H_2 and CH_4, the dissociation process yield to eliminate CH_4 only accounts for 6%. If the methane molecules observed with 4.0 Torr of TriMS in the hot-wire CVD reactor came from molecular elimination, its pressure should not exceed 4.0 Torr. In order to determine the main contributor to the formation of methane, the amount of methane produced when using 4.0 Torr of TriMS has been calculated. For this, a series of mixtures of authentic methane and helium samples with different pressures were prepared and examined the intensities of the two mass peaks. By plotting the intensity ratio of peaks at *m/z* 16 and 4 as a function of the corresponding pressure ratios, the ionization cross section ratio for CH_4 with respect to He is determined to be 1.95 ± 0.08. When using 4.0 Torr of TriMS in the reactor at a filament temperature of 1300 ^oC, the intensity ratio of peak 16 to peak 4 varies between 0.12 – 0.58. Considering the ionization cross section ratio of He to CH_4 and that the pressure of He in the reactor is constant at 16.0 Torr, the pressure of CH_4 produced is determined to be 1.0 – 4.8 Torr. Therefore, CH_4 should come mainly from the radical chain reactions, with possible minor contribution from the molecular elimination. Further support of the existence of molecular elimination of CH_4 from TriMS in our experiments comes from the observation of two new relatively strong peaks at *m/z* 84 and 98 (Figure 7-2b). The acetylene species produced *in situ* when using TriMS in the hot-wire CVD reactor is a well-known trapping agent for silylene species. [122, 176, 219]

According to Haas and Ring,[219] the reaction of $:SiH_2$ with C_2H_2 forms silylacetylene ($HC{\equiv}CSiH_3$) either by direct insertion of $:SiH_2$ into a C-H bond or by addition to the C-C triple bond to form silacyclpropene. Dimethylsilylene, the concomitant product of CH_4 elimination in Equation (7-4), once produced, reacts with acetylene yields dimethylsilylacetylene with a mass of 84 amu, as represented by Equation (7-5).



(7-5)

Similarly, 1-dimethylsilylpropyne (*m/z* 98) can be produced by the reaction between $:Si(CH_3)_2$ and propyne (*m/z* 40) generated *in situ* in the reactor. Figure 7-4 shows the intensity distributions of peaks at *m/z* 98, 84, 40, 26 and 16 as a function of time for a filament temperature of 1300 ^{o}C. The fact that these two peaks at *m/z* 84 and 98 only appears strongly when there is a good amount of methane, acetylene and propyne formed provides strong support of the existence of dimethylsilyene species formed from molecular elimination of methane.

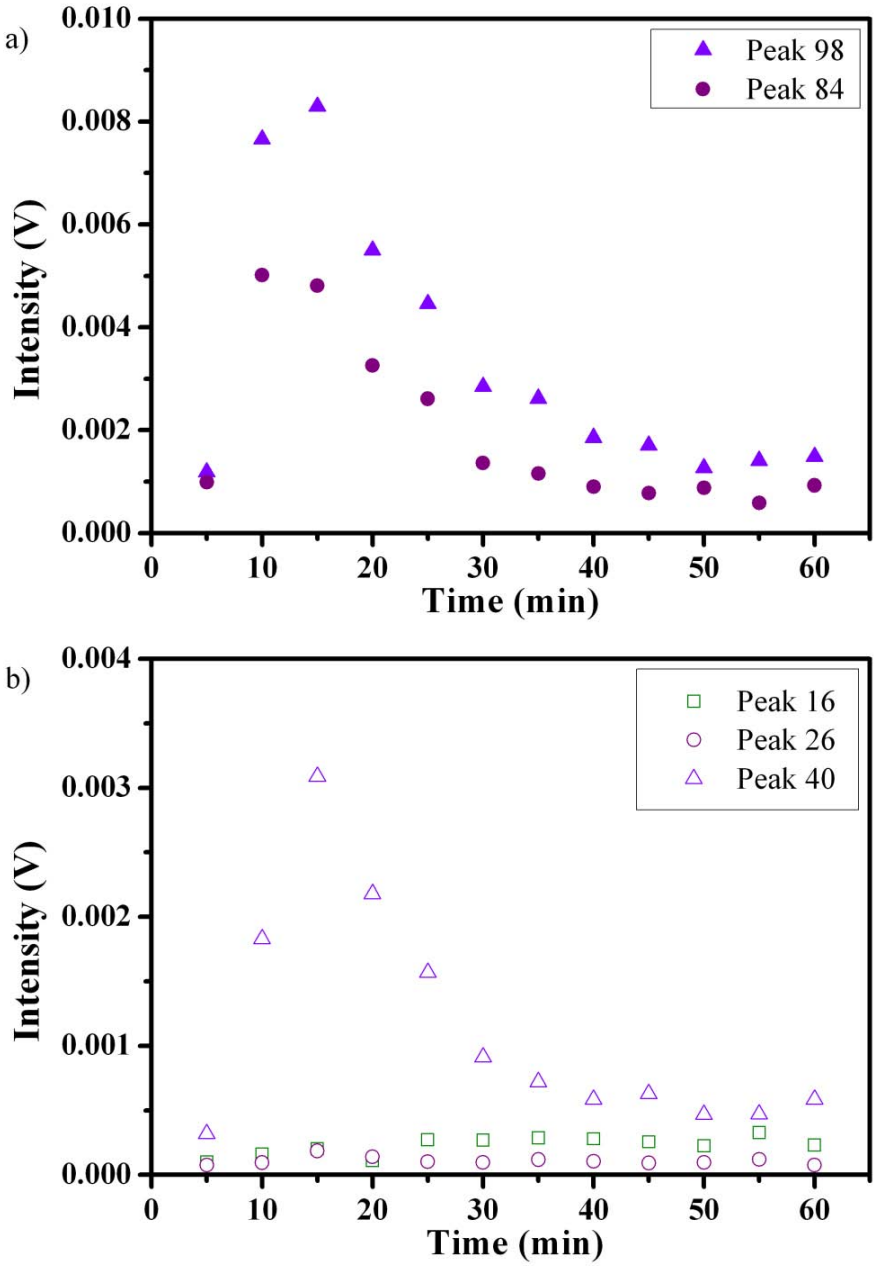


Figure 7-4: Comparisons of the intensity of the peaks at a) *m/z* 84, 98 and b) *m/z* 16, 26, 40, versus filament-on time at 1300 ^{o}C observed with 4.0 Torr of TriMS.

7.4 Formation of Hydrogen Molecules

Aside from the small hydrocarbon molecules produced when using 4.0 Torr of TriMS, a peak at *m/z* 2 representing H_2 molecule was also observed at 1300 ^{o}C, as shown

in Figure 7-2b. The H_2^+ peak started to appear very weakly at 1100 ^oC, reached a maximum intensity at 1300 ^oC, and decreased in intensity at higher temperatures. When using 0.12 Torr of TriMS, the H_2^+ peak intensity maximized at a higher temperature of 1600 ^oC. In previous studies on the pyrolysis of TriMS,[183, 184, 192, 207] H_2 was one of the two main products along with CH_4 and its formation was believed to be rate-determined by Si-H bond cleavage in TriMS (Equation (7-6)) followed by the H abstraction reaction between H radical and TriMS (Equation (7-7)).

$$(CH_3)_3SiH \longrightarrow (CH_3)_3\dot{S}i + \dot{H} \quad (7\text{-}6)$$

$$\dot{H} + (CH_3)_3SiH \longrightarrow (CH_3)_3\dot{S}i + H_2 \quad (7\text{-}7)$$

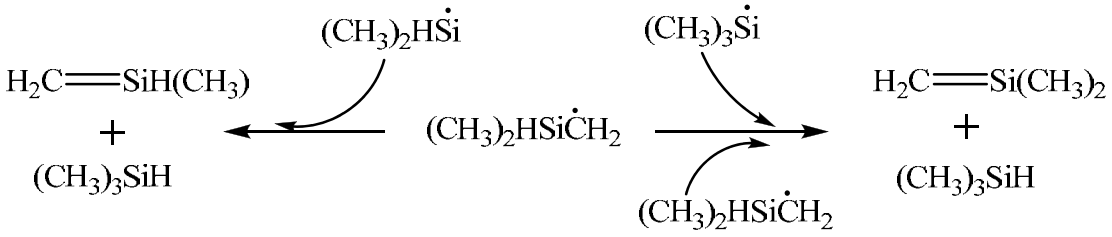
The amount ratio of H_2 to CH_4 varies in different pyrolysis studies. Davidson *et al.*[192] reported a H_2/CH_4 ratio of 0.19 – 0.20 when using 2 to 4 Torr of TriMS in a stirred-flow system between 943 and 1031 K, whereas Paquin *et al.*[184] obtained a H_2/CH_4 ratio of 3.25 at a TriMS pressure of 3.5 Torr and 983 K in a flow system with the surface coated with a silicon mirror. In our experiments with 4.0 Torr of TriMS in the hot-wire CVD reactor, the intensity ratio of the peak *m/z* 2 to that at peak *m/z* 16 varies between 1.44 and 4.10 for 1300 ^oC - 1400 ^oC. The ionization cross section ratio of H_2 to CH_4 was calibrated to be 0.88 ± 0.04 using the known mixtures with different pressure ratios. Therefore, the amount of H_2 produced in the reactor is determined to be 1.6 to 4.7 times that of CH_4. This H_2/CH_4 ratio is higher than that reported by Davidson *et al.* and comparable to or slightly higher than the result by Paquin *et al.* Following the same argument as in the discussion of methane formation, since the pressure of H_2 produced exceeds the starting pressure of TriMS at 4.0 Torr, the main contributor to the formation

of H_2 in the reactor should come from reactions (7-6) and (7-7) that are part of the radical chain reactions. However, the contribution of H_2 molecular elimination shown by Equation (7-8) cannot be discounted.

$$(CH_3)_3SiH \longrightarrow (CH_3)_2Si{=}CH_2 + H_2 \qquad (7\text{-}8)$$

7.5 Effect on the Radical Recombination and Disproportionation Reactions

As illustrated in Equation (7-1) to (7-3), the primary decomposition of TriMS and secondary H-abstraction reactions produced several Si-containing radicals such as $(CH_3)_3Si^{\bullet}$, $(CH_3)_2HSi^{\bullet}$, and $(CH_3)_2SiCH_2^{\bullet}$ in the hot-wire CVD reactor. Davidson *et al.*[183, 192, 207] has shown that the disproportionation reaction between these radicals forms the silene species, as illustrated in Scheme 7-1.



Scheme 7-1 Disproportionation reactions between Si-containing radicals

Self- and cross-cycloaddition of the silene intermediates lead to the formation of several disilacyclobutane molecules, including DMDSCB (*m/z* 116), TriMDSCB (*m/z* 130), and TMDSCB (*m/z* 144).[67] Another major radical species produced from primary decomposition is methyl. The main products from radical recombination reactions have been shown to be TMS (*m/z* 88) and HMDS (*m/z* 146).

As mentioned before, with an increased TriMS pressure to 4.0 Torr as compared to 0.12 Torr, the peaks at *m/z* 116, 130, and 144 appeared at a relatively lower temperature of 1300 ^{o}C with an increased intensity. The peak representing TMS also showed an increase with pressure, whereas the HMDS peak showed a decrease compared to those observed with 0.12 Torr TriMS. This is better illustrated in Figure 7-5, where a comparison of the intensity profiles of the five major products peaks in the high-mass region, *i.e., m/z* 88, 146, 116, 130, 144, at the filament temperature of 1300 ^{o}C for the two different TriMS pressure of 4.0 (Figure 7-5a) and 0.12 Torr (Figure 7-5b) is shown. From the comparison, it was noticed that the peak at *m/z* 88 is dominating the gas-phase chemistry for most of the reaction time ($t \geq 10$ min) at the higher pressure, whereas with an increase in pressure the peak at *m/z* 146, dominating at the lower pressure, has a lower intensity than that of TMS and became the weakest of all at $t \geq 25$ min. For the lower-pressure sample at 1300 ^{o}C (Figure 7-5b), the peak intensities increase with time indicating that there is a net formation of all products at this temperature. The intensity distribution of the same five mass peaks at an increased temperature of 1500 ^{o}C for the 0.12 Torr sample, illustrated in Figure 7-5c, showed an initial increase in the intensities followed by a decrease. This is the similar trend observed with the higher-pressure sample at a relatively lower temperature of 1300 ^{o}C.

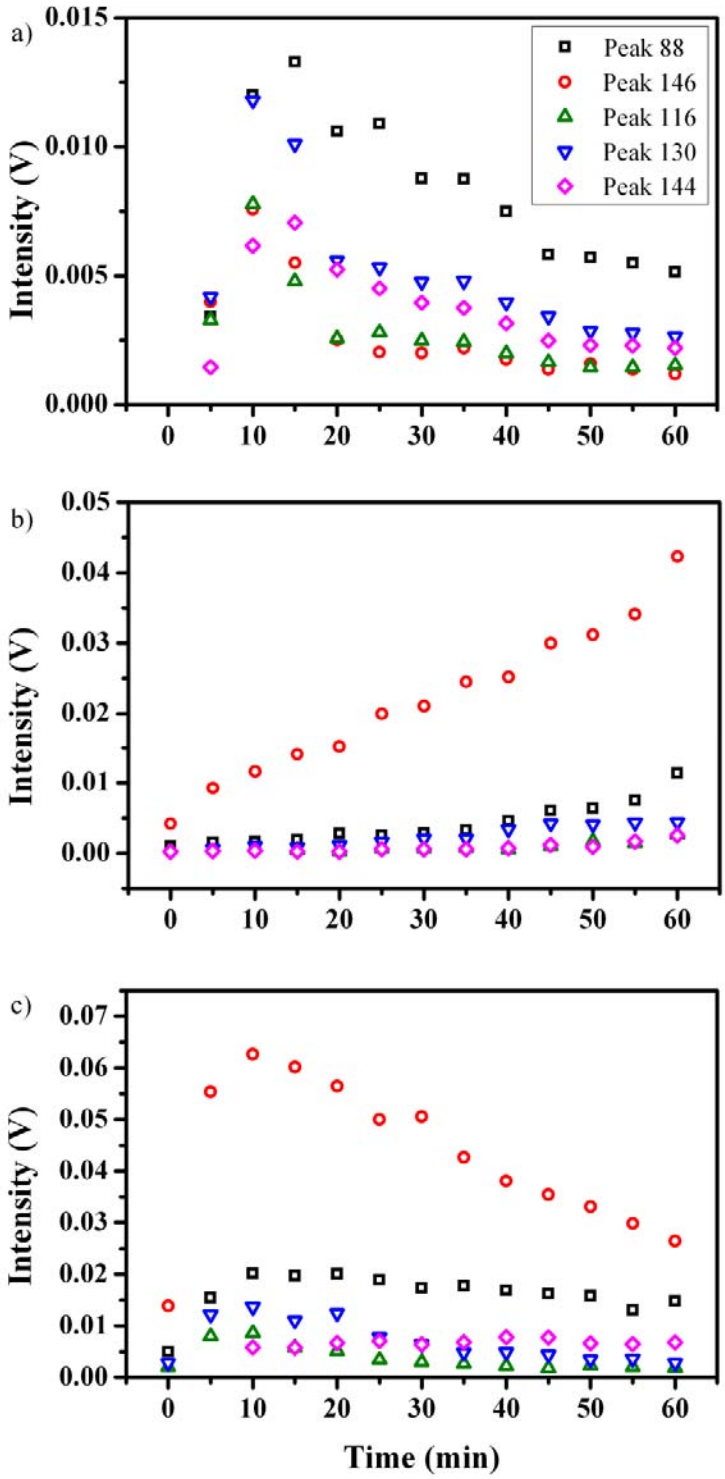


Figure 7-5: The intensity of the peaks at *m/z* 88, 146, 116, 130, and 144 versus filament-on time observed with a) 4.0 Torr of TriMS at 1300 ^{o}C, and b) 0.12 Torr of TriMS at 1300 ^{o}C, and c) 0.12 Torr of TriMS at 1500 ^{o}C.

The formation of all five products examined here involves the free radicals produced in the reactor. Among these radicals, some are methyl substituted silyl radicals (*e.g.*, $(CH_3)_3Si^{\bullet}$, $(CH_3)_2HSi^{\bullet}$), others are (silyl substituted)alkyl radicals (*e.g.*, $(CH_3)_2SiHCH_2^{\bullet}$, $^{\bullet}CH_3$). As mentioned before, with an increased TriMS pressure of 4.0 Torr, several small hydrocarbon molecules including methane, ethene, acetylene, propene and propyne have been produced. Ethene [94, 122, 176, 221, 222] and propene [122, 176] have been known to be good free radical scavengers. Therefore, it is believed that the presence of ethene and propene molecules affect significantly the availability of free radicals. Choo and Gaspar[221] have studied the addition reaction of trimethylsilyl radical to ethene in a flash photolysis system using electron spin resonance spectroscopy. They have concluded that ethene can act as an efficient silyl radical scavenger. Furthermore, the rate of this addition reaction is much faster than that of the addition of the simple alkyl radicals (*e.g.*, methyl, ethyl, n-propyl) to ethene. This fact is in agreement with the work done by Pollock *et al.*[222] where they have found that the trapping reaction of silyl radical ($^{\bullet}SiH_3$) by ethene is two to three orders of magnitude faster than its addition to alkyl radials and also more rapid than the addition reaction of the trimethylsilyl radical to ethene. Based on these observations, the formed ethene molecule will react as a silyl radical scavenger to $^{\bullet}Si(CH_3)_3$ and $^{\bullet}SiH(CH_3)_2$ radicals present in the reactor. Both HMDS and TMS originate from the radical recombination reactions; however, the self-combination reaction of trimethylsilyl radicals forms HMDS, and the combination of trimethylsilyl and methyl radicals yields TMS. The rate of the former reaction depends quadratically on the concentration of trimethylsilyl radical and that of latter exhibits a linear dependence. This

leads to a more significant decrease in the intensity of peak at *m/z* 146 relative to the one at *m/z* 88, as shown in Figure 7-5.

The occurrence of ethene scavenging reactions with $^{\bullet}Si(CH_3)_3$ and $^{\bullet}SiH(CH_3)_2$ radicals has also a direct effect on the rate of disproportionation reactions represented in Scheme 7-1. Two out of the three pathways forming dimethylsilene and methylsilene involve, respectively, $^{\bullet}Si(CH_3)_3$ and $^{\bullet}SiH(CH_3)_2$ radicals, and both rates depends linearly on the concentration of the methyl-substituted silyl radicals. A comparison of the peak intensity ratio of I(*m/z* 116)/I(*m/z* 88), I(*m/z* 130)/I(*m/z* 88), and I(*m/z* 144)/I(*m/z* 88) at filament temperatures of 1300 and 1500 ^{o}C for both sample pressures as a function of filament-on time is shown in Figure 7-6. At 1300 ^{o}C, at the first 20 minutes, the I(*m/z* 116)/I(*m/z* 88) ratio is higher for the higher TriMS pressure. This might be due to the additional contribution to the peak of *m/z* 116 from the dimethylsilylene species produced from the molecular elimination of CH_4 as illustrated in Equation (7-4). From Figure 7-4, it can be seen that the peak at *m/z* 40 representing propyne reached its maximum intensity at 20 minutes. Therefore, at a time shorter than 20 minutes, the produced propyne and also acetylene did not trap the dimethylsilylene completely. Beyond 20 minutes, the I(*m/z* 116)/I(*m/z* 88) ratio is comparable for the two TriMS pressures. This indicates that the main contributor to the peak intensity at *m/z* 116 is from the radical disproportionation reaction and due to the ethene scavenging the radicals, its intensity changes proportionately with the TMS (*m/z* 88) originated from radical combination reaction. Similar is found for the ratio of I(*m/z* 130)/I(*m/z* 88) as shown in Figure 7-6b.

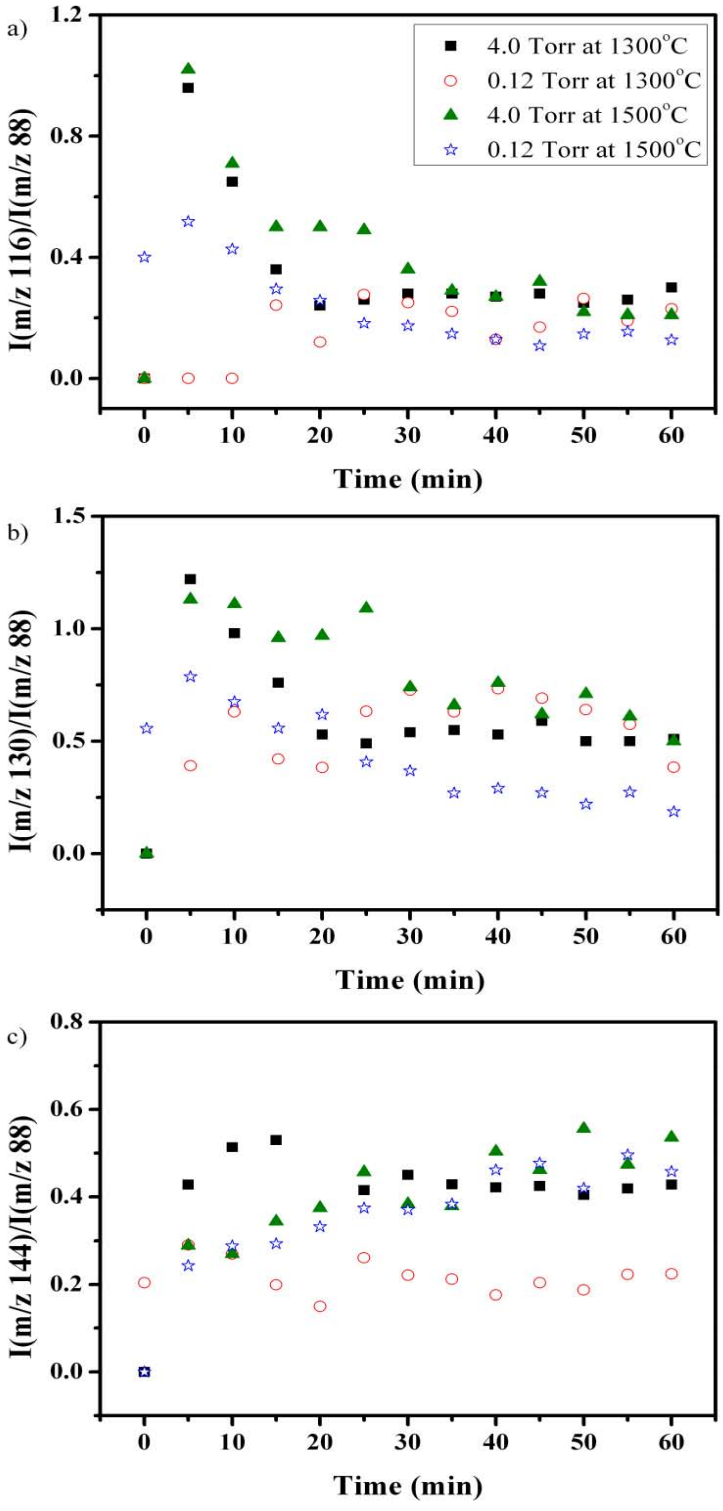


Figure 7-6: The intensity ratio of a) I(*m/z* 116)/I(*m/z* 88), b) I(*m/z* 130)/I(*m/z* 88), and c) I(*m/z* 144)/I(*m/z* 88) as a function of filament-on time for the two TriMS samples of 0.12 Torr and 4.0 Torr at the filament temperatures of 1300 ^{o}C and 1500 ^{o}C.

However, as illustrated in Figure 7-6c, the ratio of I(*m/z* 144)/I(*m/z* 88) shows a completely different trend from the other two. Here, for the lower sample pressure of 0.12 Torr, the ratio is much higher with the higher pressure for the entire reaction time of 1 hour, and the peak at *m/z* 144 only appeared at a later time ($t \geq 45$ min). The reason for this is that 1,1,3,3-tetramethyl-1,3-disilacyclobutane (*m/z* 144) is the product of dimerization of dimethylsilene which can be formed from self-disproportionation of dimethylsilylmethyl radical [$(CH_3)_2SiHCH_2^{\bullet}$] (Scheme 7-1). Dimethylsilylmethyl radical, being an alkyl radical, reacted with the free radical scavenger - ethene much less efficiently. Therefore, the amount of 1,1,3,3-tetramethyl-1,3-disilacyclobutane was not affected much as compared to those of TMS (*m/z* 88) and the other two disilacyclobutane molecules. This gives the observed increase in the ratio of I(*m/z* 144)/I(*m/z* 88) with the higher-pressure sample at 1300 ^{o}C. With an increasing temperature to 1500 ^{o}C, the three ratios generally increase with sample pressure. This indicates that the rate of disproportionation reactions with respect to the recombination reactions is enhanced with increasing pressure.

7.6 Summary

The gas-phase reaction chemistry of a 4.0 Torr of TriMS precursor gas in a hot-wire CVD reactor has been studied in this work and the results are compared with that of a 0.12 Torr of TriMS studied previously. The increase in the sample pressure leads to the formation of methane which is the first time this has been confirmed when using open-chain methyl-substituted silanes and four-membered-ring (di)silacyclobutane molecules as a precursor gas in the hot-wire CVD reactor. The formation of methane is mainly from

the radical chain reactions. However, minor contributions from molecular elimination have also been demonstrated by the chemical trapping of the concomitant silylene species from the acetylene/propyne molecules produced in-situ. Other small hydrocarbon molecules, including ethene and propene, were observed with the 4.0 Torr sample. In addition, the formation of H_2 is enhanced with increasing sample pressure.

Furthermore, the increase in the sample pressure has a direct effect on the radical recombination and disproportionation reactions. The radicals involved in these two types of reactions belong to either methyl substituted silyl radicals (*e.g.*, $(CH_3)_3Si^{\bullet}$, $(CH_3)_2HSi^{\bullet}$) or (silyl substituted)alkyl radicals (*e.g.*, $(CH_3)_2SiHCH_2^{\bullet}$, $^{\bullet}CH_3$). The availability of these radicals is significantly affected by the *in situ* produced ethene and propene, the well-known free radical scavengers. Ethene and propene traps the silyl radicals much more efficiently than the alkyl radicals, therefore, the five major products originated from the radical recombination (TMS and HMDS) and disproportionation reactions (DMDSCB, TriMDSCB, and TMDSCB) show different behavior when examining their intensity distributions as a function of reaction time and filament temperature for both sample pressures. The intensity of product peaks of TMS, DMDSCB, TriMDSCB, and TMDSCB all increases and the formation of TMS dominates the gas-phase chemistry for most of the reaction time ($t \geq 10$ min) when using high pressure of TriMS, whereas with an increase in TriMS pressure the HMDS peak, dominating at the lower pressure, decreases in intensity and becomes the weakest of all at $t \geq 25$ min.

Chapter Eight: Conclusions and Future work

Hot-wire chemical vapour deposition (HWCVD) has emerged as a new and promising technique to achieve device quality Si-based thin films. The popularity of this technique over the commonly-used deposition methods, such as PECVD and thermal CVD, is due to its numerous advantages, including high deposition rate, high gas utilization efficiency, low substrate temperature, low equipment cost, and lack of plasma induced damages to the film and the substrate. The process of HWCVD involves three main steps. The source gases are catalytically decomposed at a resistively heated wire, resulting in the formation of highly reactive radical species. These species, then, react with each other and with the abundant source gas molecules in secondary gas-phase reactions to form a variety of products. Film growth in HWCVD is believed to be induced by precursors generated from direct decomposition on the filament and/or from secondary gas-phase reactions. These final precursors dictate the resultant properties of the film that grows in the final stage of the HWCVD process. Therefore, for a better understanding of the HWCVD process and a rational optimization of film deposition, it is essential to identify the gas-phase chemical species and to study their formation mechanisms.

Among all the materials deposited by HWCVD, silicon carbide (SiC) alloy thin films have attracted a great deal of interest owing to their superior mechanical property and chemical stability as well as their applications in electronic devices. Most SiC growth proceeds through the use of separate Si- (SiH_4, Si_2H_6, or SiH_2Cl_2) and C-bearing (CH_4, C_2H_4, C_3H_8) precursors. However, the use of mixtures requires independent flow control

of each precursor. In addition, silanes and chlorosilanes are both pyrophoric and highly toxic. This has spurred a lot of interest in the investigation of alternative single-source precursors for SiC film deposition. An ideal single-source precursor would contain direct Si-C bonds and would decompose at relatively low temperatures. The simplest organosilicon compounds containing Si-C bonds are methyl-substituted silane molecules.

In this study, the primary decomposition pathways of four open chain methyl-substituted silanes, *i.e.*, monomethylsilane (MMS), dimethylsilane (DMS), trimethylsilane (TriMS), and tetramethylsilane (TMS), on heated tungsten (W) and Tantalum (Ta) filaments have been investigated by using laser ionization coupled with TOF mass spectrometry. Two complimentary ionization techniques, namely single photon ionization (SPI) using a VUV wavelength of 118 nm and a dual ionization source incorporating both SPI and laser induced electron ionization (LIEI), have been employed in this work. A common decomposition pathway, resulting in the formation of methyl and methyl-substituted silyl radicals, was found from these four precursors on W and Ta filaments. The dissociation process of these molecules on a heated metal surface is believed to be initiated by the Si-H bond cleavage and followed by Si-CH_3 bond breaking. It has been shown that the methyl radical intensity increased with temperature for both filaments in the low-temperature region, however, beyond the optimum temperature, a gradual decrease in the methyl intensity was observed for MMS, DMS, and TriMS when using Ta, whereas the intensity reaches a plateau with W. This is due to the fact that Ta is more efficient in releasing surface-bound H and forming active sites, leading to the adsorption of methyl radicals on the metal surface in the high-temperature regions. The apparent activation energy for methyl radical formation from the

dissociation of MMS, DMS, TriMS, TMS molecules on both W and Ta filaments increases with the increasing number of methyl substitution. The obtained low activation energy values for methyl radical formation in the range of 51.1 - 84.7 kJ · mol^{-1} suggests that the ejection of CH_3 radicals is accompanied by the formation of a Si moiety bound to the metal surface. Overall, TMS produces the least amount of methyl radicals on both filaments with the highest activation energy. The amount of methyl radicals produced when using MMS, DMS, and TriMS are similar but MMS gives the lowest activation energy.

In addition to methyl radical, H_2 molecule was also produced during the dissociation of these methyl-substituted silanes over W and Ta filament surfaces. Examination of the intensity of the H_2^+ peak from the four molecules has shown that it increases with temperature until reaching a plateau at around 2000 - 2100 ^oC. Similar trend has been obtained from both filaments. The effect of methyl substitution is reflected on the temperature at which the H_2^+ peak starts to appear and on the apparent activation energy (E_a) for the formation of H_2. The temperature is shifted to high end with increasing methyl substitution. The value of this activation energy is also increased from MMS to TMS. The formation of H_2 has been demonstrated to follow Langmuir-Hinshelwood mechanism, which consists of the recombination reaction between two adsorbed H atoms at the surface of the filament releasing H_2 into the gas phase. A confirmation of this mechanism is obtained by performing experiments with the deuterated isotopomers of MMS, DMS and TriMS, where the formation of D, HD and D_2 species is observed. The activation energy is also affected by the filament material. It has been found that a higher E_a value was obtained with Ta than with W. This is due to the

difference in binding energy between the H and the metal surface. In order to obtain a better understanding of this mechanism, the formation of H_2 molecule during the decomposition of MMS, DMS and TriMS is examined first in the gas-phase using *ab initio* methods. The role of the metal surface will be investigated in later stages. In this current study, *ab initio* methods at the CCSD(T)/6-311++G(3d,2p)//MP2/6-311++G(d,p) level of theory were carried out to explore the concerted and stepwise 1,1- and 1,2-H_2 elimination processes, resulting in the formation of silylene and silene species, respectively, as concomitants to H_2 in the gas-phase chemistry. These calculations showed that the concerted 1,1-H_2 elimination is the most kinetically favorable of all pathways for MMS and DMS. A comparison between the concerted and stepwise mechanism for MMS, DMS and TriMS revealed that the concerted pathway is thermodynamically favourable. From the thermodynamic and kinetic study, where the enthalpy ($\Delta H^{\neq}$), entropy ($\Delta S^{\neq}$), and Gibbs free energy ($\Delta G^{\neq}$) of activation along with reaction enthalpy (ΔH), entropy (ΔS), and Gibbs free energy (ΔG) at both 0 K and 298 K were examined, it was found that the concerted 1,1- H_2 elimination was the most kinetically and thermodynamically favourable pathway for the formation of H_2 during the decomposition of MMS and DMS molecules at both temperatures.

The products from the secondary gas-phase reactions are as important as those from the primary decomposition on the metal filaments in defining the properties of the deposited films. Therefore, it is crucial to identify these products and understand the mechanism of their formation. In this work, the secondary gas-phase reactions when using DMS and MMS as a source in a HWCVD reactor have been studied. The identification of the mechanism responsible for the formation of the main products during

the secondary gas-phase reactions using these precursors is accomplished by using the corresponding isotopomers and chemical trapping. In addition, the effect of deposition parameters, including filament material and precursor pressure on these mechanisms, was investigated. When examining the secondary gas-phase reactions for DMS, a competition between radical chain mechanism and silene/silylene mechanism is observed. At low filament temperatures, the gas-phase chemistry is dominated by the formation of 1,1,2,2-tetramethyldisilane (TMDS, 118 amu). As the filament temperature is increased, trimethylsilane and 1,3-dimethyl-1,3-disilacyclobutane (DMDSCB, 116 amu) become dominating. It has been demonstrated that TMDS is formed through silylene insertion reaction into the Si-H bond of DMS, TriMS is produced from the radical recombination reactions in the termination steps of a radical chain reaction, and the formation of DMDSCB is attributed to silene and dimethylsilylene dimerization. In addition, the effect of sample pressure on the gas-phase reaction chemistry of DMS in the HWCVD process has been studied by examining the reaction products in a reactor with 1.2 Torr and 0.12 Torr of DMS, respectively. From the comparison, it has been shown that silylene insertion reaction dominates the gas-phase chemistry when the pressure and temperature are low. As the precursor pressure is increased to 1.2 Torr, the gas-phase chemistry of DMS is governed by the radical recombination reactions. The increase in the pressure also resulted in the formation of small hydrocarbon molecules, including methane, ethene, acetylene, propene, and propyne. The *in situ* trapping of the silylene intermediates by these species is responsible for the observed switch from silylene-dominant chemistry at low pressure regime to radical-dominant chemistry at high pressure regime. The effect of another deposition parameter, which is the filament material, on the gas-phase

chemistry has also been studied. Ta filament is found to promote the formation of products generated from silylene chemistry at low temperature, whereas W filament favours radical recombination reactions at the same temperature.

The secondary gas-phase reactions with MMS in the HWCVD reactor is found to be dominated mainly by the formation of two products: 1,2-dimethyldisilane (DMDS, 90 amu) formed from methylsilylene insertion reaction into the Si-H bond in the parent molecule, and 1,3-disilacyclobutane (DSCB, 88 amu) produced from methylsilylene dimerization. Further reactions of these products with the methylsilylene intermediate produce high-mass methyl-substituted disilanes (132, 134 amu) and trisilanes (176, and 178 amu). The involvement of various possible active intermediates, such as methylsilyl radical, methylsilylene, and silene, has been investigated by experiments with the deuterated isotopomer (MMS-d_3) and chemical trapping using 1,3-butadiene and ammonia. It has been shown that the secondary gas-phase reaction chemistry with MMS involves exclusively methylsilylene species. This explains the results when examining the effect of different deposition parameters, including precursor pressure and filament material, which indicate that these parameters do not affect the chemistry at all.

Finally, the effect of sample pressure on the gas-phase reaction chemistry of TriMS in the HWCVD process has also been studied by examining the secondary gas-phase reaction products in a reactor with 4.0 Torr of TriMS and comparing with our previous results at 0.12 Torr. The increase in the sample pressure leads to the formation of other small hydrocarbon molecules including methane acetylene, ethene, propyne, and propene. The detection of methane has been confirmed for the first time when using open-chain methyl-substituted silanes and four-membered-ring (di)silacyclobutane

molecules as precursors in the HWCVD reactor. It was also demonstrated that the formation of hydrogen molecules is enhanced when the sample pressure is increased. In addition, the change in the sample pressure was found to have an effect on the radical recombination and disproportionation reactions, which is reflected in the different behavior assumed by the main products from these two reactions, tetramethylsilane (TMS), hexamethyldisilane (HMDS) from the former and three methyl-substituted disilacyclobutane (MDSCBs) from the latter. The trapping of free radicals resulted from the *in situ* produced ethene and propene molecules are responsible for the observed difference.

Identification of gas-phase reactive species and study of the secondary gas-phase reactions are considered to be essential for elucidation of the mechanism of Si-containing thin film growth in HWCVD processes. In future work, a kinetic study will help develop a comprehensive deposition model and give better insights into the optimization of thin film deposition. Previous study on TMS, TriMS and HMDS has indicated that the reaction mechanisms all fit the form of a Rice-Herzfeld mechanism. Applying the steady-state approximation in methyl radical formation, where the rate of the initiation step would be equal to the sum of the rates of the termination reactions, the rate constant of the initiation step can be determined. Experimentally, the steady-state rate of formation of the termination products could be achieved by monitoring the change in their intensities over a period of time. In this way, the rate constant of the initiation step at different pressures and temperatures can be determined. The pressure dependence of k_1 will be

studied using the factorization method of Troe[241-245], from which the high-pressure and low-pressure limit rate constant of the initiation step could be determined.

In addition, the experimental results can be compared with those from simulations using CHEMKIN,[246] a modeling program for chemical kinetics. This program can be used in HWCVD reactor systems and provides information describing chemical reaction kinetics, whether in terms of elementary reactions or global reaction mechanisms, through a group of different packages that is designed to facilitate the incorporation of complex gas-phase chemical reaction mechanisms into numerical simulations.[247-250] CHEMKIN will also help in predicting the most suitable conditions (*e.g.*, pressure and temperature ranges) for film deposition or gas-phase reaction optimization. Furthermore, thermochemical kinetics can be employed in determining the rate constant of a reaction not available from experiments or literatures by using thermodynamic properties (*e.g.*, standard reaction entropy ΔS^o and enthalpy ΔH^o). The kinetic data obtained experimentally could also help establish the thermodynamic properties for various reactions involved in the mechanism, therefore contribute to the expansion of thermodynamic database.

Finally, filament aging due to silicide and carbide formation seems to be a drawback with the HWCVD technique at low temperatures.[24, 34, 40, 211] The Shi group has studied the aging of W filament using silane and silacyclobutane molecules as source gases. When using silane and silacyclobutane (SCB) as a source gas, filament aging was found to be caused by the formation of Si or Si-W alloy.[174, 175] With 1,1,3,3-tetramethyl-1,3-disilacyclobutane (TMDSCB) as a source gas, carburization of W filament was observed, which was mainly caused by the interaction of methyl radicals with the heated

filament.[174] Hence, in order to obtain a better understanding on filament aging due to the formation of metal alloys, a study using the open chain methyl-substituted silane molecules needs to be conducted. A comparison between these open chain methyl-substituted silanes and silacyclobutanes on the filament aging process will provide a better understanding on this issue and to explore the possibility that these methyl-substituted silane molecules could be more suitable precursors for the deposition of SiC.

Appendices

SPRINGER LICENSE
TERMS AND CONDITIONS

This is a License Agreement between Rim Toukabri ("You") and Springer ("Springer") provided by Copyright Clearance Center ("CCC"). The license consists of your order details, the terms and conditions provided by Springer, and the payment terms and conditions.

All payments must be made in full to CCC. For payment instructions, please see information listed at the bottom of this form.

License Number	3176021485932
License date	Jun 25, 2013
Licensed content publisher	Springer
Licensed content publication	Journal of The American Society for Mass Spectrometry
Licensed content title	Application of laser induced electron impact ionization to the deposition chemistry in the hot-wire chemical vapor deposition process with SiH4-NH3 gas mixtures
Licensed content author	Brett Eustergerling
Licensed content date	Jan 1, 2007
Volume number	18
Issue number	11
Type of Use	Thesis/Dissertation
Portion	Figures
Author of this Springer article	No
Order reference number	
Title of your thesis / dissertation	Gas-phase Chemistry of Methyl-substituted silanes in a Hot-wire Chemical Vapour Deposition process
Expected completion date	Jul 2013
Estimated size(pages)	270
Total	0.00 CAD

Terms and Conditions

Introduction
The publisher for this copyrighted material is Springer Science + Business Media. By clicking "accept" in connection with completing this licensing transaction, you agree that the following terms and conditions apply to this transaction (along with the Billing and Payment terms and conditions established by Copyright Clearance Center, Inc. ("CCC"), at the time that you opened your Rightslink account and that are available at any time at http://myaccount.copyright.com).

Limited License
With reference to your request to reprint in your thesis material on which Springer Science and Business Media control the copyright, permission is granted, free of charge, for the use indicated in your enquiry.

Licenses are for one-time use only with a maximum distribution equal to the number that you identified in the licensing process.

This License includes use in an electronic form, provided its password protected or on the university's intranet or repository, including UMI (according to the definition at the Sherpa website: http://www.sherpa.ac.uk/romeo/). For any other electronic use, please contact Springer at (permissions.dordrecht@springer.com or permissions.heidelberg@springer.com).

The material can only be used for the purpose of defending your thesis, and with a maximum of 100 extra copies in paper.

Although Springer holds copyright to the material and is entitled to negotiate on rights, this license is only valid, subject to a courtesy information to the author (address is given with the article/chapter) and provided it concerns original material which does not carry references to other sources (if material in question appears with credit to another source, authorization from that source is required as well).

Permission free of charge on this occasion does not prejudice any rights we might have to charge for reproduction of our copyrighted material in the future.

Altering/Modifying Material: Not Permitted
You may not alter or modify the material in any manner. Abbreviations, additions, deletions and/or any other alterations shall be made only with prior written authorization of the author(s) and/or Springer Science + Business Media. (Please contact Springer at (permissions.dordrecht@springer.com or permissions.heidelberg@springer.com)

Reservation of Rights
Springer Science + Business Media reserves all rights not specifically granted in the combination of (i) the license details provided by you and accepted in the course of this

licensing transaction, (ii) these terms and conditions and (iii) CCC's Billing and Payment terms and conditions.

Copyright Notice:Disclaimer
You must include the following copyright and permission notice in connection with any reproduction of the licensed material: "Springer and the original publisher /journal title, volume, year of publication, page, chapter/article title, name(s) of author(s), figure number(s), original copyright notice) is given to the publication in which the material was originally published, by adding; with kind permission from Springer Science and Business Media"

Warranties: None

Example 1: Springer Science + Business Media makes no representations or warranties with respect to the licensed material.

Example 2: Springer Science + Business Media makes no representations or warranties with respect to the licensed material and adopts on its own behalf the limitations and disclaimers established by CCC on its behalf in its Billing and Payment terms and conditions for this licensing transaction.

Indemnity
You hereby indemnify and agree to hold harmless Springer Science + Business Media and CCC, and their respective officers, directors, employees and agents, from and against any and all claims arising out of your use of the licensed material other than as specifically authorized pursuant to this license.

No Transfer of License
This license is personal to you and may not be sublicensed, assigned, or transferred by you to any other person without Springer Science + Business Media's written permission.

No Amendment Except in Writing
This license may not be amended except in a writing signed by both parties (or, in the case of Springer Science + Business Media, by CCC on Springer Science + Business Media's behalf).

Objection to Contrary Terms
Springer Science + Business Media hereby objects to any terms contained in any purchase order, acknowledgment, check endorsement or other writing prepared by you, which terms are inconsistent with these terms and conditions or CCC's Billing and Payment terms and conditions. These terms and conditions, together with CCC's Billing and Payment terms and conditions (which are incorporated herein), comprise the entire agreement between you and Springer Science + Business Media (and CCC) concerning this licensing transaction. In the event of any conflict between your obligations established by these terms and

conditions and those established by CCC's Billing and Payment terms and conditions, these terms and conditions shall control.

Jurisdiction
All disputes that may arise in connection with this present License, or the breach thereof, shall be settled exclusively by arbitration, to be held in The Netherlands, in accordance with Dutch law, and to be conducted under the Rules of the 'Netherlands Arbitrage Instituut' (Netherlands Institute of Arbitration).***OR:***

All disputes that may arise in connection with this present License, or the breach thereof, shall be settled exclusively by arbitration, to be held in the Federal Republic of Germany, in accordance with German law.

Other terms and conditions:

v1.3

If you would like to pay for this license now, please remit this license along with your payment made payable to "COPYRIGHT CLEARANCE CENTER" otherwise you will be invoiced within 48 hours of the license date. Payment should be in the form of a check or money order referencing your account number and this invoice number RLNK501051172.
Once you receive your invoice for this order, you may pay your invoice by credit card. Please follow instructions provided at that time.

Make Payment To:
Copyright Clearance Center
Dept 001
P.O. Box 843006
Boston, MA 02284-3006

For suggestions or comments regarding this order, contact RightsLink Customer Support:customercare@copyright.com or +1-877-622-5543 (toll free in the US) or +1-978-646-2777.

Gratis licenses (referencing $0 in the Total field) are free. Please retain this printable license for your reference. No payment is required.

References

1. Martin, P. M., *Handbook of Deposition Technologies for Films and Coatings: Science, Applications and Technology*. Elsevier Science: 2009.
2. Maissel, L. I.; Glang, R., *Handbook of thin film technology*. McGraw-Hill: 1970.
3. Seshan, K., *Handbook of Thin Film Deposition Processes and Techniques*. Elsevier Science: 2001.
4. Vossen, J. L.; Kern, W., *Thin film processes II*. Academic Press: 1991.
5. Mattox, D. M., *Handbook of Physical Vapor Deposition (PVD) Processing*. Elsevier Science: 2010.
6. Park, J. H.; Sudarshan, T. S., *Chemical Vapor Deposition*. A S M International: 2001.
7. Pierson, H. O., *Handbook of chemical vapor deposition (CVD): principles, technology, and applications*. Noyes Publications: 1992.
8. Yamazaki, S.; Wada, K.; Taniguch.I, Silicon nitride prepared by SiH_4-NH_3 reaction with catalysts. *Japanese Journal of Applied Physics* **1970,** 9, (12), 1467.
9. Wiesmann, H.; Ghosh, A. K.; McMahon, T.; Strongin, M., a-Si-H produced by high-temperature thermal-decomposition of silane. *Journal of Applied Physics* **1979,** 50, (5), 3752.
10. Matsumura, H.; Tachibana, H., Amorphous silicon produced by a new thermal chemical vapor deposition method using intermediate species SiF_2. *Applied Physics Letters* **1985,** 47, (8), 833.
11. Matsumura, H., Catalytic chemical vapor-deposition (CTL-CVD) method producing high-quality hydrogenated amorphous-silicon. *Japanese Journal of Applied Physics Part 2-Letters* **1986,** 25, (12), L949.
12. Doyle, J.; Robertson, R.; Lin, G. H.; He, M. Z.; Gallagher, A., Production of high-quality amorphous-silicon films by evaporative silane surface decomposition. *Journal of Applied Physics* **1988,** 64, (6), 3215.
13. Mahan, A. H.; Carapella, J.; Nelson, B. P.; Crandall, R. S.; Balberg, I., Deposition of device quality, low H content amorphous silicon. *Journal of Applied Physics* **1991,** 69, (9), 6728.
14. Van Veenendaal, P.; Schropp, R. E. I., Processes in silicon deposition by hot-wire chemical vapor deposition. *Current Opinion in Solid State & Materials Science* **2002,** 6, (5), 465.
15. Matsumura, H., Summary of research in NEDO Cat-CVD project in Japan. *Thin Solid Films* **2001,** 395, (1-2), 1.
16. Mahan, A. H., Status of Cat-CVD (Hot Wire CVD) research in the United States. *Thin Solid Films* **2001,** 395, (1-2), 12.
17. Schropp, R. E. I., Status of Cat-CVD (Hot-Wire CVD) research in Europe. *Thin Solid Films* **2001,** 395, (1-2), 17.
18. Doyle, J. R.; Xu, Y.; Reedy, R.; Branz, H. M.; Mahan, A. H., Film stoichiometry and gas dissociation kinetics in hot-wire chemical vapor deposition of a-SiGe : H. *Thin Solid Films* **2008,** 516, (5), 526.

19. Mahan, A. H.; Xu, Y.; Gedvilas, L. M.; Reedy, R. C.; Williamson, D. L.; Datta, S.; Cohen, J. D.; Yan, B.; Branz, H. M.; Ieee, a-SiGe : H materials and devices deposited by hot wire CVD using a tantalum filament operated at low temperature. In *Conference Record of the Thirty-First IEEE Photovoltaic Specialists Conference - 2005*, 2005; pp 1397.
20. Mahan, A. H.; Xu, Y.; Gedvilas, L. M.; Williamson, D. L., A direct correlation between film structure and solar cell efficiency for HWCVD amorphous silicon germanium alloys. *Thin Solid Films* **2009,** 517, (12), 3532.
21. Nelson, B. P.; Xu, Y. Q.; Williamson, D. L.; Von Roedern, B.; Mason, A.; Heck, S.; Mahan, A. H.; Schmitt, S. E.; Gallagher, A. C.; Webb, J.; Reedy, R., Hydrogenated amorphous silicon germanium alloys grown by the hot-wire chemical vapor deposition technique. In *Amorphous and Microcrystalline Silicon Technology-1998*, Schropp, R.; Branz, H. M.; Hack, M.; Shimizu, I.; Wagner, S., Eds. 1998; Vol. 507, pp 447.
22. Xu, Y. Q.; Mahan, A. H.; Gedvilas, L. M.; Reedy, R. C.; Branz, H. M., Deposition of photosensitive hydrogenated amorphous silicon-germanium films with a tantalum hot wire. *Thin Solid Films* **2006,** 501, (1-2), 198.
23. Xu, Y. Q.; Yan, B. J.; Nelson, B. P.; Iwaniczko, E.; Reedy, R. C.; Mahan, A. H.; Branz, H., Devices fabrication with narrow-bandgap a-SiGe : H alloys deposited by HWCVD. In *Amorphous and Nanocrystalline Silicon Science and Technology-2004*, Ganguly, G.; Kondo, M.; Schiff, E. A.; Carius, R.; Biswas, R., Eds. 2004; Vol. 808, pp 617.
24. Mahan, A. H.; Dillon, A. C.; Gedvilas, L. M.; Williamson, D. L.; Perkins, J. D., Properties of thin film silicon nitride deposited by hot wire chemical vapor deposition using silane, ammonia, and hydrogen gas mixtures. *Journal of Applied Physics* **2003,** 94, (4), 2360.
25. Stannowski, B.; Rath, J. K.; Schropp, R. E. I., Hot-wire silicon nitride for thin-film transistors. *Thin Solid Films* **2001,** 395, (1-2), 339.
26. Stannowski, B.; Rath, J. K.; Schropp, R. E. I., Growth process and properties of silicon nitride deposited by hot-wire chemical vapor deposition. *Journal of Applied Physics* **2003,** 93, (5), 2618.
27. Van der Werf, C. H. M.; Goldbach, H. D.; Loffler, J.; Scarfo, A.; Kylner, A. M. C.; Stannowski, B.; ArnoldBik, W. M.; Weeber, A.; Rieffe, H.; Soppe, W. J.; Rath, J. K.; Schropp, R. E. I., Silicon nitride at high deposition rate by Hot Wire Chemical Vapor Deposition as passivating and antireflection layer on multi crystalline silicon solar cells. *Thin Solid Films* **2006,** 501, (1-2), 51.
28. Swain, B. P., Influence of process pressure on HW-CVD deposited a-SiC : H films. *Surface & Coatings Technology* **2006,** 201, (3-4), 1132.
29. Swain, B. P.; Dusane, R. O., Multiphase structure of hydrogen diluted a-SiC : H deposited by HWCVD. *Materials Chemistry and Physics* **2006,** 99, (2-3), 240.
30. Tabata, A.; Komura, Y., Preparation of nanocrystalline cubic silicon carbide thin films by hot-wire CVD at various filament-to-substrate distances. *Surface & Coatings Technology* **2007,** 201, (22-23), 8986.

31. Lee, M. S.; Bent, S. F., Bonding and thermal reactivity in thin a-SiC:H films grown by methylsilane CVD. *Journal of Physical Chemistry B* **1997,** 101, (45), 9195.
32. Lee, M. S.; Bent, S. F., Spectroscopic and thermal studies of a-SiC : H film growth: Comparison of mono-, tri-, and tetramethylsilane. *Journal of Vacuum Science & Technology a-Vacuum Surfaces and Films* **1998,** 16, (3), 1658.
33. Tange, S.; Inoue, K.; Tonokura, K.; Koshi, M., Catalytic decomposition of SiH4 on a hot filament. *Thin Solid Films* **2001,** 395, (1-2), 42.
34. Holt, J. K.; Swiatek, M.; Goodwin, D. G.; Atwater, H. A., The aging of tungsten filaments and its effect on wire surface kinetics in hot-wire chemical vapor deposition. *Journal of Applied Physics* **2002,** 92, (8), 4803.
35. Holt, J. K.; Swiatek, M.; Goodwin, D. G.; Atwater, H. A., The effect of aging on tungsten filament surface kinetics in hot-wire chemical vapor deposition of silicon. In *Amorphous and Heterogeneous Silicon-Based Films-2002*, Cohen, J. D.; Abelson, J. R.; Matsumura, H.; Robertson, J., Eds. 2002; Vol. 715, pp 165.
36. Duan, H. L.; Zaharias, G. A.; Bent, S. F., Effect of filament material on the decomposition of SiH_4 in hot wire CVD of Si-based films. In *Amorphous and Heterogeneous Silicon-Based Films-2002*, Cohen, J. D.; Abelson, J. R.; Matsumura, H.; Robertson, J., Eds. 2002; Vol. 715, pp 21.
37. Walsh, R., Bond-Dissociation Energy Values in Silicon-Containing Compounds and Some of Their Implications. *Accounts of Chemical Research* **1981,** 14, (8), 246.
38. Matsumura, H., Study on catalytic chemical vapor-deposition method to prepare hydrogenated amorphous-silicon. *Journal of Applied Physics* **1989,** 65, (11), 4396.
39. Morrison, S.; Das, U.; Madan, A., Deposition of thin film silicon using the pulsed PECVD and HWCVD techniques. *Solar Energy Materials and Solar Cells* **2003,** 76, (3), 281.
40. Van Veenendaal, P. A. T. T.; Gijzeman, O. L. J.; Rath, J. K.; Schropp, R. E. I., The influence of different catalyzers in hot-wire CVD for the deposition of polycrystalline silicon thin films. *Thin Solid Films* **2001,** 395, (1–2), 194.
41. Van Veenendaal, P. A. T. T.; Van Der Werf, C. M. H.; Rath, J. K.; Schropp, R. E. I., Influence of grain environment on open circuit voltage of hot-wire chemical vapour deposited Si:H solar cells. *Journal of Non-Crystalline Solids* **2002,** 299-302, (PART 2), 1184.
42. Duan, H. L.; Zaharias, G. A.; Bent, S. F., The effect of filament temperature on the gaseous radicals in the hot wire decomposition of silane. *Thin Solid Films* **2001,** 395, (1-2), 36.
43. Bouree, J. E.; Guillet, J.; Grattepain, C.; Chaumont, J., Quantitative analysis of tungsten, oxygen and carbon concentrations in the microcrystalline silicon films deposited by hot-wire CVD. *Thin Solid Films* **2003,** 430, (1-2), 110.
44. Molebroek, E. C.; Mahan, A. H.; Gallagher, A., Mechanisms influencing `hot-wire' deposition of hydrogenated amorphous silicon. *Journal of Applied Physics* **1997,** 82, (4), 1909.

45. Pant, A.; Russell, T. W. F.; Huff, M. C.; Aparicio, R.; Birkmire, R. W., Hot-wire chemical vapor deposition of silicon from silane: Effect of process conditions. *Industrial & Engineering Chemistry Research* **2001,** 40, (5), 1377.
46. Feng, Z. C., *SiC Power Materials: Devices and Applications*. Springer: 2004.
47. Shur, M. S.; Rumyantsev, S. L.; Levinshtein, M., *Sic Materials and Devices - Volume 1*. World Scientific: 2006.
48. Baumhauer, H., Uber die kristalle des carborundums. *Zeitschrift fur Kristallographie* **1912,** 50, 33.
49. Baumhauer, H., Uber die verschiedenen Modifikationen des Carborundums und die Erscheinung der Polytypie. *Z. Krist* **1915,** 55, 249.
50. Chow, T. P.; Ramungul, N.; Ghezzo, M. In *Recent advances in high-voltage SiC power devices*, High-Temperature Electronic Materials, Devices and Sensors Conference, 1998, 22-27 Feb 1998, 1998; 1998; pp 55.
51. Harris, G. L.; INSPEC, *Properties of silicon carbide*. INSPEC, Institution of Electrical Engineers: 1995.
52. Philip, N., SiC Technology. In *The VLSI Handbook*, CRC Press: 1999.
53. Ferreira, I.; Cabrita, A.; Fortunato, E.; Martins, R., Composition and structure of silicon-carbide alloys obtained by hot wire and hot wire plasma assisted techniques. *Vacuum* **2002,** 64, (3–4), 261.
54. Swain, B. P.; Dusane, R. O., Effect of filament temperature on HWCVD deposited a-SiC:H. *Materials Letters* **2006,** 60, (24), 2915.
55. Swain, B. P.; Gundu Rao, T. K.; Roy, M.; Gupta, J.; Dusane, R. O., Effect of H_2 dilution on Cat-CVD a-SiC:H films. *Thin Solid Films* **2006,** 501, (1–2), 173.
56. Swain, B. P.; Dusane, R. O., Effect of substrate temperature on HWCVD deposited a-SiC : H film. *Materials Letters* **2007,** 61, (25), 4731.
57. Tabata, A.; Komura, Y.; Hoshide, Y.; Narita, T.; Kondo, A., Properties of nanocrystalline cubic silicon carbide thin films prepared by hot-wire chemical vapor deposition using $SiH_4/CH_4/H_2$ at various substrate temperatures. *Japanese Journal of Applied Physics* **2008,** 47, (1), 561.
58. Komura, Y.; Tabata, A.; Narita, T.; Kanaya, M.; Kondo, A.; Mizutani, T., Film properties of nanocrystalline 3C-SiC thin films deposited on glass substrates by hot-wire chemical vapor deposition using CH_4 as a carbon source. *Japanese Journal of Applied Physics Part 1-Regular Papers Brief Communications & Review Papers* **2007,** 46, (1), 45.
59. Daimaru, T.; Tabata, A.; Mizutani, T., Structure of amorphous and microcrystalline silicon thin films prepared at various gas pressures and gas flow rates by hot-wire chemical vapor deposition. *Thin Solid Films* **2006,** 501, (1-2), 102.
60. Nakayama, H.; Takatsuji, K.; Murakami, K.; Miura, Y.; Shimoyama, N.; Machida, H., Catalytic CVD growth of Si–C and Si–C–O alloy films by using alkylsilane and related compounds. *Thin Solid Films* **2003,** 430, (1–2), 87.
61. Zaharias, G. A.; Duan, H. L.; Bent, S. F., Detecting free radicals during the hot wire chemical vapor deposition of amorphous silicon carbide films using single-source precursors. *Journal of Vacuum Science & Technology A* **2006,** 24, (3), 542.

62. Sharma, R. C.; Koshi, M., Hot filament-dissociation of $(CH_3)_3SiH$ and $(CH3)_4Si$, probed by vacuum ultra violet laser time of flight mass spectroscopy. *Spectrochimica Acta Part a-Molecular and Biomolecular Spectroscopy* **2006,** 65, (3-4), 787.
63. Yoshimura, S.; Toh, A.; Maeda, T.; Sugimoto, S.; Kiuchi, M.; Hamaguchi, S., Fragment ions of methylsilane produced by hot tungsten wires. *Japanese Journal of Applied Physics Part 1-Regular Papers Brief Communications & Review Papers* **2006,** 45, (3A), 1813.
64. Larkin, D. J., An overview of SiC epitaxial growth. *Mrs Bulletin* **1997,** 22, (3), 36.
65. Delplancke, M. P.; Powers, J. M.; Vandentop, G. J.; Salmeron, M.; Somorjai, G. A., Preparation and characterization of amorphous SiC-H thin-films. *Journal of Vacuum Science & Technology a-Vacuum Surfaces and Films* **1991,** 9, (3), 450.
66. Delplancke, M. P.; Powers, J. M.; Vandentop, G. J.; Somorjai, G. A., Preparation of $Si_xC_yH_z$ films from methylsilane by plasma-enhanced chemical vapor-deposition. *Thin Solid Films* **1991,** 202, (2), 289.
67. Habuka, H.; Ando, Y., Mechanism of silicon carbide film deposition at room temperature using monomethylsilane gas. *Journal of the Electrochemical Society* **2011,** 158, (4), H352.
68. Kaneko, T.; Hosokawa, Y.; Suga, T.; Miyakawa, N., Low-temperature growth of polycrystalline SiC by catalytic CVD from monomethylsilane. *Microelectronic Engineering* **2006,** 83, (1), 41.
69. Klein, S.; Carius, R.; Finger, F.; Houben, L., Low substrate temperature deposition of crystalline SiC using HWCVD. *Thin Solid Films* **2006,** 501, (1-2), 169.
70. Wu, Q. G.; Gleason, K. K., Plasma-enhanced chemical vapor deposition of low-k dielectric films using methylsilane, dimethylsilane, and trimethylsilane precursors. *Journal of Vacuum Science & Technology A* **2003,** 21, (2), 388.
71. Madapura, S.; Steckl, A. J.; Loboda, M., Heteroepitaxial growth of SiC on Si(100) and (111) by chemical vapor deposition using trimethylsilane. *Journal of the Electrochemical Society* **1999,** 146, (3), 1197.
72. Ohshita, Y., Reactants in sic chemical-vapor-deposition using CH_3SiH_3 as a source gas. *Journal of Crystal Growth* **1995,** 147, (1-2), 111.
73. Lee, M. S.; Bent, S. F., Temperature effects in the hot wire chemical vapor deposition of amorphous hydrogenated silicon carbon alloy. *Journal of Applied Physics* **2000,** 87, (9), 4600.
74. Fonseca, J. L. C.; Tasker, S.; Apperley, D. C.; Badyal, J. P. S., Plasma-enhanced chemical vapor deposition of organosilicon materials: A comparison of hexamethyldisilane and tetramethylsilane precursors. *Macromolecules* **1996,** 29, (5), 1705.
75. Rynders, S. W.; Scheeline, A.; Bohn, P. W., Structure evolution in a-SiC-H films prepared from tetramethylsilane. *Journal of Applied Physics* **1991,** 69, (5), 2951.
76. Tyczkowski, J.; Odrobina, E.; Kazimierski, P.; Bassler, H.; Kisiel, A.; Zema, N., Electronic-properties of plasma-deposited films prepared from tetramethylsilane. *Thin Solid Films* **1992,** 209, (2), 250.

77. Yasui, K.; Fujita, A.; Akahane, T., Preparation of microcrystalline silicon-carbide films by hydrogen-radical-enhanced chemical vapor-deposition using tetramethylsilane. *Japanese Journal of Applied Physics Part 2-Letters* **1992,** 31, (4A), L379.
78. Chiu, H. T.; Hsu, J. S., Low-pressure chemical-vapor-deposition of silicon-carbide thin-films from hexamethyldisilane. *Thin Solid Films* **1994,** 252, (1), 13.
79. Klein, S.; Dasgupta, A.; Finger, F.; Carius, R.; Bronger, T., Electronic properties of low temperature microcrystalline silicon carbide prepared by Hot Wire CVD. *Thin Solid Films* **2008,** 516, (5), 630.
80. Klein, S.; Finger, F.; Carius, R.; Lossen, J., Improved deposition rates for mu c-Si : H at low substrate temperature. *Thin Solid Films* **2006,** 501, (1-2), 43.
81. Duan, H. L.; Zaharias, G. A.; Bent, S. F., Detecting reactive species in hot wire chemical vapor deposition. *Current Opinion in Solid State & Materials Science* **2002,** 6, (5), 471.
82. Eustergerling, B. D.; Heden, M.; Shi, Y. J., Development of a new laser induced electron impact ionization source for studying the hot-wire chemical vapor deposition chemistry of silane-ammonia mixtures. *Journal of Analytical Atomic Spectrometry* **2008,** 23, (12), 1590.
83. Duan, H. L.; Zaharias, G. A.; Bent, S. F., Detecting reactive species in hot wire chemical vapor deposition. *Current Opinion in Solid State and Materials Science* **2002,** 6, (5), 471.
84. Lipson, R. H.; Dimov, S. S.; Wang, P.; Shi, Y. J.; Mao, D. M.; Hu, X. K.; Vanstone, J., Vacuum ultraviolet and extreme ultraviolet lasers: Principles, instrumentation, and applications. *Instrumentation Science & Technology* **2000,** 28, (2), 85.
85. Shi, Y. J.; Hu, X. K.; Mao, D. M.; Dimov, S. S.; Lipson, R. H., Analysis of xanthate derivatives by vacuum ultraviolet laser time-of-flight mass spectrometry. *Analytical Chemistry* **1998,** 70, (21), 4534.
86. Shi, Y. J.; Consta, S.; Das, A. K.; Mallik, B.; Lacey, D.; Lipson, R. H., A 118 nm vacuum ultraviolet laser/time-of-flight mass spectroscopic study of methanol and ethanol clusters in the vapor phase. *Journal of Chemical Physics* **2002,** 116, (16), 6990.
87. Eustergerling, B.; Heden, M.; Shi, Y., Application of laser induced electron impact ionization to the deposition chemistry in the hot-wire chemical vapor deposition process with SiH_4-NH_3 gas mixtures. *Journal of the American Society for Mass Spectrometry* **2007,** 18, (11), 1950.
88. Komura, Y.; Tabata, A.; Narita, T.; Kondo, A.; Mizutani, T., Nanocrystalline cubic silicon carbide films prepared by hot-wire chemical vapor deposition using $SiH_4/CH_4/H_2$ at a low substrate temperature. *Journal of Non-Crystalline Solids* **2006,** 352, (9-20), 1367.
89. Li, X. M.; Eustergerling, B. D.; Shi, Y. J., Mass spectrometric study of gas-phase chemistry in a hot-wire chemical vapor deposition reactor with tetramethylsilane. *International Journal of Mass Spectrometry* **2007,** 263, (2-3), 233.
90. Shi, Y. J.; Lo, B.; Tong, L.; Li, X.; Eustergerling, B. D.; Sorensen, T. S., In situ diagnostics of the decomposition of silacyclobutane on a hot filament by vacuum

ultraviolet laser ionization mass spectrometry. *Journal of Mass Spectrometry* **2007,** 42, (5), 575.
91. Tong, L.; Shi, Y. J., Gas-phase reaction chemistry of 1,1-dimethyl-1-silacyclobutane as a precursor gas in the hot-wire chemical vapor deposition process - Formation of tetramethylsilane and trimethylsilane. *Canadian Journal of Chemistry-Revue Canadienne De Chimie* **2011,** 89, (1), 19.
92. Tong, L.; Shi, Y. J., A mechanistic study of gas-phase reactions with 1,1,3,3-tetramethyl-1,3-disilacyclobutane in the hot-wire chemical vapor deposition process. *Thin Solid Films* **2009,** 517, (12), 3461.
93. Badran, I.; Forster, T. D.; Roesler, R.; Shi, Y. J., Competition of silene/silylene chemistry with free radical chain reactions using 1-methylsilacyclobutane in the hot-wire chemical vapor deposition process. *The Journal of Physical Chemistry A* **2012,** 116, (41), 10054.
94. Neudorfl, P. S.; Strausz, O. P., Pyrolysis of monomethysilane and dimethylsilane - role of molecular and radical processes. *Journal of Physical Chemistry* **1978,** 82, (2), 241.
95. Rickborn, S. F.; Rogers, D. S.; Ring, M. A.; Oneal, H. E., Kinetic and product studies of the thermal-decomposition of dimethylsilane in a single-pulse shock-tube and in a stirred flow reactor. *Journal of Physical Chemistry* **1986,** 90, (3), 408.
96. Alexander, A. G.; Strausz, O. P., Photochemistry of silicon-compounds .5. 147-nm photolysis of dimethylsilane. *Journal of Physical Chemistry* **1976,** 80, (23), 2531.
97. Nay, M. A.; Woodall, G. N. C.; Strausz, O. P.; Gunning, H. E., Mercury 6(3p1) photosensitization of methylsilanes and silane. *Journal of the American Chemical Society* **1965,** 87, (2), 179.
98. Strausz, O. P.; Obi, K.; Duholke, W. K., Photochemistry of silicon compounds .2. photolysis of methylsilane as a source of methylsilene. *Journal of the American Chemical Society* **1968,** 90, (5), 1359.
99. Gaspar, P. P.; West, R., Silylenes. In *The Chemistry of organic silicon compounds*, Rappoport, Z.; Apeloig, Y., Eds. Wiley: Chichester, 1998; Vol. 2, p 2463.
100. Gaspar, P. P.; Xiao, M.; Pae, D. H.; Berger, D. J.; Haile, T.; Chen, T.; Lei, D.; Winchester, W. R.; Jiang, P., The quest for triplet ground state silylenes. *Journal of Organometallic Chemistry* **2002,** 646, (1–2), 68.
101. Wulff, W. D.; Goure, W. F.; Barton, T. J., The role of trimethylsilylmethylsilylene in the gas-phase reactions of tetramethyldisilene. *Journal of the American Chemical Society* **1978,** 100, (19), 6236.
102. Skell, P. S.; Goldstein, E. J., Dimethylsilene: CH_3SiCH_3. *Journal of the American Chemical Society* **1964,** 86, (7), 1442.
103. Cox, B.; Purnell, H., Arrhenius parameters for silene insertion into silicon-hydrogen bonds. *Journal of the Chemical Society, Faraday Transactions 1: Physical Chemistry in Condensed Phases* **1975,** 71, (0), 859.

104. Rogers, D. S.; Oneal, H. E.; Ring, M. A., Comparative trapping kinetics of silylene .1. silylene reactions with 1,3-butadiene and acetylene and with 1,3-butadiene and methanol. *Organometallics* **1986,** 5, (7), 1467.
105. Rogers, D. S.; Walker, K. L.; Ring, M. A.; Oneal, H. E., Silylene reactions with ethylene and butadiene - mechanism and kinetics. *Organometallics* **1987,** 6, (11), 2313.
106. Barton, T. J.; Burns, S. A.; Burns, G. T., Thermochemistry of di- and trisilanyl radicals. Observations and comments on silene-to-silylene rearrangements. *Organometallics* **1982,** 1, (1), 210.
107. Barton, T. J.; Revis, A.; Davidson, I. M. T.; Ijadimaghsoodi, S.; Hughes, K. J.; Gordon, M. S., Pyrolytic, kinetic, and theoretical-studies on the isomerization of Me_2HSiCH_2 to Me_3Si. *Journal of the American Chemical Society* **1986,** 108, (14), 4022.
108. Brook, A. G.; Brook, M. A., The Chemistry of Silenes. In *Advances in Organometallic Chemistry*, F. Gordon, A. S.; Robert, W., Eds. Academic Press: 1996; Vol. Volume 39, pp 71.
109. Ziche, W.; Auner, N.; Behm, J., Silaheterocycles. 15. Cycloaddition behavior of 1,1-dichloro-2-neopentyl-2-(trimethylsilyl)silene. *Organometallics* **1992,** 11, (7), 2494.
110. Coleman, B.; Jones, M., Silenes. *Reviews of Chemical Intermediates* **1981,** 4, (1-4), 297.
111. Gusel'nikov, L. E., Hetero-π-systems from 2+2 cycloreversions. Part 1. Gusel'nikov–Flowers route to silenes and origination of the chemistry of doubly bonded silicon. *Coordination Chemistry Reviews* **2003,** 244, (1–2), 149.
112. Conlin, R. T.; Laakso, D.; Marshall, P., A theoretical investigation of donor-acceptor bonding between amines and silylenes. *Organometallics* **1994,** 13, (3), 838.
113. Kostina, S. S.; Singh, T.; Leigh, W. J., Kinetics and mechanisms of the reactions of transient silylenes with amines. *Journal of Physical Organic Chemistry* **2011,** 24, (10), 937.
114. O'Neal, H. E.; Ring, M. A.; Martin, J. G.; Navio, M. T., Kinetics of silylene insertion into N−H bonds and the mechanism and kinetics of the pyrolysis of dimethylsilylamine. *The Journal of Physical Chemistry A* **1998,** 102, (44), 8493.
115. Li, X. Investigation of gas phase chemistry of alkylsilane molecules in a hot wire chemical vapor deposition reactor. M.Sc., University of Calgary (Canada), Ann Arbor, 2008.
116. Kung, A. H., Generation of tunable picosecond VUV radiation. *Applied Physics Letters* **1974,** 25, (11), 653.
117. Schuhle, U.; Pallix, J. B.; Becker, C. H., Surface analysis of bulk polymers using single and multiple photon ionization. *Journal of Vacuum Science & Technology A: Vacuum, Surfaces, and Films* **1988,** 6, (3), 936.
118. Eustergerling, B.; Heden, M.; Shi, Y. J., Application of laser induced electron impact ionization to the deposition chemistry in the hot-wire chemical vapor deposition process with SiH_4-NH_3 gas mixtures. *Journal of the American Society for Mass Spectrometry* **2007,** 18, (11), 1950.

119. Wiley, W. C.; McLaren, I. H., Time-of-flight mass spectrometer with improved resolution. *Review of Scientific Instruments* **1955,** 26, (12), 1150.
120. Tannenbaum, S.; Kaye, S.; Lewenz, G. F., Synthesis and properties of some alkylsilanes. *Journal of the American Chemical Society* **1953,** 75, (15), 3753.
121. Sidorov, D. V.; Storozhenko, P. A.; Shutova, O. G.; Kozhevnikov, B. E., Synthesis of high-purity alkylsilanes. *Theoretical Foundations of Chemical Engineering* **2007,** 41, (5), 668.
122. Sawrey, B. A.; Oneal, H. E.; Ring, M. A., The gas-phase decomposition of methylsilane .2. mechanisms of decomposition under static system conditions. *International Journal of Chemical Kinetics* **1984,** 16, (1), 23.
123. Sawrey, B. A.; Oneal, H. E.; Ring, M. A.; Coffey, D., The gas-phase decomposition of methylsilane .1. mechanism of decomposition under shock-tube conditions. *International Journal of Chemical Kinetics* **1984,** 16, (1), 7.
124. Sawrey, B. A.; Oneal, H. E.; Ring, M. A.; Coffey, D., The gas-phase decomposition of methylsilane .3. kinetics. *International Journal of Chemical Kinetics* **1984,** 16, (1), 31.
125. Binkley, J. S.; Pople, J. A., Møller–Plesset theory for atomic ground state energies. *International Journal of Quantum Chemistry* **1975,** 9, (2), 229.
126. Bartlett, R. J., Coupled-cluster approach to molecular structure and spectra: a step toward predictive quantum chemistry. *The Journal of Physical Chemistry* **1989,** 93, (5), 1697.
127. Frisch, M. J.; Trucks, G. W.; Schlegel, H. B.; Scuseria, G. E.; Robb, M. A.; Cheeseman, J. R.; Montgomery, J. A.; Vreven, T.; Kudin, K. N.; Burant, J. C.; Millam, J. M.; Iyengar, S. S.; Tomasi, J.; Barone, V.; Mennucci, B.; Cossi, M.; Scalmani, G.; Rega, N.; Petersson, G. A.; Nakatsuji, H.; Hada, M.; Ehara, M.; Toyota, K.; Fukuda, R.; Hasegawa, J.; Ishida, M.; Nakajima, T.; Honda, Y.; Kitao, O.; Nakai, H.; Klene, M.; Li, X.; Knox, J. E.; Hratchian, H. P.; Cross, J. B.; Bakken, V.; Adamo, C.; Jaramillo, J.; Gomperts, R.; Stratmann, R. E.; Yazyev, O.; Austin, A. J.; Cammi, R.; Pomelli, C.; Ochterski, J. W.; Ayala, P. Y.; Morokuma, K.; Voth, G. A.; Salvador, P.; Dannenberg, J. J.; Zakrzewski, V. G.; Dapprich, S.; Daniels, A. D.; Strain, M. C.; Farkas, O.; Malick, D. K.; Rabuck, A. D.; Raghavachari, K.; Foresman, J. B.; Ortiz, J. V.; Cui, Q.; Baboul, A. G.; Clifford, S.; Cioslowski, J.; Stefanov, B. B.; Liu, G.; Liashenko, A.; Piskorz, P.; Komaromi, I.; Martin, R. L.; Fox, D. J.; Keith, T.; Laham, A.; Peng, C. Y.; Nanayakkara, A.; Challacombe, M.; Gill, P. M. W.; Johnson, B.; Chen, W.; Wong, M. W.; Gonzalez, C.; Pople, J. A., Gaussian 03, Revision C.02. In 2003.
128. Scott, A. P.; Radom, L., HARMONIC vibrational frequencies: An evaluation of Hartree−Fock, Møller−Plesset, quadratic configuration interaction, density functional theory, and semiempirical scale factors. *The Journal of Physical Chemistry* **1996,** 100, (41), 16502.
129. Johnson, A. D.; Perrin, J.; Mucha, J. A.; Ibbotson, D. E., Kinetics of SiC CVD - surface decomposition of silacyclobutane and methylsilane. *Journal of Physical Chemistry* **1993,** 97, (49), 12937.
130. Wu, Q.; Gleason, K. K., Plasma-enhanced chemical vapor deposition of low-k dielectric films using methylsilane, dimethylsilane, and trimethylsilane

precursors. *Journal of Vacuum Science & Technology A: Vacuum, Surfaces, and Films* **2003,** 21, (2), 388.
131. Yasui, K.; Asada, K.; Akahane, T., Epitaxial growth of 3C-SiC films on Si substrates by triode plasma CVD using dimethylsilane. *Applied Surface Science* **2000,** 159–160, (0), 556.
132. Joubert, O.; Fuard, D.; Monget, C.; Weidman, T., Plasma polymerized methylsilane. III. Process optimization for 193 nm lithography applications. *Journal of Vacuum Science & Technology B* **2000,** 18, (2), 793.
133. Wrobel, A. M.; Walkiewicz-Pietrzykowska, A., Mechanism of the initiation step in atomic hydrogen-induced CVD of amorphous hydrogenated silicon-carbon films from single-source precursors. *Chemical Vapor Deposition* **1998,** 4, (4), 133.
134. Herlin, N.; Lefebvre, M.; Pealat, M.; Perrin, J., Investigation of the chemical vapor-deposition of silicon-carbide from tetramethylsilane by insitu temperature and gas-composition measurements. *Journal of Physical Chemistry* **1992,** 96, (17), 7063.
135. Itoh, T.; Kawasaki, T.; Takai, Y.; Yoshida, N.; Nonomura, S., Properties of hetero-structured SiC_X films deposited by hot-wire CVD using SiH_3CH_3 as carbon source. *Thin Solid Films* **2008,** 516, (5), 641.
136. Chen, T.; Kohler, F.; Heidt, A.; Huang, Y.; Finger, F.; Carius, R., Microstructure and electronic properties of microcrystalline silicon carbide thin films prepared by hot-wire CVD. *Thin Solid Films* **2011,** 519, (14), 4511.
137. Badran, I.; Forster, T. D.; Roesler, R.; Shi, Y. J., Competition of silene/silylene chemistry with free radical chain reactions using 1-methylsilacyclobutane in the hot-wire chemical vapor deposition process. *Journal of Physical Chemistry A* **2012,** 116, (41), 10054.
138. Tong, L.; Shi, Y. J., Decomposition of 1,1-dimethyl-1-silacyclobutane on a tungsten filament - evidence of both ring C-C and ring Si-C bond cleavages. *Journal of Mass Spectrometry* **2010,** 45, (2), 215.
139. Harris, S. J.; Weiner, A. M.; Perry, T. A., Measurement of stable species present during filament-assisted diamond growth. *Applied Physics Letters* **1988,** 53, (17), 1605.
140. Goodwin, D. G., Simulations of high-rate diamond synthesis - methyl as growth species. *Applied Physics Letters* **1991,** 59, (3), 277.
141. Harris, S. J.; Martin, L. R., Methyl versus acetylene as diamond growth species. *Journal of Materials Research* **1990,** 5, (11), 2313.
142. Martin, L. R.; Hill, M., A flow-tube study of diamond film growth: methane versus acetylene. *Journal of Materials Science Letters* **1990,** 9, (6), 621.
143. Harris, S. J., Mechanism for diamond growth from methyl radicals. *Applied Physics Letters* **1990,** 56, (23), 2298.
144. Winters, H. F.; Seki, H.; Rye, R. R.; Coltrin, M. E., Interaction of hydrogen, methane, ethylene, and cyclopentane with hot tungsten - implications for the growth of diamond films. *Journal of Applied Physics* **1994,** 76, (2), 1228.
145. Harris, S. J.; Weiner, A. M., Methyl radical and h-atom concentrations during diamond growth. *Journal of Applied Physics* **1990,** 67, (10), 6520.

146. Tong, L.; Shi, Y. J., Carburization of tungsten filaments in a hot-wire chemical vapor deposition process using 1,1,3,3-tetramethyl-1,3-disilacyclobutane. *ACS Applied Materials & Interfaces* **2009,** 1, (9), 1919.
147. Shi, Y. J.; Badran, I.; Tkalych, A.; Kan, W. H.; Thangadurai, V., Growth of crystalline tungsten carbides using 1,1,3,3-tetramethyl-1,3-disilacyclobutane on a heated tungsten filament. *Journal of Physical Chemistry C* **2013,** 117, (7), 3389.
148. Hostetler, M. J.; Nuzzo, R. G.; Girolami, G. S., Reactions of primary organosilanes on transition-metal surfaces - identification of the first surface-bound silylynes. *Journal of the American Chemical Society* **1994,** 116, (25), 11608.
149. Spencer, M. J. S.; Nyberg, G. L., Adsorption of methylsilane on copper surfaces. *Surface Science* **2003,** 543, (1-3), 162.
150. Bradshaw, D. I.; Moyes, R. B.; Wells, P. B., Reactions of methylsilane at the surfaces of nickel, rhodium and tungsten. *Journal of the Chemical Society-Faraday Transactions I* **1980,** 76, 979.
151. Roberts, M. W.; Ross, J. R. H., Chemisorption and decomposition of tetramethylsilane over tungsten and iron surfaces. *Journal of the Chemical Society-Faraday Transactions I* **1972,** 68, (591), 221.
152. Casserly, T. B.; Gleason, K. K., Enthalpies of formation and reaction for primary reactions of methyl- and methylmethoxysilanes from density functional theory. *Plasma Processes and Polymers* **2005,** 2, (9), 669.
153. Gusel'nikov, L. E.; Avakyan, V. G.; Gusel'nikov, S. L., Effect of the electronic structure of substituents at the silicon atom on the structure and bond energies of methylhydrosilanes and silenes. *Russian Journal of General Chemistry* **2001,** 71, (12), 1933.
154. Zeigarnik, A. V.; Valdes-Perez, R. E.; Myatkovskaya, O. N., C-C bond scission in ethane hydrogenolysis. *Journal of Physical Chemistry B* **2000,** 104, (45), 10578.
155. Foster, M.; Darlington, B.; Scharff, J.; Campion, A., Surface chemistry of alkylsilanes on Si(100)2x1. *Surface Science* **1997,** 375, (1), 35.
156. Shinohara, M.; Maehama, T.; Niwano, M., Adsorption and decomposition of methylsilanes on Si(100). *Applied Surface Science* **2000,** 162, 161.
157. Takatsuka, T.; Fujiu, M.; Sakuraba, M.; Matsuura, T.; Murota, J., Surface reaction of CH_3SiH_3 on Ge(100) and Si(100). *Applied Surface Science* **2000,** 162, 156.
158. Lin, J. L.; Bent, B. E., Two mechanisms for formation of methyl radicals during the thermal decomposition of methyl iodide on a copper surface. *The Journal of Physical Chemistry* **1993,** 97, (38), 9713.
159. Wang, G. C.; Li, J.; Xu, X. F.; Li, R. F.; Nakamura, J., The relationship between adsorption energies of methyl on metals and the metallic electronic properties: A first-principles DFT study. *Journal of Computational Chemistry* **2005,** 26, (9), 871.
160. Kua, J.; Faglioni, F.; Goddard, W. A., Thermochemistry for hydrocarbon intermediates chemisorbed on metal surfaces: $CH_{n-m}(CH_3)_m$ with n=1, 2, 3 and m <= n on Pt, Ir, Os, Pd, Ph, and Ru. *Journal of the American Chemical Society* **2000,** 122, (10), 2309.

161. Comerford, D. W.; Smith, J. A.; Ashfold, M. N. R.; Mankelevich, Y. A., On the mechanism of H atom production in hot filament activated H_2 and CH_4/H_2 gas mixtures. *Journal of Chemical Physics* **2009,** 131, (4).
162. Van der Werf, C. H. M.; van Veenendaal, P. A. T. T.; van Veen, M. K.; Hardeman, A. J.; Rusche, M. Y. S.; Rath, J. K.; Schropp, R. E. I., The influence of the filament temperature on the structure of hot-wire deposited silicon. *Thin Solid Films* **2003,** 430, (1–2), 46.
163. Celii, F. G.; Butler, J. E., Hydrogen-atom detection in the filament-assisted diamond deposition environment. *Applied Physics Letters* **1989,** 54, (11), 1031.
164. Ferreira, I.; Aguas, H.; Mendes, L.; Martins, R., Role of the hot wire filament temperature on the structure and morphology of the nanocrystalline silicon p-doped films. *Applied Surface Science* **1999,** 144-45, 690.
165. Banholzer, W., Understanding the mechanism of cvd diamond. *Surface & Coatings Technology* **1992,** 53, (1), 1.
166. Liu, H. M.; Dandy, D. S., Studies on nucleation process in diamond cvd - an overview of recent developments. *Diamond and Related Materials* **1995,** 4, (10), 1173.
167. May, P. W., Diamond thin films: a 21st-century material. *Philosophical Transactions of the Royal Society of London Series a-Mathematical Physical and Engineering Sciences* **2000,** 358, (1766), 473.
168. Lee, S. T.; Lin, Z. D.; Jiang, X., CVD diamond films: nucleation and growth. *Materials Science & Engineering R-Reports* **1999,** 25, (4), 123.
169. Cifre, J.; Bertomeu, J.; Puigdollers, J.; Polo, M. C.; Andreu, J.; Lloret, A., Polycrystalline silicon films obtained by hot-wire chemical vapour deposition. *Applied Physics A* **1994,** 59, (6), 645.
170. Matsumura, H., Formation of silicon-based thin films prepared by catalytic chemical vapor deposition (Cat-CVD) method. *Japanese Journal of Applied Physics Part 1-Regular Papers Short Notes & Review Papers* **1998,** 37, (6A), 3175.
171. Mahan, A. H.; Yang, J.; Guha, S.; Williamson, D. L., Structural changes in a-Si : H film crystallinity with high H dilution. *Physical Review B* **2000,** 61, (3), 1677.
172. Honda, K.; Ohdaira, K.; Matsumura, H., A novel method for suppressing silicidation of tungsten catalyzer during silane decomposition in Cat-CVD. *Thin Solid Films* **2008,** 516, (5), 826.
173. Knoesen, D.; Arendse, C.; Halindintwali, S.; Muller, T., Extension of the lifetime of tantalum filaments in the hot-wire (Cat) chemical vapor deposition process. *Thin Solid Films* **2008,** 516, (5), 822.
174. Shi, Y. J.; Tong, L.; Eustergerling, B. D.; Li, X. M., Silicidation and carburization of the tungsten filament in HWCVD with silacyclobutane precursor gases. *Thin Solid Films* **2011,** 519, (14), 4442.
175. Tong, L.; Sveen, C. E.; Shi, Y. J., Study of tungsten filament aging in hot-wire chemical vapor deposition with silacyclobutane as a source gas and the H_2 etching effect. *Journal of Applied Physics* **2008,** 103, (12).

176. Ring, M. A.; Oneal, H. E.; Rickborn, S. F.; Sawrey, B. A., Kinetics of the high-temperature thermal-decomposition of silanes and alkylsilanes. *Organometallics* **1983,** 2, (12), 1891.
177. Davidson, I. M. T.; Ring, M. A., Primary processes in the low-pressure pyrolysis of methylsilane. *Journal of the Chemical Society-Faraday Transactions I* **1980,** 76, 1520.
178. Neudorfl, P. S.; Lown, E. M.; Safarik, I.; Jodhan, A.; Strausz, O. P., Mechanism of the gas-phase thermolysis of monomethylsilane. *Journal of the American Chemical Society* **1987,** 109, (19), 5780.
179. Oneal, H. E.; Ring, M. A., Mechanism of the thermal-decomposition of dimethylsilane at atmospheric pressures in the gas-phase. *Organometallics* **1988,** 7, (5), 1017.
180. Gordon, M. S.; Truong, T. N., Potential primary pyrolysis processes of methylsilane. *Chemical Physics Letters* **1987,** 142, (1-2), 110.
181. Davidson, I. M. T.; Lambert, C. A., Mechanisms of pyrolysis and bond dissociation energies in trimethylsilane. *Journal of the Chemical Society A: Inorganic, Physical, Theoretical* **1971,** 0, (0), 882.
182. Davidson, I. M. T.; Lambert, C. A., A kinetic study of the pyrolysis of trimethylsilane. *Journal of the Chemical Society D: Chemical Communications* **1969,** 0, (21), 1276.
183. Baldwin, A. C.; Davidson, I. M. T.; Reed, M. D., Mechanism of thermolysis of tetramethylsilane and trimethylsilane. *Journal of the Chemical Society-Faraday Transactions I* **1978,** 74, 2171.
184. Paquin, D. P.; Oconnor, R. J.; Ring, M. A., Pyrolysis of trimethylgermane and trimethylsilane. *Journal of Organometallic Chemistry* **1974,** 80, (3), 341.
185. Bradshaw, D. I.; Moyes, R. B.; Wells, P. B., Fast catalysis of a hydrogen-exchange reaction at low-temperatures by gold. *Journal of the Chemical Society-Chemical Communications* **1975**, (5), 137.
186. Dubois, L. H.; Zegarski, B. R., The decomposition of alkyl silanes ($SiMe_nH_{4-n}$,0-less-than-or-equal-to-n-less-than-or-equal-to-4) on Ni(100). *Journal of Vacuum Science & Technology a-Vacuum Surfaces and Films* **1988,** 6, (3), 870.
187. Roberge, R.; Sandorfy, C.; Matthews, J. I.; Strausz, O. P., Far ultraviolet and hel photoelectron-spectra of alkyl and fluorine substituted silane derivatives. *Journal of Chemical Physics* **1978,** 69, (11), 5105.
188. Herzberg, G., Dissociation energy and ionization potential of molecular hydrogen. *Physical Review Letters* **1969,** 23, (19), 1081.
189. Berkowitz, J.; Ellison, G. B.; Gutman, D., Three methods to measure RH bond energies. *The Journal of Physical Chemistry* **1994,** 98, (11), 2744.
190. Hase, W. L.; Mazac, C. J.; Simons, J. W., Decomposition kinetics of chemically activated dimethylsilane and ethylsilane. *Journal of the American Chemical Society* **1973,** 95, (11), 3454.
191. Alexander, A. G.; Strausz, O. P., Photochemistry of silicon compounds. 5. The 147-nm photolysis of dimethylsilane. *The Journal of Physical Chemistry* **1976,** 80, (23), 2531.

192. Davidson, I. M.; Lambert, C. A., Mechanisms of pyrolysis and bond dissociation energies in trimethylsilane. *Journal of the Chemical Society a -Inorganic Physical Theoretical* **1971**, (7), 882.
193. Paquin, D. P.; O'Connor, R. J.; Ring, M. A., The pyrolysis of trimethylgermane and trimethylsilane. *Journal of Organometallic Chemistry* **1974,** 80, (3), 341.
194. Morisset, S.; Aguillon, F.; Sizun, M.; Sidis, V., Wave-packet study of H_2 formation on a graphite surface through the Langmuir--Hinshelwood mechanism. *The Journal of Chemical Physics* **2005,** 122, (19), 194702.
195. Obi, K.; Clement, A.; Gunning, H. E.; Strausz, O. P., Photochemistry of silicon compounds. III. Vacuum-ultraviolet photolysis of methylsilane. *Journal of the American Chemical Society* **1969,** 91, (7), 1622.
196. Ring, M. A.; Oneal, H. E., Mechanism of the thermally induced gas-phase decomposition of silane - a revisitation. *Journal of Physical Chemistry* **1992,** 96, (26), 10848.
197. Kohanek, J. J.; Estacio, P.; Ring, M. A., Pyrolysis of methylgermane and methylsilane. *Inorganic Chemistry* **1969,** 8, (11), 2516.
198. Ring, M. A.; Puentes, M. J.; Oneal, H. E., Pyrolysis of monosilane. *Journal of the American Chemical Society* **1970,** 92, (16), 4845.
199. Tong, L. Gas-phase chemistry and tungsten filament aging in hot-wire chemical vapor deposition with silacyclobutanes. M.Sc., University of Calgary (Canada), Canada, 2009.
200. Frese, K. W., Calculation of surface binding-energy for hydrogen, oxygen, and carbon-atoms on metallic surfaces. *Surface Science* **1987,** 182, (1-2), 85.
201. Toyoshima, I.; Somorjai, G. A., Heats of Chemisorption of O_2, H_2, CO, CO_2, and N_2 on Polycrystalline and Single Crystal Transition Metal Surfaces. *Catalysis Reviews* **1979,** 19, (1), 105.
202. Reynolds, T. W.; Aeronautics, U. S. N.; Administration, S., *Adsorption-desorption behavior of homogeneous and heterogeneous metal surfaces*. National Aeronautics and Space Administration: 1968.
203. Bond, A. C.; Brockway, L. O., The molecular structures of mono-, di- and trimethylsilane1. *Journal of the American Chemical Society* **1954,** 76, (12), 3312.
204. Owens, T. R.; Harrington, C. R.; Pace, T. C. S.; Leigh, W. J., Steric effects on silene reactivity. The effects of ortho-methyl substituents on the kinetics and mechanisms of the reactions of 1,1-diarylsilenes with nucleophiles. *Organometallics* **2003,** 22, (26), 5518.
205. Wu, Y.-D.; Wong, C.-L., Substituent effect on the dissociation energy of the Si-H bond: a density functional study. *The Journal of Organic Chemistry* **1995,** 60, (4), 821.
206. Walsh, R., Thermochemistry. In *Organic Silicon Compounds (1989)*, John Wiley & Sons, Ltd: 2004; pp 371.
207. Davidson, I. M.; Lambert, C. A., A kinetic study of pyrolysis of trimethylsilane. *Journal of the Chemical Society D-Chemical Communications* **1969**, (21), 1276.
208. Badran, I.; Rauk, A.; Shi, Y. J., Theoretical study on the ring-opening of 1,3-disilacyclobutane and H_2 elimination. *The Journal of Physical Chemistry A* **2012,** 116, (48), 11806.

209. Clifford, R. P.; Gowenloc.Bg; Stevenso.J; Johnson, C. A. F., Pyrolysis of organometallic compounds .4. kinetic studies of decomposition of tetramethylsilane. *Journal of Organometallic Chemistry* **1972,** 34, (1), 53.
210. Mahan, A. H., Hot wire chemical vapor deposition of Si containing materials for solar cells. *Solar Energy Materials and Solar Cells* **2003,** 78, (1-4), 299.
211. Fonrodona, M.; Soler, D.; Asensi, J.; Bertomeu, J.; Andreu, J., Studies on grain boundaries in nanocrystalline silicon grown by hot-wire CVD. *Journal of Non-Crystalline Solids* **2002,** 299, 14.
212. Shi, Y. J.; Li, X. M.; Toukabri, R.; Tong, L., Effect of Si–H bond on the gas-phase chemistry of trimethylsilane in the hot wire chemical vapor deposition process. *The Journal of Physical Chemistry A* **2011,** 115, (37), 10290.
213. Clarke, M. P.; Davidson, I. M. T., Mechanism of addition of silanediyls (silylenes) to buta-1,3-diene. *Journal of the Chemical Society-Chemical Communications* **1988**, (3), 241.
214. Conlin, R. T.; Wood, D. L., Evidence for the isomerization of 1-methylsilene to dimethylsilylene. *Journal of the American Chemical Society* **1981,** 103, (7), 1843.
215. Zhao, Q.; Li, J. C.; Zhou, H.; Wang, H.; Wang, B.; Yan, H., Parameters determining crystallinity in β-SiC thin films prepared by catalytic chemical vapor deposition. *Journal of Crystal Growth* **2004,** 260, (1–2), 176.
216. Berkowitz, J.; Greene, J. P.; Cho, H.; Ruscic, B., The ionization potentials of CH_4 and CD_4. *The Journal of Chemical Physics* **1987,** 86, (2), 674.
217. Plessis, P.; Marmet, P., Electroionization study of acetylene and fragment ions. *International Journal of Mass Spectrometry and Ion Processes* **1986,** 70, (1), 23.
218. Taylor, J. E.; Milazzo, T. S., A comparative study of the pyrolyses of the tetramethyl derivatives of silicon, germanium, and tin using a wall-less reactor. *The Journal of Physical Chemistry* **1978,** 82, (8), 847.
219. Haas, C. H.; Ring, M. A., Reaction of silyl radical and silylene with acetylene and application of orbital symmetry to the pyrolysis of silane and disilane. *Inorganic Chemistry* **1975,** 14, (9), 2253.
220. Al-Rubaiey, N.; Carpenter, I. W.; Walsh, R.; Becerra, R.; Gordon, M. S., Direct gas-phase kinetic studies of silylene addition reactions: SiH_2+C_3H_6, SiH_2+i-C_4H_8, and $SiMe_2$+C_2H_4. The effects of methyl substitution on strain energies in siliranes. *Journal of Physical Chemistry A* **1998,** 102, (44), 8564.
221. Choo, K. Y.; Gaspar, P. P., Addition of trimethylsilyl radical to ethylene. Flash photolysis-electron spin resonance kinetic study. *Journal of the American Chemical Society* **1974,** 96, (5), 1284.
222. Pollock, T. L.; Sandhu, H. S.; Jodhan, A.; Strausz, O. P., Photochemistry of silicon compounds. IV. Mercury photosensitization of disilane. *Journal of the American Chemical Society* **1973,** 95, (4), 1017.
223. Oliphant, C.; Arendse, C.; Prins, S.; Malgas, G.; Knoesen, D., Structural evolution of a Ta-filament during hot-wire chemical vapour deposition of Silicon investigated by electron backscatter diffraction. *Journal of Materials Science* **2012,** 47, (5), 2405.
224. Oliphant, C. J.; Arendse, C. J.; Malgas, G. F.; Motaung, D. E.; Muller, T. F. G.; Halindintwali, S.; Julies, B. A.; Knoesen, D., Filament poisoning at typical carbon

nanotube deposition conditions by hot-filament CVD. *Journal of Materials Science* **2009,** 44, (10), 2610.
225. Davidson, I. M., Factors influencing formation of silylenes in pyrolysis of silicon compounds. *Journal of Organometallic Chemistry* **1970,** 24, (1), 97.
226. Obi, K.; Clement, A.; Gunning, H. E.; Strausz, O. P., Photochemistry of silicon compounds .3. vacuumm-ultraviolet photolysis of methylsilane. *Journal of the American Chemical Society* **1969,** 91, (7), 1622.
227. Loboda, M. J.; Seifferly, J. A.; Dall, F. C., Plasma-enhanced chemical-vapor-deposition of a-SiC-H films from organosilicon precursors. *Journal of Vacuum Science & Technology a-Vacuum Surfaces and Films* **1994,** 12, (1), 90.
228. Ohshita, Y., Low-temperature p-doped SiC growth by chemical-vapor-deposition using CH_3SiH_3/Ph_3 gas. *Journal of the Electrochemical Society* **1995,** 142, (3), 1002.
229. Krotz, G.; Legner, W.; Muller, G.; Grueninger, H. W.; Smith, L.; Leese, B.; Jones, A.; Rushworth, S., Structural and electronic characterization of beta-SiC films on si grown from mono-methylsilane precursors. *Materials Science and Engineering B-Solid State Materials for Advanced Technology* **1995,** 29, (1-3), 154.
230. Johnson, A. D.; Perrin, J.; Mucha, J. A.; Ibbotson, D. E., Chemical vapor-deposition of SiC from silacyclobutane and methylsilane. In *Chemical Perspectives of Microelectronic Materials Iii*, Abernathy, C. R.; Bates, C. W.; Bohling, D. A.; Hobson, W. S., Eds. 1993; Vol. 282, pp 451.
231. Liu, C. W.; Sturm, J. C., Low temperature chemical vapor deposition growth of beta-SiC on (100) Si using methylsilane and device characteristics. *Journal of Applied Physics* **1997,** 82, (9), 4558.
232. Guselnikov, L. E.; Nametkin, N. S.; Vdovin, V. M., Unstable silicon analogs of unsaturated-compounds. *Accounts of Chemical Research* **1975,** 8, (1), 18.
233. Maier, G.; Mihm, G.; Reisenauer, H. P., Silaethene. *Angewandte Chemie-International Edition in English* **1981,** 20, (6-7), 597.
234. Conlin, R. T.; Gaspar, P. P., Evidence for the dimerization of dimethylsilylene to tetramethyldisilene. *Journal of the American Chemical Society* **1976,** 98, (3), 868.
235. Apeloig, Y., Theoretical aspects of organosilicon compounds. In *The Chemistry of Organosilicon Compounds*, Wiley, J., Ed. S. Patai and Z. Rappoport: New York, 1989; Vol. 1, pp 57.
236. Chambreau, S. D.; Lemieux, J.; Wang, L.; Zhang, J., Mechanistic studies of the pyrolysis of 1,3-butadiene, 1,3-butadiene-1,1,4,4-d4, 1,2-butadiene, and 2-butyne by supersonic jet/photoionization mass spectrometry. *The Journal of Physical Chemistry A* **2005,** 109, (10), 2190.
237. Shinohara, M.; Kimura, Y.; Shoji, D.; Niwano, M., Infrared study of carbon incorporation during chemical vapor deposition of SiC using methylsilanes. *Applied Surface Science* **2001,** 175, 591.
238. Wrobel, A. M.; Walkiewicz-Pietrzykowska, A.; Stasiak, M.; Aoki, T.; Hatanaka, Y.; Szumilewicz, J., Reactivity of alkylsilanes and alkylcarbosilanes in atomic hydrogen-induced chemical vapor deposition. *Journal of the Electrochemical Society* **1998,** 145, (3), 1060.

239. Tong, L.; Shi, Y. J., Decomposition of 1,1-dimethyl-1-silacyclobutane on a tungsten filament—evidence of both ring C-C and ring Si-C bond cleavages. *Journal of Mass Spectrometry* **2010,** 45, (2), 215.
240. Band, S. J.; Davidson, I. M.; Lambert, C. A., Bond dissociation energies - electron impact studies on some trimethylsilyl compounds. *Journal of the Chemical Society a -Inorganic Physical Theoretical* **1968**, (9), 2068.
241. Malko, M. W.; Troe, J., Analysis of the unimolecular reaction N_2O_5 + M reversible NO_2 + NO_3 + M. *International Journal of Chemical Kinetics* **1982,** 14, (4), 399.
242. Cawood, C. N.; Furue, H.; Mousavipour, S. H.; Pacey, P. D., Comment on "Initiation and abstraction reactions in the pyrolysis of acetone". *Journal of Physical Chemistry A* **2003,** 107, (11), 1896.
243. Cawood, C. N.; Furue, H.; Mousavipour, S. H.; Pacey, P. D., Comment on "initiation and abstraction reactions in the pyrolysis of acetone". *Journal of Physical Chemistry B* **2003,** 107, (11), 2618.
244. Mousavipour, S. H.; Pacey, P. D., Initiation and abstraction reactions in the pyrolysis of acetone. *Journal of Physical Chemistry* **1996,** 100, (9), 3573.
245. Mousavipour, S. H.; Saheb, V.; Ramezani, S., Kinetics and mechanism of pyrolysis of methyltrichlorosilane. *Journal of Physical Chemistry A* **2004,** 108, (11), 1946.
246. Kee, R.; Rupley, F.; Miller, J.; Coltrin, M.; Grcar, J.; Meeks, E.; Moffat, H.; Lutz, A.; Dixon-Lewis, G.; Smooke, M., Chemkin Collection. *Reaction Design Inc., San Diego, CA* **2000**.
247. Coltrin, M. E.; Ho, P.; Moffat, H. K.; Buss, R. J., Chemical kinetics in chemical vapor deposition: growth of silicon dioxide from tetraethoxysilane (TEOS). *Thin Solid Films* **2000,** 365, (2), 251.
248. Tsang, R. S.; May, P. W.; Ashfold, M. N. R., Modelling of the gas phase chemistry during diamond CVD: the role of different hydrocarbon species. *Diamond and Related Materials* **1999,** 8, (2–5), 242.
249. Tsang, R. S.; May, P. W.; Cole, J.; Ashfold, M. N. R., Simulations of the hot-filament diamond CVD gas-phase environment: direct comparison with experimental measurements. *Diamond and Related Materials* **1999,** 8, (8–9), 1388.
250. Coltrin, M. E.; Kee, R. J.; Rupley, F. M., Surface chemkin: A general formalism and software for analyzing heterogeneous chemical kinetics at a gas-surface interface. *International Journal of Chemical Kinetics* **1991,** 23, (12), 1111.